SCHOOL OF ELECTRICAL AND ELECTRONIC ENGINEERING
ELECTRIC POWER SYSTEMS RESEARCH GROUP

INVESTIGATION OF ENERGY STORAGE SYSTEM AND DEMAND SIDE RESPONSE FOR DISTRIBUTION NETWORKS

A THESIS PRESENTED FOR THE DEGREE OF DOCTOR OF PHILOSOPHY

Jialiang Yi

February 2016

Abstract

The UK government has a target of achieving an 80% reduction in CO_2 emissions with respect to the values from 1990 by 2050. Therefore, renewables based distributed generations (DGs) coupled with substantial electrification of the transport and heat sectors though low carbon technologies (LCTs), will be essential to achieve this target. The anticipated proliferation of these technologies will necessitate major opportunities and challenges to the operation and planning of future distribution networks.

Smartgrid technologies and techniques, such as energy storage systems (ESSs), demand side response (DSR) and real time thermal ratings (RTTRs), provide flexible, economic and expandable solutions to these challenges without resorting to network reinforcement. This research investigates the use of ESS and DSR in future distribution networks to facilitate LCTs with a focus on the management and resolution of thermal constraints and steady state voltage limit violation problems. Firstly, two control schemes based on sensitivity factors and cost sensitivity factors are proposed. Next, the impacts of a range of sources of uncertainties, arising from existing and future elements of the electrical energy system, are studied. The impacts of electric vehicle charging are investigated with Monte Carlo simulation (MCS). Furthermore, to deal with uncertainties efficiently, a scheduling scheme based on robust optimization (RO) is developed. Two approaches have been introduced to estimate the trade-off between the cost and the probability of constraint violations. Finally, the performance of this scheme is evaluated.

The results of this research show the importance of dealing with uncertainties appropriately. Simulation results demonstrate the capability and effectiveness of the proposed RO based scheduling scheme to facilitate DG and LCTs, in the presence of a range of source of uncertainties. The findings from this research provide valuable solution and guidance to facilitate DG and LCTs using ESS, DSR and RTTR in future distribution networks.

Declaration

I hereby declare that this thesis is a record of work undertaken by myself, that it has not been the subject of any previous application for a degree, and that all sources of information have been duly acknowledged.

Acknowledgement

I would like to express my gratitude to my supervisors, Professor Phil Taylor and Dr Pádraig Lyons. Without their support, supervision, expertise, efforts, encouragement and inspiration, this research would have been impossible. The lessons they have taught me go far beyond the PhD.

I would like to thank Northern Powergrid for the supports during and after the Customer-led Network Revolution project. Special thanks to Ian Lloyd, Rosie Hetherington, Stuart Brown, Andrew Webster and David Miller for providing support, data, network models and especially their expertise and experiences.

I would like to thank all the colleagues in the CLNR project, Robin Wardle, Dr Lorna Bang, Peter Davison and Dr Pengfei Wang. This project has been an unforgettable journey. At the same time, I must acknowledge my colleagues in the electric power group especially Dr Neal Wade, Myriam Neaimeh, Dr Simon Blake, Dr Mansoureh Zangiabadi, Dr Haris Patsios, Dr Tianxiang Jiang, Dr David Greenwood and Dr Lei Wang for all the collaborations, advices and helpful discussions. Most importantly I would like to thank you all for your friendship and all the happy and sour moments we shared together.

Above all, I would like to thank my parents for their unwavering love, faith and support (mentally and financially!). None of these would have been possible if they have ever given up on me since I was born.

List of Publications

Journal Papers

- **J. Yi**, P. Lyons, P. Davison, P. Wang, P. Taylor, "Robust Scheduling Scheme for Energy Storage to Facilitate High Penetration of Renewables," *IEEE Transactions on Sustainable Energy,*. **7**(2): 797-807.
- M. Neaimeh, R. Wardle, A. Jenkins, **J. Yi** , G. Hill, P. Lyons, Y. Hübner , P. Blythe, P. Taylor, (2015). "A probabilistic approach to combining smart meter and electric vehicle charging data to investigate distribution network impacts." Applied Energy **157**(0): 688-698.
- P. Wang, D. H. Liang, **J. Yi**, P. F. Lyons, P. J. Davison, and P. C. Taylor, "Integrating Electrical Energy Storage Into Coordinated Voltage Control Schemes for Distribution Networks," *Smart Grid, IEEE Transactions* on, vol. 5, pp. 1018-1032, 2014.

Conference papers

- **J. Yi**, P. Wang, P. C. Taylor, P. J. Davison, P. F. Lyons, D. Liang, et al., "Distribution network voltage control using energy storage and demand side response," in *Innovative Smart Grid Technologies (ISGT Europe)*, 2012 3rd IEEE PES International Conference and Exhibition on, 2012, pp. 1-8.
- P. Wang, **J. Yi**, P. Lyons, D. Liang, P. Taylor, D. Miller, et al., "Customer Led Network Revolution - Integrating renewable energy into LV networks using energy storage," in *Integration of Renewables into the Distribution Grid*, CIRED 2012 Workshop, 2012, pp. 1-4.
- M. Neaimeh, G. Hill, P. Blythe, R. Wardle, **J. Yi**, and P. Taylor, "Integrating smart meter and electric vehicle charging data to predict distribution network impacts," in *Innovative Smart Grid Technologies Europe* (ISGT EUROPE), 2013 4th IEEE/PES, 2013, pp. 1-5.
- S. Blake, **J. Yi**, P. Taylor, D. Miller, and I. Lloyd, "Using electrical energy storage to support customers under faulted network conditions," in Electricity Distribution (CIRED 2013), 22nd International Conference and Exhibition on, 2013, pp. 1-4.

Selected Reports

J. Yi and S. Blake, "Analysis of Industrial and Commercial Demand Side Response for Powerflow Management", CLNR trial Analysis, 2014. Available: http://www.networkrevolution.co.uk/wp-content/uploads/2014/12/CLNR-Trial-Analysis-IC-DSR-for-Powerflow-Management.pdf

- **J. Yi** and P. Lyons, "Electrical Energy Storage 1 (2.5MVA/5MWh) and Enhanced Automatic Voltage Control", CLNR trial Analysis, 2014. Available: http://www.networkrevolution.co.uk/wp-content/uploads/2014/12/CLNR-L119-CLNR-Trial-Analysis-EES1-and-EAVC1-Voltage-Control-at-Rise-Carr.pdf
- **J. Yi**, T. Jiang, P. Davison and P. Lyons, "Electrical Energy Storage 1 (2.5MVA/5MWh) Powerflow Management at Rise Carr" , CLNR trial Analysis, 2014. Available: http://www.networkrevolution.co.uk/wp-content/uploads/2014/12/CLNR-Trial-Analysis-EES1-Powerflow-Management-at-Rise-Carr.-2pdf.pdf

  J. Yi and P. Lyons, "Industrial and Commercial Demand Side Response + Grand Unified Scheme Voltage Control", CLNR trial Analysis, 2014. Available: http://www.networkrevolution.co.uk/wp-content/uploads/2014/12/CLNR-Trial-Analysis-IC-DSR-and-GUS-Voltage-Control.pdf
- T. Jiang, **J. Yi**, S. Blake and P. Lyons, "Residential Demand Side Response for Powerflow Management", CLNR trial Analysis, 2015. Available: http://www.networkrevolution.co.uk/wp-content/uploads/2015/04/CLNR-L223-Residential-DSR-for-Powerflow-Management-v0-5.pdf
- T. Jiang, P. Lyons, P. Wang and **J. Yi**, "Electrical Energy Storage 2 (100kVA/200kWh) Powerflow Management", CLNR trial Analysis, 2014. Available: http://www.networkrevolution.co.uk/wp-content/uploads/2014/12/CLNR-Trial-Analysis-EES2-Autonomous-Powerflow.pdf
- P. Wang, T. Jiang, P. Lyons and **J. Yi** "Tap changing Secondary Transformer Autonomous and Grand Unified Scheme voltage control" , CLNR trial Analysis, 2014. Available: http://www.networkrevolution.co.uk/wp-content/uploads/2014/12/CLNR-Trial-Analysis-Tapchanging-Secondary-Transformer-Automonous-and-GUS-Voltage-Control1.pdf
- P. Lyons, T. Jiang, P. Wang and **J. Yi** "Analysis of collaborative voltage control on high voltage and low voltage networks", CLNR trial Analysis, 2014. Available: http://www.networkrevolution.co.uk/wp-content/uploads/2014/12/CLNR-L135-CLNR-Trial-Analysis-Collaborative-voltage-control-on-HV-and-LV-networks.pdf

Acronyms

Acronym	Definition
ANN	Artificial neural network
AC	Alternating current
ARMA	Autoregressive moving average
ASHP	Air source heat pump
BESS	Battery energy storage systems
BoU	Budget of uncertainty
BPNN	Back-propagation neural network
CB	Capacitor bank
CBM	Cumulant-based method
CCP	Chance constraint programming
CHP	Combined heat and power
CLNR	Customer led network revolution
CoP	Coefficient of performance
CSF	Cost sensitivity factor
DC	Direct current
DCOPF	Direct current optimal power flow
DG	Distributed generation
DLC	Direct load control
DN	Distribution network
DNO	Distribution network operator
DoD	Depth of discharge
DSM	Demand side management
DSR	Demand side response
ELM	Extreme learning machine

ESS	Energy storage system
EV	Electric vehicle
EWH	Electric water heater
GB	Great Britain
GP	Gaussian processes
HIL	Hardware in the loop
HV	High voltage
I&C	Industrial and commercial
ICT	Information and communications technology
LCT	Low carbon technology
LV	Low voltage
MAPE	Mean absolute percentage error
MCS	Monte Carlo Simulation
M-GRNN	Modified general regression neutral network
MODM	Multi-objective decision making
MV	Medium voltage
OBoU	Optimal budget of uncertainty
OHL	Overhead line
OLTC	On load tap changer
OPF	Optimal power flow
PDF	Probability density function
PEM	Price elasticity matrices
PEM	Point estimation methods
PFCSF	Power flow cost sensitivity factor
PFF	Participation factor forecaster
PFM	Power flow management

PFSF	Power flow sensitivity factor
PHS	Pumped hydroelectric storage
PoS	Probability of success
PSO	Partial swarm optimization
PV	Photovoltaic
RBFNN	Radial basis function neural network
RDSR	Residential DSR
RES	Renewable energy sources
RMSE	Root means square error
RO	Robust optimization
RTP	Real time price
RTTR	Real time thermal rating
SD	Standard deviation
SF	Sensitivity factor
SME	Small and medium enterprise
SO	Stochastic optimization
SoC	State-of-Charge
SoH	State-of-Health
ST	Short term
STLF	Short term load forecast
ToU	Time of use
UC	Unit commitment
V2G	Vehicle to grid
VCSF	Voltage cost sensitivity factor
VSF	Voltage sensitivity factor
VST	Very short term

VSTLF	Very short term load forecast

Nomenclature

Symbol	Definition	Unit
ΔV	voltage change	pu
V_S	nominal voltage	Pu
P_{ESS}	real power import/export from ESS	kW/MW
Q_{ESS}	reactive power import/export from ESS	kVAr
R	resistance	Ω
X	inductive reactance	Ω
$VSF_{i,k}$	voltage sensitivity factor from bus k to bus i which represents the voltage change at bus i due to the power injection at bus k	pu/kW
ΔV_i	voltage change at bus i	pu
ΔP_k	real power injection change at bus k	kW/MW
ΔQ_k	reactive power injection change at bus k	kVAr
ΔS_k	apparent power injection change at bus k	kVA
$\boldsymbol{\theta}$	vector of angle difference between busbars	Radian
$\boldsymbol{V}$	vector of voltage of busbars	N/A
$\boldsymbol{J}$	Jacobian matrix	N/A
$\boldsymbol{J^{-1}}$	inverse Jacobian matrix	N/A
$\boldsymbol{P}$	vector of net real power injection	N/A
$\boldsymbol{Q}$	vector of net reactive power injection	N/A
$\partial\Delta\boldsymbol{\theta}/\partial\boldsymbol{P}$	matrix for the partial derivatives of $\boldsymbol{\theta}$ to $\Delta\boldsymbol{P}$	N/A
$\partial\Delta\boldsymbol{\theta}/\partial\boldsymbol{Q}$	matrix for the partial derivatives of $\boldsymbol{\theta}$ to $\Delta\boldsymbol{Q}$	N/A
$\partial\Delta\boldsymbol{V}/\partial\boldsymbol{P}$	matrix for the partial derivatives of $\Delta\boldsymbol{V}$ to $\boldsymbol{P}$	N/A
$\partial\Delta\boldsymbol{V}/\partial\boldsymbol{Q}$	matrix for the partial derivatives of $\Delta\boldsymbol{V}$ to $\boldsymbol{Q}$	N/A
$PFSF_{ij,k}$	Power flow sensitivity factor from bus k to branch ij	MVA
ΔS_{ij}	apparent power flow change of branch ij	kVA
$VCSF_{i,k}$	voltage cost sensitivity factor from bus k to bus i	pu/£
C_k	the cost of real power injection at bus k	MW/£
$PFCSF_{i,k}$	power flow cost sensitivity factor from bus k to bus i	MVA/£
$C_{ESS,Charge}$	cost for charging ESS	£/kW

$C_{ESS,Discharge}$	cost for discharging ESS	£/kW
$C_{Capital,ESS}$	capital cost of ESS	£
$N_{Cycle,ESS}$	total charge and discharge cycle over the lifetime of the selected ESS	N/A
$P_{ESS,Rating}$	rated real power output of the ESS	kW
SoC	State-of-Charge	%
$SoC_{Upperlimit}$	the upper limit for SoC	%
k_{ESS}	is a factor represents the impact of SoC on the cost of operating the ESS. This reflects a disincentive to discharging the ESS at a low state of charge and a disincentive to charging the ESS at a high SoC	N/A
C_{RDSR}	is the cost of RDSR service per kW	£/kW
$C_{Capital,RDSR}$	is the cost of RDSR service per year	£
N_{RDSR}	is the maximum number of service requests of RDSR in a year	N/A
P_{RDSR}	is the reduction of RDSR customer consumption	kW
$C_{I\&C}$	is the cost of I&C service per kW	£/kW
$C_{Capital,I\&C}$	is the total cost of I&C DSR service per year	£
$N_{I\&C}$	is the maximum number of service requests of I&C DSR in a year	N/A
$P_{I\&C}$	is the estimated real power reduction delivered by the I&C DSR customer	kW
$P_{ESS,Rating}$	real power rating of ESS	kW
$Q_{ESS,Rating}$	reactive power rating of ESS	kVAr
$S_{ESS,Rating}$	apparent power rating of ESS	kVA
$VSFP_{i,ESS}$	real power voltage sensitivity factor from ESS to busbar i	pu/kW
$VSFQ_{i,ESS}$	reactive power voltage sensitivity factor from ESS to busbar i	pu/kVAr
E	Expectation	N/A
$Real_t$	the real value	N/A
Pre_t	the predicted value	N/A
pr	probability	N/A
$MAPE$	mean absolute percentage error	N/A

ε	normalised prediction error	N/A
μ	mean	N/A
σ	standard deviation	N/A
κ	kurtosis	N/A
$RMSE$	root mean square error	N/A
q_c	convective heat exchange	J
q_s	impact of solar radiation	J
q_r	radiative heat exchange	J
C_{q_r}	a coefficient to account for factors such as emission effect	N/A
$\boldsymbol{x}$	input vector	N/A
$\boldsymbol{y}$	output vector	N/A
$g()$	general nonlinear function	N/A
$h()$	general nonlinear function for inequality constraints	N/A
$\boldsymbol{b}$	the constraints vector	N/A
$\boldsymbol{c}$	vector of coefficients for the cost function	N/A
$\boldsymbol{c}'$	inverse vector of coefficients for the cost function	N/A
$\boldsymbol{A}$	matrix of constants for constraints	N/A
a_{ij}	the nominal value of the elements of $\boldsymbol{A}$ in the i^{th} row and the j^{th} column	N/A
$\hat{a}_{ij}$	maximum variation of a_{ij}	N/A
$\tilde{a}_{ij}$	real value of a_{ij}	N/A
$\boldsymbol{D}$	matrix of coefficients for equality constraints	N/A
$\boldsymbol{e}$	right hand side vector of equality constraints	N/A
$\boldsymbol{l}$	lower limit of decision variables	N/A
$\boldsymbol{u}$	upper limit of decision variables	N/A
$\boldsymbol{w}$	maximum of the cost function	N/A
T	total number of timesteps	N/A
t	number of timestep, integer between 0 to T	N/A
N_{ESS}	total number of ESS	N/A
C_{ESS_m}	cost of charging or discharging ESS m	£/kW
$P_{ESS_m}^t$	power import/export of ESS m at time t	kW
k_1	positive coefficient	N/A
k_2	negative coefficient for the state of health	N/A

$C_{ESS_m,Capital}$	capital cost of ESS m	£
SoH_{ESS_m}	State-of-Health of ESS m	N/A
$S^t_{ij,Forecast}$	forecasted load flow through branch ij at time t, based on powerflow calculations at the forecast stage	MVA
$PFSF^t_{ij,ESS_m}$	PFSF of ESS m to branch ij at time t	MVA/MW
$PFSF^t_{ij,RES_n}$	PFSF of RES n to branch ij at time t	MVA/MW
$PFSF^t_{ij,Bus_p}$	PFSF of busbar p to branch ij at time t	MVA/MW
N_{ESS}	total number of ESS	N/A
N_{RES}	total number of renewable energy sources	N/A
N_{Bus}	total number of buses	N/A
$\Delta P^t_{RES_n}$	error of RES power output at time t	MW
$\Delta P^t_{Bus_p}$	error of RES power output at time t	MW
$P^t_{RES_n,Forecast}$	the forecasted output of RES n at time t	MW
$P^t_{Bus_p,Forecast}$	the forecasted load of busbar p at time t	MW
$V_{Min,i}$	lower voltage limits of busbar i	pu
$V_{Max,i}$	upper voltage limits of busbar i	pu
$V^t_{i,Forecast}$	forecasted voltage of busbar i at time t based on load flow calculations at the forecast stage	pu
VSF^t_{i,EES_m}	voltage sensitivity factor from ESS m to busbar i at time t	pu
VSF^t_{i,RES_n}	voltage sensitivity factor from RES n to busbar i at time t	pu
$VSF^t_{i,Busp}$	voltage sensitivity factor from busbar p to busbar i at time t	pu
$SoC^t_{ESS_m}$	SoC of ESS at time t	%
Δt	duration of each timestep	N/A
$\eta_{ESS_m,discharge}$	discharge efficiency of ESS m	%
$\eta_{ESS_m,charge}$	charge efficiency of ESS m	%
$d^t_{ESS_m}$	binary variable, $d = 1$ if discharge and $d = 0$ if charge	N/A
E_{ESS_m}	energy capacity of the ESS m	kWh
$SoC^t_{ESS_m,Min}$	lower limit of SoC for ESS m at time t	%
$SoC^t_{ESS_m,Max}$	upper limit of SoC for ESS m at time t	%
$\boldsymbol{P}^t_{ESS}$	real power import or export of ESS m at time t	kW

$\tilde{S}_{ij,RTTR}^{t}$	uncertainty value of predicted RTTR of branch ij at time t	kVA
$\Delta\tilde{P}_{RES_n}^{t}$	uncertainty value of predicted power output of RES n at time t	kW
$\Delta\tilde{P}_{Bus_p}^{t}$	uncertainty value of load forecast of busbar p at time t	kW
N_u	maximum number of uncertainty	N/A
N_{Total}	total number of Monte Carlo samples	N/A
N_{Vio}	number of violations recorded.	N/A
N_{DSR}	total number of DSR	N/A
$PFSF_{ij,DSR_q}^{t}$	power flow sensitivity factor of DSR q to branch ij	MVA/MW
VSF_{i,DSR_q}^{t}	voltage sensitivity factor of DSR q to bus i	MVA/MW
$P_{DSR_q}^{t}$	power decrease or increase due to DSR q	kW
$\tilde{P}_{DSR_q}^{t}$	uncertain power decrease of increase due to DSR q	kW

Table of Contents

Table of Figures

List of Tables

Chapter 1. Introduction

1.1 Background

Governmental policy around the world is incentivising the decarbonisation of energy infrastructure. The UK government, for example, has a target of achieving an 80% reduction in CO_2 emissions with respect to the values from 1990 by 2050 [1]. In the UK, CO_2 accounted for 74% of the UK's greenhouse gas emissions in 1990 and increased to over 80% in 2013 [2]. Figure 1.1 shows a breakdown of CO_2 emissions by sector, in percentage of UK total. Energy supply, transport, business and residential sectors account for 78% of total UK CO_2 emissions in 2013. Energy supply was responsible for 32% of total CO_2 emissions in the UK, 180.8 million tonnes of carbon dioxide equivalent, in 2013. Transport and residential sectors contribute 20% and 13% respectively of total CO_2 emissions. Road transport and residential heating and cooking are large consumers of fossil fuels and are the most significant sources of emissions in the transport and residential sectors, respectively.

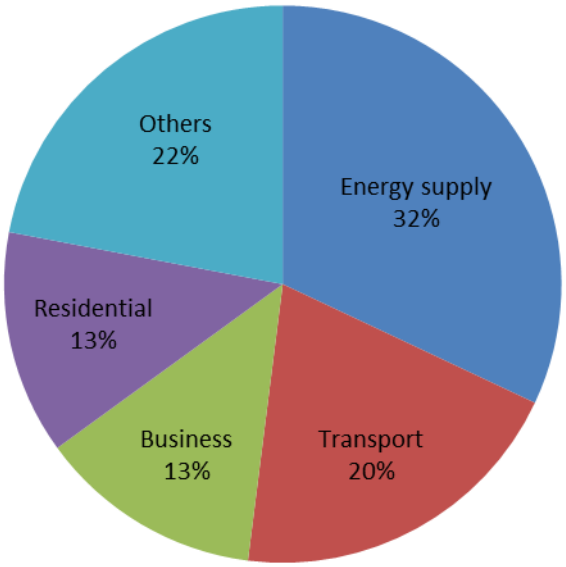

Figure 1.1 UK CO_2 Emissions by Sector in Percentage of Total UK Emissions [2]

Therefore, renewables based electricity generation, from windfarms and photovoltaics coupled with substantial electrification of the transport and heat sectors though low carbon technologies (LCTs) such as electric vehicles (EVs) and air source heat pumps (ASHPs), will be essential to achieve the required reductions in carbon emissions. The anticipated proliferation of these technologies in future energy systems will necessitate major changes to the operation and planning of future distribution networks.

1.1.1 Distributed Generation

Distributed generation (DG), especially renewable energy source (RES), are playing an important role in decarbonising the energy supply. For example, wind generation and solar photovoltaics (PV) convert wind and solar energy into electrical energy. Installed capacities of wind and PV have increased dramatically since 2010. As indicated in Figure 1.2, the installed capacity of PV increased from 0.1 GW to 5.4 GW. For onshore and offshore wind, the installed capacities increased from 4.1 GW and 1.3GW to 8.5 GW and 4.5 GW, respectively.

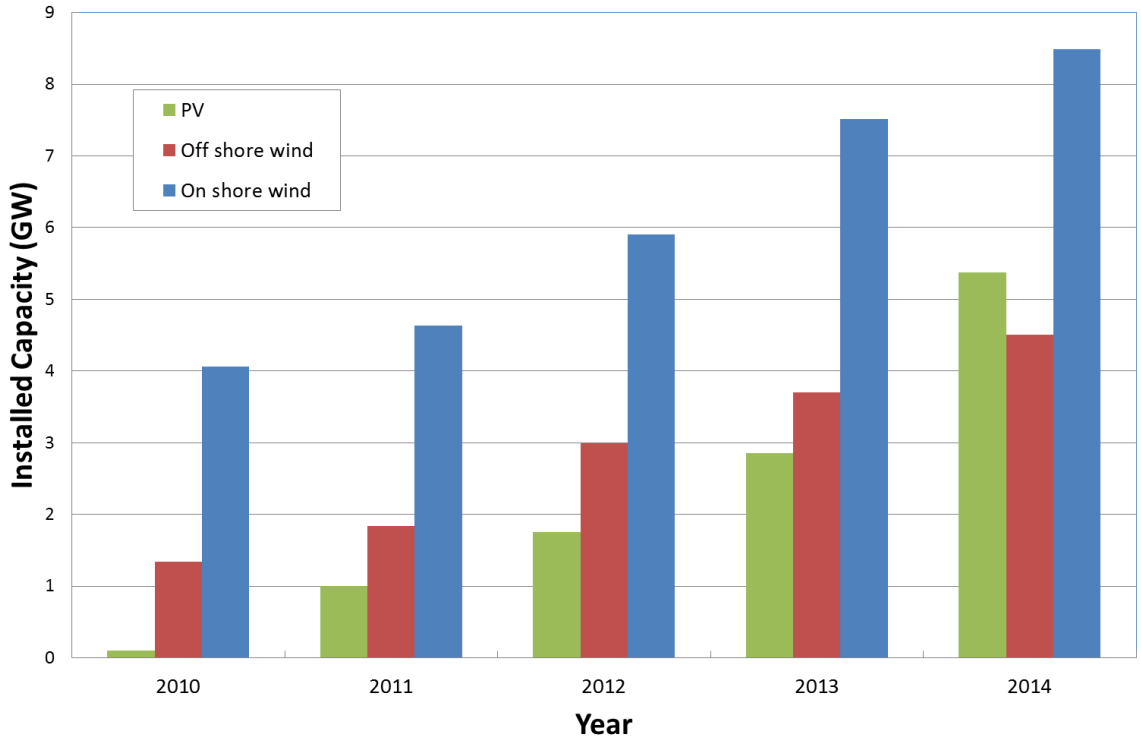

Figure 1.2 Installed Capacity of PV and Wind Generation in the UK from 2010 to 2014 [3]

1.1.2 Air Source Heat Pumps

ASHPs are seen as key technology in the decarbonisation of domestic heating. In comparison with conventional boilers, which burn natural gas, ASHPs transfer heat from the outside to the inside of buildings using electrical energy. This allows an ASHP to generate far more heat than a conventional electrical heating system. The efficiency of ASHP is measured by coefficient of performance (CoP). CoP is the ratio between the amount of thermal energy transferred for heating and the electrical energy consumed by ASHP. CoP can be influenced by many factors including the temperature difference between the inside and outside of the building. Experimental results from ASHPs in residential buildings in Italy show that the CoP

is typically above 2.5 [4]. Other studies have determined that the power consumption of ASHPs varies between 1.5kW to 4.5kW [5].

1.1.3 Electric Vehicles

Electric vehicles (EVs) include a range of technologies including plug-in EVs (PEVs), battery EVs and extended-range EVs. EVs use electrical motors instead of, or in conjunction with, internal combustion engines. When driven from the battery energy storage on board, EVs produce no pollution or CO_2 during driving. If the batteries are charged from renewable sources, EVs do not produce any emissions. Even when EV batteries are charged from non-renewable based generation, they still provide opportunities to deal with emissions centrally.

Plug-in EVs are charged from three categories of chargers [6, 7], which are summarized in Table 1.1.

	Connection	Power (kW)
Level 1	Single phase	1.5 – 3
Level 2	Single phase	10 - 20
Level 3	Three phase	> 40

Table 1.1 EV Charing Connection Type and Power Range

Level 1 and Level 2 chargers are suitable for home charging. Compared to normal household peak demand, the power consumption of Level 1 and Level 2 chargers are relatively large. Level 3 refers to fast chargers and these high power chargers require appropriate infrastructures. The impacts of EV charging on existing electrical infrastructures have been extensively studied [8-10]. It has been found that if not well managed, even a low penetration of EVs can still cause network constraints violations.

1.2 Challenges Faced by Conventional Distribution Networks

Traditionally, power systems have been considered in terms of three areas: power generation, power transmission and power distribution. In the UK, distribution network operators (DNOs) manage electrical networks from 132kV to 0.4kV. The connection of DGs and LCTs to distribution networks brings new opportunities and challenges to DNOs.

Power systems were previously designed to deliver power from large-scale generators to where the demand was required, via the transmission networks and distribution networks, from high voltage (HV) to the low voltage (LV) system. However, with more DG and LCTs

connected within distribution networks, this model is becoming outdated as power can be supplied locally and even be exported back to the transmission networks in some cases.

Moreover, due to the connection of large quantities of renewables based intermittent generation such as wind and PV panels the availability and location of generation is becoming less predictable. Moreover, with the proliferation of new technologies such as EVs and ASHPs, the prediction of load profiles are becoming less predictable and unified.

1.2.1 Voltage Control

DG can lead to voltage rise problems. In the UK, steady state voltage limits for networks above 1kV and below 132kV are ±6% of the nominal voltage and -6%/+10% for LV networks [11]. In distribution networks, especially in LV networks where on-load tap changers (OLTCs) are not used, the tap positions of transformers are normally set so that secondary voltages at the LV busbars are close to the high voltage limits to maximise the capability of the network to accommodate load. Thus, during periods of low load and high DG real power export, it is likely that high voltage limits are violated.

The connection of distributed PV, ASHPs and EVs are less likely to be planned by DNOs and therefore can increase unbalance between different phases and different feeders. The increased unbalance between feeders in radial networks is challenging for OLTCs. OLTCs change the voltages of all the feeders downstream uniformly. As a result, in a substation where one feeder has low voltage problems due to load while another feeder has high voltage problems due to DG, an OLTC cannot solve both sets of problems if they occur simultaneously. Similarly, as unplanned generation and additional load will be distributed across the phases of an LV feeder voltage phase unbalance is likely to be more severe than before.

DGs and LCTs can pose challenges for voltage control devices controlling individual feeders. Conventionally, capacitor banks (CB) and in-line regulators are used for feeder voltage control. However, at the remote ends of medium voltage (MV) feeders and LV networks, normally there are no measurements. Without measurements and accurate state estimation information, controlling voltages at the remote ends of MV and LV feeders is difficult.

1.2.2 Power Flow

The ratings of transformers and cables indicate their capabilities for transferring power. High penetrations of DG can cause power flow problems including reverse power flow and overload.

Traditionally, distribution networks are designed to transmit power in the same direction moving from HV to LV or from substations to the remote ends of feeders. Bidirectional power flows can be challenging to network control and protection as existing systems and technology has been designed to cope with the traditional model of power flow. RESs, especially wind energy, may not be at the same location as load, thus in weak networks with high penetrations of DG, during low demand period, reverse power flow is likely to occur. For cables and transformers without OLTCs, the reverse power ratings are equal to their normal ratings. However, the reverse ratings of primary transformers equipped with certain types of OLTC can be constrained. For example, it is found that the reverse rating of some 33/11.5kV, 7.5MVA primary transformer is reduced to 66.3% of the forward rating [11].

Both large penetrations of DG and load increase due to LCTs can cause overloads in transformers, overhead lines and underground cables. Overloads or thermal constraint violations are conventionally alleviated by network reinforcement which is expensive and requires considerable planning [12, 13]. The ratings of transformers and branches used in system planning and design are to meet peak demand or generation and are therefore typically not fully utilised. Enhanced DG control can also be used to alleviate thermal constraints. This includes curtailment of real power and management of reactive power of DG. DG curtailment is the most common method to deal with generation driven overloads. However, DG curtailment reduces environmental and economic benefits of RESs. Some DG, depending on the type and technology, has the capability to inject or absorb reactive power. In addition, the use of reactive power can be effective for voltage control in networks particularly in networks with higher X/R ratios. In MV and LV distribution networks, where the X/R ratio is relatively lower, reactive power is less effective for voltage control. It should be noted that the injection or absorption of reactive power changes the power factor and can increase the losses across the system.

1.2.3 Uncertainties

Conventionally, distribution networks are operated and planned using predictable load profiles with the majority of the real power supplied from large generators via the transmission system. The generation dispatch schedules are developed, at the transmission system operator level, based on day-ahead load forecasts coupled with sufficient reserve.

However, this simple model is no longer valid as the level and types of uncertainty in power systems are increasing with the increasing penetration of RESs and LCTs connecting to distribution networks [14-17]. The result of these changes is that the load and generation

profiles used for planning systems are becoming more unpredictable and thus forecast errors will increase. The electrification of the transport and heating not only increase the demand but also make load forecast a more difficult task. For instance, due to the spatial and temporal uncertainty of EV charging, it is difficult to predict the charging profiles. The usage of domestic ASHP is decided by heat demand which can be influenced by many factors such as ambient temperature and the use of hot water. As a result, the electricity demand of LCTs is difficult to predict as well. Besides, renewable based generation is less or even not controllable.

With the presence of these increasing uncertainties in the power system conventional technologies and techniques are therefore not adequate. The increasing number and level of uncertainties will greatly increase operation costs and trigger network reinforcement unless these uncertainties are understood, managed and planned for appropriately.

1.3 Energy storage

Electrical energy cannot be stored easily therefore the existing operational model within power systems is to maintain the balance between load and generation as accurately as possible. Due to the uncertainties in predicting load and generation some mismatch is unavoidable. These mismatches are conventionally managed using controllable generation, controllable load (if available) and energy storage systems (ESSs). ESSs store electrical energy in other forms such as chemical, thermal or gravitational potential energy and decouple load and generation. Battery energy storage systems (BESSs), for instance, convert electrical energy into chemical energy during charging and convert chemical energy into electrical energy during discharge.

The characteristics of BESSs such as high energy density and fast response rate make it suitable for various power system applications [18-20]. Pumped hydroelectric storage (PHS) has been used for meeting peak demand, absorb excess generation and frequency control. However, in comparison with BESS, PHS is slower to respond and is also restricted by location. BESSs, on the other hand, have faster response times and are less restricted in terms of location. BESSs have no moving parts and therefore, in comparison to technologies such as compressed air energy storage and flywheel energy storage, are suitable to be installed in residential area or at a smaller scale.

Furthermore, in distribution networks, real power flow is much higher than reactive power. This means that the same change in the magnitude of real power has a much higher impact on the magnitude of apparent power than that using reactive power. Therefore, compared with

other technologies which use reactive power, such as static synchronous compensator, real power from ESS is more effective.

However, a number of limitations of BESSs still exist. Currently the cost of BESSs is still very high and the number of charge and discharge cycles of BESSs can result in relatively short operational lifetimes. Moreover, over-charging or over-discharging of BESSs can result in irreversible damage to the battery cells. To protect fragile and expensive BESSs, conservative approaches are normally taken to the design and management of BESSs. For instance, tighter SoC limits than their technical limits are often used to protect BESSs from over-charge and over-discharge.

The difficulty of observing the complex chemical reactions within the cells makes measuring state-of-charge (SoC) and the state-of-health (SoH) of batteries extremely challenging. Inaccuracies in SoC measurements have additional impacts on the operational regimes of the available energy resource in order to protect the battery.

Understanding and measuring battery degradation and SoH is very important to maximising the value of BESSs, due to their high capital costs and limited numbers of charge-discharge cycles. SoH can be indicated by internal resistance, available capacity, voltage and remaining charge and discharge cycles [21]. Aggressive use of BESS such as deep depth of discharge (DoD) and fast charge and discharge have serious effects on the SoH of BESSs.

1.4 Demand Side Response

Power systems used to be designed to meet peak demands by scheduling and controlling centralized large-scale fossil fuel based plant based on predictable load forecasts. The generators used to supply the peak demand usually have higher costs and are typically less efficient, more carbon intensive generating plants. Therefore, exploiting the customers' flexibility through DSR and reducing reliance on this generating plant is crucial to reducing the carbon emissions of the electrical energy system. It has been estimated that a 5% shift of peak demand can deliver an annual network investment saving of £14m and a daily carbon emission saving of up to 1,250 tCO_2 [22].

Demand side response (DSR) is able to reduce peak demand but also can be used to facilitate RESs. During periods when generation is in excess of demand, for example during periods of large wind generation export, bringing load forward, which results in generation and demand mismatches being minimised, can avoid RES curtailment. DSR has also been shown to have the capability to reduce the requirement for network reinforcement [23].

There are still a number of barriers to the implementation of DSR. How much demand can be reduced or increased is difficult to determine and uncertain. The recuperation of energy after DSR services have been delivered is known as pay back. The magnitude, duration and effects of the pay back of DSR need to be further investigated. The uncertainties associated with DSR need to be understood and managed. Furthermore, there is a lack of a regulatory framework and incentive mechanism for DSR which is currently limiting the adoption of DSR in the UK. Finally, customers' awareness of the potential benefits of DSR needs to be improved.

1.5 Real Time Thermal Rating

The ratings of conductors are conventionally defined by a set of predefined and conservative weather conditions. For instance, according to the UK standard, the rating for overhead lines (OHL) are calculated based on assumptions of the weather conditions of 0.5m/s wind speed and an ambient temperature of 2°C in winter and 20°C in summer [24].

Real time thermal rating (RTTR) considers the real time temperature of conductors as the constraint of the conductors' capacity. The impacts of environmental conditions on RTTR have been explored in [25]. The cooling of conductors is influenced by environmental factors including ambient and soil temperature, wind speed, wind direction and solar irradiance. For OHLs, the most significant factors are wind speed and ambient temperature [26]. For electric cables (underground), their ratings are mostly influenced by thermal resistance of the insulation and the soil. The ratings of power transformers are limited by the hot spot temperature of the windings. For distribution transformers, which are normally naturally cooled by air externally, the most significant environmental factor is air temperature [25, 27, 28].

Deploying RTTR in collaboration with other technologies has been shown to be able increase the capability of distribution networks' to accommodate RESs and LCTs [29]. In comparison with static rating, RTTR can increase the current carrying capability of conductors [27]. In previous studies, it is found that the implementation of RTTR can reduce loss of load expectation of up to 67% [30].

1.6 Research objectives

The research detailed in this thesis focussed on the management and resolution of thermal constraints and steady state voltage limit violation problems in distribution networks. The aim of the research is to provide an alternative solution to network reinforcement, which has high cost and requires extensive planning and construction work.

This research aims to investigate the use of ESS and DSR in future distribution networks to facilitate LCTs as an alternative to network reinforcement. In summary, the research question of this thesis is: if and when ESS and DSR can be alternative to network reinforcement? The main research objectives are detailed below:

- To investigate the impacts of high penetrations of DG and LCTs on future smart distribution networks in terms of voltage and power flow;
- To understand the limitations of current control strategies for ESS and DSR in future distribution network scenarios where high penetrations of DG and LCTs exist;
- To understand the impacts of a range of sources of uncertainties, arising from existing and future elements of the electrical energy system, on the performance of conventional control algorithms;
- To develop and evaluate control strategies for ESS and DSR to facilitate DG and LCTs in the presence of a range of source of uncertainties.

1.7 Thesis outline

The rest of this thesis is organised as follows: Chapter 2 provides a literature review on ESS and DSR. The technologies and benefits of ESS are introduced first. The state of the art of control and scheduling strategies for grid scale ESS is provided. This is followed by a description of the benefits and challenges for DSR. Current approaches for DSR control and scheduling are also examined. In the following section, coordinated control methods for ESS and DSR are reviewed. Finally, conclusions are drawn on the use of EES and DSR in future distribution networks.

In Chapter 3, the calculation of SFs is described and control schemes based on SFs are proposed. The use of sensitivity factors (SFs), namely voltage sensitivity factors (VSF) and power flow sensitivity factors (PFSFs) in this thesis, is an important method to linearize the quadratic power flow equation. Initially, two methods to calculate SFs are introduced. Next, based on SFs, cost sensitivity factors (CSFs) are introduced. Finally, A SF and a CSF based control schemes which use ESS and DSR collaboratively are presented.

Chapter 4 describes uncertainties that exist in power system scheduling problems and methods to deal with uncertainties. The sources of uncertainty, including load forecast, wind forecast, RTTR, SoC and DSR, are introduced first. Methods to deal with uncertainty are presented. To illustrate the impact of uncertainty on a distribution network an example of using Monte Carlo simulation (MCS) to explore the impacts of EV charging on distribution networks is given.

In Chapter 5, tackling uncertainty with robust optimization (RO) is detailed. The formulation and solution of an uncertainty linear optimization problem is introduced. The three stages of RO formulations are presented. This is followed by a description of the implementation and validation of RO in Python.

Chapter 6 applies RO to solve a power flow management (PFM) problem which integrates ESS and DSR. The concept of budget of uncertainty (BoU) and optimal budget of uncertainty (OBoU) is proposed to realise the trade-off between the probability of success (PoS) and the cost. Two methods to calculate OBoU are proposed.

In Chapter 7, case studies based on IEEE 14 and 118 busbar networks are given to illustrate the advantages of the proposed method. Simulation results show that the proposed scheduling scheme is able to reduce the requirement for ESS, compared to conventional techniques.

In Chapter 8 and Chapter 9, a discussion of the findings and the implications of this research is presented and key findings are summarised.

Chapter 2. Literature Review

2.1 Introduction

In the previous chapter, the challenges to future distribution networks due to the anticipated widespread proliferation of LCTs that are required to enable the decarbonisation of the energy sector are presented. ESS and DSR are key technologies in enabling a smart approach to economically managing these changes to the supply, transmission, distribution and consumption of electrical energy.

In this chapter, a review of the roles and capabilities of ESS and DSR, under the supervision of supervisory smart control systems in future distribution networks is presented. In section 2.4, previous work on the coordinated, collaborative operation and scheduling of ESS and DSR in distribution networks is evaluated. Finally, a summary of the current capabilities and limitations of advanced network management systems which integrate ESS and DSR to manage voltage and thermal constraints in future distribution network is discussed. The limitations of current research are summarised.

2.2 Energy Storage

2.2.1 Benefits of Energy Storage in Electrical Energy Systems

Due to differences in the operation and management of today's electrical energy systems throughout the world and the flexibility of energy storage the benefits of energy storage vary. In the following section, the key benefits provided by energy storage to distribution and transmission networks worldwide is presented. The benefits of ESS include:

1. ***Voltage control and power flow management***

   The use of energy storage to provide voltage control and power flow management has been demonstrated in [31, 32]. In [31], a battery energy storage system (BESS) was deployed in an area of 11kV distribution network in the UK to control voltage and alleviate thermal constraints. It was found that the 0.4MW, 0.2MWh BESS deployed in an 11kV distribution network was capable of reducing the number of thermal excursions.

2. ***Energy Arbitrage***

   Generating profit by selling energy when the cost of energy is high and buying energy when the cost is low is known as arbitrage. To do this effectively requires accurate prediction of future energy prices which is influenced by factors such as generation availability and load. A robust bidding strategy for a windfarm and an ESS, which

considers the uncertainty in electrical energy price and wind power export forecasting, has been developed previously [33]. In [34], the economic viability of arbitrage with cryogenic ESS considering day-ahead and week-ahead electricity prices is evaluated.

3. ***Ancillary Services***

   Energy storage has been previously shown to be able to provide ancillary services including frequency response/operating reserves [35]. Energy storage can be used to support black starts [36, 37]. ESS can be used to improve power quality and stability, especially in LV networks and microgrids [38-40].

4. ***Facilitate renewables***

   Previous work has demonstrated, using a validated Great Britain (GB) power system model, it has been shown that with 8GW, 800GWh energy storage, the maximum capacity of wind based generation can be increased from 35GW to 42GW and the critical excess electricity production can be reduced from 8.21GWh to 4.35GWh [41].

5. ***Regulatory***

   Energy storage has the capability to reduce customer minutes lost, and can also assist in compliance with ER P2/6 [42], the UK energy security standard. In addition, energy storage has also been shown to reduce generator curtailment [31, 43].

2.2.2 Grid Scale Energy Storage Technologies and Services

The capabilities of a wide range of grid scale energy storage technologies to provide energy system services have been investigated previously [18, 44-48].

In [47], the characteristics, current development state and potential usage of grid scale energy storage technologies are summarised and evaluated. Key characteristics that were identified include the current rated (energy) capacities and the discharge time duration at rated power of the energy storage systems under evaluation. These key characteristics were mapped to the key challenges and services that are required in the energy market. This mapping is expressed diagrammatically in Figure 2.1. It can be seen that the characteristics of BESSs currently map to the requirements of smartgrid and distribution network applications.

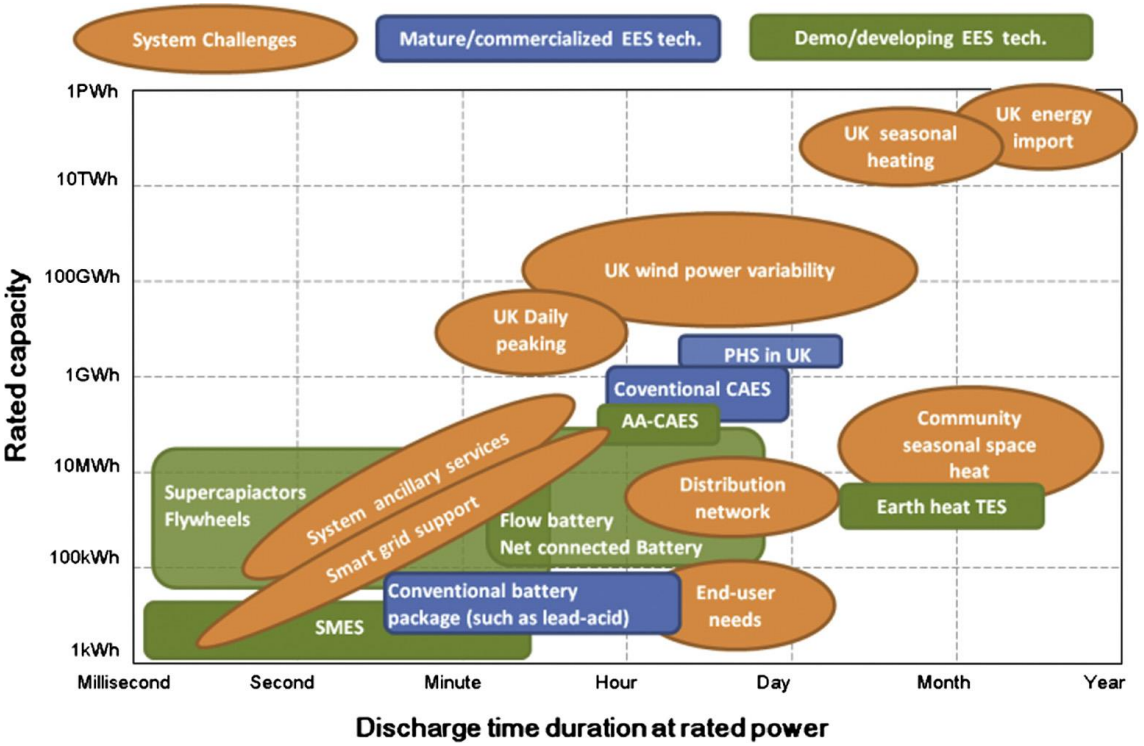

Figure 2.1 Characteristics, State and Potential Application of Electrical Energy Storage Technologies [47]

2.2.3 Energy Storage Control and Scheduling

In [49], an introduction to the use of BESS to enable the integration of PV based generation, is given. Three control modes for BESS were defined, namely ramp rate control, frequency response and reactive support. In reactive support mode, BESS is used to import/export reactive power for power factor correction and distribution network loss reduction. To support the development of the control for BESS a Hardware in the Loop (HIL) test bed was developed. The final control strategy presented in this paper is based on ramp rate control, with the ramp rate of the BESS export change limited to 50kW/min. However; the control strategy developed is not optimised.

A multi-objective control strategy for BESS to defer network reinforcement due to the increasing penetration of PV has previously been developed [50]. A detailed BESS model is proposed and this model is able to simulate the round trip efficiency, SOC, single and three-phase real, reactive and apparent power rating of BESS. The objectives of the optimisation algorithm are voltage control, power flow management and minimisation of annual cost. The trade-off between voltage control and power flow management is realized by using a weighting factor. The third objective, annual cost minimisation is modelled as a constraint. The annual cost calculation includes asset depreciation cost, fixed capital cost and maintenance costs and average energy cost per unit of time.

An optimal operation strategy for an ESS, connected to a wind generator, in a day-ahead market is proposed in [51]. The ESS is used to store renewable energy from the wind generator in order to maximize the revenue generated for selling energy to the market. A discrete time battery model, which models the battery dynamics including SOC, temperature and current, has been built and adopted. The overall optimization problem is solved with a forward dynamic programming algorithm.

Several studies focus on the real and reactive power import/export ratio of ESS to control voltage and manage power flows. The effectiveness of reactive power to control voltage is dependent on the X/R ratio of the network. In [52], six control strategies with different real and reactive power priorities and ratios have been used for voltage control and reducing reverse power flow. The strengths and weaknesses have been evaluated through simulations with an 11kV network model. In [53] an operation strategy for BESS, is proposed for distribution network voltage support. The real and reactive power ratio is determined by the conductance and the susceptance of the Thevenin equivalent of the upstream network. This method is introduced in [54]. Eight dispersed Zn/Br flow batteries are deployed in a rural distribution network at different locations for voltage control [55]. In this work three voltage control strategies have been developed and comparatively evaluated. However, it was found that reactive power had minimal effect on the voltages in the case study network under investigation.

Optimal power flow (OPF) techniques have also been used to develop control algorithms for the control and scheduling of ESS [56-58]. However, direct integration of ESS into conventional OPF techniques is not usually possible. The main challenges to integrating ESS into OPF based control algorithms are:

- Finite discharge/charge capability of ESS;
- Accurate determination of available discharge and charge capability of ESS;
- The quadratic relationship between real, reactive and apparent power rating.

In [56], an ESS is instructed to charge during off-peak periods and discharge during peak periods. Maximum real power import and export is decided by the maximum mismatch between generation and load. In this paper, the charge and discharge operation periods are fixed. In [57], an optimised flexible charge and discharge scheduler for ESS is proposed. However, this scheduler only allows one charge and discharge cycle per day and is not able to deal with the uncertainty of forecast. In [58], the authors proposed a dynamic programming approach based solver for OPF problems with ESS, with a focus on microgrid application.

The proposed formulation minimises the cost of importing electricity from the main grid. In [59], OPF equation has been modified to solve an ESS scheduling problem. In this work, the cost function minimizes the cost of generation. The cost of using ESS is not considered.

Rule based control techniques have been used for ESS control [60, 61]. In [60], a rule based control strategy is proposed to dispatch intermittent renewable based generation. The objective of this control strategy is to maintain the combined export power from renewables and BESS to a predefined setpoint. In [61], ESS is used in collaboration with OLTC for voltage control. The concepts of cost sensitivity factors are proposed. The proposed methodology uses the most effective intervention.

Paper [62] presents a coordinated control of distributed ESS with tap changer transformers for voltage rise mitigation due to high PV penetration. In this proposed system, distributed ESSs are located next to PV and are coordinated by the central controller. When a voltage excursion occurs, the transformer responds initially and ensures that the bus voltage is within limits. Real power import/export signals will be sent to the ESSs to absorb the reverse power flow or shave the peak load. Real power import/export signals will not be sent until the tap operation is over. The maximum DoD of the BESS is limited to 20% (over 80% SOC) to prolong the cycle lifetime of the ESSs.

2.2.4 Use of Real and Reactive Power Ratio for Voltage Control and Power Flow Management

As energy storage can provide multiple services with both real and reactive power, it is important to understand the relationships between voltages and power flows of the system and the real and reactive power import/export from ESS units.

The voltage change due to real and reactive power injection from ESS can be estimated by

$$\Delta V = \frac{(P_{ESS}R + Q_{ESS}X)}{V_S} \quad \textbf{(2.1)}$$

where

ΔV	the voltage change
V_S	the nominal voltage
P_{ESS}	the real power import/export from ESS
Q_{ESS}	the reactive power import/export from ESS
R	line resistance
X	line inductive reactance

In transmission networks where the X/R ratio is high, reactive power is more effective for voltage control. On the contrary, in distribution networks, where the X/R ratio is relatively lower, real power is more effective to control voltage. However, the available real power resource is finite and is limited by the capacity of the ESS. Reactive power is less effective for voltage control but is unlimited in time.

Similarly, when using energy storage for power flow management problems, real power has a higher sensitivity factor but the effective cost of real power is higher as well. Reactive power is less effective but costs less.

The trade-off between using real and reactive power is illustrated by Figure 2.2 below. Reactive power of ESS is not time limited therefore using reactive power only is purely a cost prioritized approach. However, injecting too much reactive power will cause large voltage change and also increase network losses. When voltage constraints and losses are considered, more real power should be used. Exporting real power only is a technically driven approach. Real power is an effective solution for power flow management, however, when the energy capacity of the ESS unit is approaching its limits as well as the duration of the violation of limits or constraints are considered, more reactive power should be used.

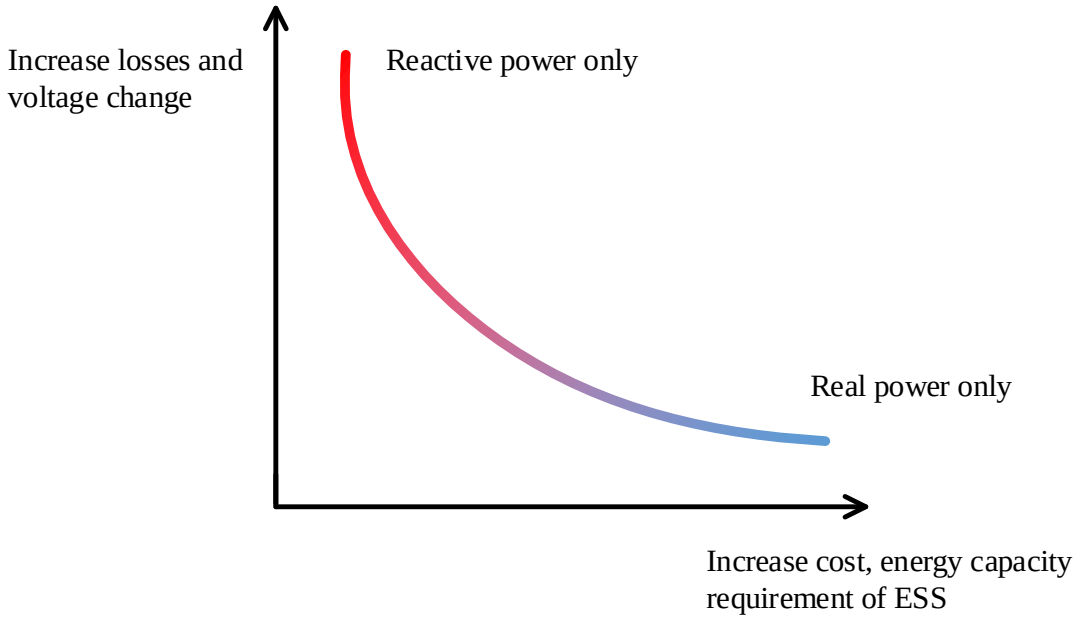

Figure 2.2 Illustration of the Trade-off Between Real and Reactive Power

2.3 Demand side response

Demand side management (DSM) is defined as any activity carried out on the demand side of energy systems [63]. DSM, therefore, encompasses activities such as energy efficiency, time of use (ToU) tariffs, DSR and spinning reserve (SR). DSR increases or decreases the load in

the system by changing the behaviour of customers. The term DSM is often used as an alternative to DSR and two words could be considered to be interchangeable. In this thesis, the term DSR is used for this activity and is used to emphasise that the behaviour of real customers is far less controllable in comparison with other elements of the energy system such as large-scale generation plant, ESS and interconnectors.

There are two principal approaches to DSR. The first approach is direct load control (DLC) [64-69]. In this approach, the operation of appliances is controlled or scheduled by utilities, aggregators or controllers such as home automation devices. The other approach influences how customers use energy by changing the price of electricity. Most popular methods of this approach include ToU tariffs [70, 71] and dynamic or real time pricing [72, 73].

As DSR has the impact of bringing forward and/or delaying electrical energy consumption, it can therefore, be seen as another form of energy storage. For instance, performing DSR through the use of refrigerators [74], electric water heaters (EWH) [68, 75], heat pumps [76] and other thermal energy storage techniques [77] can also be viewed as an exchange between electrical energy and thermal energy systems with energy stored thermally. An example of this process would be a request for a demand reduction from a group of domestic heat pump equipped households for an hour. During this period energy is effectively taken from the thermal store (the households) and made available to the electrical energy system. Following the completion of the DSR request the thermal store needs to be recharged and thus the heat pumps are switched back on recuperating the energy back to the households from the electrical system. This recuperation of energy from the electrical system is known as payback [78]. More intuitionally, DSR with EVs, such as optimal charging control [79] and vehicle to grid (V2G) [80] is realized by controlling the ESS on board of EVs.

2.3.1 Benefits and Challenges of Demand Side Response

The classification, benefits, future opportunities and challenges for DSR have been reported in various studies [22, 23, 81-83]. The benefits of DSR include but are not limited to:

- Reducing the generation margin;
- Deferring network infrastructure reinforcement;
- Improving the efficiency of network operation;
- Reducing carbon emissions;
- Reducing energy costs for customers;
- Reducing or avoiding RES curtailment.

The challenges for rolling out DSR in large scale include:

- Customers' awareness of the possibilities (financial and otherwise) that DSR provides needs to be improved;
- The load reduction or increase and payback of DSR is difficult to predict;
- Essential infrastructures such as smart meters and information and communications technology (ICT) are required;
- A Market structure is required to develop business cases.

2.3.2 DSR Control and Scheduling

In this section, the state of the art of DSR control and scheduling strategies is reviewed.

In paper [84], a DC-Optimal Power Flow (DCOPF) based algorithm is used to improve the utilisation of the existing network capacity. This framework is applied to on an11kV radial distribution network to evaluate the benefits of collaborative deployment of energy storage and DSM. In this work, it is assumed that 10% of peak load can be shifted.

An interdisciplinary method to evaluate the reinforcement deferring effect of DSR has been previously proposed [85]. Power flow sensitivity factors, thermal vulnerability factors and social index factors are used to identify the best location for DSM and evaluate the social acceptance within the network area. A load control strategy to enable LV network voltage control is presented in [86]. The control scheme increases the real power consumption in an LV network to mitigate voltage rise problems due to a wind farm connection.

In [87], thermal loads with high thermal inertia are used for short-term voltage support. During a low voltage event, thermal loads are disconnected to mitigate the impacts of induction motors. Thermal loads are reconnected when the voltage is recovers. It was shown that this control strategy can thus improve voltage stability.

A pricing method based on Vickery-Clarke-Groves (VCG) mechanism is proposed in [88]. VCG mechanism is a pricing method which aims to encourage efficient energy consumption and at the same time maximizes the benefits of the customers. The VCG mechanism makes decisions based on the consumption of customers. It is found that this method can encourage customers to reduce consumption; however, the formulation introduced in this paper is computationally intensive and also requires two-way communication.

When the on and off state and the duration of operation of DSR enabled appliances are considered, the controlling and scheduling problem for these services become a mixed-integer problem. Solving mixed-integer problems (MIP) by deterministic techniques can pose a number of challenges. For instance, MIPs are no-convex, difficult to solve and computational

intensive. Heuristic optimisation techniques have been used to overcome these challenge [66, 89-91]. For instance, in [89], a day-ahead load scheduling problem is formulated as a minimization problem. The proposed formulation takes planned load profiles as input. The planned load profile is provided by a smart grid manager and aims to maximize the use of RES and the economic benefits. The operation of the appliances is scheduled so that the difference between the scheduled total consumption and the planned load profile is minimised.

Game theory based methods have also been proposed for DSR scheduling [92, 93]. Most scheduling methods require the knowledge of the energy consumption of customers while game theory based methods can protect the privacy of customers [92]. In this paper, the proposed energy consumption scheduling scheme is able to achieve the Nash equilibrium among the participating users.

In [94], a multi-objective decision making (MODM) method for DSR in LV residential distribution networks is developed to resolve transformer thermal contraints. The MODM process decides which load is disconnected or delayed. The proposed process is based on a decision making matrix. The decision making matrix has five criteria, including user priority, flexibility, satisfaction, power similarity and high power consumption. However, this proposed method may not be suitable for large scale applications due to the heavy communication requirements.

2.4 Coordinated ESS and DSR control

In this section, coordinated ESS and DSR control methods are reviewed. Normally, ESS and DSR are treated in isolation or even competitively.

In [95], a distributed on-line algorithm is proposed for energy utilization among multiple households. In this paper, it is assumed that each household is equipped with an ESS. ESS is used to store excess DG real power export and supply local demand when the DG real power export is low.

ESS and DSR are used cooperatively for microgrid frequency control during islanding [96, 97]. ESS units with short response times, such as flywheels, are used for primary frequency control. Controllable micro-sources, which are relatively slower to respond to control signals, are used for secondary frequency control. Load curtailment is implemented if there is insufficient generation reserve in the microgrid or if the SoC of ESS is low.

In [75] and [76], BESS and DSR have been used for distribution system voltage and frequency control. DSR is used for frequency control only while BESS is used for both

voltage and frequency control. Real power from BESS is used for frequency control while reactive power is used for voltage control. In this application, heat pumps [76] and EWH [75] are used for frequency control as DSR appliances.

2.5 Discussion and Conclusion

ESS has the capability to provide a number of services which assist in the operation of distribution networks. This will be particularly important in future networks with large penetrations of LCTs such as wind generation, PV, EVs and heat pumps which are likely to increase demands on distribution networks and make it increasingly difficult to predict load and generation. However, the greatest challenge to the widespread adoption of this technology is the high cost of ESS in distribution networks, therefore it is crucial that the control and scheduling of these units maximises their impacts on the energy system.

The limitations of previous research are summarized below:

- The majority of previous research has focused on DSM rather than DSR

The assumption that demand is fully controllable has been previously shown to be not always true as customers are not always going to accept requests for demand response. Thus the response in terms of magnitude and duration is uncertain. Therefore, designing a control or scheduling system that assumes that response is fully or highly controllable is likely to result in relatively poor performance.

- Static rating is used rather than RTTR

Similarly, for power flow management problems, much of the previous work assumes a static asset rating rather than using RTTR. Compared to static rating, RTTR can enhance the utilization of cables and transformer and thus reduce the requirement for ESS and DSR.

- Uncertainty is ignored in many works

Furthermore, the majority of previous research ignores the stochasticity of load, DG, RTTR and DSR. In a scheduling problem in a future smartgrid, with the increasing penetration of LCTs, it is likely that forecast values will have limited accuracy, particularly as the time horizon extends beyond a few hours. Without careful consideration of the uncertainty of all these factors, the decisions made by any control system or scheduling strategy are likely to be either excessively conservative or risky.

- Lack of coordinated operation of ESS and DSR

Finally, little previous work has considered the coordinated operation of ESS and DSR and has usually considered the control of these devices in isolation. ESS is fully controllable and

fast response device with higher cost and limited resource. Compared to ESS, DSR is normally less or even not controllable, slow to response however has a relatively lower cost. At the same time, DSR resource or capacity is less constrained compared to ESS. For example, if backup generators are used to provide DSR, the DSR resource is only limited by the fuel. The next chapter will illustrate the complementary features of ESS and DSR which make the combination of ESS and DSR an attractive solution.

Chapter 3. Sensitivity Factors and Sensitivity Factors Based Control Schemes

3.1 Introduction

In this chapter, sensitivity factor (SF), namely voltage sensitivity factor (VSF) and power flow sensitivity factors (PFSF), based control schemes are introduced. Load flow calculation is a non-linear process and optimization techniques, such as interior-point methods (IPM) and least sequential square methods, are well established for non-linear functions. However, most analytical methods dealing with uncertain problems can only be applied to linear problems. The use of VSF and PFSF is a linearization of the full quadratic alternating current (AC) loadflow calculation. In this chapter, how to derive VSF and PFSF from loadflow equations is detailed first. The SFs can be derived from the full AC loadflow equation or direct current (DC) load flow. Next, an incremental method to calculate VSF and PFSF is introduced.

A control scheme with ESS and DSR based on SFs is detailed in section 3.4. Fast response ESS, such as BESS, can provide fast response upon receiving request however it has a limited energy resource. On the contrary, DSR is more likely to provide longer service but is slower to respond. This control scheme uses ESS to deal with the magnitude and delay uncertainty of DSR. However, SFs dao not consider the cost of using ESS and DSR.

In section 3.5, cost sensitivity factors (CSFs) are introduced to quantify the effectiveness of the per unit cost for changing voltage and power flow by using ESS and DSR. A control scheme based on CSFs is proposed in section 3.6. CSF enables the evaluation of an intervention using both technical and commercial considerations. The proposed control schemes are tested with real trial network and device models used in the CLNR project. The case study shows that, by using ESS and DSR collaboratively, the control schemes are able to reduce the size requirements for ESS and enable the use of DSR without resorting to network reinforcement.

In section 3.7 the limitation of using sensitivity factors is discussed based on a practical example using IEEE 14 bus network.

3.2 Deriving Voltage Sensitivity Factor and Power Flow Sensitivity Factor from Jacobian Matrix

Jacobian matrix is the matrix of first order partial derivatives of voltage angle and voltage to real and reactive power mismatch. In this section, calculating voltage sensitivity factors and power flow sensitivity factors based on Jacobian Matrix is introduced.

3.2.1 VSF

VSF is the voltage change at busbar i due to the real or reactive power injection or extraction at busbar k

$$VSF_{i,k}^{P} = \frac{\Delta V_i}{\Delta P_k}$$

or

$$VSF_{i,k}^{Q} = \frac{\Delta V_i}{\Delta Q_k} \quad \textbf{(3.1)}$$

or

$$VSF_{i,k}^{S} = \frac{\Delta V_i}{\Delta S_k}$$

where

$VSF_{i,k}^{P}$ the voltage sensitivity factor from bus k to bus i which represents the voltage change at bus i due to real power injection at bus k

$VSF_{i,k}^{Q}$ the voltage sensitivity factor from bus k to bus i which represents the voltage change at bus i due to reactive power injection at bus k

$VSF_{i,k}^{S}$ the voltage sensitivity factor from bus k to bus i which represents the voltage change at bus i due to apparent power injection at bus k

ΔV_i the voltage change at bus i

ΔP_k the real power injection change at bus k

ΔQ_k the reactive power injection change at bus k

ΔS_k the apparent power injection change at bus k

VSF can be derived from the inverse Jacobian matrix. The inverse Jacobian matrix is given below. Detailed explanation is given in Appendix A.

$$\begin{bmatrix} \Delta \boldsymbol{\theta} \\ \Delta \boldsymbol{V}/\boldsymbol{V} \end{bmatrix} = -\boldsymbol{J}^{-1} \begin{bmatrix} \Delta \boldsymbol{P} \\ \Delta \boldsymbol{Q} \end{bmatrix} = -\begin{bmatrix} \dfrac{\partial \boldsymbol{\theta}}{\partial \boldsymbol{P}} & \dfrac{\partial \boldsymbol{\theta}}{\partial \boldsymbol{Q}} \\ \dfrac{\partial \Delta \boldsymbol{V}}{\partial \boldsymbol{P}} & \dfrac{\partial \Delta \boldsymbol{V}}{\partial \boldsymbol{Q}} \end{bmatrix} \begin{bmatrix} \Delta \boldsymbol{P} \\ \Delta \boldsymbol{Q} \end{bmatrix} \quad \textbf{(3.2)}$$

where

$\boldsymbol{\theta}$ the vector of angle difference between busbars

$\boldsymbol{V}$ the vector of voltage of busbars

$\boldsymbol{J}$	the Jacobian matrix
$\boldsymbol{J^{-1}}$	the inverse Jacobian matrix
$\boldsymbol{P}$	the vector of net real power injection
$\boldsymbol{Q}$	the vector of net reactive power injection
$\partial\Delta\boldsymbol{\theta}/\partial\boldsymbol{P}$	the matrix for the partial derivatives of $\boldsymbol{\theta}$ to $\Delta\boldsymbol{P}$
$\partial\Delta\boldsymbol{\theta}/\partial\boldsymbol{Q}$	the matrix for the partial derivatives of $\boldsymbol{\theta}$ to $\Delta\boldsymbol{Q}$
$\partial\Delta\boldsymbol{V}/\partial\boldsymbol{P}$	the matrix for the partial derivatives of $\Delta\boldsymbol{V}$ to $\boldsymbol{P}$
$\partial\Delta\boldsymbol{V}/\partial\boldsymbol{Q}$	the matrix for the partial derivatives of $\Delta\boldsymbol{V}$ to $\boldsymbol{Q}$

Thus, for a small ΔP_k and ΔQ_k VSF can be represented by the elements in the inverse Jacobian matrix $\boldsymbol{J^{-1}}$

$$VSF_{i,k}^{P} = \frac{\Delta V_i}{\Delta P_k} \approx \frac{\partial \Delta V_i}{\partial P_k}$$

or

$$VSF_{i,k}^{Q} = \frac{\Delta V_i}{\Delta Q_k} \approx \frac{\partial \Delta V_i}{\partial Q_k} \quad \textbf{(3.3)}$$

3.2.2 PFSF

PFSF in this research is defined as the change of powerflow through a branch from bus i to bus j, or branch ij, due to the real or reactive power injection or extraction from busbar k.

$$PFSF_{ij,k}^{P} = \frac{\Delta S_{ij}}{\Delta P_k}$$

or

$$\boldsymbol{PFSF_{ij,k}^{Q} = \frac{\Delta S_{ij}}{\Delta Q_k}} \quad \textbf{(3.4)}$$

or

$$PFSF_{ij,k}^{S} = \frac{\Delta S_{ij}}{\Delta S_k}$$

where

$PFSF_{ij,k}^{P}$	Power flow sensitivity factor from bus k to branch ij due to real power

$PFSF_{ij,k}^{Q}$	Power flow sensitivity factor from bus k to branch ij due to reactive power
$PFSF_{ij,k}^{S}$	Power flow sensitivity factor from bus k to branch ij due to apparent power
ΔS_{ij}	apparent power flow change of branch ij

Deriving PFSF from full AC loadflow can be complicated due to the fact that the Jacobian matrix only reflects the relationship between the angle of bus i, j and the net power injection from busbar k. In some applications, DC loadflow is applied to calculate PFSF [98-100]. In DC loadflow, the resistance on the branches and reactive power is ignored. All voltage magnitudes are assumed to be 1.0 p.u.. DC loadflow only calculates the real power and the voltage angle. The assumptions for DC loadflow include:

i. Reactive power is neglected
ii. The relationship between the real power and the voltage magnitude is neglected
iii. All voltage magnitudes are assumed to be 1.0
iv. Resistance on branches is neglected

In transmission networks, where the X/R ratio is high and sufficient voltage support exist, the above assumptions are valid and DC loadflow is a reasonable simplification. DC loadflow is extensively applied in transmission network unit dispatch and control. However, in distribution networks, the X/R ratio is lower than that of transmission networks and neglecting the resistance can cause calculation errors. Besides, in distribution networks, especially for distribution networks with long feeders or with large penetrations of DG or LCTs, the voltage profiles will be more volatile. It may not be reasonable to assume that the magnitude of voltage is 1.0. Thus, using DC loadflow derived PFSF for distribution network control and optimization is likely to lead to large errors.

3.3 VSF and PFSF Calculation Based on Incremental Method

In this section, an incremental method for calculating sensitivity factors is introduced. This method calculates sensitivity factors by comparing two loadflow results. The first loadflow is used as the baseline. A small power injection change to one of the busbars in this network is then applied. By calculating the difference between voltage and power flow in two load flow results, the voltage and power flow sensitivity factors can be calculated. The process of the

incremental method is illustrated in the flow chart below. Figure 3.1 shows the process to calculate the $VSF_{i,k}$ and $PFSF_{ij,k}$ due to the real power injection from bus k.

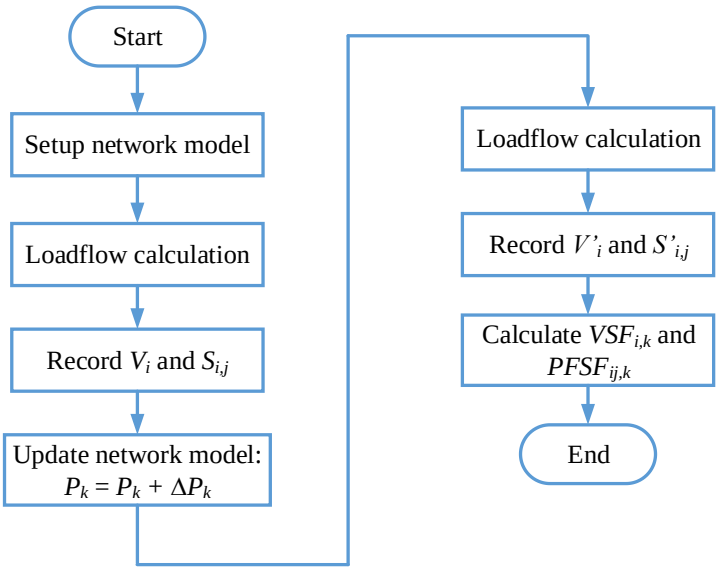

Figure 3.1 Incremental Method for Calculating VSF and PFSF

First, the network model is setup to enable a loadflow calculation. Real and reactive load or generation for each busbar is defined at this stage. Second, a normal full AC loadflow calculation is carried out, the voltage of bus i, V_i and the power flow through branch ij, S_{ij} is recorded. Next, the net injection of bus k, $P_k = P_{k,generation} - P_{k,load}$ is replaced by $P_k + \Delta P_k$, ΔP_k is a small increment in real, reactive or apparent power. Loadflow is carried out again with the updated network model to calculate the new voltage of bus i, V'_i and the power flow through branch ij, S'_{ij}. Finally, the sensitivity factors can be calculated as

$$VSF_{i,k} = \frac{\Delta V_i}{\Delta P_k} = \frac{V'_i - V_i}{\Delta P_k} \quad \textbf{(3.5)}$$

$$PFSF_{ij,k} = \frac{\Delta S_{ij}}{\Delta P_k} = \frac{S'_{ij} - S_{ij}}{\Delta P_k} \quad \textbf{(3.6)}$$

3.4 Sensitivity Factor Based Control Scheme

In this section, a new application of ESS and DSR operating collaboratively to enable voltage control within distribution networks is introduced. This work has been published in paper [101]. The author's contributions in this work include design, implementation and evaluation of this control scheme. In this scheme, industrial and commercial (I&C) DSR and ESS have been used collaboratively to mitigate voltage violations in a rural distribution network under a future scenario.

Voltage and power flow sensitivity factors have been used for voltage control and power flow management in [102] and [103]. In [102], VSF and PFSF are used in a coordinated control scheme for solving voltage and thermal limit violations with DGs. It is found in this work that sensitivity factor based control scheme is fast-to-deploy and flexible.

3.4.1 Proposed control scheme

High penetrations of LCTs are likely to cause voltage drop problems in distribution networks. In order to mitigate the violation of steady-state voltage limits caused by the increasing penetration of LCTs, the proposed control system uses industrial and commercial (I&C) DSR and ESS collaboratively to mitigate voltage violations in a rural distribution network. ESS has is able to provide fast response however has a finite resource. The capability of ESS to provide real power support is limited by the SoC. On the contrary, I&C DSR is normally slow to response but is less constrained by resource. To reduce the requirement for the resource of ESS and achieve a high response rate for voltage excursions, the proposed collaborative control system will instruct the ESS to operate first and export real power to increase the voltage in the network. The real power export from ESS increases or decreases at a step size of 10kW. If the excursion is sustained, the scheme will call DSR. There is no reactive power output from ESS because a typical distribution network has a low X/R ratio and the impact of reactive power on voltage control is limited.

Since the ESS has a finite resource, a possible scenario arises such that if the voltage problem cannot be solved with the available capacity of the ESS, the under voltage problem would remain. The availability of DSR services will be checked at the occurrence of the under voltage events. The available DSR services will be checked against power flow constraints so that they will not cause thermal violations. The collaborative control scheme will therefore call this response in order to provide security to the operation of the ESS. When operation of the DSR is confirmed and the steady-state voltage is within limits, the collaborative voltage control system will instruct the ESS to reduce real power export and thus conserve its limited resource. The flowchart of this control scheme is illustrated in Figure 3.2.

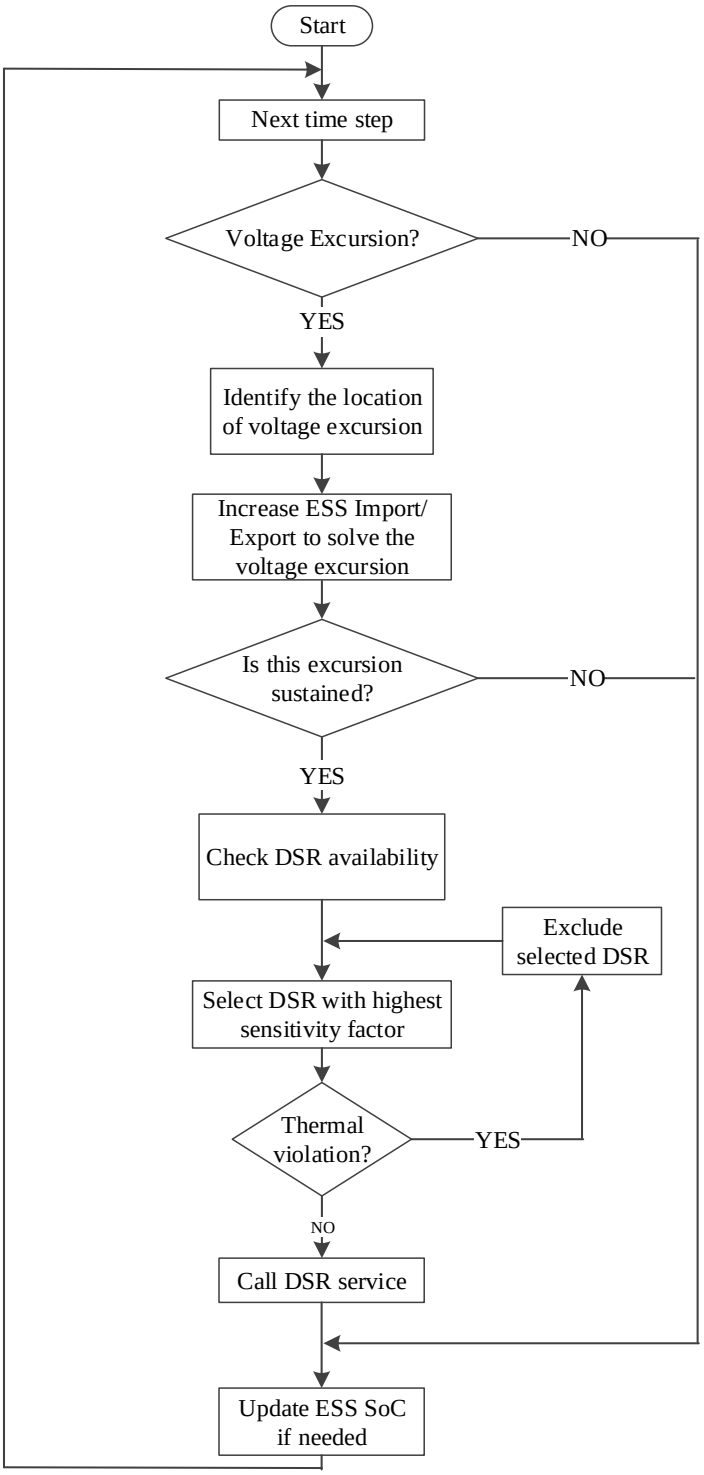

Figure 3.2 Flow Chart for Sensitivity Factor Based Control Scheme

The control scheme can be applied to solve over voltage problems by charging ESS and increasing demand. By replacing VSFs with PFSFs and checking voltage constraints, this control scheme is also able to deal with power flow management (PFM) problems.

3.4.2 Case Study Network

A typical rural network in Northumberland, England, owned by Northern Powergrid has been selected as the case study network. Figure 3.3 shows the schematic diagram and the smart grid technologies which have been installed. Two 20kV feeders and an LV network have been modelled in detail. As can be seen in this figure, two 66/20kV transformers are used for voltage control at the primary substation. A mechanically switched capacitor bank and two in-line regulators are already deployed on this system for voltage control purposes for the feeders and at present, are operated according to the standard DNO voltage control practice.

A future smartgrid scenario is presented. DSR customers A and B, and an LCT cluster with associated ESS system are located towards the remote end of one of the 20kV feeders. The power consumption of DSR customer A is 0.8 MW and backup generators are used by DSR customer A to provide demand reduction. When the backup generators are used, the power consumption of this customer reduces to less than 10kW. DSR customer B provides response service by reducing its consumption and the power reduction is not constant. DSR customers A and B are not located at the end of the MV feeder due to the rating of the cable. An LCT cluster is a LV network with high penetrations of LCTs. The LCT cluster in this case study has 230 customers and a higher penetration of EV and ASHP ownership than the remaining network. The apparent power rating and the capacity of the energy storage system, are 100kVA and 200kWh, respectively.

To enable evaluation of the voltage control scheme SCADA data from the case study network and the LCT models have been used to develop realistic future scenarios and associated consumer load profiles. These load profiles exceed the capabilities of the existing network infrastructure and conventional infrastructural upgrade would be the most likely option to resolve this. The capability of the proposed control strategy to address the limitations of the existing network is evaluated by solving an MV and an LV voltage excursion, respectively.

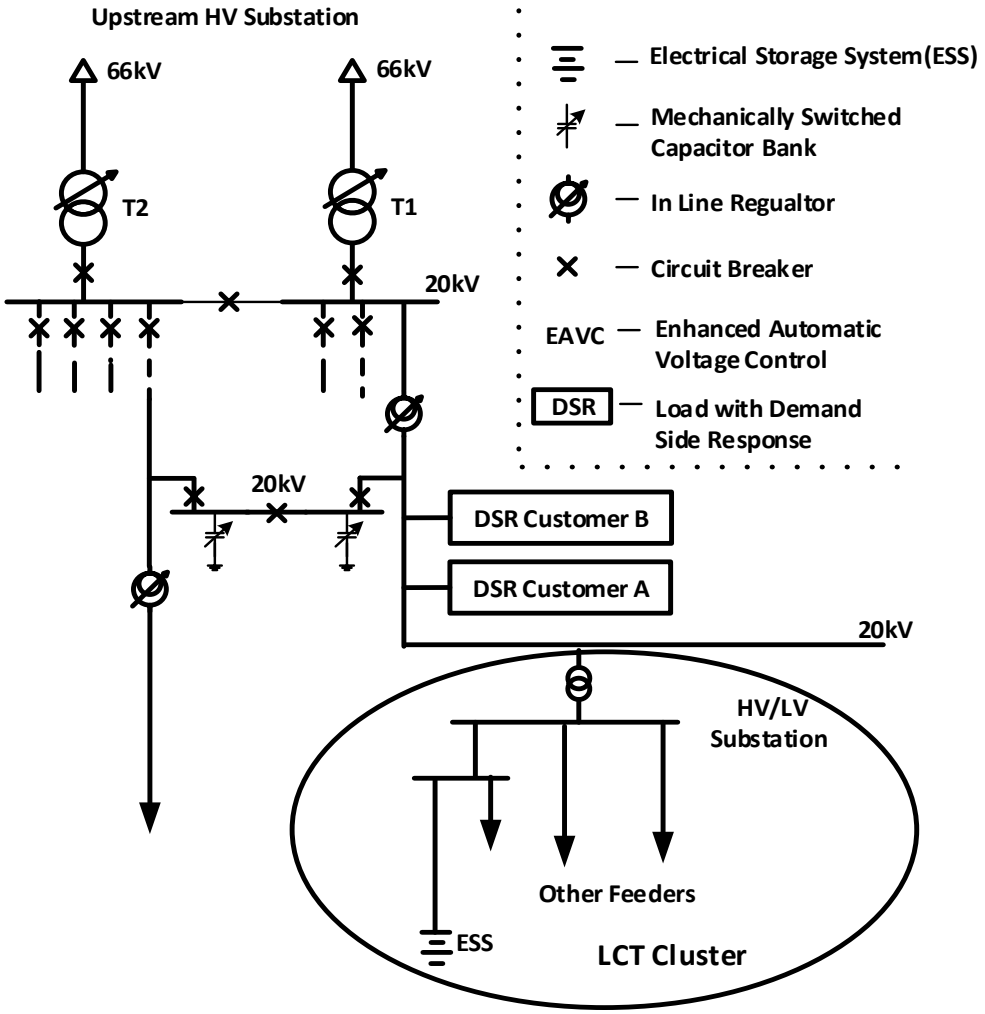

Figure 3.3 Schematic Diagram of the 20kV Case-Study Network.

The demand profile of this distribution network, measured by the present SCADA system, is illustrated in Figure 3.4. The resolution of the original SCADA measurements is half-hour. This data has been linear interpolated into 1 minute resolution. The blue trace indicates the typical load profile during a winter day, when the highest load was recorded, in the period from December 2010 to January 2012. The peak demand which occurs between 02:00 and 03:00 is due to electrical storage heating and a high uptake of the economy seven tariff. The additional peak between 14:00 and 16:00 is the result of a Super Tariff in this area which gives a lower electricity price for six hours overnight and two hours in the afternoon.

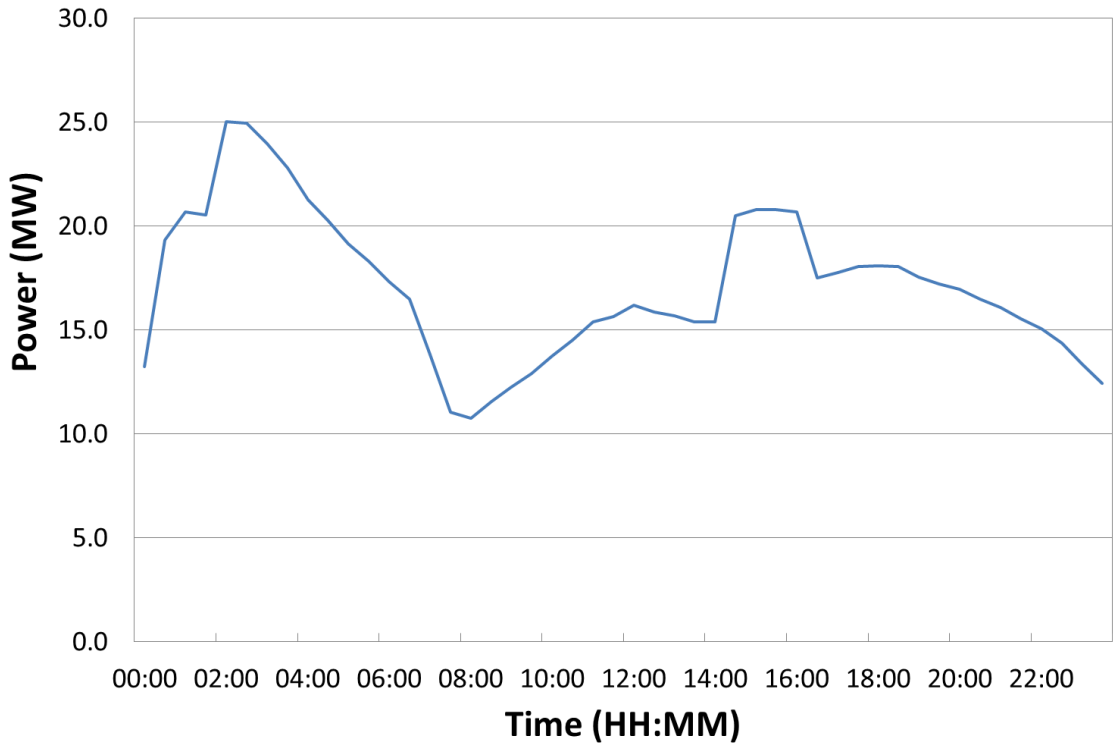

Figure 3.4 Current Load Profile in the case-Study Network

The proposed decentralised control strategy is applied to mitigate voltage limit violations at the remote end of an MV feeder, over 25 miles in length, and the remote end of an LV feeder. Unlike a centralised control system, which coordinates other network interventions such as the capacitor bank, the local decentralized control system minimizes the requirement of communication.

Modelling methodology

A network model has been developed using IPSA2. The LV section of the distribution network with ESS is illustrated in Figure 3.5. The model is based on detailed network data supplied by Northern Powergrid. The longest branch of the longest LV feeder has been modelled in detail, due to the likelihood of voltage problems occurring. Loading on Branch 2 of this feeder and the remaining LV feeders are represented by lumped loads.

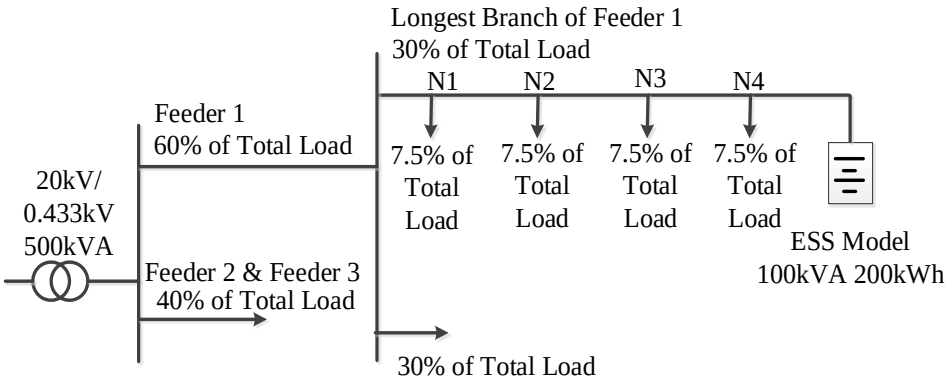

Figure 3.5 Model of LV Distribution Network

ESS has been modelled in this system such that it can import/export real and/or reactive power in any combination within its rating. DSR is modelled as a controllable load. The ESS model and DSR model capabilities are extended using Python 2.7, which has been adopted as a scripting language in IPSA2, to automate control of the network model and the load flow engine.

Model validation

The network model has been validated against load flow results from an existing model within Northern Powergrid. The busbar voltages and feeder currents calculated in both models have been found to be in good agreement.

The network model has also been validated using measured data from both the HV/LV and primary substation sites. Real load data have been used in the IPSA2 network model. Load flow calculations have been carried out and the results were compared to the measured data. The model was found to be able to reproduce LV voltages to within 1% accuracy.

Low carbon technologies

Experiments have been carried out to analyse the charging profile of an EV (Mitsubishi, i-MiEV) [101]. Results indicate that, during charging, the power consumed by the EV is initially constant, followed by a period where the charge current reduces as the EV reaches full charge. Profiles were derived from a range of initial states-of-charge. These results have been used within the EV modelling methodology in this thesis.

Previous work has characterised EV users and analysed the daily usage patterns of vehicles [104]. According to this report, roughly 25% of trip purposes are for commuting. The blue

trace detailed in Figure 3.6 shows the probability of commuting vehicles being at home. It can be seen that from 21:00 until 06:00 the next day, the probability of commuting vehicles being at home is over 90%. During the hours from 09:00 until 16:00, the probability of commuting vehicles being at home is lower than 30%. Similarly, for all other purposes, such as food shopping and business, the probability of vehicles being at home from 21:00 until 06:00 next day and from 09:00 until 16:00 are over 90% and below 80% respectively.

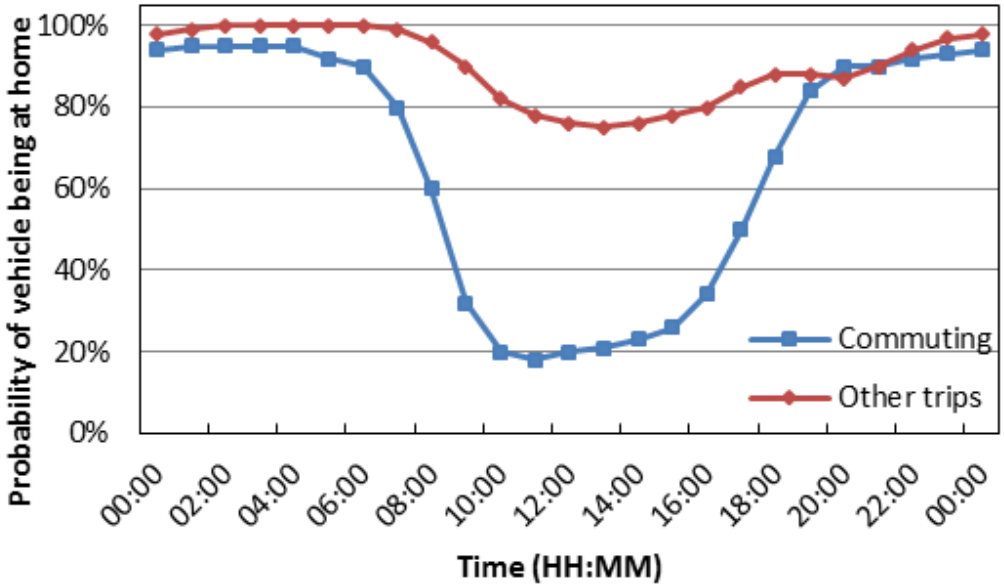

Figure 3.6 Probability of Vehicles Being at Home [104].

Under the tariffs described earlier, customers have a lower electricity price for six hours in the night and two hours in the afternoon. Considering the higher probability of vehicles being at home at night, it could be assumed that most EV users would tend to charge EVs during this period, instead of in the afternoon. It is also reported that, without a fast charging infrastructure, most EVs have an initial state of charge of 60% to 70% prior to charging [104]. Due to the high cost of a fast charging infrastructure and the rurality of the area under consideration, it is reasonable to make the assumption that there would be minimal fast charging units available. Therefore, at the start of a charge, the EVs' SOC is assumed to be between 60% and 70%. An aggregated charging curve based on the assumptions above; with a 15% penetration of EVs in the cluster is given in Figure 3.7.

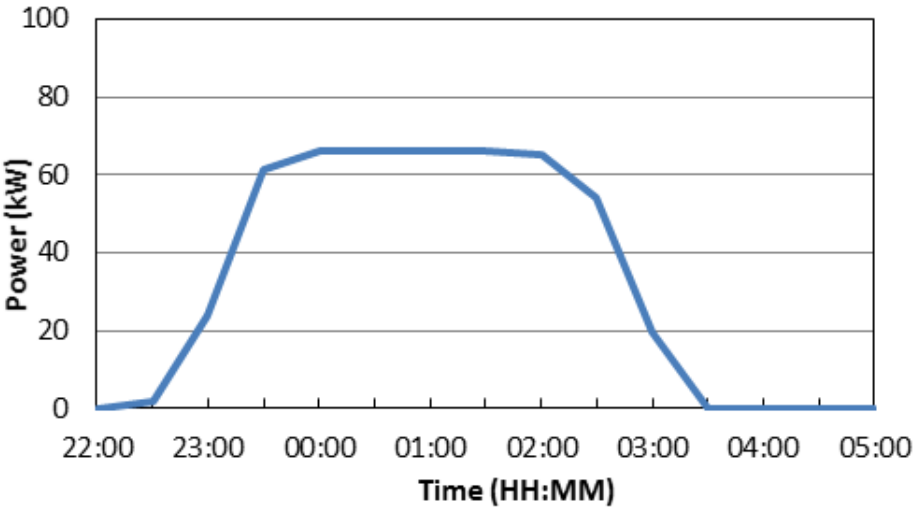

Figure 3.7 Aggregated EV charging curve in the LCT cluster during night time.

Work has been previously carried out in order to derive thermal profiles for typical UK building stock. Generic building data was used as an input to the models in combination with temperature data from a site in the UK. Multiple occupancy scenarios for each considered building type (detached, semi-detached, flat, mid-terrace) are derived and aggregated in order to generate the final thermal profile [105]. The results were found to agree favourably with UK national statistics. In order to generate the electrical profile of the air-source heat pump (ASHP), the thermal profiles for the required building types have been scaled according to the methodology outlined in [106]. The methodology requires that the thermal profile be scaled down by the coefficient of performance (COP) of the ASHP. A value of 3 has been chosen for the ASHP system under consideration in line with previous work [106]. The derived electrical demand profiles of detached and semi-detached properties are given in Figure 3.8.

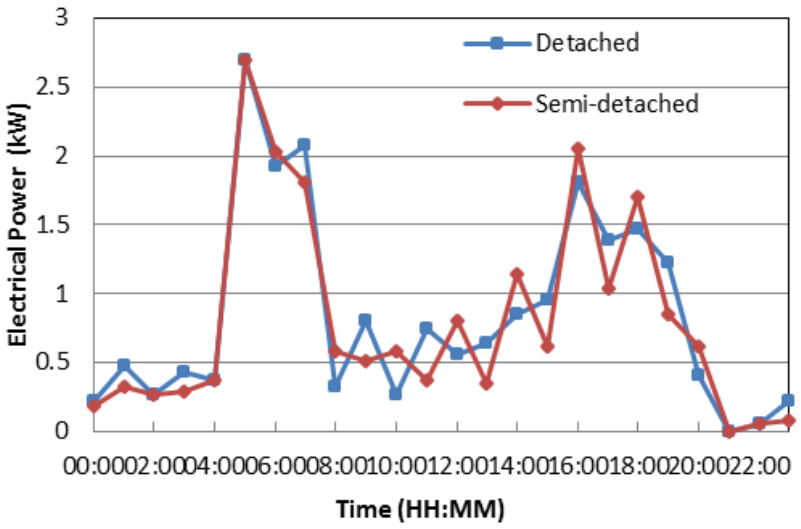

Figure 3.8 Derived electrical demand for detached and semi-detached properties.

To derive the ASHP electrical demand profiles for this work, detached and semi-detached properties have been used, in a ratio of 9:1 respectively. This is in accordance with previous simulations of rural networks [106]. Figure 3.9 shows the total demand curve due to the ASHP load, with an assumed penetration of 45%.

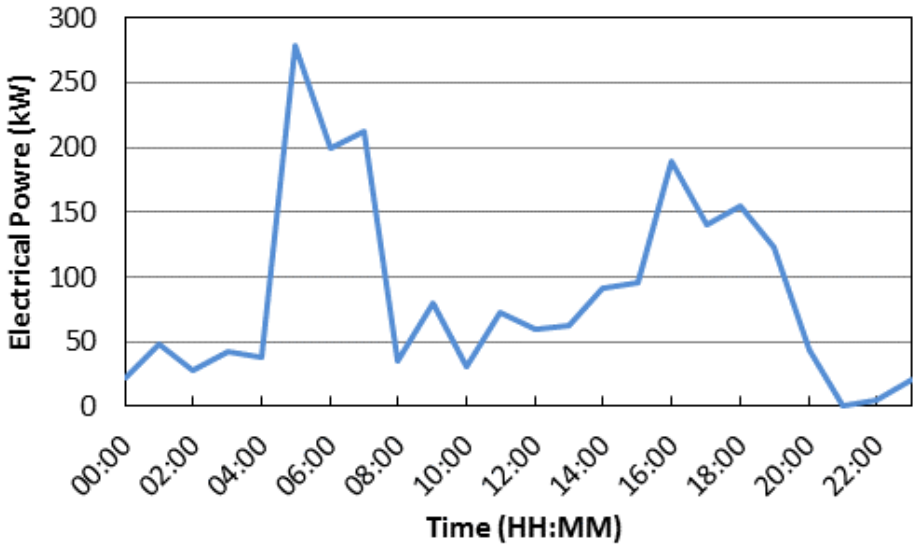

Figure 3.9 Aggregated ASHP electrical demand curve in the LCT cluster.

The EV and ASHP demand profiles have been added to the LCT cluster and the remaining network. The number of LCTs added is calculated based on the number of customers and the penetration of the LCTs.

Voltage Profile

Based on the validated network model and the load profile illustrated in Figure 3.4, the voltage profile of the remote end of the feeder in the future scenario can be calculated. The simulated voltage profile is plotted in Figure 3.10. The red curve is the load profile in this network with LCTs. The scattered blue line is the voltage profile due to the load change. Three voltage excursions can be observed on this graph. The first excursion between 00:00 and 03:00 is due to EV charging and the existing tariff. The second and third excursion is due to the use of ASHP in the morning. It should be noted that currently existing voltage control interventions, including OLTCs, in-line regulators and capacitor banks are still in use in this case study.

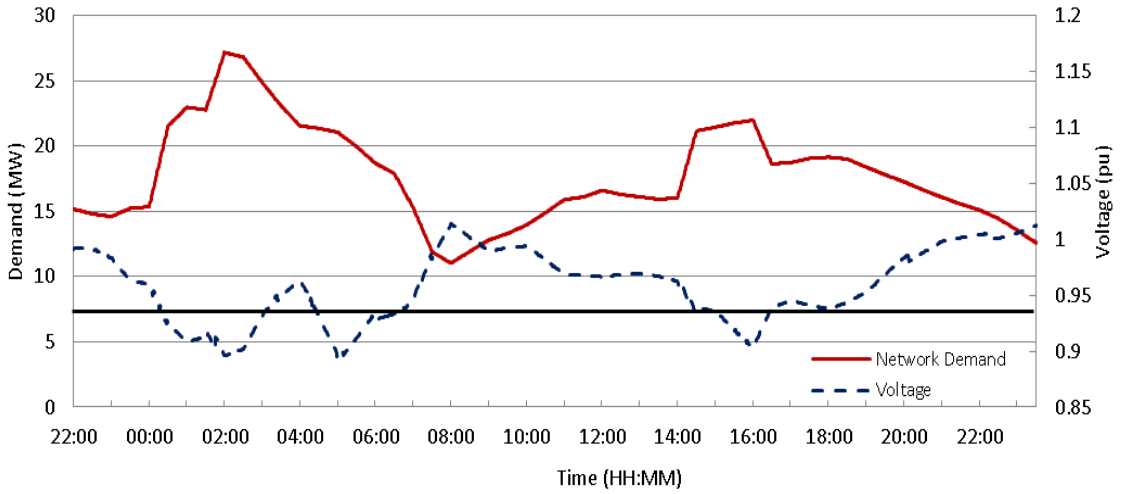

Figure 3.10 Voltage Profile in 24 Hours

Simulation results indicate that, with the higher penetrations of LCTs, detailed earlier, in the modelled LV network, and a 10% penetration of both EVs and ASHPs across the whole network, the voltage at the remote end of the longest LV feeder will drop below the statutory limit (0.94pu in the UK). This will occur during the night-time peak period, early morning and afternoon peak time. The voltage is lower than 0.94pu from 00:00 to 03:00 due to EV charging. The large power consumption of ASHPs in the early morning will result in a voltage drop between 04:00 and 07:00. From 14:00 to 16:00, another peak can be observed due to the additional ASHP consumption in combination with the present network peak.

The locations of the smartgrid interventions, ESS and DSR customers, are located at nodes with high VSFs to locations where low voltage limit violations are observed.

3.4.3 Simulation results

The proposed control scheme has been applied to this network with the derived load profile with LCTs. In this section, voltage profiles with the implementation of the proposed control scheme are reported. It is assumed that, the ESS is fully charged at the beginning of the simulation.

Under voltage due to night peak

In this case, collaborative voltage control is carried out using ESS and DSR customer B. Customer B is called due to its 24 hour operation. The simulation results illustrating the operation of the ESS and DSR customer B to control voltage during the mid-night peak period are shown below in Figure 3.11 and Figure 3.12. In Figure 3.11, the voltage profile between 23:30 to 04:00 is plotted. It can be seen that the voltage dropped below the 0.94pu limit, at approximately 00:15 in the morning. The ESS then injected 10kW of real power into

the grid to bring the voltage back above the limit and, at the same time, the DSR command was issued. After 20 minutes, the consumption of DSR customer B started to reduce but did not reach a stable level until 01:00. At this time, installed monitoring equipment showed that the voltage of the network was close to the statutory limit therefore the collaborative voltage control scheme decided to maintain the output of the ESS, in order to prevent a further voltage problem. However, around 45 minutes later, when the voltage again went below the limit, the ESS started to inject more power into the network to maintain the voltage above limit.

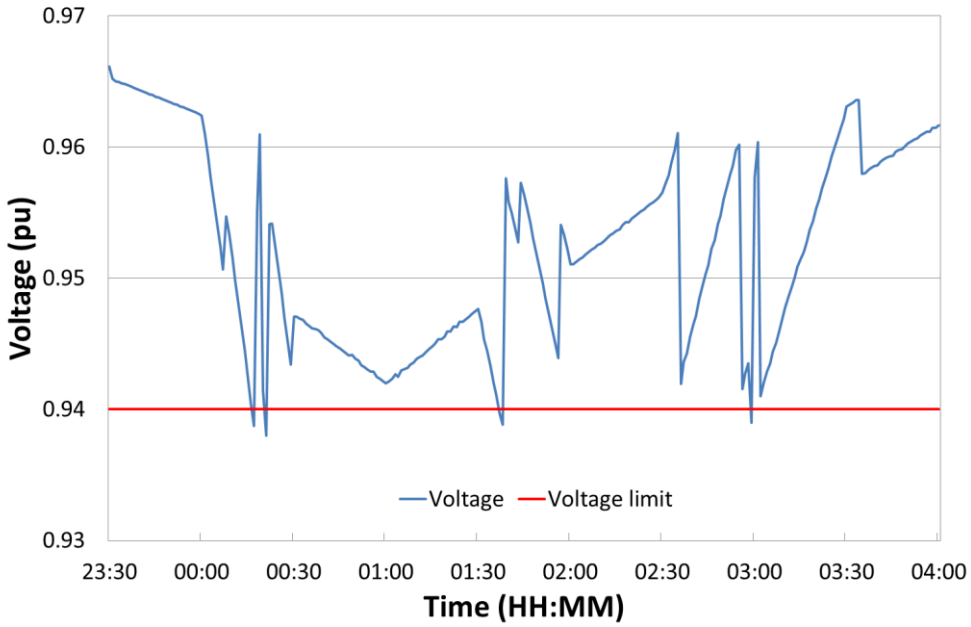

Figure 3.11 Voltage Profile with DSR Customer B and ESS During the Night Peak Period

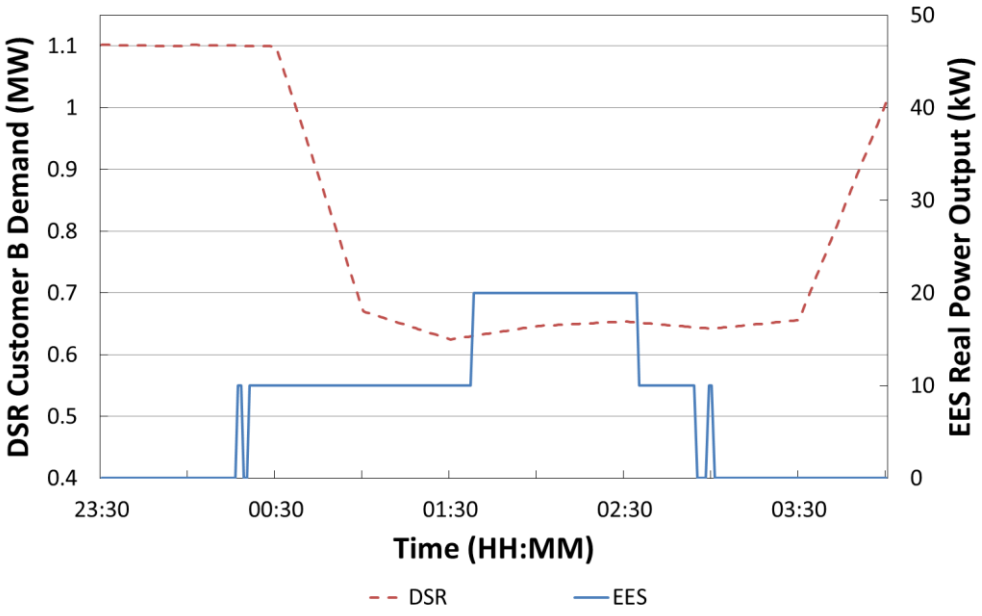

Figure 3.12 DSR Customer B Demand and Real Power Output of ESS.

Under voltage due to morning peak

During the early morning peak period, a voltage problem was fixed purely by the ESS. A DSR operation was not called in consideration from Customer B as the number of DSR operations available in a day is limited for this customer. Customer A was unavailable as the voltage problem occurred in the early morning. This customer is assumed to operate a typical 09:00 to 17:00 working day and is not preferred to provide a DSR outside these hours. This case also helps to illustrate the potential unavailability of DSR as well as customer flexibility.

The voltage profile between 04:00 and 07:00 is plotted in Figure 3.13. Real power output of the ESS will increase in steps when an under voltage problem occurs and will decrease in steps when the voltage goes up to 0.96pu to reserve available capacity.

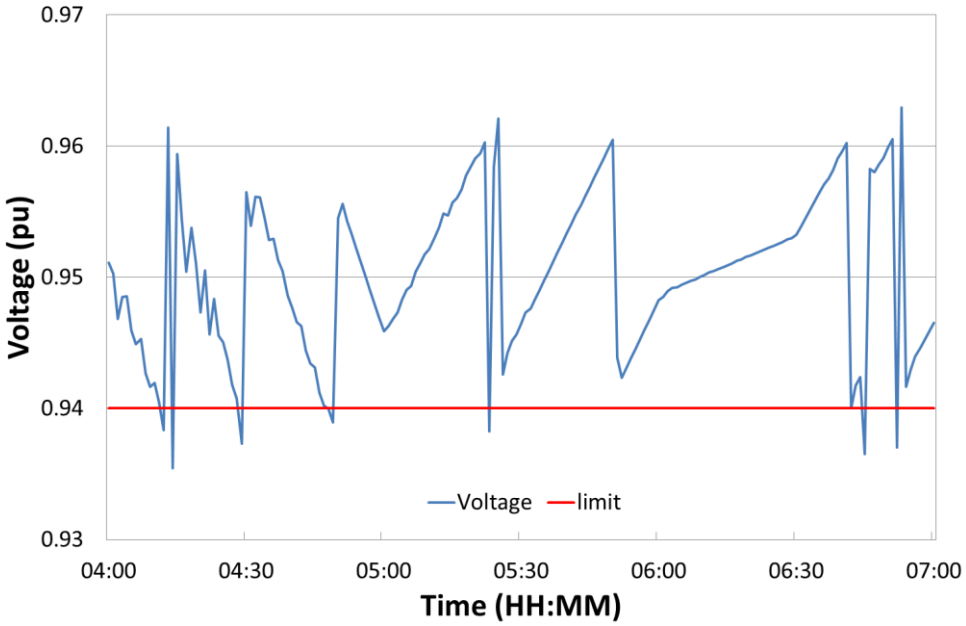

Figure 3.13. Voltage profile at the end of the feeder with ESS control only during the morning peak period.

The real power export from ESS is plotted in Figure 3.14. As can be observed, the ESS increases and decreases its power output in a step of 10 kW so that the voltage at the end of the feeder is maintained within the range of 0.94p.u. and 0.96p.u..

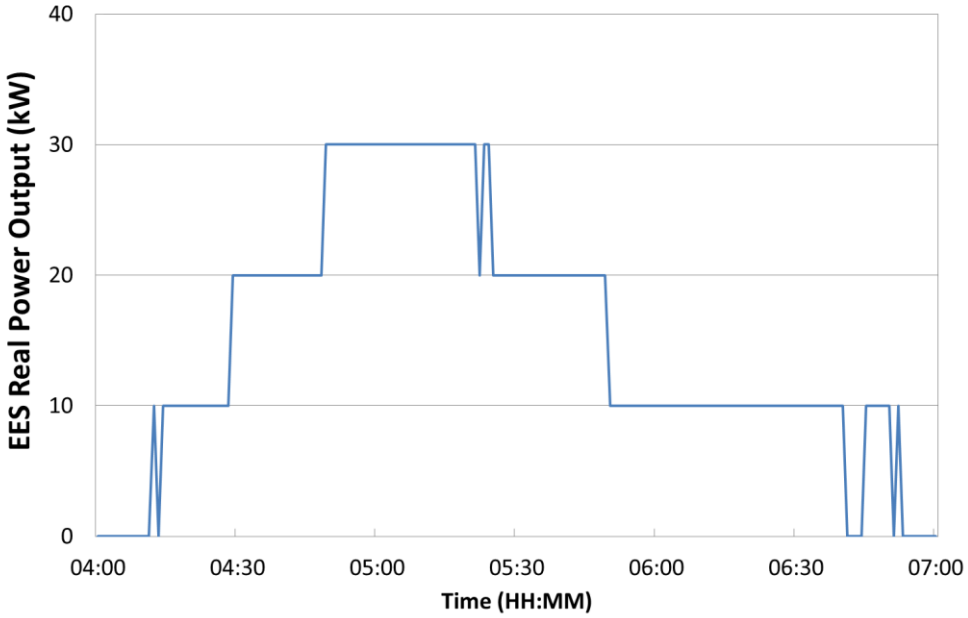

Figure 3.14. ESS real power output during the morning peak period.

Under voltage due to afternoon peak

A similar simulation was carried out to investigate the collaborative operation of ESS and DSR customer A, as illustrated in Figure 3.15 and Figure 3.16. In order to cope with the voltage problem during the afternoon peak, at approximately 14:25, voltage dropped below 0.94pu and continued to decrease. ESS reacted first to bring the voltage back to 0.96pu. A DSR command was issued at the same time to customer A. After 20 minutes, at 14:45, the demand of customer A decreased to 0 in a very short period of time. Despite the magnitude of customer A's response, at 15:30, the voltage violated the limit again due to the increasing load. As a result, the ESS started to inject real power into the network again.

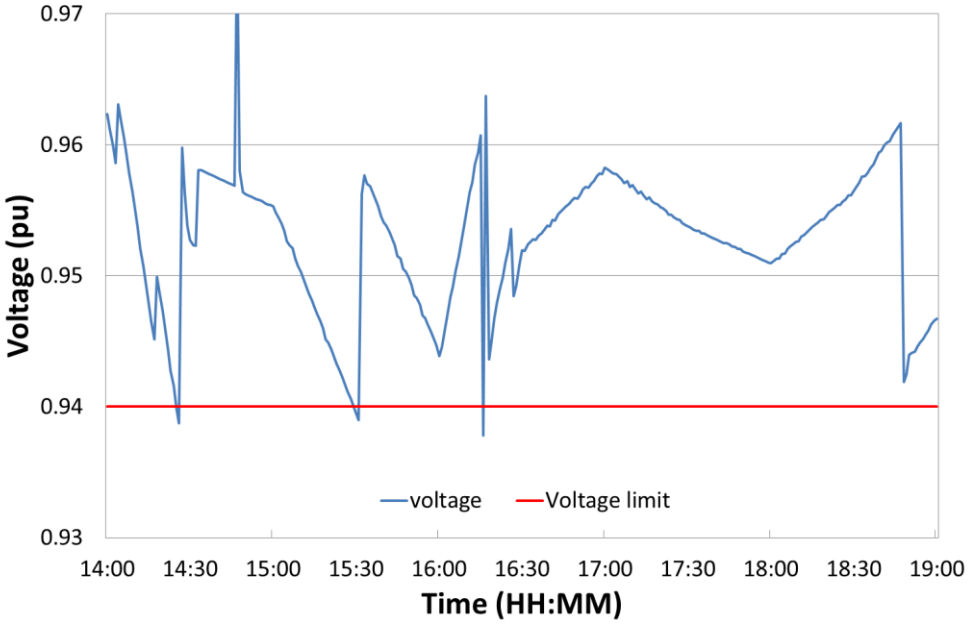

Figure 3.15. Voltage Profile with ESS and DSR Customer A During the Afternoon Peak Period.

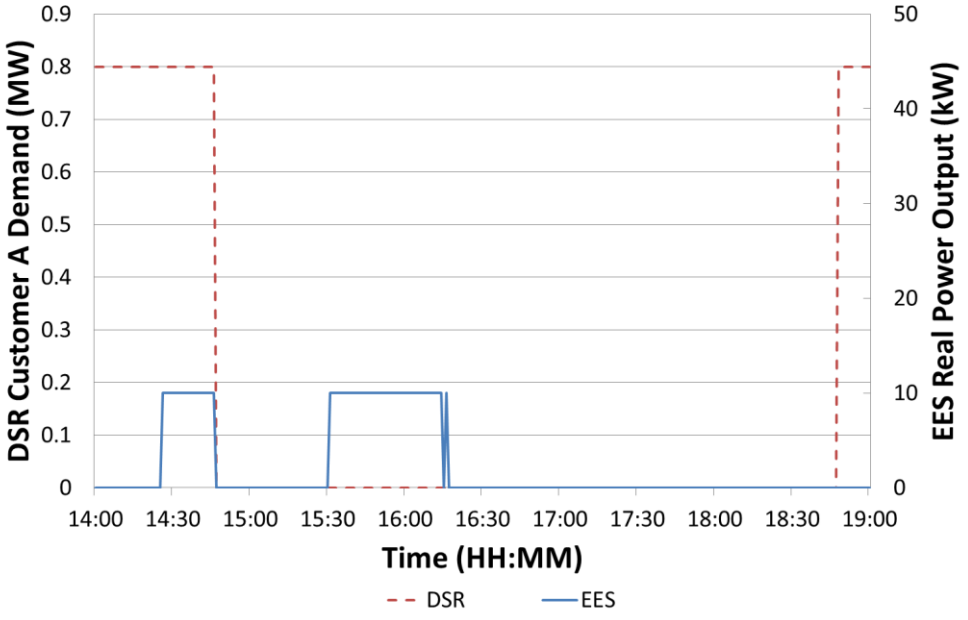

Figure 3.16. DSR customer a consumption and ESS real power output during the afternoon peak period.

The energy outputs of ESS in the simulation are 35.8 kWh, 45.1 kWh and 11.0 kWh, respectively. It is estimated that this presents a percentage change of SOC of 17.9%, 22.6% and 5.5% based on the 200kWh capacity ESS. The total depth-of-discharge (DoD) therefore is 46.0%. Based on this estimation, if the initial state of charge of the ESS is greater than 46%

(and the Lithium-Ion battery is capable of a maximum DOD of 100%) the ESS will not require re-charging during one day.

Additional simulations showed that if the battery bank of the ESS were to have been optimally re-charged throughout the day using a methodology not considered as part of this scheme, the ESS would have not be required to achieve a deep discharge which could potentially damage the battery.

3.5 Cost Sensitivity Factors

In this section, the concept of cost sensitivity factors (CSF) is introduced. Sensitivity factors indicate the technical effectiveness of the controllable devices such as ESS and OLTC. By considering the cost of using the controllable devices, CSF is able to represent both the technical and economical effectiveness. The use of VCSF and PFCSF has been proposed in [61]. VCSF and PFCSF are proposed in order to represent the cost of a change in the voltage at node i or powerflow through branch ij with respect to the cost of injecting or retracting real or reactive power from bus k. The VSF from bus k to bus i has been introduced in section 3.2. Assuming the cost of 1 MW injection of real power at bus k is C_k, VCSF is defined as

$$VCSF_{i,k} = \frac{\Delta V_i}{\Delta P_k \cdot C_k} = \frac{VSF_{i,k}}{C_k} \tag{3.7}$$

where

$VCSF_{i,k}$ voltage cost sensitivity factor from bus k to bus i

C_k the cost of real power injection at bus k (MW/£)

Based on this definition, PFCSF can be defined as

$$PFCSF_{i,k} = \frac{\Delta S_{ij}}{\Delta P_k \cdot C_k} = \frac{PFSF_{ij,k}}{C_k} \tag{3.8}$$

where

$PFCSF_{i,k}$ power flow cost sensitivity factor from bus k to branch ij

VCSF and PFCSF quantify the effectiveness of the per unit cost for changing voltage and power flow. Thus, VCSF and PFCSF enable a control strategy to evaluate an intervention using both technical and commercial considerations.

3.6 CSF Based Control Scheme

This section presents a decentralized voltage control strategy which utilises DSR from ESS, I&C DSR and residential DSR (RDSR). The control strategy is designed to be cognisant of the DSR characteristics demonstrated in real DSR trials, and of the actual ESS systems. In this section, DSR is regarded as a participatory action which relies on the consent and involvement of network users, both commercial and residential, to achieve a demand increase or reduction. The participatory view of DSR recognises the need to consider the social implications of altering when and how load is consumed. This approach to DSR introduces a degree of uncertainty to the level and duration of response to DSR calls. The control strategy described in this section uses ESS as a technical solution to manage the uncertainty linked with the participatory nature of the other DSR options by using ESS in a buffer mode, in which the fast and flexible response provided by ESS is used to mitigate the slower and less certain DSR responses. The concept of VCSFs is used within the control strategy to enable selection of the most cost effective deployments of DSR. Although the control scheme presented in this section is for voltage control, by replacing VCSF with PFCSF, this control scheme is also adequate to perform PFM.

Compared to the control scheme proposed in section 3.4, the following improvements have been made:

1. Both real and reactive power of ESS has been used. An algorithm has been devised to optimize the capability of ESS
2. Cost functions for DSR and ESS have been developed and considered. The use of CSFs considers both the technical and economical effectiveness of ESS and DSR

In this work, it is the author's contribution of developing the cost functions of DSR services, designing the control strategy, calculating SFs and CSFs, implementing the control strategy on the case study network and analysing the results.

3.6.1 Cost functions of DSR

In order to quantify the cost of each DSR service, cost functions for ESS, RDSR and I&C DSR are proposed. The cost function considers the capital costs, power ratings and the number of cycles available of DSR services. Based on the values above, the cost function for each DSR in the unit of £/kW can be derived. The cost functions enable comparison between different DSR in different forms in terms of cost of real power.

ESS cost function

The cost function of ESS exporting and importing real power is defined as

Charge:

$$C_{ESS,Charge} = \frac{C_{Capital,ESS}}{N_{Cycle,ESS} \cdot P_{ESS,Rating}} - \left(SoC_{Upperlimit} - SoC\right) \cdot k_{ESS} \quad \textbf{(3.9)}$$

Discharging:

$$C_{ESS,Discharge} = \frac{C_{Capital,ESS}}{N_{Cycle,ESS} \cdot P_{ESS,Rating}} - \left(SoC - SoC_{Lowlimit}\right) \cdot k_{ESS} \quad \textbf{(3.10)}$$

where

$C_{ESS,Charge}$	the cost for charging ESS (£/kW)
$C_{ESS,Discharge}$	the cost for discharging ESS (£/kW)
$C_{Capital,ESS}$	the capital cost of ESS (£)
$N_{Cycle,ESS}$	the total charge and discharge cycle over the lifetime of the selected ESS
$P_{ESS,Rating}$	the rated real power output of the ESS (kW)
SoC	State-of-Charge
$SoC_{Upperlimit}$	the upper limit for SoC
$SoC_{Lowlimit}$	the lower limit for SoC
k_{ESS}	a factor represents the impact of SoC on the cost of operating the ESS. This reflects a disincentive to discharging the ESS at a low SoC and a disincentive to charging the ESS at a high SoC

The cost functions for import and export of real power for the ESS given in equation (3.9) and (3.10) are not the actual costs of using the ESS. For real power, the cost function is a combination of capital investment and an offset to account for a changing SoC. k_{ESS} is a positive number and according to the cost function, the cost of charging the ESS at a high SOC will be higher than charging at a lower SOC to prevent over-charge. Similarly, the cost of discharging the ESS at a lower SOC will be more expensive than at a higher SOC.

RDSR cost function

The cost of RDSR C_{RDSR} (£/kW) is estimated based on the total cost of calling RDSR in a year $C_{Capital,RDSR}$ (£), maximum number of service requests of RDSR in a year N_{RDSR} and

reduction in customer consumption P_{RDSR} (kW). The total cost of calling RDSR $C_{Capital,RDSR}$ per year is based on the value of reducing demand at peak periods and the associated conventional network reinforcement costs. The cost of RDSR is given by:

$$C_{RDSR} = \frac{C_{Capital,RDSR}}{N_{RDSR} \cdot P_{RDSR}} \quad \textbf{(3.11)}$$

Where

C_{RDSR} the cost of RDSR service per kW (£/kW)

$C_{Capital,RDSR}$ the cost of RDSR service per year (£)

N_{RDSR} the maximum number of service requests of RDSR in a year

P_{RDSR} the reduction of RDSR customer consumption (kW)

I&C DSR cost function

Similar to the cost of RDSR service, the cost of I&C DSR$C_{I\&C}$ is defined by:

$$C_{I\&C} = \frac{C_{Capital,I\&C}}{N_{I\&C} \cdot P_{I\&C}} \quad \textbf{(3.12)}$$

Where

$C_{I\&C}$ the cost of I&C service per kW (£)

$C_{Capital,I\&C}$ the total cost of I&C DSR service per year (£)

$N_{I\&C}$ the maximum number of service requests of I&C DSR in a year

$P_{I\&C}$ the estimated real power reduction delivered by the I&C DSR customer

3.6.2 Proposed Control Strategy

CSF based decentralized control scheme

The proposed control strategy consists of two stages, an initial routine and the main control routine which runs the CSF algorithm. The initial stage detects a sustained under or over voltage condition at the key locations or critical nodes on the network and initiates the *ESS Buffer Mode*. The *ESS Buffer Mode* provides fast acting response ensures corrective action before other DSR services can be switched in. In addition, this control routine mitigates against the uncertainty in DSR response and voltage excursion severity. These critical nodes are identified by offline analysis utilizing the network model and data. By analysing the results of large numbers of load flow calculations, using annualised load data, the nodes that

are likely to experience sustained highest and lowest voltage can be determined. The nodes with the highest number of voltage limit violations recorded in the period will be designated as the critical nodes.

The proposed control strategy is illustrated in Figure 3.17. When the voltage at one of the pre-defined critical nodes violates the statutory limits of 0.94 pu and 1.1 pu, the *ESS Buffer Mode* is initiated and increases the ESS system real and reactive power export or import. An algorithm has been devised which seeks to optimize the capability of an ESS system to mitigate voltage problems. If the excursion persists, then the ESS is instructed to increase the real and reactive power import or export. The ESS is disengaged if the voltage returns within the ESS disengage voltage thresholds. This disengage thresholds are chosen so that the act of disengaging the ESS does not result in voltages moving outside the statutory limits.

The main control routine, which runs the VCSF algorithm and calls conventional DSR as well as ESS, will be initiated when the control system detects that the ESS has operated longer than the threshold of 10 minutes in the *ESS Buffer Mode*. The VCSF control algorithm will check the availability of all the DSR services first. The available DSR with the highest VCSF will be selected. Next, the selected DSR will be checked against branch thermal limits. The selected DSR will be excluded if it causes a thermal violation. The DSR with the second highest VCSF will then be selected and checked for thermal violation.

Following initiation of the VCSF routine, the *ESS Buffer Mode* routine adjusts the ESS outputs to minimise the use of the system while maintaining the voltages within the statutory limits. Moreover, in the case of an unsuccessful DSR service request or if the DSR is unable to correct the voltage excursion, the ESS real and reactive power setpoints will be adjusted such that the voltage is maintained within statutory limits.

The SOC of the ESS is managed by comparing the SOC with an SOC threshold. If $SoC > SoC_{Dischargethreshold}$ or $SoC < SoC_{Chargethreshold}$ and the voltage is less than or greater than the respective discharge or charge thresholds, the ESS starts to discharge or charge as necessary.

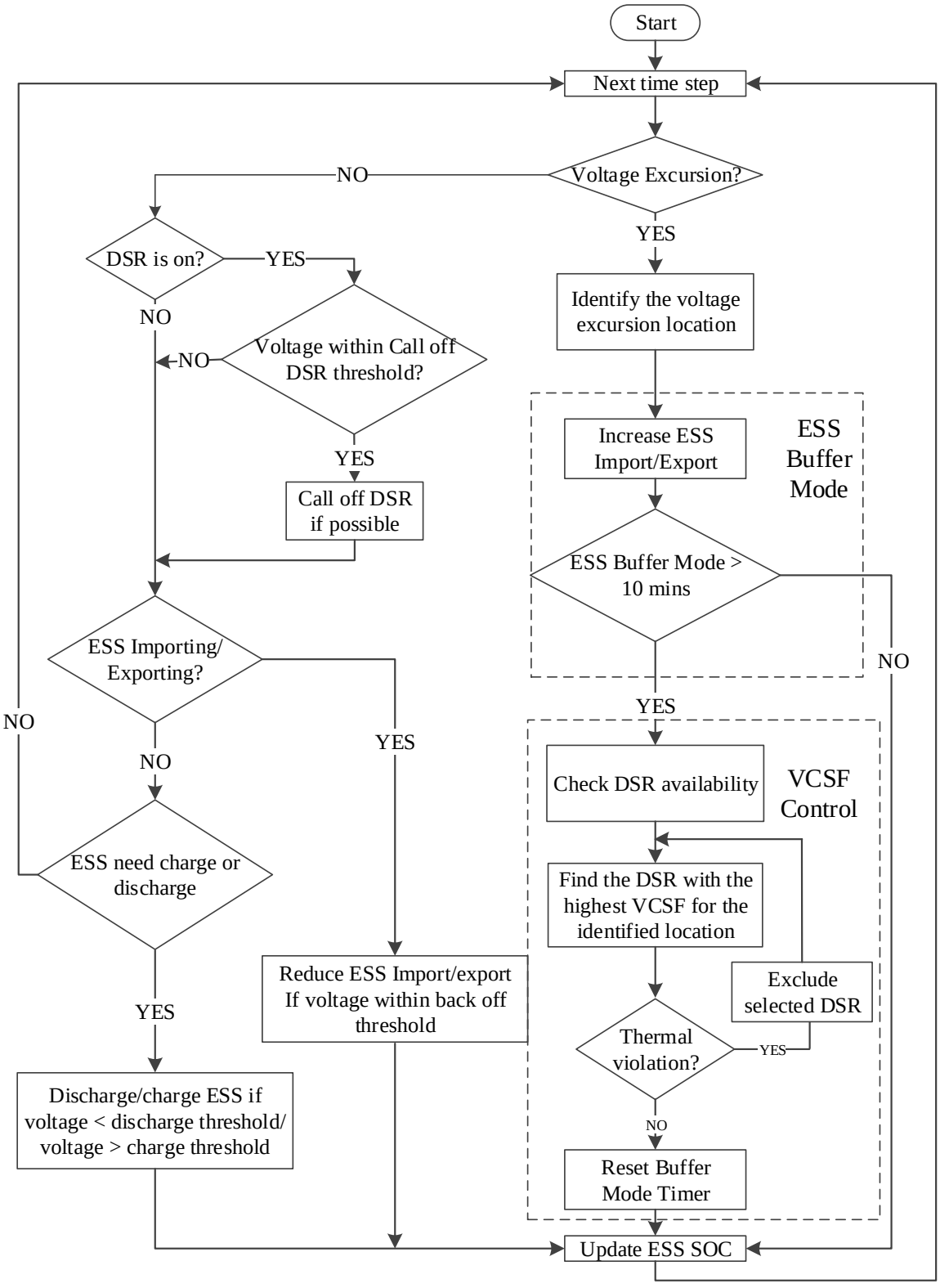

Figure 3.17 Flow Chart of VCSF Voltage Control Strategy

Real/reactive power setpoint algorithm

The real and reactive power import/export P_{ESS} and Q_{ESS} from the ESS is limited by the rated real power $P_{ESS,Rating}$, the rated reactive power $Q_{ESS,Rating}$and the apparent power rating $S_{ESS,Rating}$ of the ESS.

$$|P_{ESS}| \leq P_{ESS,Rating} \tag{3.13}$$

$$|Q_{ESS}| \leq Q_{ESS,Rating} \tag{3.14}$$

$$S_{ESS} = \sqrt{P_{ESS}^2 + Q_{ESS}^2} \leq S_{ESS,Rating} \tag{3.15}$$

where

$P_{ESS,Rating}$ the real power rating of ESS

$Q_{ESS,Rating}$ the reactive power rating of ESS

$S_{ESS,Rating}$ the apparent power rating of ESS

The real and reactive power import/export of the ESS will ramp up in the ratios specified by equation (3.16). This ratio minimises the apparent power import and export S_{ESS}. It has been proved that, the ratio of real and reactive power will vary depending on the location of voltage excursion.

$$\frac{P_{ESS}}{Q_{ESS}} = \frac{VSFP_{i,ESS}}{VSFQ_{i,ESS}} \tag{3.16}$$

where

$VSFP_{i,ESS}$ is the real power voltage sensitivity factor from ESS to busbar i

$VSFQ_{i,ESS}$ is the reactive power voltage sensitivity factor from ESS to busbar i

The proof of this conclusion is presented below. The voltage change ΔV_i at location i due to P_{ESS} and Q_{ESS} ·can be expressed as:

$$\Delta V_i = P_{ESS} \cdot VSFP_{i,ESS} + Q_{ESS} \cdot VSFQ_{i,ESS} \tag{3.17}$$

This can be re-written as:

$$Q_{ESS} = \frac{\Delta V_i}{VSFQ_{i,ESS}} - \frac{VSFP_{i,ESS}}{VSFQ_{i,ESS}} \cdot P_{ESS} \tag{3.18}$$

The line expressed by this equation is shown in Figure 3.18. S_{ESS} is the distance between the origin and the point (P_{ESS}, Q_{ESS}) along the line.

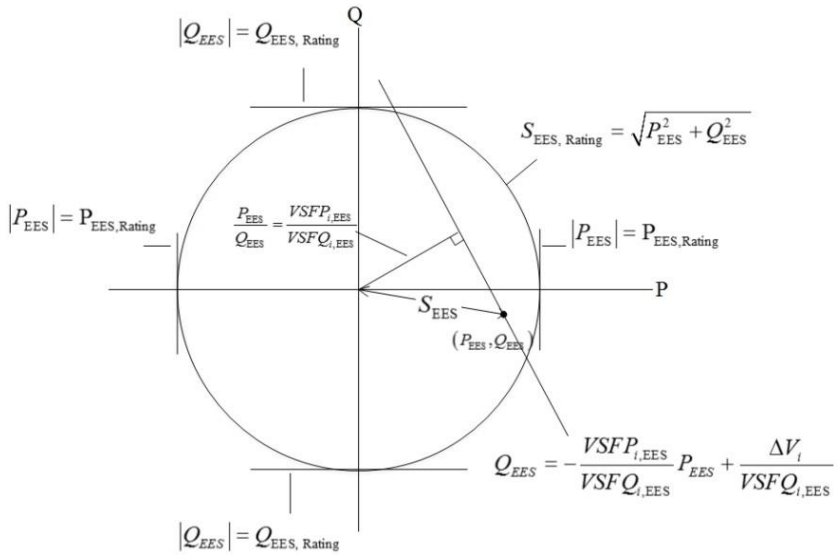

Figure 3.18 ESS Real/Reactive Power Setpoint Algorithm

It can be seen from Figure 3.18 that the minimum apparent power S_{EES} to provide the voltage change ΔV_i is expressed graphically by a line perpendicular to the original line which passes through the origin. The slope *m* of the line is given by

$$m = \frac{VSFQ_{i,ESS}}{VSFP_{i,ESS}} \tag{3.19}$$

3.6.3 Case Study Network

As illustrated in Figure 3.20, a representative rural network in the North East of England, owned by Northern Powergrid has been selected as the case study network. A detailed MV and LV network model has been built and validated by MV and LV measurements. A mechanically switched capacitor bank is already deployed on this system for voltage control purposes. The LV network schematic is given in Figure 3.19.

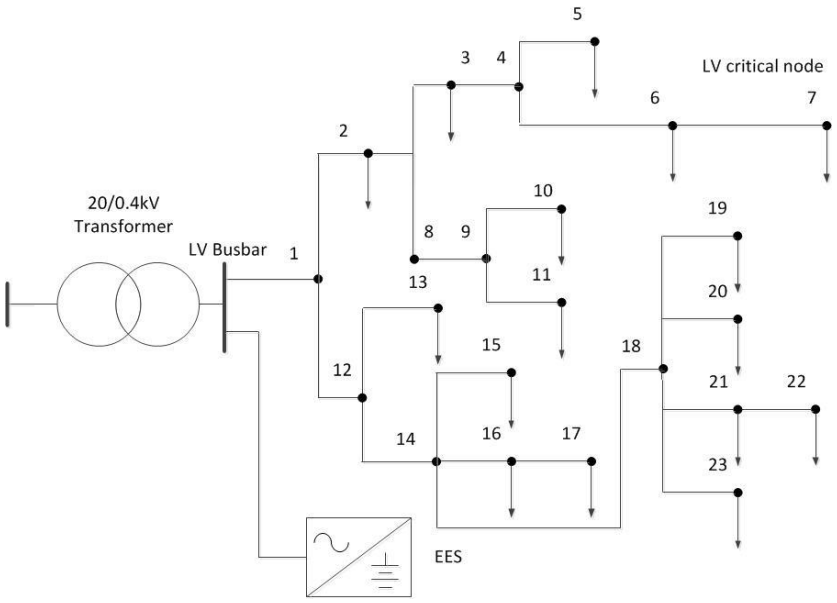

Figure 3.19 LV Network Diagram showing location of the EES device and connected loads.

Compared to the case study network presented in section 3.4.2, the location of smartgrid interventions and the size of ESS have been modified for the purpose of this study. I&C DSR customer A, an MV/LV substation and I&C DSR customer B locate toward the end of the MV feeder. As part of the CLNR project an ESS system has been installed on the LV side (0.4kV) of the MV/LV transformer. The system is located at the LV busbar to maximize its capability to mitigate voltage limit violations on the MV and LV systems. All residential customers in the LV network are assumed to be RDSR enabled.

The location of DSR B has been revised to facilitate the evaluation of this CSF based control scheme. In the case study scenario used in section 3.4, DSR A and DSR B are located next to each other and both upstream of the LCT cluster. As a result, the VSFs from DSR A and DSR B to the end of the MV and the LV feeder are identical. In this case study, DSR B is relocated downstream the LCT cluster. As shown in Table 3.1, this relocation increased the VSF of DSR B to the end of the MV and the LV feeder. With the same per MW cost, this arrangement makes DSR B a more effective solution to solve voltage limit violations.

Critical nodes have been defined by using the methodology introduced in section 3.6.2 and illustrated in Figure 3.20. SCADA data for a period of 18 months has been used as an input to the network model. Critical nodes were identified from running the network model for two scenarios

i. present SCADA data
ii. present SCADA data with post inclusion of the LCT devices.

In the second scenario investigated, the penetrations of LCTs are formulated on the assumption that there is a 30% domestic penetration rate of ASHPs and EVs evenly distributed across the LV LCT cluster of 230 residential customers. Alignment was found between the critical nodes for both cases.

The proposed decentralised control strategy is applied to mitigate voltage limit violations at the remote end of an MV feeder, over 25 miles in length, and the remote end of an LV feeder. Unlike a centralised control system, which coordinates other network interventions such as the capacitor bank, the local decentralized control system minimizes the requirement of communication.

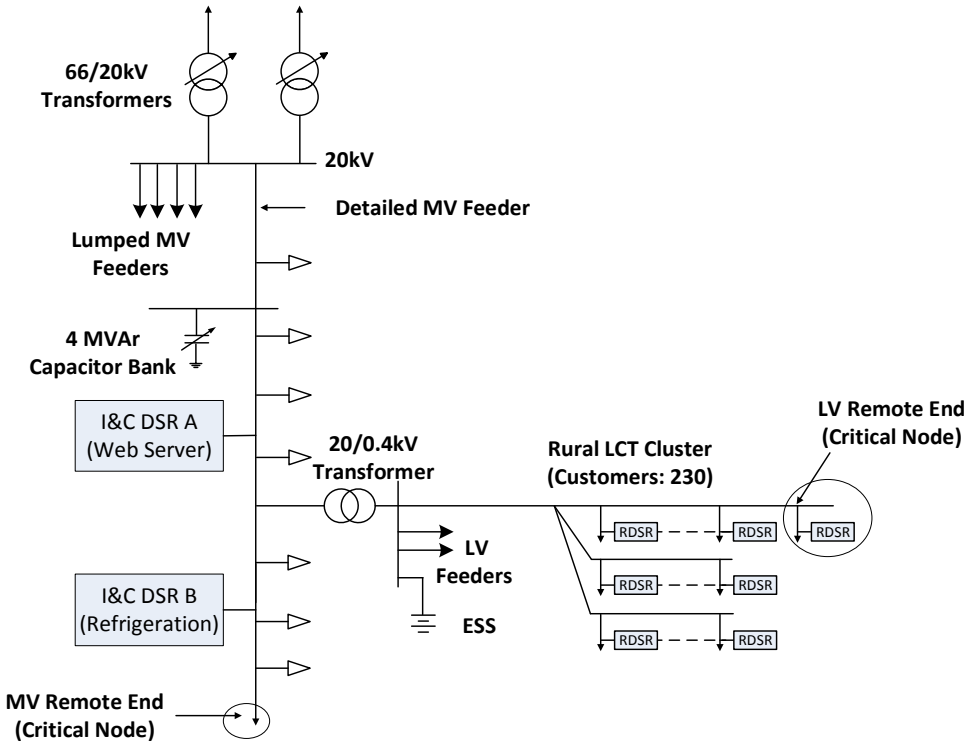

Figure 3.20 Schematic diagram of the case-study network with future scenario industrial and commercial customers

Average domestic load data from [107] has been applied to the residential customers in the LV network. [107] contains historical data from over 5000 domestic smart meter customers, covering the period from May 2011 to April 2012. This data set can be sub-divided into a number of individual categories, which contain details such as rurality, income, thermal building performance and age of the occupants. The original dataset was filtered by social variables in order to match the demographic of the case study network area. The domestic load profile based on the smart meter data is aligned with the actual customers in the case study area.

Previous work, has shown that LCT distributions tend to be clustered, for example a high penetration of new technologies along a particular LV feeder [108]. The ASHP consumer modelling method and approach is detailed in [101]. EV consumer modelling is based on real trial data from 19,872 charging events of 340 vehicles (electric, pure hybrid and fuel cell vehicles) from December 2009 to June 2011 [108].

DSR modelling

A high resolution energy demand model, the CREST demand model [109-111], was used to simulate detailed residential load data and assess when DSR appliances, wet appliances (washing machines, tumble driers and dishwashers as identified in [112]) were being used throughout a typical day. The CREST demand model was modified to reflect the location and the demographics of the consumers connected on the LV feeder, by calibrating the average household energy consumption to that of the regional average of 5,235 kWh annual electricity consumption [113] and the regional household size. The DSR resource profile, shown in Figure 3.21, was generated by averaging the simulation model over a run of 1000 for a typical January weekend. The synthesized data was validated against the real smart meter data to ensure that the simulated data was representative of the feeder.

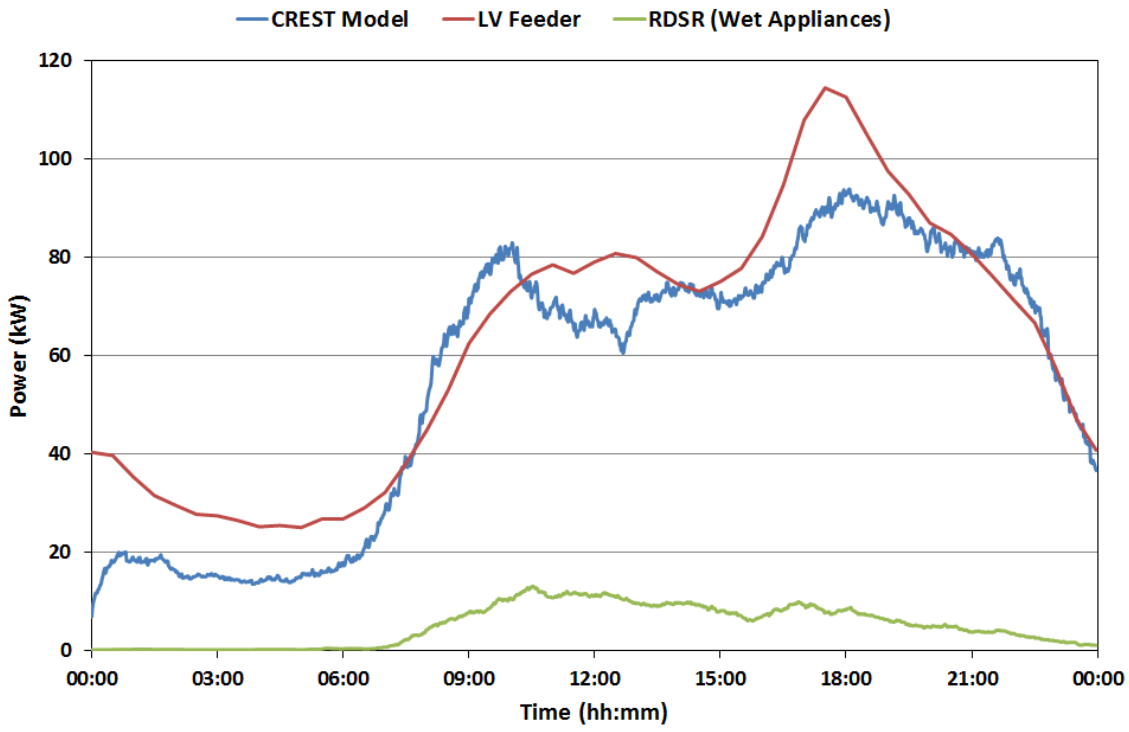

Figure 3.21 Rurality filtered aggregated smart meter, simulated and simulated wet goods load profiles of non-gas connected customers

In order to validate the RDSR simulation results, the total simulated domestic profile was compared against the derived smart meter load curve and was found to have a correlation coefficient of 0.90, it was therefore assumed that a degree of confidence could be taken that the DSR resource profile is also representative of the LV feeder This confirms that the simulated DSR resource profile was representative of the customers along the LV feeder.

RDSR is achieved with a broadcast call for demand reduction by delaying the start of RDSR wet appliances, and a reduction in HP demand and EV charging. In line with the participatory DSR approach taken, the time at which the displaced loads are redeployed is determined by the network user or residential consumer rather than the DNO. The EES system deployed in the CLNR project uses lithium ion iron nano-phosphate technology. The size of EES used in this case study has a real power and energy rating of 300 kW and 600 kWh, respectively.

I&C DSR customer models are based on the real half-hourly consumption figures recorded during the CLNR project DSR trials [101]. The delay time of I&C DSR was 10 minutes. I&C DSR services are provided in the forms of backup diesel generators (I&C DSR A) and reducing power consumption (I&C DSR B). The durations of the I&C DSR service are two hours.

VSFs, DSR costs and VCSFs

The VSFs for the case-study network critical nodes with respect to the nodes where DSR service was available were derived by running offline power flow calculations. These are given in Table 3.1. In the case where the DSR service is delivered by multiple consumers at multiple locations, as in the case of RDSR, the change in load is distributed evenly across all the consumers in the model. The resultant voltage change at the critical node and the total load change is used to calculate the VSF. All loads in the case study area are assumed to be constant power loads.

	LV critical node	MV critical node
RDSR	18.9×10^{-3}	3.55×10^{-3}
ESS	7.73×10^{-3}	3.52×10^{-3}
I&C DSR A	3.65×10^{-3}	3.27×10^{-3}
I&C DSR B	4.00×10^{-3}	3.60×10^{-3}

Table 3.1 Voltage Sensitivity Factors for Critical Nodes (pu/100kW)

The numbers in Table 3.1 represent the technical effectiveness of the smartgrid interventions for voltage control for the critical nodes. For instance, for the LV critical node, RDSR has the

highest sensitivity factor, therefore is the most effective intervention for dealing with voltage problem at the LV critical node. I&C DSR B has the highest VSF to the MV critical node and as a result is the most effective intervention. I&C DSR customer B is more effective than I&C DSR customer A for voltage control at the MV critical node because the electrical distance of I&C DSR customer B is closer than that of I&C DSR customer A.

The costs of the DSR services used in this study are summarised in Table 3.2. The costs are derived based on the cost functions defined in section 3.6.1. For RDSR it is assumed that an average of 15 service requests per year will be called with an overall value of £50/kW. The I&C DSR costs are example costs of the contractual arrangements that have been used as part of the CLNR project. The capital cost of ESS from the CLNR project has been used to estimate the cost of using ESS.

DSR	RDSR	ESS $(SoC = SoC_{Upper\_limit})$	I&C DSR A	I&C DSR B
Cost (£/kW)	3.33	15.00	0.90	0.90

Table 3.2 DSR Costs

The VSFs given in Table 3.1 can be seen as $\Delta V_i(\mathrm{pu/kW})$ and the costs listed in Table 3.2 can be expressed as £/kW. These VSFs and costs result in the VCSFs of DSR busbars to the critical nodes as shown in Table 3.3. The VCSFs are calculated based on equation (3.7).

VCSF	LV critical node	MV critical node
RDSR	$56.6\text{x}10^{-6}$	$10.7\text{x}10^{-6}$
ESS$(SoC = SoC_{Discharge_{threshold}})$	$5.20\text{x}10^{-6}$	$2.3\text{x}10^{-6}$
I&C DSR A	$40.6\text{x}10^{-6}$	$36.4\text{x}10^{-6}$
I&C DSR B	$44.4\text{x}10^{-6}$	$40.0\text{x}10^{-6}$

Table 3.3 Voltage-Cost Sensitivity Factors for Critical Nodes (pu/£)

Comparing Table 3.3 to Table 3.1, it can be observed that, for LV critical node, RDSR has the highest VCSFs due to the high VSF and low cost, therefore, in order to achieve the same voltage change at the LV critical node, RDSR results in the lowest cost. On the contrary, although the VSF from ESS to the LV critical node is higher than I&C DSR customers, the VCSF is lower due to its high cost. This indicates that the cost of using I&C DSR customers for voltage control of the LV critical node will be lower than using ESS.

For the MV critical node, as can be seen in Table 3.1 the VSFs of RDSR and I&C DSR customers are similar, however, due to the low costs of the I&C DSR customers, the I&C DSR customers would have lower cost for controlling voltage at the MV critical node.

Control System Architecture

Figure 3.22 illustrates the proposed decentralized control system architecture that has been modelled with the case study network. The network monitoring detects a sustained voltage excursion and the supervisory controller selects the DSR service with the highest VCSF, shown along the bottom of the figure, in order to resolve the network voltage violation. The supervisory controller has two functions. The first, shown by the equation on the left, calculates the optimum real power set point for the ESS to relieve the voltage excursion. The second control routine is initiated if the voltage excursion persists longer than 10 minutes. This routine evaluates the VCSFs to select the cost minimized DSR service to take.

As can be seen, I&C and RDSR service request is issued via a one way communication. It is assumed that there is a direct link between the controller and the I&C DSR customers. On the other hand, a broadcast command will be issued to all the RDSR customers when RDSR is requested. Communication between the ESS system and the controller is more detailed with the ESS returning data regarding its charge/discharge capability in real time. With knowledge of the ESS's state of charge (SOC), the supervisory controller can update the ESS cost function which indicates its capability to supply the desired response.

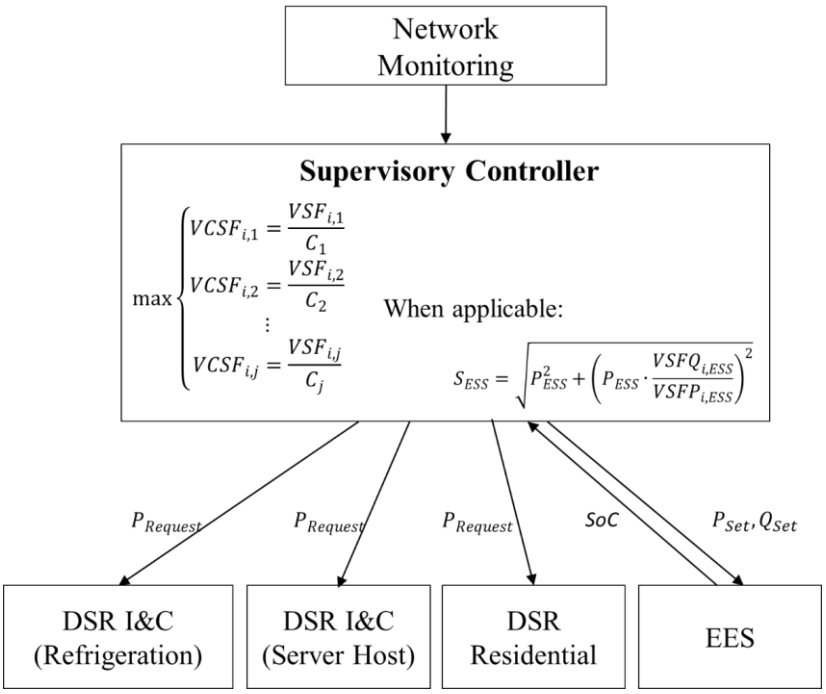

Figure 3.22 Supervisory DSR control system architecture

3.6.4 Results

To enable evaluation of the voltage control scheme SCADA data from the case study network, smart meter data and the LCT models have been used to develop realistic future scenarios and associated consumer load profiles. These load profiles exceed the capabilities of the existing network infrastructure and conventional infrastructural upgrade would be the most likely option to resolve this. The capability of the proposed control strategy to address the limitations of the existing network is evaluated by solving an MV and an LV voltage excursion, respectively.

MV voltage excursions on existing network infrastructure

The MV voltage excursion occurs during a spring weekday morning between 08:00 to 13:30. The MV and LV voltage profiles under the future scenario are illustrated in Figure 3.23. Four MV voltage excursions and an LV voltage excursion can be observed in this figure.

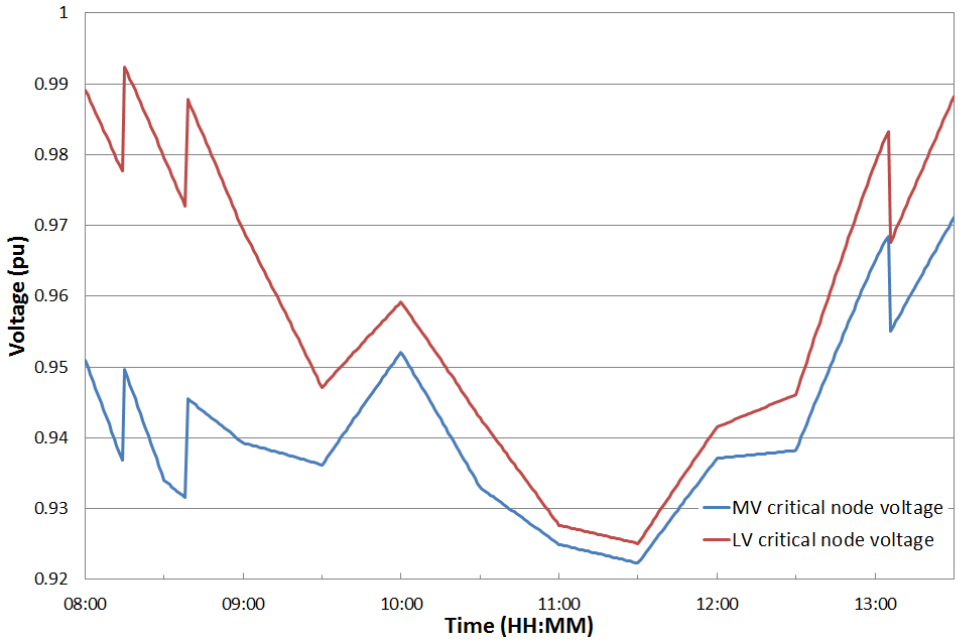

Figure 3.23 Voltage Profiles under Future Scenario Using Existing Network Infrastructure with No Control Actions

MV voltage excursion mitigation

DSR profiles during this excursion are plotted in Figure 3.24 and the voltage profiles with control action taken are given in Figure 3.25. When the first MV voltage excursion happens, the controller instructs the ESS to discharge. After 10 minutes, the under voltage excursion still exists and a DSR request is sent to I&C DSR customer B as it provides the cheapest DSR service at this time. The ESS reduces its export power when DSR B operation is confirmed and the MV voltage is above the reduce ESS export threshold. In this case study, the threshold

is 0.945p.u. The DSR B service comes to its end after two hours. ESS is used again in the buffer mode and DSR A is called to solve the continuing under voltage excursion.

It should be noted that the ratio of the real and reactive power output from the ESS system is 0.995 and as a result the real and reactive power curves cannot be clearly seen in Figure 3.24.

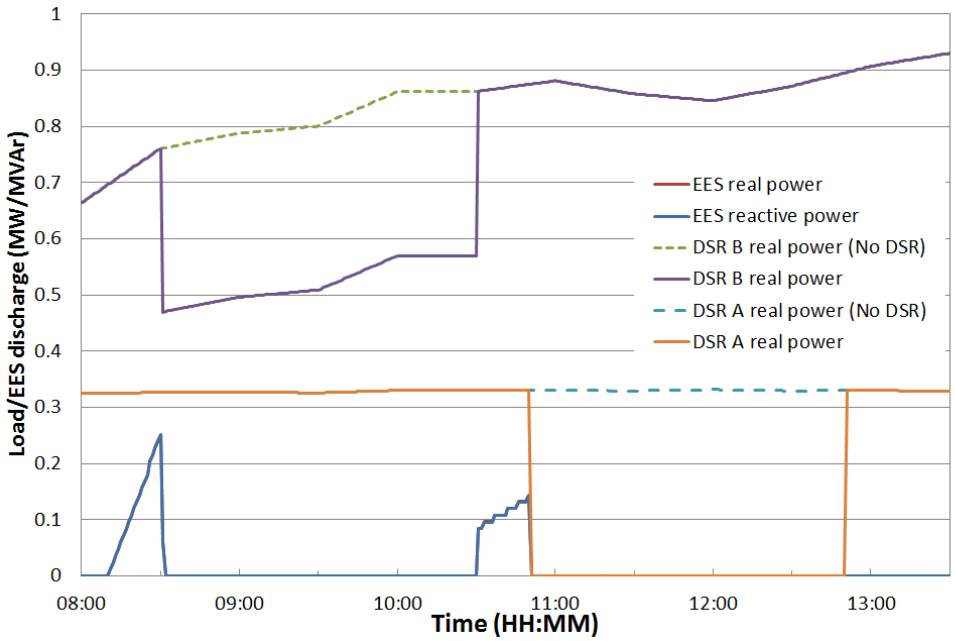

Figure 3.24 DSR profiles during MV voltage excursion control under future scenario with decentralised voltage control strategy

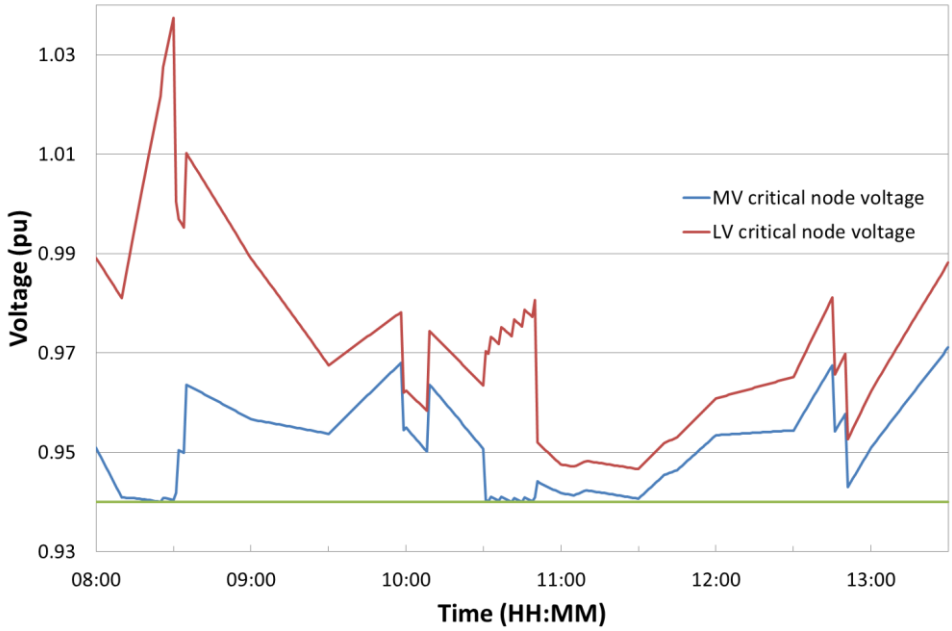

Figure 3.25 Voltage profiles with control actions under future scenario with decentralised voltage control strategy

LV voltage excursions on existing network infrastructure

The voltage profiles of an LV under voltage event during a winter weekend afternoon are illustrated in Figure 3.26. The LV voltage excursion occurs first and this is followed by an MV voltage violation.

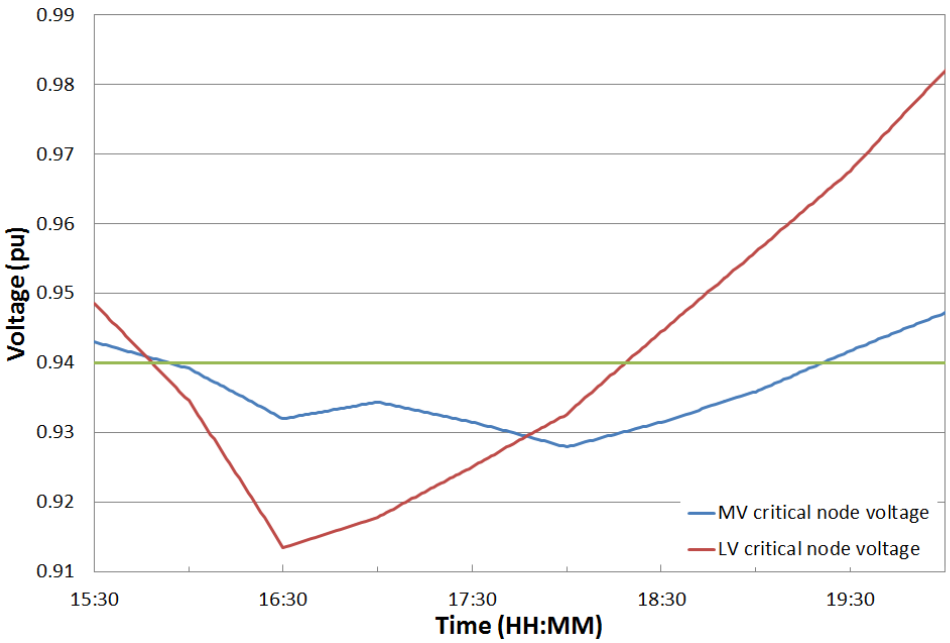

Figure 3.26 Voltage Profiles with No Control Actions

It can be seen in Figure 3.27, that RDSR service is called at the end of the ESS buffer mode as it has the highest VCSF with respect to the LV critical node even though the I&C DSR have larger potential reduction and lower costs (£/kW). In this simulation, it is assumed that a random percentage of customers between 60% and 80% respond to the DSR request and the percentage of customer responding at each LV node is equal.

At 17:20, a sustained MV voltage limit violation is detected and I&C DSR B service is requested. When the consumption of DSR customer B is reduced, the LV voltage is above the call-off RDSR threshold and RDSR is called off.

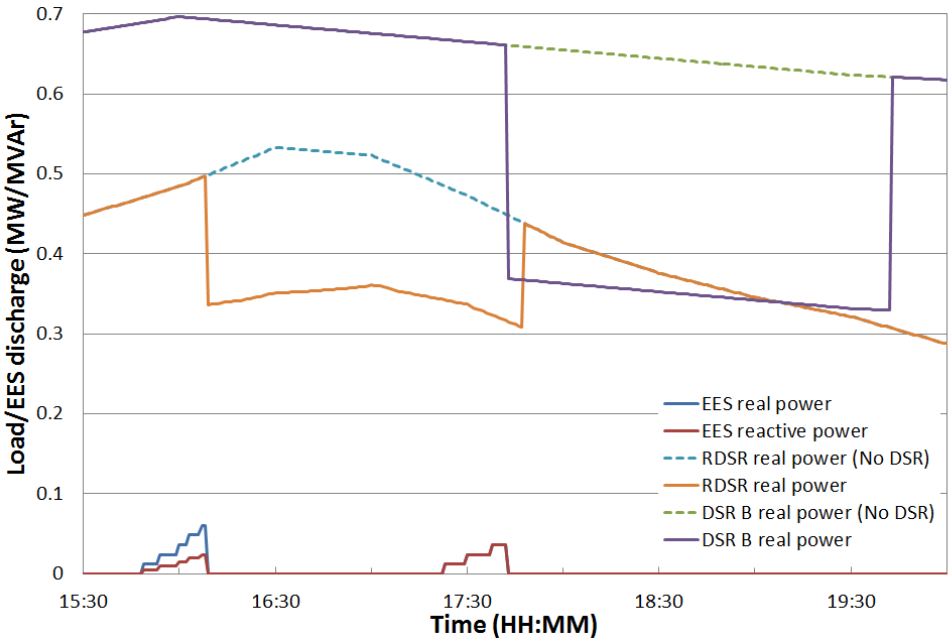

Figure 3.27 DSR profiles during LV voltage excursion

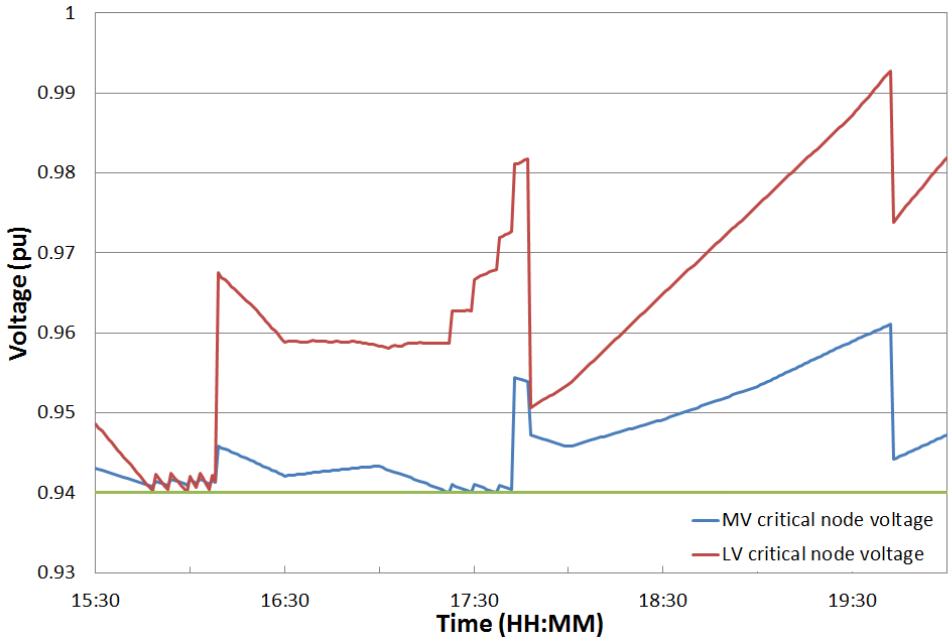

Figure 3.28 Voltage profiles with control actions during LV voltage excursion

3.6.5 Extension and Application of VCSF Based Control Scheme

The use of VCSF is extended by Want in [61]. In this paper, a coordinated voltage control scheme utilizing ESS is presented, for future distribution networks with large, clustered distributions of low carbon technologies (LCTs) in terms of both feeder and phase location. In this paper, ESS is used collaboratively with OLTC at the primary substation. OLTC changes the voltage of downstream feeders evenly. Therefore, in scenarios where one feeder has over voltage problem due to DG while another feeder has low voltage problem due to load and LCTs, OLTC is not able to solve the problem. In [61], VCSF is used to select the most

effective control intervention from a range of ESS which is then used reduce the voltage divergence between two feeders. Once the feeder voltage divergence factor is reduced within a threshold, OLTC can be applied to solve the voltage problem.

The benefits of the ESS integrated scheme over conventional voltage control schemes are demonstrated by realizing a set of network scenarios on a case study network both in simulation and in network-in-the-loop (NIL) emulation at a smart grid laboratory facility. The case study uses a rigorously validated model of an actual GB distribution network with multiple EES installations. It was found that the EES integrated voltage control scheme is able to provide increased capability over conventional voltage control schemes and increase the value of EES to network operation.

3.7 The Limitation of VSF and PFSF

VSF and PFSF linearize the non-linear power flow equations therefore it is important to understand their accuracy. VSF and PFSF are accurate estimations when the state of the network only changes slightly. The inaccuracy of sensitivity factors only has a small impact on the performance of the control schemes proposed in this chapter. The sensitivity factor and cost sensitivity factor based control schemes only use sensitivity factors to select the most effective control intervention. Besides, fast response ESS is used in buffer mode so that potential future excursions can be dealt with.

The derivative ${}^{\partial V_i}/_{\partial P_k}$ from the inverse Jacobian matrix is used to approximate VSF. However, as shown below

$$\frac{\partial P_i}{\partial V_j} = -V_i\left(G_{ij}\cos\theta_{ij} + B_{ij}\sin\theta_{ij}\right), i \neq j \quad \textbf{(3.20)}$$

$$\frac{\partial \Delta P_i}{\partial V_i} V_i = -V_i^2 G_{ii} - P_i \quad \textbf{(3.21)}$$

${}^{\partial V_i}/_{\partial P_k}$ is a function of G_{ij}, B_{ij}, V_i, P_i and θ_{ij}. G_{ij} and B_{ij} are network parameters depending on the topology of the network. V_i, P_i and θ_{ij} are decided by the operating point of the system. This means the derivative ${}^{\partial V_i}/_{\partial P_k}$ is not constant. Thus, for a fixed network, VSF is dependent on the operating point of the system. VSF and PFSF will change when the operating point of the system changes. The reasons for operation point change include but not limited to:

- Load increase and decrease
- Generation increase and decrease
- Generator connection or disconnection

- Line connection or disconnection
- Energy storage charge and discharge
- Capacitor bank operation
- On load tap changer (OLTC) operation

Due to the uncertainty of load and generation, the exact operating point of the system is unknown. Thus, it is very difficult to calculate accurate sensitivity factors in advance. Furthermore, when VSFs and PFSFs are used for ESS control, the operating point of the system after ESS is engaged is unknown before the control decision is made. Next, an example using the IEEE 14 busbar network is given to show the errors in VSF and PFSF. There are two reasons to use the standard IEEE network rather than a real distribution network. Firstly, in radial distribution networks, the sensitivity factors, especially PFSFs, are relatively constant due to the radial topology of the network. Secondly, tests carried out on a standard network can be more easily repeated. Therefore it is more appropriate to use the IEEE standard meshed network for the purpose of this study. The sketch diagram of the network is given below.

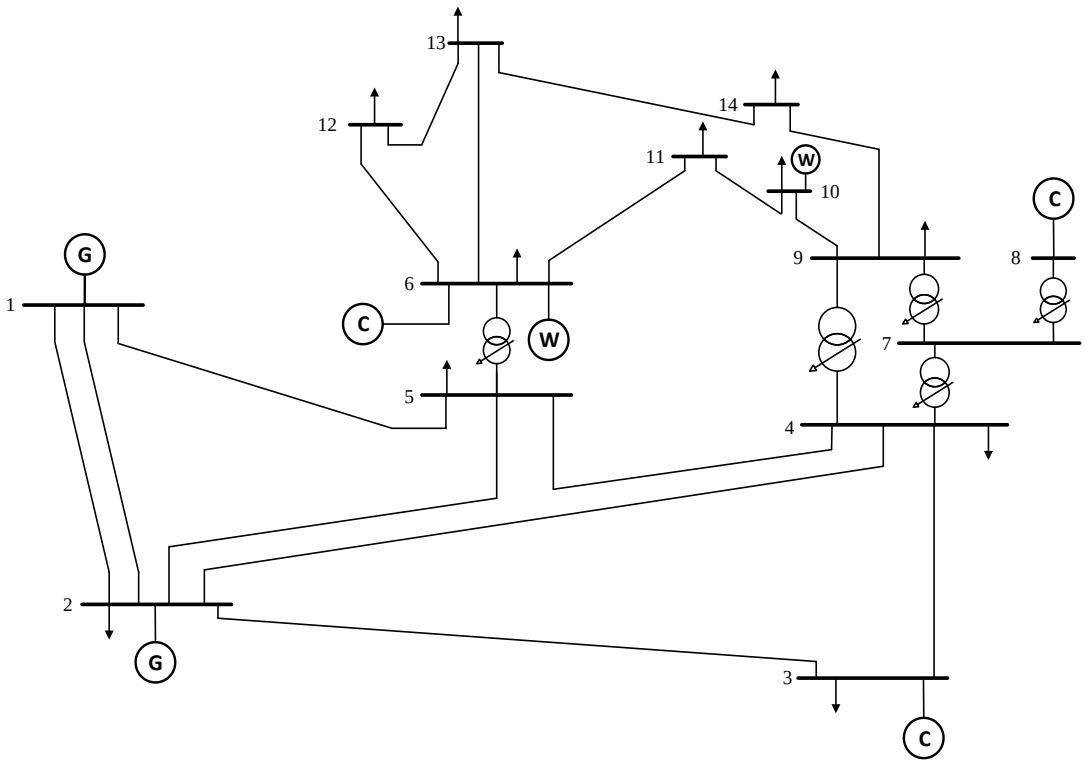

Figure 3.29 IEEE 14 Busbar Network

Firstly, VSFs are calculated based on Jacobian matrix. PFSFs, on the other hand, are derived from with DC loadflow. Next, both VSFs and PFSFs are calculated with the incremental

method. The VSF from bus 12 to bus 6 and the PFSF from bus 12 to branch from bus 9 to bus 14 are used for comparison.

3.7.1 VSF

As illustrated in Figure 3.30, the red dot is the VSF derived from the inversed Jacobian matrix $\boldsymbol{J}^{-1}$ while the blue trace is the VSF calculated with the incremental method. For the incremental method, the VSF is calculated as

$$VSF_{6,12} = \frac{\Delta V_6}{\Delta P_{12}} \tag{3.22}$$

Where

$VSF_{6,12}$ is the VSF from busbar 12 to busbar 6

ΔV_6 is the voltage change at busbar 6

ΔP_{12} is the power injection change at busbar 12

A series of ΔP_{12} values from 0.5MW to 10MW at a step size of 0.5MW have been used. The VSF is given in the unit of pu/MW. As can be observed, the VSF calculated by the Jacobian matrix method is larger than that of the incremental method. For the incremental method, the calculated VSFs reduce when ΔP_{12} increases.

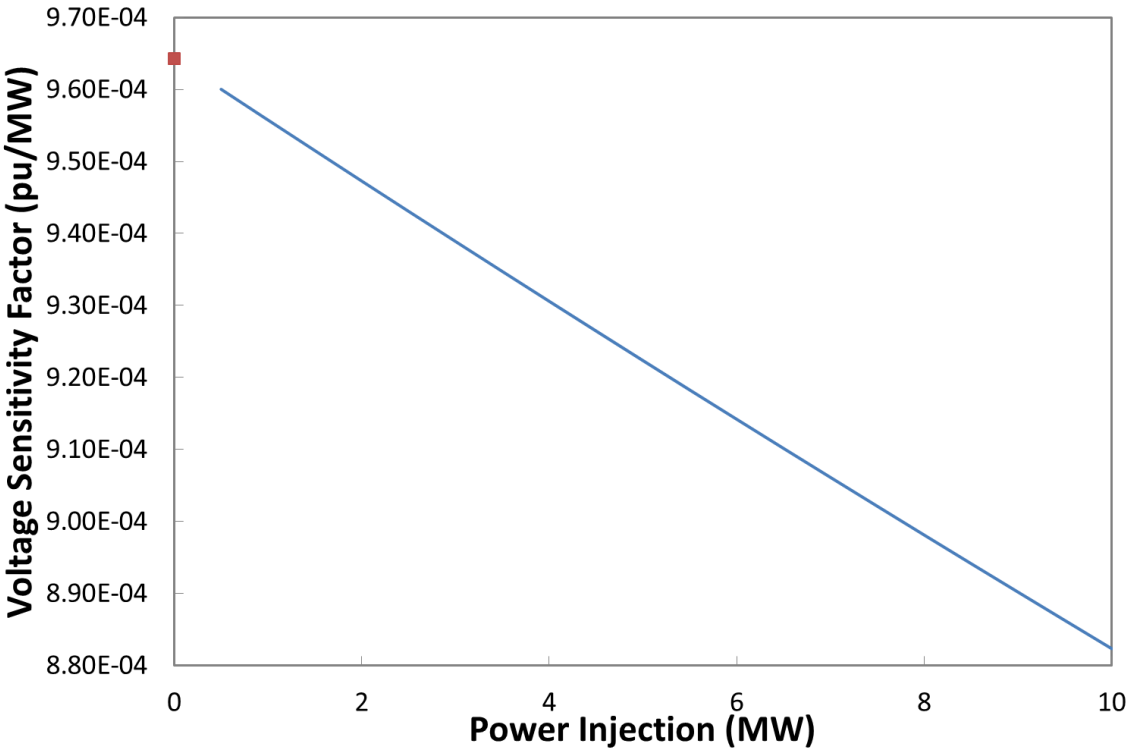

Figure 3.30 VSF based on Jacobian Matrix Method and Incremental Method

The VSFs calculated based on different methods are given in Table 3.4.

	VSF_{Jacobian}	$VSF_{\Delta P_{12}=0.5MW}$	$VSF_{\Delta P_{12}=10W}$
Calculation method	Jacobian Matrix	$\Delta P_{12} = 0.5\text{MW}$	$\Delta P_{12} = 10\text{MW}$
Value (1e-4pu/MW)	9.64	9.60	8.82

Table 3.4 VSF Results from Jacobian Matrix and Incremental Method based on $\Delta \boldsymbol{P_{12}} = \mathbf{0.5MW}$ and $\Delta \boldsymbol{P_{12}} = \mathbf{10MW}$

The voltage change at bus 6 due to a 10MW real power injection from bus 12, based on loadflow calculation, is 8.82×10^{-3}pu. To achieve the same voltage change, the power injection estimated by VSF_{Jocobian} and $VSF_{\Delta P_{12}=0.5MW}$ is

$$P_{\text{Jocobian}} = \frac{\Delta V}{VSF_{\text{Jocobian}}} = \frac{8.82 \times 10^{-3} pu}{9.64 \times 10^{-4} pu/MW} \approx 9.15MW \quad \textbf{(3.23)}$$

$$P_{\Delta P_{12}=0.5MW} = \frac{\Delta V}{VSF_{\Delta P_{12}=0.5MW}} = \frac{8.82 \times 10^{-3} pu}{9.60 \times 10^{-4} pu/MW} \approx 9.19MW \quad \textbf{(3.24)}$$

As can be observed using VSFs for voltage control without feedback can be inaccurate. The variation of VSF is not a linear process and is influenced by many factors. The nonlinear change of VSF is shown below in Figure 3.31. In this graph, VSFs are calculated under the same condition as the example given above. The power injection has been extended to 50MW. In this graph, the blue plain curve is the voltage of bus 6. The red plain curve is the VSF calculated based on the incremental method. The dotted straight lines indicate the corresponding trends of the plain curves. As can be observed, both the voltage and VSF change is not linear.

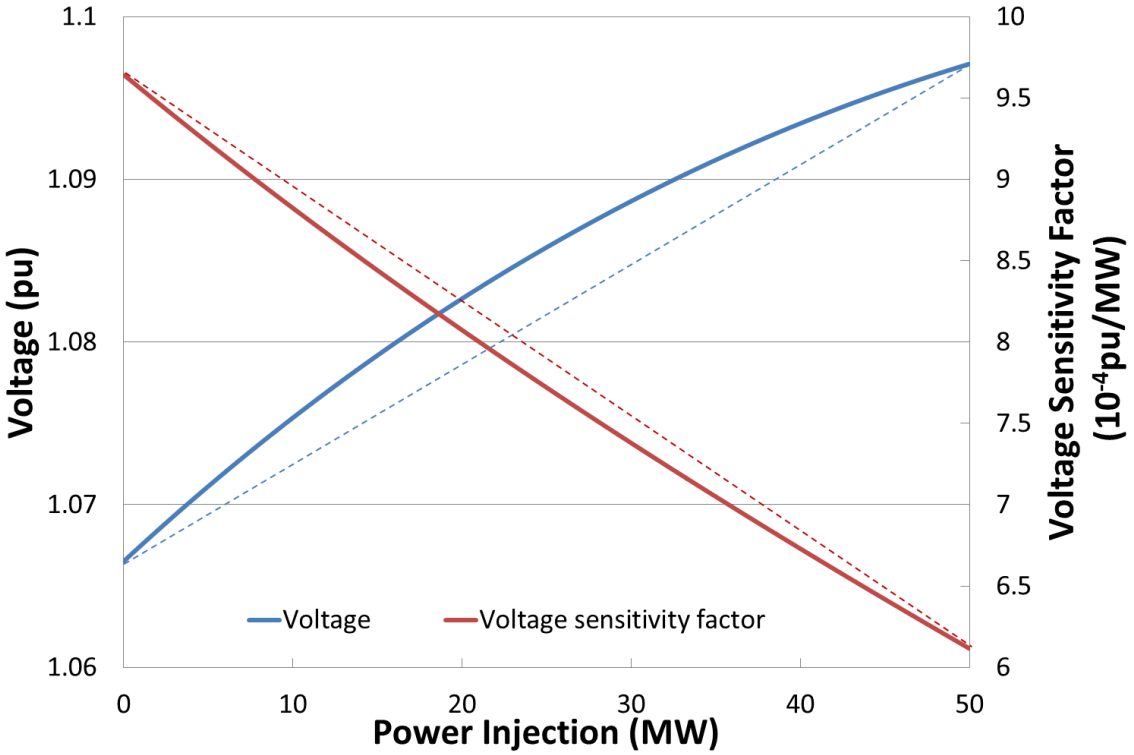

Figure 3.31 Voltage and Voltage Sensitivity Factor Change due to Power Injection

3.7.2 PFSF

PFSF calculated from DC loadflow and the incremental method is illustrated in Figure 3.32. The PFSF calculated by DC loadflow method is 0.19MVA/MW while the PFSFs calculated by the incremental method are 0.14MVA/MW approximately.

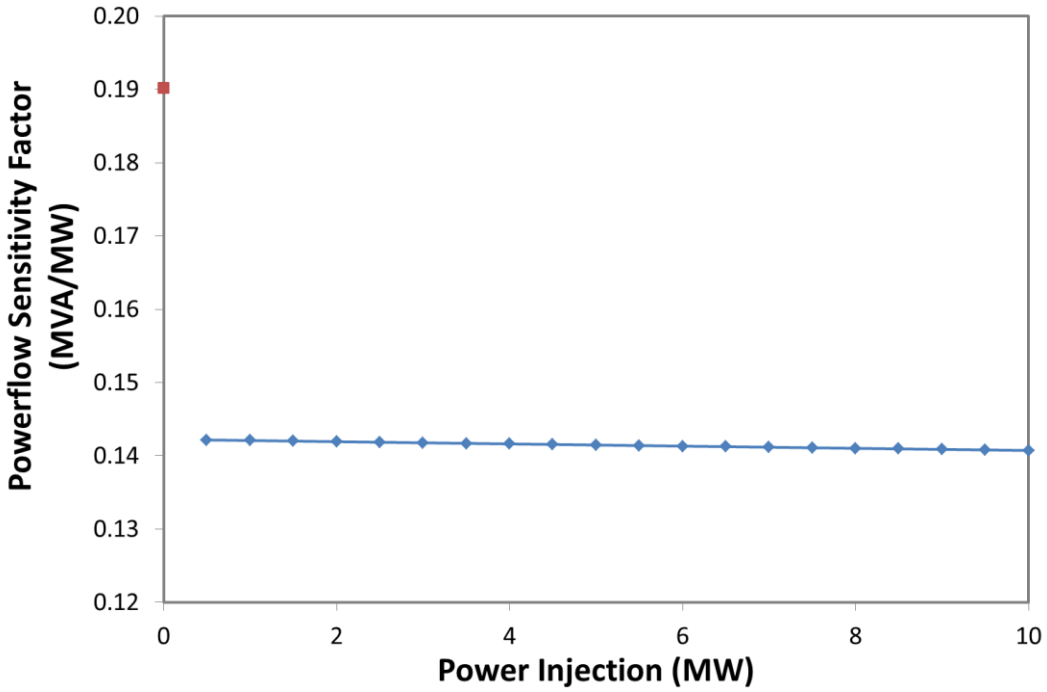

Figure 3.32 PFSF based on Jacobian Matrix Method and Incremental Method

3.8 Discussion and Conclusion

In this chapter, VSFs and PFSFs are introduced. VSFs and PFSFs represent the busbar voltage or branch powerflow change due to a change of busbar net power injection. Two methods to derive VSFs and PFSFs are detailed in section 3.2 and section 3.3. VSFs and PFSFs can be derived from power flow calculation process or calculated by the incremental method. The partial derivatives of the voltage magnitude or angle to the net real or reactive power injection can be used to calculate VSFs and PFSFs. DC loadflow is also used to calculate PFSFs due to its simplicity, compared to full AC Jacobian matrix. On the other hand, the incremental method calculates the sensitivity factors by comparing two loadflow results. When the real power injection change ΔP_k or the reactive power injection change ΔQ_k is small, loadflow based sensitivity factor calculation methods are more accurate. DC loadflow based method can be inaccurate when applied to distribution networks due to its assumptions. The incremental method is relatively easier to implement and more flexible. The incremental method can be configured to calculate apparent power related sensitivity factors such as ${}^{\Delta V_i}/_{\Delta S_k}$ and ${}^{\Delta S_{ij}}/_{\Delta S_k}$. This characteristic is important for smartgrid technologies such as ESS and DG, which have four-quadrant operation capability. For ESS, the use of a combination of real and reactive power can reduce the power and energy requirements [31]. Furthermore, as shown in section 3.6.3, the incremental method is also suitable to calculate the SFs from a cluster of RDSR customers. However, as shown in section 3.7, one challenge for the incremental method is the selection of an appropriate power change $\Delta S_k/\Delta P_k/\Delta Q_k$.

In section 3.6, VCSFs and PFCSFs are proposed to enable a control strategy to evaluate an intervention using both technical and commercial considerations. The value of using DSR for voltage control in comparison with conventional techniques has been investigated. Multiple forms of DSR (three in case study) with varying magnitudes, locations and characteristics have been considered in this chapter. Cost functions for ESS, I&C DSR and RDSR have been developed, based on the cost of real ESS systems, real I&C DSR trial contracts and the value of RDSR to DNOs respectively. Electrical distance between the smart grid interventions and the location of the voltage excursions have been taken into account by utilizing VSF. The concept of VCSF is derived based on the cost functions and VSFs to quantify the effectiveness of voltage control with operating various DSR at a unit cost.

The strategies have been evaluated using a validated real network model and a realistic future scenario extrapolated from a large smart meter data set, which considers social, technical and commercial aspects, SCADA data and EV charging and ASHP loading profiles based on

literature and previous work. In this scenario the present voltage control system is no longer able to function successfully. The RDSR models developed in this work utilise an improved CREST demand model. The I&C DSR models are based on real trial results and the ESS model based on real device have been adopted.

The evaluation illustrates how the control strategy can be used as an attractive alternative to network reinforcement to solve the uncertain voltage problems due to the unpredictable rate and distribution of LCT installations. The proposed methods require no knowledge of the probability density functions (PDFs) of DSR uncertainty. However, the limitations of the proposed control schemes include:

- The proposed schemes are passive control schemes which respond to measurements. Without forecast and planning, such schemes may be inadequate to deal with predictable future excursions. An example is given below. In Table 3.5, two available DSR services are given for illustration purposes.

•	PFSF(MVA/MW)	Cost (£/MW)	PFCSF (MVA/£)	Magnitude (MW)	Total cost (£)
DSR A	0.5	5	0.1	10	50
DSR B	0.5	10	0.05	2.5	25

Table 3.5 An Example of Two Available DSR Services to Solve an Thermal Violation

As can be seen in Table 3.5, it is assumed DSR A and DSR B have the same PFSF to a branch. Due to DSR A's lower per MW cost, it has a higher PFCSF. However, the total cost of using DSR A, which is the product of cost and magnitude, is higher than that of DSR B. Both DSR are capable to solve the 1MW thermal violation of the branch. Thus, the DSR service with higher PFCSF, DSR A in this case, will be chosen despite the fact that DSR B is able to solve the thermal violation with a lower total cost.

- Compared to optimization based techniques, such as OPF, the proposed schemes may not able to provide a solution with minimum cost.
- The proposed control schemes do not take into consideration the timescale of ESS and DSR. ESS SoC management is critical to maximize its value. Due to the current high cost, under-utilised ESS is unlikely to be cost beneficial while over charge or discharge ESS can damage its state-of-health (SoH).

- In the presence of a range of source of uncertainties, conventional methods which fail to understood, manage and plan for uncertainties appropriately can result in expensive use of ESS and DSR.

Chapter 4. Uncertainties in the Power System

4.1 Introduction

Uncertainty exists in the process of power system analysis, control, scheduling and planning. As shown in Chapter 2, most techniques assume that the input data is certain and accurate and the output or decisions can be implemented with little or no error. However, this is not always the case. This chapter examines sources of uncertainty involved in a power system scheduling problem. The uncertainties reviewed in this research include load, wind speed and wind power, real time thermal rating, state-of-charge estimation error and I&C DSR.

To deal with uncertainty, two main types of methods can be used. The first type is to use conventional methods with extra margins, such as extra generation reserve or increased reserved capacity. The second type is probabilistic methods. The state of the art of probabilistic methods to deal with uncertainty in power system analysis and control is reviewed in section 4.3. Probabilistic methods reviewed in this chapter include point estimation methods (PEM), cumulant based method, chance constrained programing (CCP) method and Monte Carlo simulation (MCS). As part of this thesis, MCS is used to investigate the impacts of electric vehicle (EV) charging. This example shows how MCS can be used for complex systems. In section 4.5, a literature review of using robust optimization (RO) techniques to deal with uncertainty is given. In the conclusion, a comparison between probabilistic methods and RO techniques are included.

4.2 Source of uncertainty

4.2.1 Load Forecast Uncertainty

With the adoption of low carbon technologies (LCTs), electricity demand becomes potentially more volatile and non-linear. Accurate very short term (VST) and short term (ST) load forecasting, therefore plays an important role in DN control and scheduling. Very short term load forecast (VSTLF) refers to predictions ranging from minutes to hours. Short term load forecast (STLF) covers the range from one hour to up to a week [114].

The time range covered by these two categories of predictions techniques is suitable for the scheduling of ESS and DSR in hours-ahead or day-ahead application. Therefore, in this section, the performance of state-of-art VST load forecast and ST load forecast techniques are reviewed and compared. The performance of the algorithms is compared using mean absolute percentage error (MAPE) as a common metric.

MAPE is defined as,

$$MAPE = \frac{100}{N}\sum_{t=1}^{N}\left|\frac{Real_t - Pre_t}{Real_t}\right| \quad \textbf{(4.1)}$$

Where

$MAPE$	is mean absolute percentage error
$Real_t$	is the real value
Pre_t	is the predicted value
N	is the number of samples
t	is the index for the sample

The review provided in this section focuses on the performance of ST and VST load forecast techniques, which has a direct impact on the performance of scheduling algorithms. However, it is difficult to have a fair comparison between different techniques because they are tested on different networks with different voltage levels, number and type of customers.

Paper [114] proposes a methodology for VST load forecast. The case study network has a peak load of 35.96MW. Tests are carried out for normal weekday and special days such as Thanksgiving Day. For normal days, the proposed multi-objective forecasting method has a minimum MAPE of 0.987% and a maximum of 2.040%. For special days, the corresponding number is 1.034% and 1.642%. The computing time of the proposed method is within 1 minute for the case study network. Autoregressive moving average (ARMA) has a worse performance and the minimum MAPE for normal day and special day is 2.453% and 1.673%, respectively.

Zhang proposed an ensemble model of extreme learning machine (ELM) in [115]. ELM features fast learning speed however suffers from stability problems. By taking an ensemble learning scheme, ELM can be used for high quality load forecasting. The proposed model is tested with historical data and compared with a back-propagation neural network (BPNN) and radial basis function neural network (RBFNN). Simulation results show that the proposed method has a better performance than single ELM, BPNN and RBFNN method. The MAPE of the ensemble ELM model is 1.82% and that of single ELM, BPNN and RBFNN is 2.89%, 2.93% and 2.86%, respectively.

A modified general regression neutral network (M-GRNN) is proposed in [116] for higher forecasting speed and a procedure to automatically reduce the number of inputs. Tests are carried out for load at HV and MV substations. Simulation results show that for global load, the MAPE is between 2.76% to 3.46% and the calculation time is less than 0.01 second. For

MV substation, the MAPE is between 2.58% to 8.60% approximately. The relationship between the voltage level and capacity of substations and the MAPE is not obvious. However, the MAPE for MV substation is greater than that of HV substation due to smaller number of customers.

In paper [117] Fan developed a semi-parametric additive model to estimate the nonlinear relationship between the demand and the driver variables. The forecasting result is compared with an artificial neural network (ANN) based model and a hybrid model proposed in [118]. The average MAPE of the proposed additive model, ANN and the hybrid model is 1.88%, 2.81% and 2.14%, respectively. The maximum and minimum MAPE of the additive model is 2.38% and 1.41%. The peak load of the case study network is 10 approximately GW.

A semi-parametric additive model is developed in [119] for local short and middle term load forecasting. 10 minute measurement data from 2260 substations have been used. Both middle term and ST forecast have been carried out in this paper. For ST load forecast, forecast results have MAPE values of 1.4% and 1.9%, depending on the temperature input. It is also found that a three-day ahead forecast temperature data with a MAPE of 30% will introduce an extra 0.5% error in the result.

The results achieved by the methods examined in this section are summarised below in table 4.1

Method	MAPE	Comments
GP Ensemble [114]	0.99 - 2.04%	Normal days
ARMA [114]	2.45 – 7.85%	Normal days
GP Ensemble [114]	1.03 – 1.64%	Special days
ARMA [114]	1.67 – 15.40%	Special days
Single ELM [115]	2.89%	Generalised performance
ELM ensemble [115]	1.82%	Generalised performance
BPNN [115]	2.93%	Generalised performance
RBFNN [115]	2.86%	Generalised performance
M-GRNN [116]	2.76 – 3.46%	Global load: HV substations
M-GRNN [116]	2.58 – 8.60%	Local load: MV substations
Additive model [117]	1.41 – 2.38%	Approximately 10 GW of load
ANN [117]	2.81%	Approximately 10 GW of load, averaged results
Hybrid model [118]	2.14%	Approximately 10 GW of load, averaged results
Additive model [119]	1.4 – 1.9%	

Table 4.1 Summary of Very Short Term and Short Term Load Forecast Results

The performance of VST and ST load forecast depends on the methodology adopted, the accuracy of input data, normal or special day, number of customers in the network etc. As a result, it is difficult to draw a simple conclusion of the uncertainty level or distribution of VSTLF and STLF. The case study networks in [114], [116] and [119] are high voltage and medium voltage distribution networks and at the same time, the computational time of the proposed methods is suitable for real time application. As a result, based on the test results presented, it is reasonable to assume that the uncertainty of VST load forecast and ST load forecast for distribution network is 1% to 10%.

Some load forecast procedures only give a estimation point but not the distribution of error [120]. Most sources drawn from literature only give an average MAPE value, such as [114], [116] and [119]. Paper [117] listed the results for 48 steps in a day but the sample size may not be large enough for statistical analysis.

4.2.2 Wind Forecast and Windfarm Output Forecast

This section reviews the errors in wind and windfarm output forecast. It should be noted that, the distribution of wind speeds is different to the distribution of wind speed forecast errors. As illustrated in Figure 4.1, the distribution of wind speed demonstrates the variability of wind speed over a period of time. On the other hand, the distribution of wind speed forecast error shows the likelihood of wind speed forecasting being inaccurate. Similarly, the distribution of wind power and wind power forecast errors are different concepts. The error of wind speed forecast and wind power forecast has more impact on the performance on the controllers and schedulers; therefore this section investigate the error of wind speed forecast and wind power forecast.

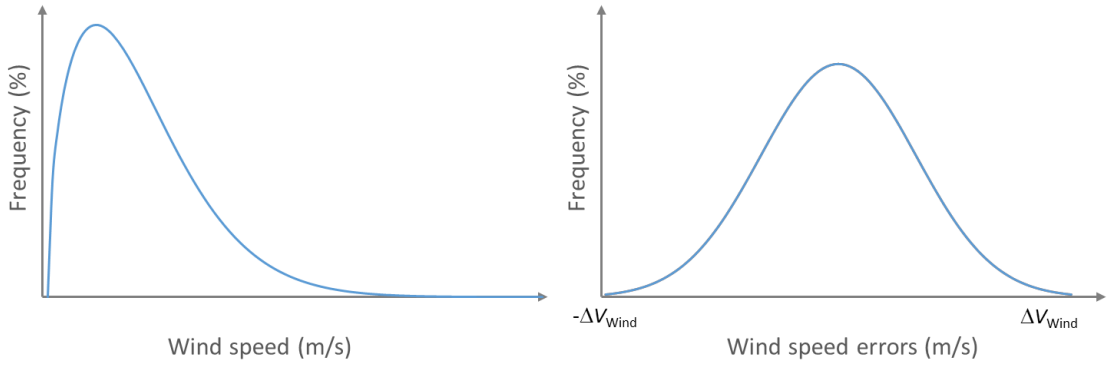

Figure 4.1 Illustration of the Difference between the Distribution of Wind Speed (Left) and the Distribution of Wind Speed Error (Right)

There is limited work on the error of wind speed forecast and wind power forecast. Wind speed and wind power forecast errors for six wind farms have been studied in [121]. Wind speed is predicted for 6, 12, 18, 24, 36 and 48 hours ahead. Real wind speed is measured every 5 minutes. The predicted wind speed is compared to hourly-averaged real wind speed. The forecast value pre_t and the measured value $real_t$ is compared in root mean square error (RMSE). RMSE is given as

$$RMSE = \sqrt{\overline{\varepsilon^2}} = \sqrt{\overline{(pre_t - real_t)^2}} \tag{4.2}$$

Normalized RMSE is given as

$$NRMSE = \frac{\sqrt{\overline{\varepsilon^2}}}{\overline{pre_t}} = \frac{\sqrt{\overline{(pre_t - real_t)^2}}}{\overline{pre_t}} \tag{4.3}$$

It is found in this paper the RMSE for wind speed forecast generally increases over the prediction horizon. For one of the test wind farms, the normalized RMSE at 6 hours is 38% and that of 48 hours is 55%.

An example of forecast errors for one of the test sites are illustrated in Figure 4.2. The predicted values are for one of the windfarms for 12 hours ahead at 10 meters height. The errors between predicted values and the measurements are plotted as shaded histogram. The solid line shows a normal distribution with the same mean and SD. It can be seen that the distribution of the errors reasonably follow a normal distribution.

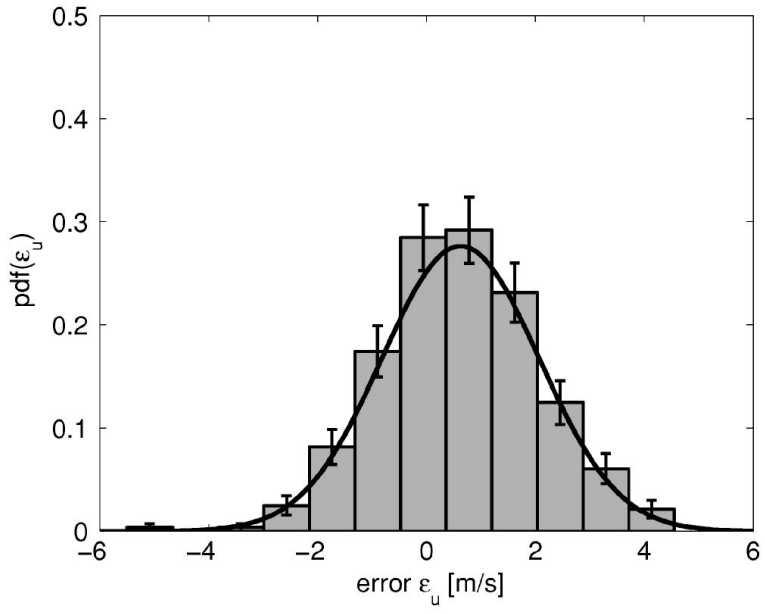

Figure 4.2 Probability density of Wind Speed Forecast Errors (12hours ahead) for One of the test wind farms [121]

However, the error in wind power does not follow normal distribution. An example of wind power forecast error is given in [121].

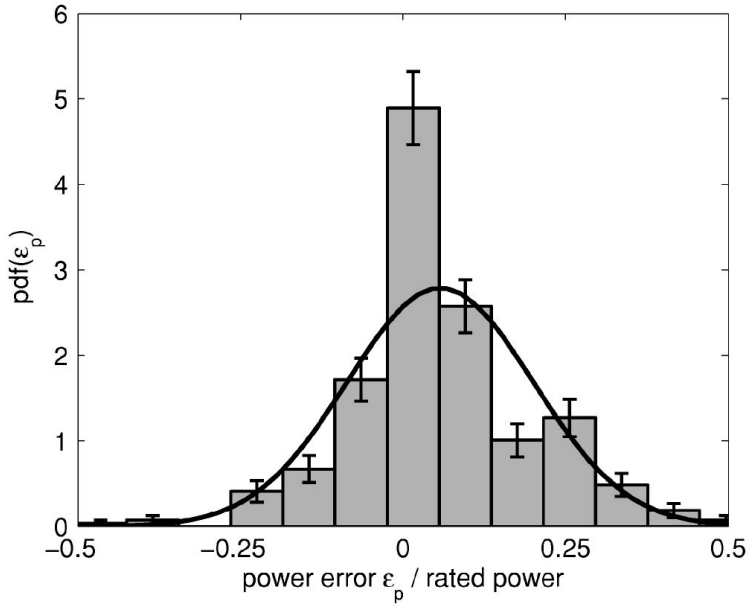

Figure 4.3 Probability density of Wind Power Forecast Errors (12hours ahead) for One of the test wind farms [121]

Due to the non-linear relationship between wind speed and wind power, wind power forecast error is difficult to be obtained. Different conclusions have been given regarding the distribution of wind power forecast error. In [122], wind power forecast error is divided into 50 bins and it is found that the error follows a Beta distribution. In [123] it is found that the distribution of wind power forecast error is fat tailed so that it cannot be modelled as a normal distribution. Kurtosis is used to check the tail of the distribution. The kurtosis κ of a distribution whose mean $\mu = 0$ is defined as

$$\kappa = \frac{E(\varepsilon^4)}{\sigma^4} \tag{4.4}$$

In which, ε is normalised prediction error, σ is the standard deviation and E is the expectation operator,

$$E(x) = x_1 \cdot pr_1 + x_2 \cdot pr_2 + \cdots + x_k \cdot pr_k \tag{4.5}$$

Where pr denotes the probability. When $\kappa > 3$, the distribution is a fat-tailed distribution. A histogram of 24-h forecast error data with $\kappa = 4.8$ is plotted with a Gaussian and a Laplace PDF. It can be seen that the distribution of error fits better with a Laplace distribution.

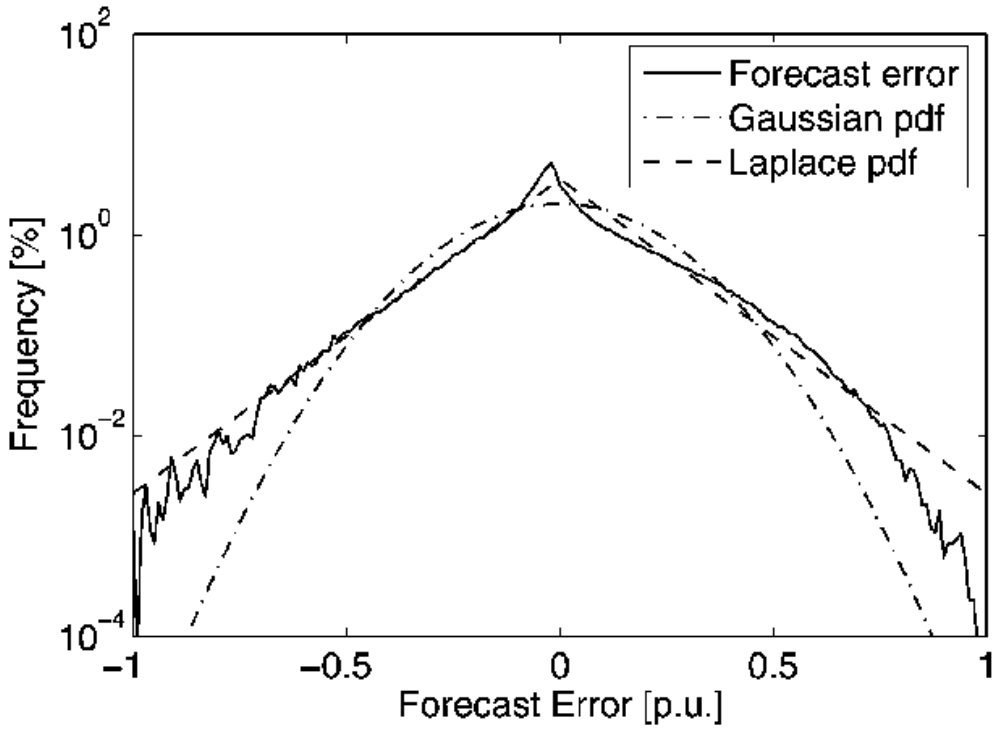

Figure 4.4 Comparison of a histogram of 24-h forecast error data (kurtosis 4.8) with Gaussian and Laplace pdf having the same standard deviation as the forecast error [123]

A Beta PDF is used to describe the error and good alignment was found. The studies of [121-123] are carried out with wind power data of a least 6 hours intervals. In [124], the distribution of wind power forecast error is examined at various and smaller intervals. The study in this work shows that Cauchy distribution outperforms other types of distributions.

In conclusion, it can be seen that the distribution of wind power forecast error is difficult to be represented by distribution functions accurately. Most wind forecast models or techniques gives a single-value point forecast [123, 125]. However, techniques which can provide wind power forecast with intervals are available. In [126], two neural network based methods have been used for short term wind power generation forecast. The proposed methods construct prediction intervals with 90% confidence level. ELM method has been used in [127] and simulation results show a good performance. A hybrid intelligent algorithm combining ELM and particle swarm optimization (PSO) is proposed in [128] and proved effective.

4.2.3 Real Time Thermal Rating

The accuracy of RTTR calculation can be influenced by component thermal model input error [129, 130] and environmental conditions [25, 131, 132]. Michiorri carried out sensitivity analyse on how environmental conditions effect real time rating. In this paper, RTTR models of overhead lines, electric cables and power transformers are introduced.

The maximum current capacities of OHL, electric cables and transformers are non-linear functions of the environmental factors such as air temperature and wind speed. For instance, to calculate the maximum current for a given operating temperature of OHL, the energy balance, as described below, needs to be maintained

$$q_c + q_r = q_s + I^2 r \tag{4.6}$$

Where

q_c the convective heat exchange

q_s the impact of solar radiation

q_r the radiative heat exchange

I the current on the OHL

r the resistance of the OHL

The radiative heat exchange is function of conductor temperature T_c and air temperature T_a

$$q_r = C_{q_r}(T_c^4 - T_a^4) \tag{4.7}$$

Where

C_{q_r} a coefficient to account for factors such as emission effect

As can be observed from equation (4.6) and (4.7), the maximum current capability of OHL is dependent on air temperature based on a non-linear relationship. Thus, if the uncertainties in the environmental conditions are considered, the RTTR of the conductors will become uncertain and the uncertainty is unlikely to be described by PDF.

In Table 4.2, the sensitivities of RTTRs to some environmental conditions are given. As can be observed, wind speed has the largest impact on the real time rating of overhead lines. The ratings of electric cables are mainly influenced by thermal resistance of the insulation and the soil. For a transformer uses oil and air and internal and external coolant and there is forced cooling, its rating is influenced mostly by air temperature.

		Overhead lines (Lynx 50)				Electric cables ($150mm^2$)		Transformers (ONAN 45)
parameter (credible mid-range value)		Ws (8m/s)	Wd ($\frac{\pi}{4} rad$)	Ta^{δ} (15°C)	Sr ($500W/m^2$)	R_T (1.2WK/m)	Ts (10°C)	Ta (15°C)
Variation from mid-range value	-50%	-23.86%	-11.38%	+10.80%	+0.72%	+31.46%	+3.00%	+6.11%
	-25%	-10.73%	-4.97%	+5.52%	+0.36%	+12.36%	+1.50%	+3.09%
	-10%	-4.07%	-1.85%	+2.24%	+0.15%	+6.18%	+0.60%	+1.24%
	10%	+3.84%	+1.66%	-2,29%	-0.15%	-4.49%	-0.60%	-1.25%
	25%	+9.22%	+3.82%	-5.81%	-0.36%	-8.99%	-1.50%	-3.16%
	50%	+17.40%	+6.54%	-11.96%	-0.73%	-16.48%	-3.00%	-6.40%

Table 4.2 Environmental condition sensitivity analysis (parameter variation versus rating variation) [25]

4.2.4 State-of-Charge

A number of techniques have been developed to estimate the SoC of BESS [133-138]. Due to the difficulty of observing complex electrochemical reactions and measuring electrical and chemical parameters within the batteries, it is a challenging task to measure the SoC accurately.

SoC can be measured by open circuit voltage or current integration method. However, both methods have their drawbacks. Open circuit voltage is not available until the battery is disconnected and therefore this technique cannot be applied online. Besides, most open circuit voltage based methods do not consider the parameter variations and therefore are not accurate enough. On the other hand, current integration techniques are subject to the errors in current measurement. The errors also accumulate over time. In previous works, 5-15% errors in SoC estimation have been reported [138, 139].

The SoC measurements are reported for a 2.5MVA, 5MWh Li-Ion ESS during a field trial are reported. This ESS is installed as part of the CLNR project [101, 140]. Figure 4.5 compares the measured SoC from the battery management system and the calculated SoC based on the power import and export recorded at one minute resolution.

As can be observed, during the charge period between 00:00 to 07:00, the measured SoC is higher than the calculated SoC. During the discharge period between 09:00 to 18:00, the measured SoC is lower than that of the calculated. The error between the measured and calculated SoC reduces when the BESS is idle. The correlation coefficient between the SoC error and power export is 0.77, which indicates a relatively high correlation between the two values.

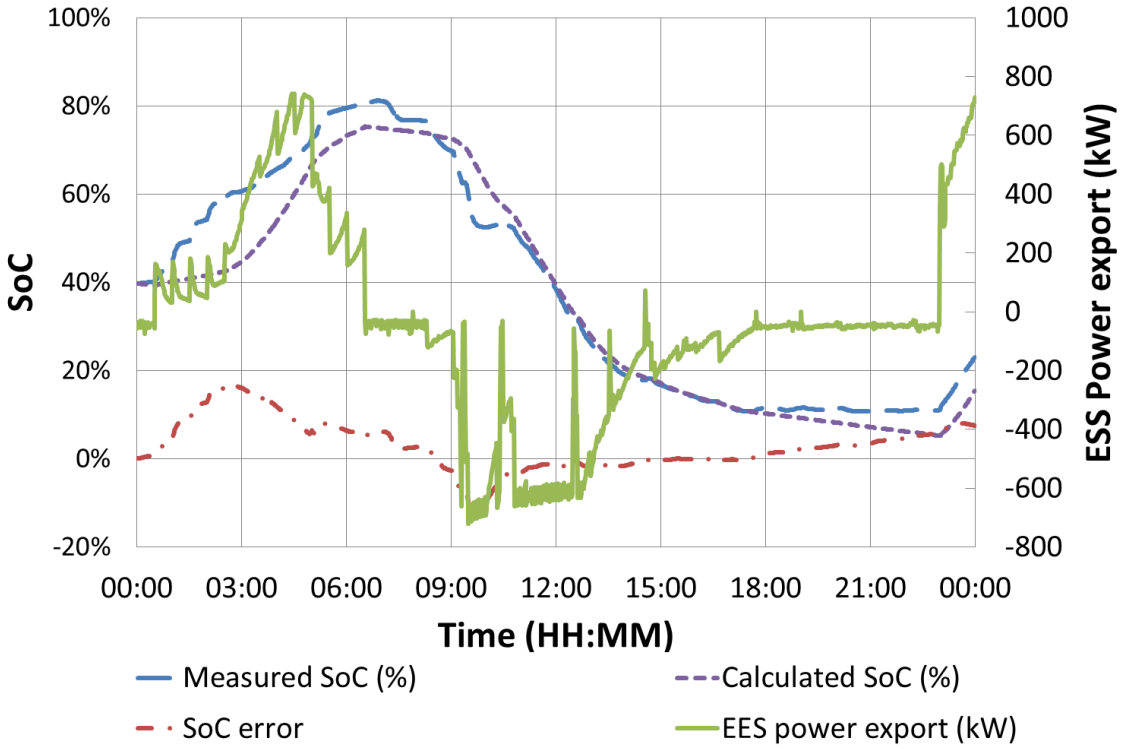

Figure 4.5 ESS Measured and Calculated SoC

In summary, it can be observed that, with in short period of time, the error of SoC estimation varies with real power. However, the error of SoC is not a linear function of the real power import/export of the BESS. Therefore it is difficult to provide an accurate mathematical description of this error such as PDF.

4.2.5 Industrial and Commercial DSR

This section introduces I&C DSR trial results from the CLNR projects. The results have been reported and published in conference paper [101] and reports [141, 142]. In the CLNR project, residential, small and medium enterprise (SME) and I&C customers have participated in demand response programmes. I&C DSR trials have been carried out in 2012 and 2014 to investigate DSR customers' flexibility and response characteristics. Three I&C customers have participated in the initial series of thirteen DSR trials in 2012. Nine out of the thirteen requests for demand response were successful. The author's contribution is analysing the trial results regarding the uncertainty in response success rates, reduction magnitude and delay.

Figure 4.6 illustrates the half hourly energy consumption and average power consumption of customer A, during DSR trial A.1. The blue bar represents the half hourly consumption of customer A, obtained from meter readings, and the red trace represents the average real power consumption.

In this trial, the DSR command was issued from a control room at 14:50. On receiving the signal, a diesel generator was engaged, to supply power to meet the customer demand. The customer load was thus reduced by over 800kW for four hours. It should be noted, however, that there was a delay of approximately 20 minutes before customer consumption was actually reduced.

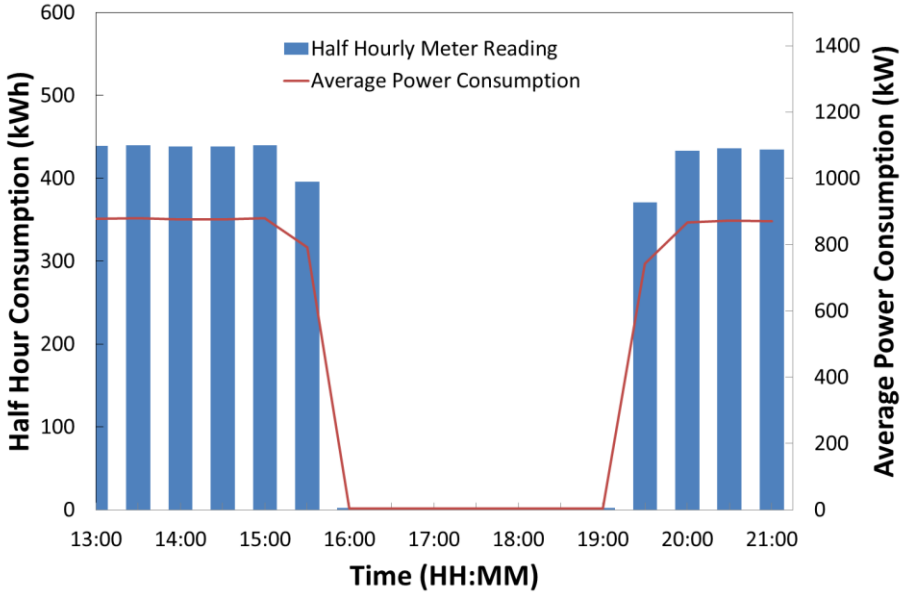

Figure 4.6 I&C Customer A DSR profile in DSR trial A.1

In trial A.2, the DSR instruction was confirmed before 11:00 and DSR commenced at 15:00. The half hourly meter readings and average power are shown below Figure 4.7.

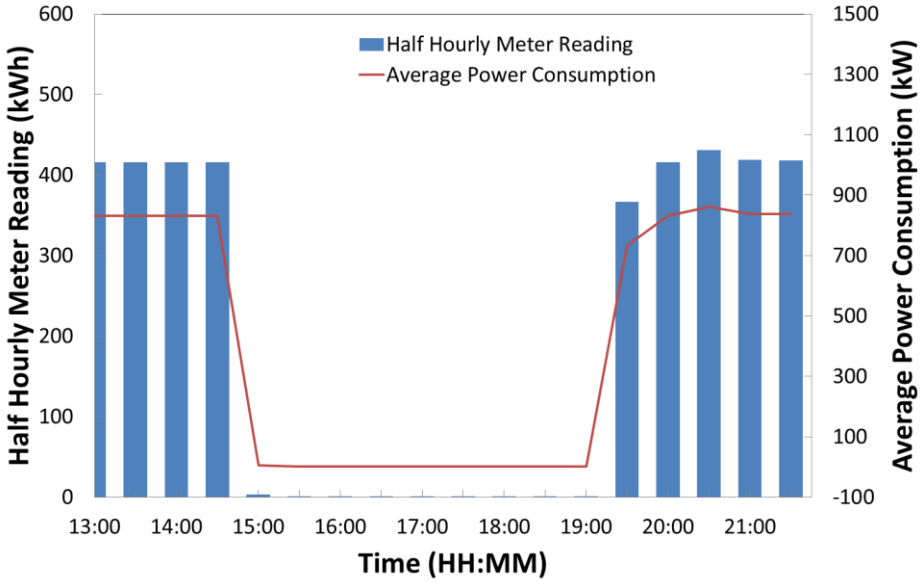

Figure 4.7 I&C Customer A DSR profile in DSR trial A.2

Comparing Figure 4.6 and Figure 4.7, it can be seen that the response of A.1 is much slower than that in A.2. Due to the use of the diesel generator to supply the local load, power consumption was reduced to 2kW within 2 minutes and remained constant. Similarly, when the invoked DSR came to an end, load was restored within a 2 minute period.

The load of Customer B consists primarily of refrigeration. In contrast to customer A, the load was varied by reducing consumption as opposed to engaging on site backup generation. A DSR profile, for this customer, (DSR trial B.1) is illustrated in Figure 4.8. DSR commenced at 15:00 and lasted until 19:00. During this period, the half hourly energy consumption of customer B was reduced from 1200kWh to approximately 600 kWh.

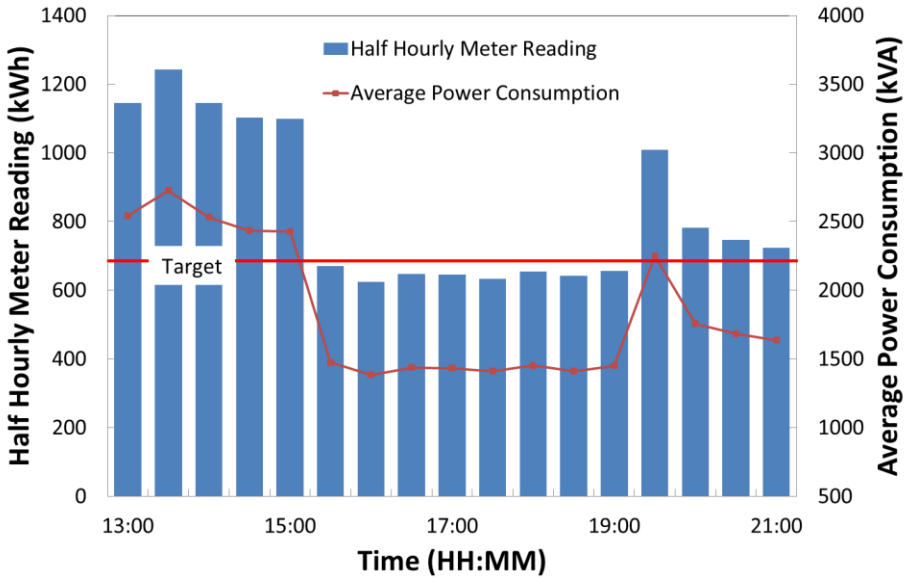

Figure 4.8 I&C Customer B DSR profile in DSR trial B.1

As mentioned previously, not all trials resulted in a successful response from the customers. Reasons for unsuccessful DSR include; failure to respond, or an inability to reduce enough load to meet the target half hourly energy consumption. For example, in one trial, the diesel generator used on the site of customer A experienced failure and therefore the site was unable to respond.

The half hourly energy consumption and average power curves from trial B.2 are given in Figure 4.9. The DSR command was confirmed before 11:00 and DSR started at 15:00. It can be seen that the half hourly energy consumption started to decrease and dropped from 1195.9kWh at 15:00 to 950.2kWh at 15:30. However the reduction was smaller than the agreed target and therefore the DSR was deemed to be unsuccessful. The load on the site did not drop below the target until 17:30, at which point the DSR was considered to be successful.

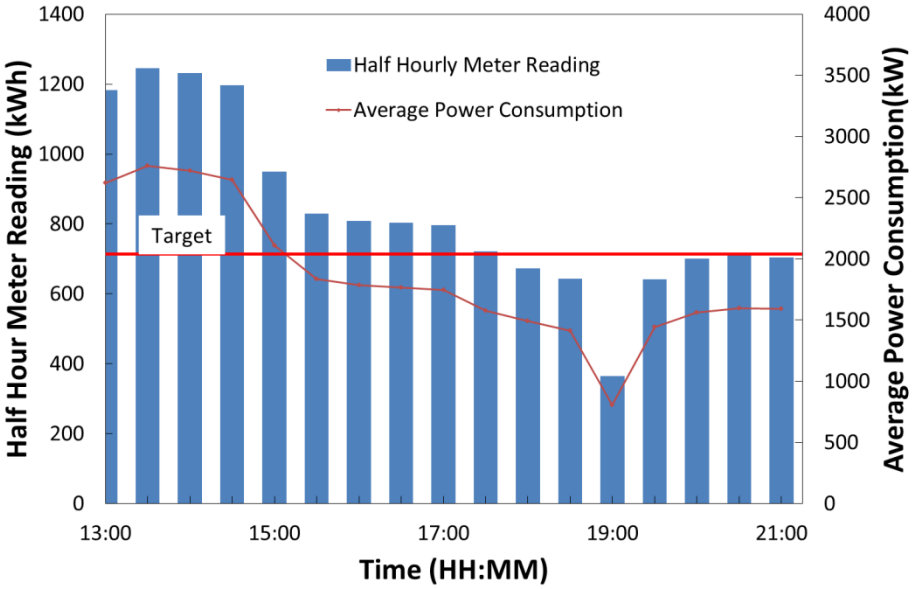

Figure 4.9 I&C Customer B DSR profile in DSR trial B.2

In summary, with I&C DSR, there is uncertainty regarding:

- If there will be a response;
- If there is a response, how long is the delay;
- How much reduction/increase can be provided.

4.3 Probabilistic Methods to Deal with Uncertainty

4.3.1 Introduction

In this section, methods for dealing with uncertainty are reviewed. Consider a non-linear system which can be described as

$$\boldsymbol{y} = g(\boldsymbol{x}) \tag{4.8}$$

Where

$\boldsymbol{x}$	the input vector
$\boldsymbol{y}$	the output vector
g	a general nonlinear function

When $\boldsymbol{x}$ is uncertain, $\boldsymbol{y}$ becomes uncertain as well. In this thesis, uncertain values, vectors and matrices are marked with an accent as shown below. Equation (4.8) then becomes,

$$\tilde{\boldsymbol{y}} = g(\tilde{\boldsymbol{x}}) \tag{4.9}$$

The goal of probabilistic methods is to study the PDF of $\boldsymbol{y}$ if the PDF of $\boldsymbol{x}$ is known. In this section, methods to deal with uncertainty are introduced. Stochastic problems can be solved by simulation based methods, analytical methods and a combination of both [143]. Mont Carlo simulation (MCS) is a simulation based method. This method is detailed in section 4.3.4 and applied to explore the impacts of EV charging on distribution networks in section 4.4. Analytical methods reviewed in this chapter include point estimate method and cumulant based method. Chance constraint programming method can be a mix of PEM and cumulant methods.

Methods have also been developed to solve uncertain optimization problems. The general form of a constrained optimization problem can be described as

$$\begin{aligned} &\min f(\boldsymbol{x}) \\ \textit{Subject to} \quad & \\ &g(\boldsymbol{x}) = 0 \\ &h(\boldsymbol{x}) \leq \boldsymbol{b} \end{aligned} \tag{4.10}$$

Where

$\boldsymbol{x}$	the input vector
$\boldsymbol{y}$	the output vector
g	a general nonlinear function for equality constraints
h	a general nonlinear function for inequality constraints
$\boldsymbol{b}$	the constraints vector

If uncertainties are considered, the problem described by equation (4.10) becomes

$$\begin{aligned} &\min \tilde{f}(\tilde{\boldsymbol{x}}) \\ &s.t.\, \tilde{g}(\tilde{\boldsymbol{x}}) = 0 \\ &\tilde{h}(\tilde{\boldsymbol{x}}) \leq \tilde{\boldsymbol{b}} \end{aligned} \tag{4.11}$$

In equation (4.11), the uncertainties in g and h are also considered.

4.3.2 Point Estimate Method

The goal of PEM methods is to calculate the PDF of the output $\boldsymbol{y}$ in equation (4.9) based on the uncertainty of $\boldsymbol{x}$. The PEM method calculates the PDF of $\boldsymbol{y}$ based on the deterministic analysis of the selected points, or scenarios. The number of scenarios selected is based on the number of uncertain values in $\boldsymbol{x}$. For each uncertain entry in $\boldsymbol{x}$, two values, or concentrations, are selected on each side of the nominal value. The corresponding value of $\boldsymbol{y}$ is calculated for

each concentration. In the end, the PDF of $\boldsymbol{y}$ can be calculated. The procedure for PEM is detailed below:

1. Determine the number of uncertain values in $\boldsymbol{x}$, denoted as N_u
2. Determine the locations of concentrations for each uncertain variable $x_k (1 \leq k \leq N_u)$, $\xi_{k,1}$ and $\xi_{k,2}$. The concentrations are two points on each side of the nominal value x_k
3. Replace x_k in $\boldsymbol{x}$ with one of its concentration $x_{k,i} = x_k + \xi_{k,i}$, $i = 1,2$. The updated $\boldsymbol{x}$ is denoted as $\boldsymbol{x}_{k,i}$
4. Use $x_{k,i}$ to calculate $\boldsymbol{y}_{k,i} = g(\boldsymbol{x}_{k,i})$ deterministically
5. When all $\boldsymbol{y}_{k,i}$ have been calculated, calculate the moments of $\boldsymbol{y}$ by

$$E(\boldsymbol{y}) \cong \sum_{k=1}^{n} \sum_{i=1}^{2} P_{k,i} \boldsymbol{y}_{k,i}$$
$$E(\boldsymbol{y}^2) \cong \sum_{k=1}^{n} \sum_{i=1}^{2} P_{k,i} \boldsymbol{y}_{k,i}^2 \quad \textbf{(4.12)}$$

   where $P_{k,i}$ is the probability of the $\boldsymbol{y}_{k,i}$. The concept and calculation of moments is introduced in Appendix C.
6. Based on the calculated moments of $\boldsymbol{y}$, the mean and standard deviation of $\boldsymbol{y}$ can be calculated

$$\mu_{\boldsymbol{y}} = E(\boldsymbol{y})$$
$$\sigma_{\boldsymbol{y}} = \sqrt{E(\boldsymbol{y}^2) - \mu_{\boldsymbol{y}}^2} \quad \textbf{(4.13)}$$

PEM technique has been adopted to solve probabilistic power flow (PPF) problems in [143]. A power flow problem is a non-linear formulation which can be described by equation (4.8). The proposed PPF algorithm considers uncertain nodal power injections and calculates the PDF of branch loadflows.

PEM method can be used to solve optimal power flow (OPF) problems with uncertainty. An OPF problem is an optimization problem which can be generalized as equation equation (4.10). OPF problems, unlike a power flow problem, need to be transformed into equality problems as stated in equation (4.8). OPF problems can be transformed into the form of (4.8) by applying interior point method (IPM) [144, 145]. In [146], PEM is used to calculate the mean and standard deviations of locational marginal prices (LMPs) under the uncertainty of load. Later works introduce the correlation between uncertain values into PPF and probabilistic OPF (POPF) problems [147-149]. Most POPF approaches assume all uncertain

values follow normal distributions or have identical first three order moments i.e. the same mean, variance and skewness. Meanwhile, most POPF approaches are highly dependent on the techniques which transform OPF into an equality equation. A POPF approach is proposed in [150] to avoid these assumptions. In this work, correlated uncertain inputs following different distributions are transformed into uncorrelated normal distributed values so that the POPF problem can be solved.

PEM based PPF and POPF techniques require relatively low computing burden, only $2n + 1$ times of PF or OPF calculations are required. This process does not require linearization of the non-linear equation. However, the accuracy of PEM based POPF methods is reduced when the number of uncertainties increases or when the smoothness of the OPF output reduces [146].

4.3.3 Cumulant-based method

Cumulant base method (CBM) for probabilistic power flow analysis has been introduced in [151]. The cumulant is one of the numerical characteristics for a series of random values. The cumulant and the process to calculate cumulant are introduced in Appendix C. Unlike mean and standard deviation (SD), cumulants can be operated directly. The process of a Cumulant-based method to solve (4.9) is given below

1. Linearize $h(\boldsymbol{x})$
2. Prepare the density function of $\boldsymbol{x}$
3. Calculate the cumulants of $\boldsymbol{x}$
4. Calculate the cumulants of $\boldsymbol{y}$
5. Based on the cumulants of $\boldsymbol{y}$, calculate the probability distribution of $\boldsymbol{y}$

Cumulant based power flow has been used in [152] to calculate the distribution of busbar voltages due to the uncertainty of wind power and load. Cumulant based PPF is used in [153] to study the impacts of PV generation on transmission networks.

In [154], a cumulant based POPF methodology is proposed. In this work, Gaussian and Gamma distributions are decomposed into a series of normal distributions using Gram-Charlier A series. An OPF formulation is transformed into an equality equation using logarithmic barrier IPM. This work is extended in [155] so that the correlations between uncertain values can be dealt with. An POPF based on cumulant method for dispatching purposes, which takes into account the uncertainty of PV and load, is proposed in [156]. In

[157], two methods to construct the PDF for the output, Maximum Entropy method and Gram-Charlier method, are compared.

Similar to most PEM methods, the process to solve a POPF problem with cumulant based method is highly dependent on the specific solver for the OPF problem. Furthermore, cumulant based method only applies to linear problems. The linearization of PF or OPF problems may lead to large errors, especially in distribution network where the X/R ratio is low.

4.3.4 Monte Carlo Simulation

Monte Carlo Simulation (MCS) is an approach to study the behaviour of complex systems by analysing a large number of random samples. For the problem introduced in (4.9), by sampling a large number of input values $\boldsymbol{x}$, the probability density function (PDF) or expectation of $\boldsymbol{y}$ can be calculated. An introduction to this technique can be found in [158]. The application of MCS to solve power system stochastic problems has been introduced in [145, 151, 159]. The flowchart of applying MCS for a loadflow calculation is presented below in Figure 4.10.

$\boldsymbol{x}_i$ is a sample of the input value. Depending on the purpose of the study, $\boldsymbol{x}_i$ may consist of the load at each bus, the output of RES and on and off state of components. $\boldsymbol{y}_i$ is the loadflow results based on the input $\boldsymbol{x}_i$. $\boldsymbol{y}_i$ consists of loadflow results such as busbar voltage and loadflow through branches.

In this process, firstly, the initial sample size N is set to 0. A random sample of input x_i is generated and its corresponding output y_i can be calculated. Next, the expectation of y_i can be calculated as

$$E(\boldsymbol{y}) = \frac{1}{N}\sum_{i=1}^{N} \boldsymbol{y}_i \tag{4.14}$$

At the end of each iteration, the convergence should be checked. The convergence can be checked by the variance of $E(\boldsymbol{y})$. The variance of $E(\boldsymbol{y})$ is given as

$$V\big(E(\boldsymbol{y})\big) = \frac{V(\boldsymbol{y})}{N} \tag{4.15}$$

Where

$V\big(E(\boldsymbol{y})\big)$ is the variance of the expectation of $\boldsymbol{y}$

$V(\boldsymbol{y})$ is the variance of Y and $V(\boldsymbol{y})$ is given as

$$V(\boldsymbol{y}) = \frac{1}{N-1}\sum_{i=1}^{N}\left(\boldsymbol{y}_i - E(\boldsymbol{y})\right)^2 \quad \textbf{(4.16)}$$

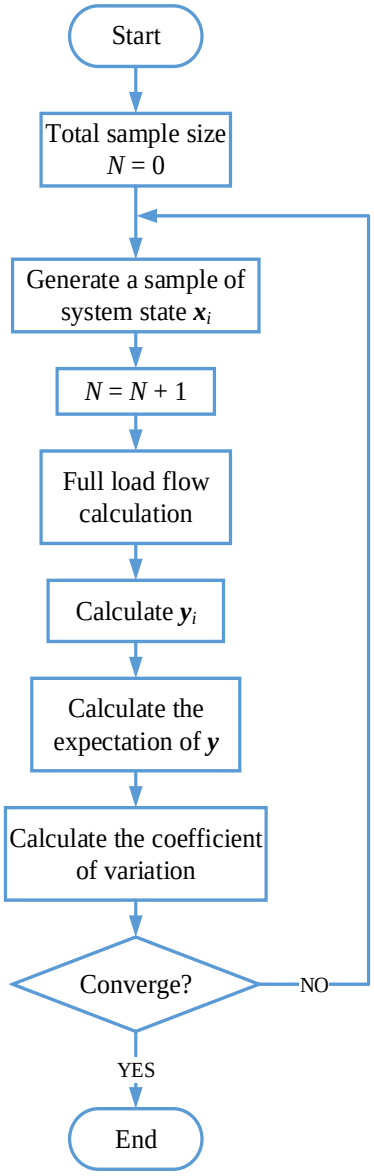

Figure 4.10 Flowchart of Monte Carlo Study

The condition of a converged MCS can be defined as the variance of $E(\boldsymbol{y})$ is smaller than a desired tolerance

$$V\left(E(\boldsymbol{y})\right) \leq \propto \quad \textbf{(4.17)}$$

MCS can be easily adopted to complex systems and doesn't require simplification of the system under study, which means the result of MCS is able to capture the nonlinear

characteristic of $h(\boldsymbol{x})$. However, MCS requires heavy computation burden due to the need for generating and evaluating a large number of samples.

4.3.5 Chance Constrained Programming Method

The chance constrained programing (CCP) method has been used to solve OPF or planning problems under uncertainty [160-163]. A general optimization problem is given in (4.10). When $\boldsymbol{x}$ is uncertain, the objective function and constraints become uncertain as well. The goal of CCP is to find a solution $\boldsymbol{x}'$ that minimises the expectation of the cost function, meanwhile, ensuring the constraints are satisfied to a predefined probability. This can be expressed as

$$\begin{aligned} &\min E\big(f(\boldsymbol{x}')\big) \\ &s.t.\, Pr\begin{pmatrix} g(\boldsymbol{x}') = 0 \\ h(\boldsymbol{x}') \le \boldsymbol{b} \end{pmatrix} \ge \propto \end{aligned} \tag{4.18}$$

Where

$E\big(f(\boldsymbol{x}')\big)$	the expectation of the cost function
$\Pr\begin{pmatrix} g(\boldsymbol{x}') = 0 \\ h(\boldsymbol{x}') \le \boldsymbol{b} \end{pmatrix}$	the probability of the constraints being satisfied
$\propto$	a predefined probability which is acceptable for constraints being satisfied

One of the challenges for CCP formulated problem is the difficulty of calculating the probability of constraints violation, i.e. to calculate $Pr\begin{pmatrix} g(\boldsymbol{u}) = 0 \\ h(\boldsymbol{u}) \le b \end{pmatrix}$. In [160] an OPF problem is formulated as a CCP problem and solved by Monte Carlo simulation (MCS). The sparse-grid method is used to solve CCP based OPF problem in [161]. However, the sparse-grid method only applies for uncertainties following Gaussian distribution and requires high computation time. In [162], a CCP based uncertain OPF problem is linearized first and then solved by a back-mapping approach. This approach requires the linearization of OPF problem and also only applied for Gaussian distribution. Paper [163] proposes a multi-objective OPF formulation for renewable energy integration. This problem is formulated as a CCP problem and solved by a heuristic algorithm, group search optimization method. This method has been adopted to find the optimal solution $\boldsymbol{u}$ and the probability of constraints violation is estimated by PEM method.

The other limitation of CCP based method is the difficulty of providing a solution with 100% reliability of probability of success (PoS). CCP based problem is normally solved by finding a solution that satisfies

$$\min E\big(f(\boldsymbol{u})\big)$$
$$s.t.\, 1 - Pr\begin{pmatrix} g(\boldsymbol{u}) = 0 \\ h(\boldsymbol{u}) \leq b \end{pmatrix} \leq 1{-}\propto \tag{4.19}$$

If high PoS is required, $1{-}\propto$ is a very small number. Dealing with a very small number is challenging in such a process. Therefore, it is challenging for CCP based approaches to provide a highly reliable solution.

4.4 Investigating the Impact of EV Charging Using MCS

As introduced in section 4.3.4, a MCS study can be applied to complex systems which are difficult to describe mathematically. In future DNs, where the customers' behaviours become more stochastic and less predictable, load forecast will be more challenging. The correlation between the household electricity usage and EV charging events is difficult to describe mathematically. As a result, MCS is employed to investigate the impact of EV charging on DNs.

In this section, a case study is presented using MCS to study the impact of EV charging on distribution networks. This work has been published in [164] and [165]. In this case study real world EV charging profiles data and smart meter data measurements are combined using MCS technique. Next, the combined load profiles are applied on three distribution networks to investigate the impact of EV uptake. The impacts under study include steady state voltage drop, power flow on the MV/LV transformer and unbalance. Modelling of the case study networks, applying the combined load profiles upon case study networks and accessing the impacts on voltage drop and power flow is carried out as part of the research in this thesis. The code for this work is given in Appendix B.

4.4.1 Data

In this work load profiles applied in the case study networks are composed of smart meter load profiles and EV charging profiles.

The EV data is collected from the SwitchEV project which trialled 44 EVs in the North East of England between 2010 and 2013. The cars were fitted with data loggers that captured more than 85,000 EV journeys recorded second by second and over 19,000 recharging events recorded minute by minute at more than 650 public and 260 private charging points [166,

167]. High resolution spatial and temporal data of EV driving and charging events were collected, processed and analysed during the SwitchEV project. The dataset gave insight and illustrated the stochastic nature of real world behaviour of EV users. The project recruited different types of users- private and fleet drivers. They had access to an extensive charging infrastructure (home, work, public). The majority of vehicles used in the trial are production vehicles available on the market and were provided by Nissan (LEAF) and Peugeot (iOn). A total of 125 different users were recruited for the duration of the project [167]. As a result, the data collected from the SwitchEV trial captured how people would use an electric car in a real-world context.

The smart meter data was collected via the CLNR project. This is the UK's largest trial of smart grids and it provided domestic load profiles of half-hourly power consumption data collected from nearly 9000 smart meters. In addition, the CLNR smart meter data set [168] is parameterised by socio-economic variables which allow the selection of representative load profiles appropriate to the network customer population under study. The four-year CLNR project also provided network data and extensively validated network models based on existing local distribution networks operated by the regional DNO, Northern Powergrid.

In order to understand present and emerging load and distributed generation patterns, the CLNR project is conducting monitoring trials using data from over 9000 smart meters placed in residential locations in the UK. The smart meter dataset is classified by household income, presence of under 5 s or over 65 s, tenure, household thermal efficiency and area classification (urban/rural). UK Office for National Statistics (ONS) data was used to determine the characteristics of the study areas of this work, which are summarised in Table 4.3 along with the electricity network characteristics. Using the parameters in Table 4.3, a representative population of residential load profiles was extracted from the CLNR dataset representing the study areas. Properties in the two regions are mostly mid-20^{th} century semi-detached houses with adjoining off-street parking. Some communal parking facilities are also evident. Vehicle ownership is high and many households own more than one car. Given these observations, these populations are used as model populations of potential future EV owners on their respective networks.

	Urban	Rural
Substation	6.6kV/400V, 500 kVA	20kV/400V, 315 kVA
Feeders	4	2
Total LV customers	288	189
Number of customers per LV feeder	A – 59, B – 66, C – 84, D - 79	A – 123, B – 66
Vehicle ownership	86%	74.6%
No. of vehicles in vehicle-owning households	1.7	1.5
ONS morphology code	1 (Urban)	3 (Rural)
House thermal efficiency	Medium	Medium
Percentage households with under 5s or over 65s	44%	40%
Equivalent annual income (gross)	60%: > £30 k 35%: £15-£30 k 5%: < £15k	18%: > £30 k 62%: £15 - £30 k 20%: <£15 k
Tenure	Effective 100% home ownership	37% Renting 63% Owned
Household occupancy	97%	97%

Table 4.3 Summary of LV Network and Population Parameters

4.4.2 Case Study Networks

Three case study networks have been used for this study. The case study networks include two networks from the CLNR project and the UK generic network (UKGDS).

One rural and one urban network within Northern Powergrid's licence area have been used to enable the evaluation of questions of load growth and active network management. Models of the trial networks have been developed in IPSA2, a steady-state power system simulation application, and these have been extensively validated with two years of detailed network data and against existing DNO network models (using data provided by Northern Powergrid). This study uses this set of models and data as a foundation for the examination of EV load impacts. The urban network under study, Figure 4.11, is a 6.6 kV network supplying approximately 6000 customers, with a mixed load curve and an early-evening peak. One particular HV/LV substation supplying 288 customers via a 500 kVA transformer and 4 LV feeders is studied in detail as a test case for EV penetration.

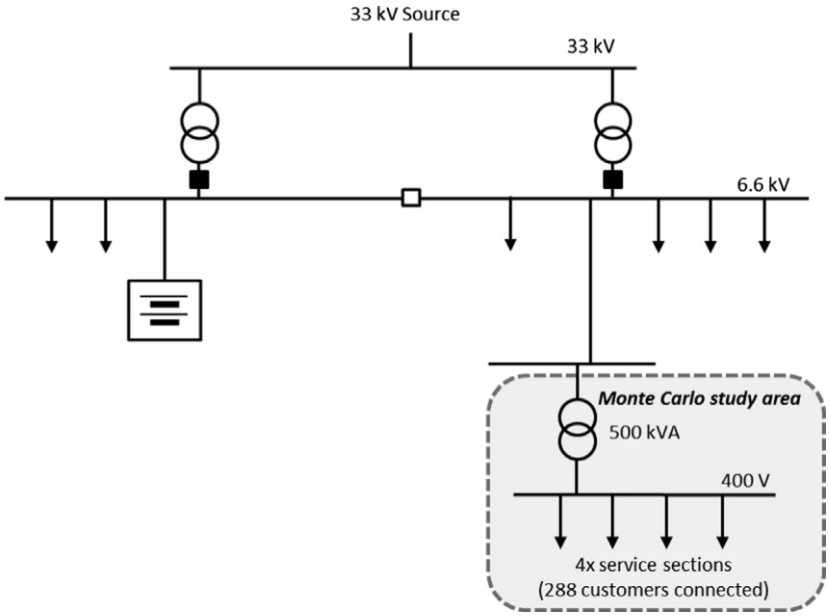

Figure 4.11 Diagram of the 6.6 kV case-study urban network used in steady-state IPSA2 study

Figure 4.12 shows the rural network under investigation. This network has previously used in Chapter 3 to evaluate the sensitivity factor and CSF based control scheme. This network consists of a 20 kV feeder, approximately 25 miles long, supplying a number of towns in Northumberland in northern England. Three HV/LV substations supply one of these towns; and this paper focuses on one of these substations which supplies 189 residential properties through two multiply-branched LV feeders. The LV network sections under study are exclusively residential with no industrial or commercial facilities or public EV charging infrastructure supplied by the HV/LV transformer.

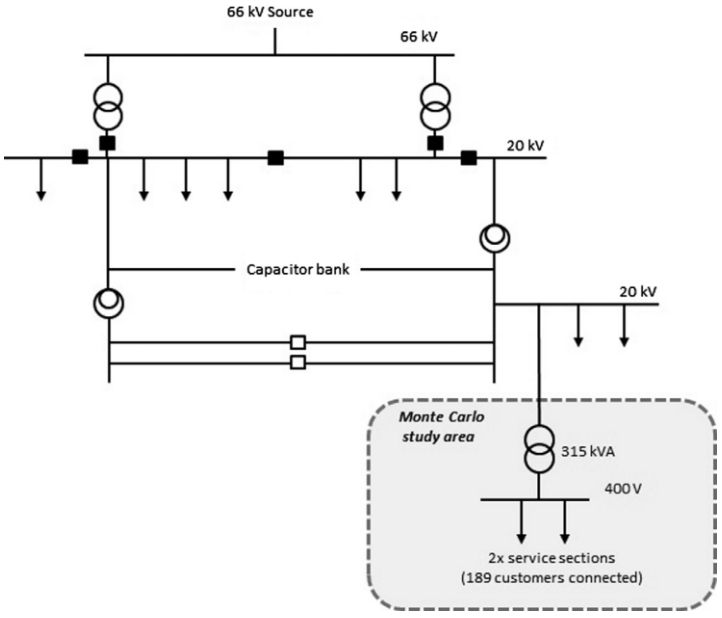

Figure 4.12 Diagram of the 20 kV case-study rural network used in steady-state IPSA2 study

In addition, a generic network as shown in Figure 4.13, based on [169], has been studied. This network has been deemed to be a representative of a heavily loaded UK distribution network by UK DNOs who were involved in specifying and creating it. It consists of a 33 kV source feeding two 15 MVA 33/11 kV transformers. There are six 11 kV feeders, each of which have eight 500 kVA 11/0.4 kV transformers equally spaced along 3 km of underground cable. Downstream of each 500 kVA transformer are 4 LV feeders of 300 m in length with 96 customers spaced equally along each feeder. The population parameters for the 386 customers under study on the generic network were assumed to be the same as the urban network described previously in Table 4.3. The rural and urban networks give an indication as to the problems that could be encountered in different types of networks. However, all networks are different and therefore the modelling of a specific system is required to establish if localised problems exist. The generic network has been used in this study in order to draw broad and generalizable conclusions across the UK distribution networks as a whole.

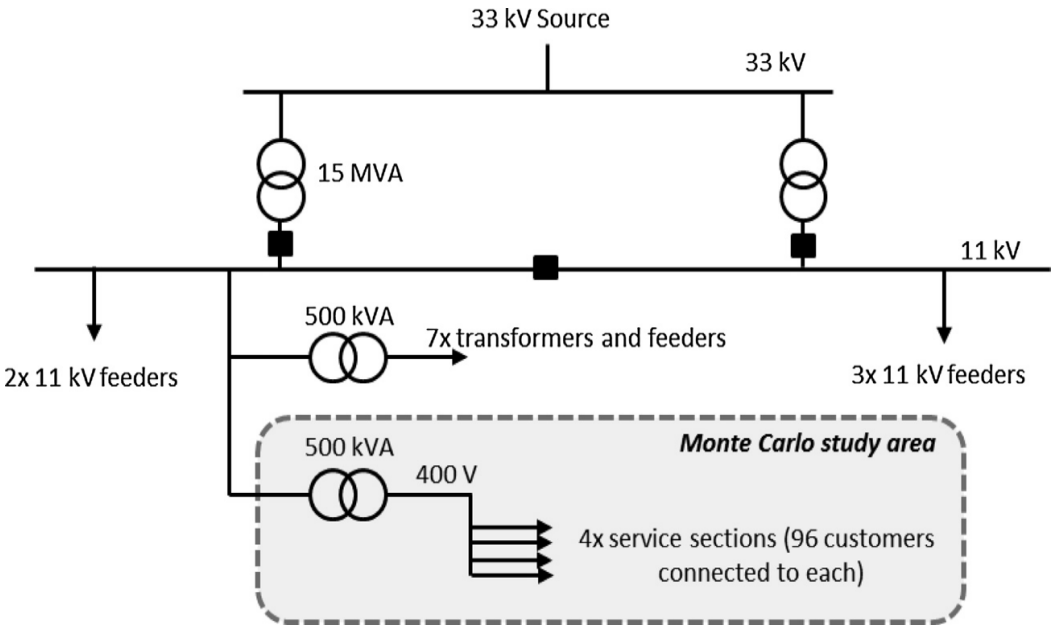

Figure 4.13 UK generic network used in steady-state IPSA2 study

4.4.3 MCS Study

Monte Carlo Simulation (MCS) was used to build up a distribution of possible demands on the trial networks. Data for the simulation was produced by sampling the domestic load profile and EV charging profile populations. Households on the LV networks were randomly assigned load profiles in proportion to the local demographic makeup. A defined percentage of these users, corresponding to a level of EV penetration, were further assigned an EV load profile which was added to their base domestic profile. EV penetration is defined as the ratio of EVs to the number of vehicle- owning households. For the case of the urban network with

288 customers and a vehicle ownership of 86%, 60% penetration (149 EVs) represents an approximate nominal upper bound on the test networks whereupon all households owning more than one vehicle have an EV as the second vehicle. 1000 simulated peak days (i.e. 1000 simulation runs) were generated to ensure adequate variation of customer behaviour, EV charging profiles and customer location on the network. The generation of multiple random configurations naturally captures any spatial concentration of households with EVs (e.g. at the remote end of the longest feeder) which could cause additional voltage drops. Figure 4.14 shows some illustrative examples from the urban profiles population assigned to customers. A configuration of the urban network with 60% EV penetration at 18.00 on the peak demand day was examined to ensure that stable results had been obtained with 1000 MCS trials. With 1000 trials, the mean transformer demand had converged to a stable 385.8 kVA (standard error 0.29 kVA). The standard deviation of the distribution of transformer demands had also stabilised to 9.1 kVA. Thus the distributions produced by the simulated trials are stable and provide reliable estimators of the simulated demand.

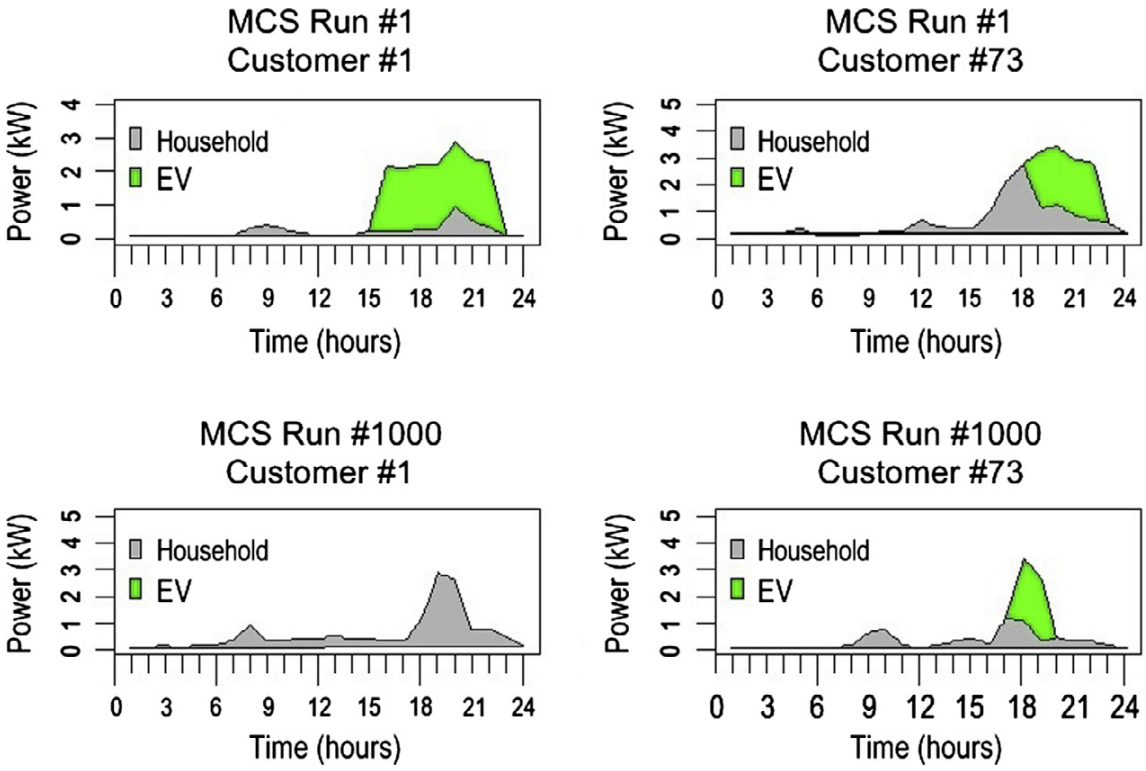

Figure 4.14 Example of peak day load profiles for 2 customers (#1 and #73) on the network for 2 different MCS runs (run #1 and 1000). Each MCS run generates a population of customers as defined by the network topology

4.4.4 Results

Transformer loading

The power demand profiles for the urban and rural LV networks on the test day for EV penetration values that produce loading exceeding the transformer thermal limit are plotted in Figure 4.15 and Figure 4.16. As can be observed in Figure 4.15, using the 97.5th upper demand bound, the urban network is not compromised even at 60% EV penetration, although at this point the load is approaching the transformer rating (500 kVA).

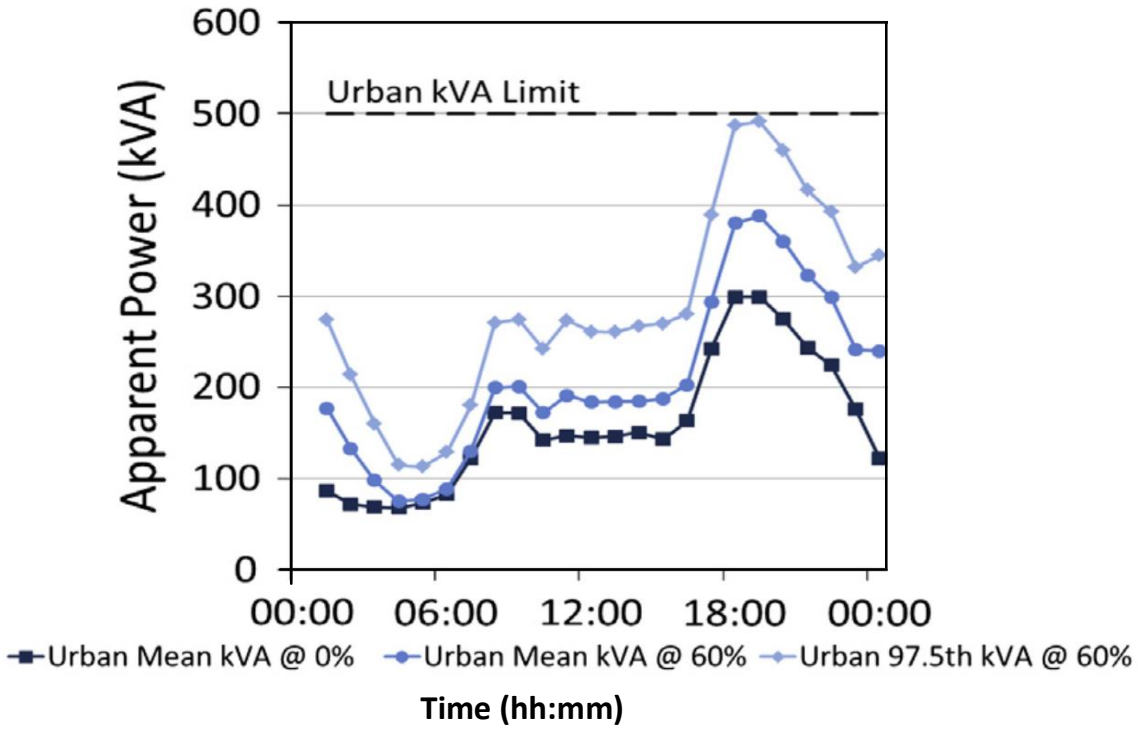

Figure 4.15 Test Day Critical Demand for Urban Network

However, as can be seen in Figure 4.16, during the afternoon peak, the power flow on the transformer exceeded its rating at 15% EV penetration using 97.5th upper demand bound.

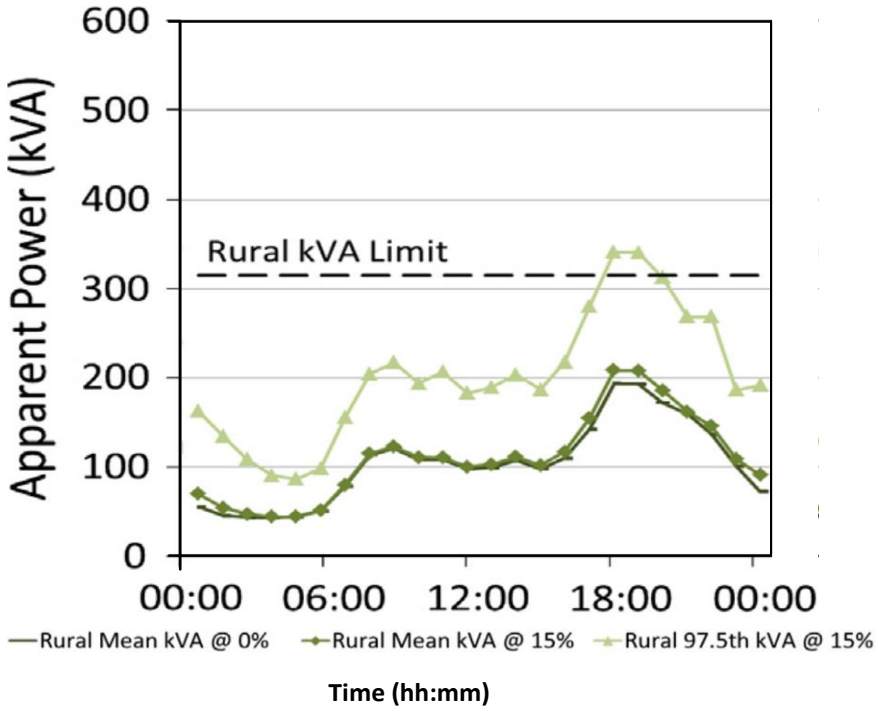

Figure 4.16 Test Day Critical Demand for Rural Network.

The demand profiles with 15% to 60% penetration of EVs are plotted in Figure 4.17. As can be observed, using the 97.5th upper demand bound, in the generic network the rating of the transformer is violated at 40% EV penetration (Max@ 40%).

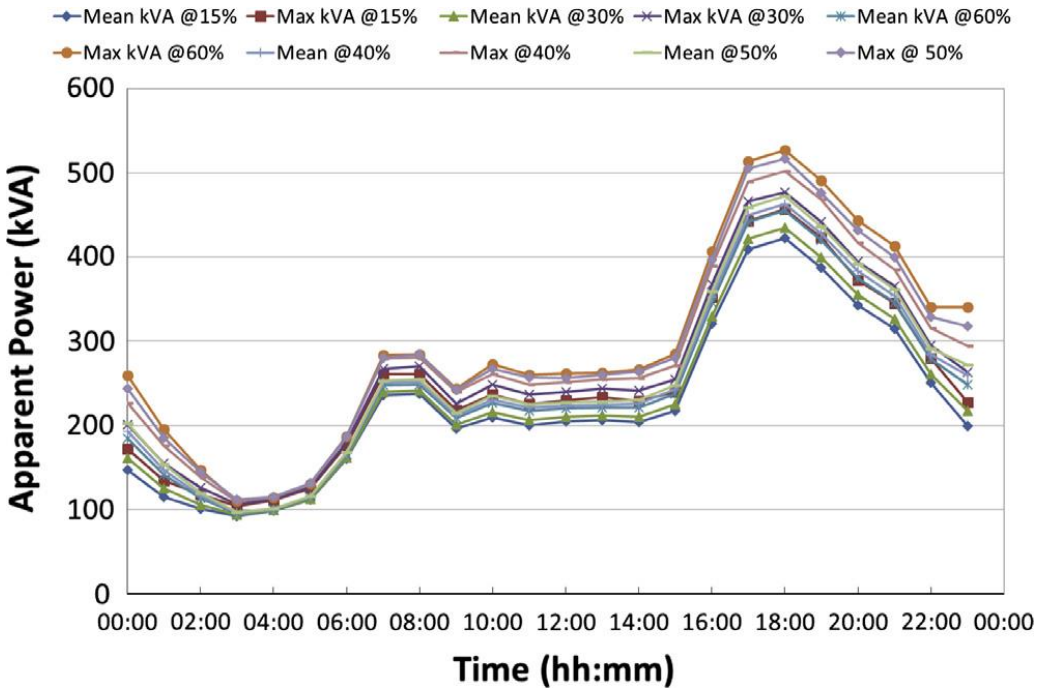

Figure 4.17 Test Day Critical Demand for the Generic Network.

Voltage drop

Table 4.4 shows the maximum voltage changes occurring at times of 97.5% of the load for the rural and urban networks. The voltage change is calculated by comparing the voltages at the secondary side of the MV/LV transformer to the end of the feeders. As can be seen in Table 4.4, the maximum voltage change in rural network is 5.39% and 2.90% in urban network. The voltage magnitude in LV networks is required to be within the statutory limits +10%/-6% [170]. According to this standard, such voltage change does not cause voltage excursions.

	Average Load 0% EVs	Average Load 15% EVs Rural 60% EVs Urban	97.5% Load 15% EVs Rural 60% EV Urban
ΔV – Rural	2.33%	2.52%	5.39%
ΔV – Urban	1.4%	1.72%	2.90%

Table 4.4 Maximum Voltage Changes on the Test Networks (negative sign indicates a voltage drop)

Similarly in Table 4.5 and 60% EV penetration with 97.5% of the load did not cause voltage problems in the generic LV distribution network.

Lowest Voltage	15% EVs	30% EVs	60% EVs
ΔV – Mean (%)	1.58	1.64	1.73
ΔV – Max (%)	2.67	2.79	3.02

Table 4.5 Maximum Voltage Changes in the Generic LV Network (negative sign indicates a voltage drop)

4.4.5 Conclusion

This study uses real world datasets to study the impacts of the uptake of EV on distribution networks. Case studies on three types of distribution networks show that the spatial, temporal and behavioural diversity of EV charging demand can alleviate the impacts on distribution networks. In other words, if these uncertainties are not well understood or managed, the voltage drop and power flow through the transformers will be overestimated.

MCS technique presents a few advantages to other analytical methods, when applied to the problem investigated in this section. In this problem, some factors such as EV charging and

home appliances usage behaviours are difficult to be described mathematically. Therefore, analytical methods are unlikely to be able to tackle such a complex system. However, MCS technique makes full use of the real world datasets by deriving samples based on the EV charging and smart meter profiles. Besides, no assumptions and linearization are made during this process.

The disadvantages of MCS also exist. First of all, MCS poses heavy computational burden. In this case, hourly profiles have been used and a total number of 1,000 numbers of samples are tested. For each case study network, 24,000 load flow calculations are needed. Therefore, it is unlikely to use MCS in real time decision making process. Secondly, similar to analytical methods, MCS requires detailed information about the uncertainty input, although this does not need to be described mathematically. When there is only partial or inaccurate information of the uncertainty, MCS may fail as well. Finally, the limit for variance of the expectation needs to be decided carefully. If this convergence limit is set too high, the results may not be accurate enough. On the other hand, if the limit is too low, extra and unnecessary tests will be carried out.

4.5 Robust optimisation

Robust optimisation (RO) is an approach to transform uncertain linear optimisation (ULO) problems to another form so that they can be solved deterministically. RO has been applied to solve unit commitment (UC) problems, DSR and planning. This section exams the state of the art of the application of RO in power systems.

The general form of an optimization problem has been introduced in section 4.3.1. Equation (4.11) describes a constrained uncertain optimization problem. To solve this problem by RO, equation (4.11) need to be linearized. A standard linear optimization problem can be represented as

$$\begin{aligned} &min\ \boldsymbol{c}'\boldsymbol{x} \\ &s.t.\ \boldsymbol{A}\boldsymbol{x} \leq \boldsymbol{b} \end{aligned} \tag{4.20}$$

where

$\boldsymbol{c}$	the vector of coefficients for the cost function
$\boldsymbol{c}'$	the inverse vector of coefficients for the cost function
$\boldsymbol{x}$	the decision variables or control variables
$\boldsymbol{A}$	the matrix of constants for constraints

$\boldsymbol{b}$ the right hand side vector of constraints

Considering the uncertainties in $\boldsymbol{c}$, $\boldsymbol{x}$, $\boldsymbol{A}$ and $\boldsymbol{b}$, equation (4.20) becomes

$$\begin{aligned} &min\, \tilde{\boldsymbol{c}}'\tilde{\boldsymbol{x}} \\ &s.t. \tilde{\boldsymbol{A}}\tilde{\boldsymbol{x}} \leq \tilde{\boldsymbol{b}} \end{aligned} \quad \textbf{(4.21)}$$

Unlike other methods, RO does not require the PDF of all the uncertainty values. It is assumed that all the uncertain values vary in a given range, or uncertainty interval. For instance, if one of the elements of a_{ij}, in the i^{th} row and the j^{th} column, is uncertain, then the real value of $\tilde{a}_{ij}$ follows

$$a_{ij} - \hat{a}_{ij} \leq \tilde{a}_{ij} \leq a_{ij} + \hat{a}_{ij} \quad \textbf{(4.22)}$$

Where

a_{ij} the nominal value of the elements of $\boldsymbol{A}$ in the i^{th} row and the j^{th} column

$\hat{a}_{ij}$ the maximum variation of a_{ij}

$\tilde{a}_{ij}$ the real value of a_{ij}

RO has been applied to solve uncertain UC problems [171-182]. A two-stage adaptive RO formulation to security constrained UC problems is proposed in [182] to deal with the uncertainty of DG and load. A practical method to solve the adaptive model is developed and numerical experiments with real data are carried out. The conclusion shows that RO reduces the total dispatch costs significantly and this advantage is amplified when the level of load variation is higher. In [175], UC problem considering the uncertainty of wind power output is solved by RO. Simulation results indicate that the RO approach is able to tackle the worst case scenario and pumped hydro storage can act as substitutes of thermal generators on increasing the system robustness. A RO based UC formulation to deal with the uncertainty of DSR and wind energy is introduced in [174].

A real time demand response model for scheduling household appliances responding to real time price (RTP) is proposed in [183] to deal with the uncertainty of electricity price. It is found that RO based scheduling scheme is able to reduce the electricity bill of customers. Paper [184] evaluates the real-time price-based demand side management (DSM) for residential appliances via stochastic optimisation (SO) and robust optimisation approaches. The algorithm is designed to schedule the operation of plugin electric vehicle, dishwasher,

cloth dryer, electric water heater, air conditioner and oven. The conclusion shows that both SO and RO approach is able to reduce electricity bill cost. SO based method can achieve a higher cost reduction however introduces higher computational burden. RO is used for load scheduling in [185] considering the uncertainty of electricity price and renewable generation. The price of electricity is modelled as a piecewise linear function of demand.

A RO algorithm is applied for the scheduling of combined heat and power (CHP), boiler and BESS [186]. This formulation minimise the cost of import/export electricity to the grid and the fuel (gas) cost of CHP and boiler. Uncertainties considered in this paper are solar irradiance and electric and heat load.

A reactive power optimization approach for intermittent windfarm integration based on RO is proposed in [187]. Voltage change due to reactive power injection is estimated by voltage sensitivity factor, derived from Jacobian matrix. Simulation results on a 30-busbar IEEE network show that the proposed method is able to reduce system loss by 10.2%.

RO algorithm is used to forecast the maximum plug-in hybrid electric vehicles (PHEVs) penetration [188]. The objective function minimises the cost and emission of generation due to the increasing penetration of PHEVs. The constraints in this paper include zonal power balance, transmission line rating, power generation capacity, generation emission constraints and the penetration constraints of PHEV.

Compared with techniques such as MCS, the limitation of RO is that linearization of the nonlinear formulation is required. The linearization process may introduce calculation errors. Furthermore, the output of RO is a solution $\boldsymbol{x}$ which satisfies the constraints and minimizes the cost function in the presence of the uncertainties. On the other hand, methods such as PEM and CBM can provide the PDF of the output $\boldsymbol{y}$, which gives an better indication of the impacts of the uncertainty of input $\boldsymbol{x}$.

However, compared with most methods for dealing with uncertainty there are many benefits of RO. First of all, RO only requires uncertainty intervals, which are easier to access than detailed information of PDF. This is a useful strength as the accurate PDFs of uncertain values can be difficult to access. If the PDF inputs are not available or inaccurate, most methods will fail to perform. Meanwhile, compared to MCS, RO poses a much lower computing burden. The computation required by RO is to solve the optimization formulation. Finally, within RO, the level of conservatism can be easily adjusted. CCP formulation can be used to adjust the probability of constraint violation as well, however, cannot guarantee 100%

probability of success (PoS). RO can provide a feasible solution and guarantees the PoS of up to 100%.

4.6 Conclusion and discussion

In this chapter, the sources of uncertainties are reviewed first. It has been found that, uncertainty exists in load, wind and wind power, RTTR, SoC and I&C DSR. It can also be seen that the PDFs of uncertainty is often difficult to access and unlikely to be normally distributed.

Methods to deal with uncertainties are compared below in Table 4.6. Conventional in the first row stands for conventional techniques with extra margins. In this table, input type refers to the type of input for uncertainty values.

	Input type	Computational burden	Linearization	Compute the PDF of output
Conventional	Interval	Low	N/A	No
PEM	PDF	Low	Yes	Yes
CBM	PDF	Low	Yes	Yes
MCS	PDF	High	No	Yes
CCP	PDF	Can be high	N/A	No
RO	Uncertainty interval	Low	Yes	No

Table 4.6 Comparison of Different Techniques to Deal with Uncertainty

MCS, CCP and analytical probabilistic methods, such as PEM and CBM, require the PDFs of the uncertainty values. However, conventional techniques with extra margins and RO only need the interval for the uncertainty values. PEM, CBM, MCS and CCP methods are not adequate to solve problems when the PDFs of uncertain values are not available or not accurate.

MCS requires high computational time compared to other methods. If MCS is used by CCP methods to evaluate the distribution of output, also requires high computational burden. If the system under study is non-linear, PEM, CBM and RO based method need to linearize the system and/or assume a linear superstation of probabilities. MCS does not require linearization of the non-linear system. Depending on the methods adopted, conventional techniques with extra margins and CCP may not require linearization.

PEM, CBM and MCS methods are able to compute the PDF of the output values, if the PDF of uncertain input values are provided. Conventional techniques with extra margins can be conservative. For CCP based methods, it is difficult to compute a solution with high reliabilities.

The focus of the reminder of this thesis is RO, which appears to be the most suitable solution a scheduling problem for ESS and DSR. Thus, RO will be investigated throughout the rest of this thesis. The mathematical principle of RO is investigated in the next chapter. Three development stages of RO are introduced. The key parameter in RO, budget of uncertainty (BoU), which is used to enable the trade-off between cost and the PoS, is introduced. In Chapter 6, RO is applied to a scheduling problem for ESS and DSR with the presence of a range of source of uncertainties including load, DG and DSR.

Chapter 5. Introduction to Robust Optimisation

5.1 Introduction

As shown in Chapter 2 and Chapter 4, little previous work has considered the uncertainty of load, generation, DSR and RTTR. Most methods, which are able to deal with uncertainty, require the PDF of uncertainty. Robust optimisation (RO) has been found to be the most suitable solution for solving a scheduling problem for ESS and DSR with only partial information on their uncertainties. RO is an approach to transform an uncertain linear optimisation (ULO) problem into an optimization problem with certain parameters, so that it can be solved deterministically. In this chapter, RO is introduced and the implementation of RO in Python is detailed.

The importance of dealing with uncertainty is described in section 5.2. This is followed by a general formulation of ULO problems in section 5.3. Three key stages of the development of the RO algorithm are detailed. Compared with other probabilistic methods, RO presents a few advantages. First of all, RO can protect all the constraints against uncertainty. Secondly, RO only requires the uncertainty intervals of the uncertain values. This is a very valuable feature, since, as shown in the previous chapter, PDFs of the uncertainties considered in this thesis are difficult to access. Last but not least, the use of RO enables a trade-off between the cost and the risk. In an ULO problem, the risk is the probability of constraint violations. The trade-off is realized by tuning a coefficient defined in the algorithm named budget of uncertainty (BoU). BoU and probability bounds of constraint violations are introduced in Section 5.4. Finally, the implementation of RO in Python is detailed.

5.2 Linear optimisation problem with uncertainty

Most optimisation techniques are based on the assumption that all the data is certain and accurate. In reality, this is seldom the case. The need for dealing with uncertainty has been previously demonstrated [189]. In [189], a linear programming problem with 1000 variables and 410 constraints is used to demonstrate the impacts of uncertainty. A 0.1% error is applied to one of the entries in this problem. It is found that the solution to the new linear programming problem does not always satisfy the original constraints. The violation of constraints can be as large as 450%.

5.2.1 Types of uncertainty

In [190], data uncertainty is categorised into three types as follows:

I. *Prediction uncertainty*

Scheduling or planning problems can be formulated as linear or non-linear optimization problems. When they are solved, some of the data entries, such as future demand and electricity price for the next few hours, do not exist. It is unlikely for the predictions to be entirely accurate. The error in load forecasting or future demand [172, 191], wind generation forecasting [175], annual growth rate of EVs [188] and electricity price [184] can be represented by this type of uncertainty.

II. *Measurement uncertainty*

Some of the data cannot be measured exactly or their values are varying. For example, in power systems, voltage and current measurements can be inaccurate. Furthermore, voltage and power flow sensitivity factors, as shown in Chapter 3, would vary depending on the network conditions. Such uncertainties can be classified as measurement uncertainties.

III. *Implementation uncertainty*

Some of the decision variables cannot be implemented exactly as computed. For instance, in a scheduling problem, when a demand side response decision is made and requested, the delay, magnitude and duration of load reduction or increase that will be provided by the customers, is not likely to be exactly the same as that scheduled.

5.2.2 General formulation of a ULO problem

This section introduces the generalized formulation for an LO problem with uncertainty. An LO problem can be expressed as:

$$max\ \boldsymbol{c}'\boldsymbol{x}$$

subject to

$$\begin{aligned} \boldsymbol{A}\boldsymbol{x} &\leq \boldsymbol{b} \\ \boldsymbol{D}\boldsymbol{x} &= \boldsymbol{e} \\ \boldsymbol{l} \leq \boldsymbol{x} &\leq \boldsymbol{u} \end{aligned} \qquad \textbf{(5.1)}$$

Where

$\boldsymbol{c}$	the vector of coefficients for the cost function
$\boldsymbol{c}'$	the inverse of $\boldsymbol{c}$
$\boldsymbol{x}$	the array of decision variables or control variables
$\boldsymbol{A}$	the matrix of constants for constraints

$\boldsymbol{b}$ the right hand side vector of constraints

$\boldsymbol{D}$ the matrix of coefficients for equality constraints

$\boldsymbol{e}$ the right hand side vector of equality constraints

$\boldsymbol{l}$ the lower limit of decision variables

$\boldsymbol{u}$ the upper limit of decision variables

Uncertainty can exist in all parts of the LO problem. Type I prediction uncertainty and type II measurement uncertainty can exist in the constant vectors ($\boldsymbol{c}$, $\boldsymbol{b}$, $\boldsymbol{l}$ and $\boldsymbol{u}$) and matrix $\boldsymbol{A}$. The uncertainty of decision variable $\boldsymbol{x}$ can be categorised as type III implementation uncertainty. In the following section, it is shown how the uncertainties can be handled by only considering the uncertainty of the elements in $\boldsymbol{A}$. This enables the simplification of the ULO problem.

Uncertainty in inequality constants

By introducing an auxiliary control variable $\boldsymbol{y} = 1$, the constraints can be reformulated as

$$\begin{gathered} max\ \boldsymbol{c}'\boldsymbol{x} \\ s.t. \boldsymbol{A}\boldsymbol{x} - \boldsymbol{b}\boldsymbol{y} \leq \boldsymbol{0} \\ \boldsymbol{x} - \boldsymbol{u}\boldsymbol{y} \leq \boldsymbol{0} \\ -\boldsymbol{x} + \boldsymbol{l}\boldsymbol{y} \leq \boldsymbol{0} \end{gathered} \tag{5.2}$$

Thus, the uncertainties in $\boldsymbol{b}, \boldsymbol{l}$ and $\boldsymbol{u}$ can be represented by the uncertainty in a new constraints coefficient matrix

$$\boldsymbol{A}' = \begin{bmatrix} \boldsymbol{A} & -\boldsymbol{b} \\ \boldsymbol{D_n} & -\boldsymbol{u} \\ -\boldsymbol{D_n} & \boldsymbol{l} \end{bmatrix} \tag{5.3}$$

where

$\boldsymbol{D_n}$ is a diagonal matrix and for $i = 1,2, \dots, n$, $\boldsymbol{D_{ii}} = 1$, $\boldsymbol{D_{ij,i\neq j}} = 0$

$$D_n = \begin{bmatrix} 1 & & & \\ & 1 & & \\ & & \ddots & \\ & & & 1 \end{bmatrix} \tag{5.4}$$

Thus, equation (5.2) becomes

$$\begin{gathered} max\ \boldsymbol{c}'\boldsymbol{x} \\ s.t. \begin{bmatrix} \boldsymbol{A} & -\boldsymbol{b} \\ \boldsymbol{D_n} & -\boldsymbol{u} \\ -\boldsymbol{D_n} & \boldsymbol{l} \end{bmatrix} \begin{bmatrix} \boldsymbol{x} \\ \boldsymbol{y} \end{bmatrix} \leq \boldsymbol{0} \end{gathered} \tag{5.5}$$

Uncertainty in equality constraints

Equality constraints

$$\boldsymbol{Dx = e} \tag{5.6}$$

can be reformulated as two inequality constraints

$$\boldsymbol{-e \leq Dx \leq e} \tag{5.7}$$

Uncertainty in the cost function

A cost function with uncertainty can be modelled by introducing an extra constraint [192]

$$\boldsymbol{w - c'x \leq 0} \tag{5.8}$$

where

$\boldsymbol{w}$ the maximum of the cost function

Uncertainty in the control variables

The uncertainties in control variables $\boldsymbol{x}$, or the implementation uncertainties, can be modelled as the product of multiplying an uncertainty coefficient a_{ij} and a certain control variable x_j.

In the end, a ULO problem can be generalised as

$$\begin{gathered} max\ \boldsymbol{c'x} \\ s.t.\ \widetilde{\boldsymbol{A}}\boldsymbol{x} \leq \boldsymbol{b} \end{gathered} \tag{5.9}$$

The accent character ~ stands for uncertainty. This formulation is able to represent the three types of uncertainties introduced earlier.

5.2.3 Uncertainty model

In 5.2.2, it has been shown that uncertainties in an LO problem can be modelled as the uncertainties in the coefficient matrix $\boldsymbol{A}$. Next, the uncertainty model of each entry $a_{ij} \in \boldsymbol{A}$ is introduced. In RO, unlike other approaches, such as analytical probabilistic methods or Monte Carlo simulation, only the interval of an uncertainty value is required. It is assumed that the real value of a_{ij} takes a value symmetrically in the range of $\left[a_{ij} - \hat{a}_{ij}, a_{ij} + \hat{a}_{ij}\right]$. The range, in this research, is called the uncertainty interval (UI).

$$a_{ij} - \hat{a}_{ij} \leq \tilde{a}_{ij} \leq a_{ij} + \hat{a}_{ij} \quad \textbf{(5.10)}$$

where

a_{ij} the nominal value

$\tilde{a}_{ij}$ the real value of a_{ij}

$\hat{a}_{ij}$ the maximum variation of a_{ij}

Next a variable η is defined to measure the level of uncertainty:

$$\eta_{ij} = \frac{\tilde{a}_{ij} - a_{ij}}{\hat{a}_{ij}} \quad \textbf{(5.11)}$$

thus

$$-1 \leq \eta_{ij} \leq 1 \quad \textbf{(5.12)}$$

It is assumed that η_{ij} is symmetrically distributed and each uncertainty value is independent. The advantage of using a UI instead of a probabilistic distribution function (PDF) is that, a UI can be easily derived from historical data. In contrast, PDFs may not be derived easily or cannot be derived at all.

5.3 Robust optimization

Robust optimisation transforms an ULO problem to an optimization problem without uncertain inputs so that it can be solved deterministically. Three key approaches are selected and introduced in this section to illustrate how this technique is developed and enhanced. Further details and mathematical derivations of the technique can be found in [189, 190, 192-194].

The concept of RO was first proposed by Soyster in 1973 [193]. Ben-Tal and Nemirovski extended Soyster's research in [189] to reduce the level of conservatism. However, in Ben-Tal and Nemirovski's work, a ULO formulation is transformed into a non-linear optimization formulation. Based on previous work of Soyster and Ben-Tal, Bertsimas and Sim proposed a new formulation in [192], which enables a ULO problem to be solved as a new LO problem.

5.3.1 Soyster's formulation

Soyster's formulation is a very conservative approach as it protects the constraints against the worst case scenario [193]. Considering the general formulation given in (5.9) if the

probability of constraints violations is required to be 0, Soyster proposed that, a feasible solution of this problem $\boldsymbol{x}^*$ must obey

$$max\, \tilde{\boldsymbol{A}}\boldsymbol{x}^* = max\left[\sum_j (a_{ij} + \hat{a}_{ij})x_j^*\right] = \sum_j a_{ij}x_j^* + max\left[\sum_{j\in J_i} \hat{a}_{ij}x_j^*\right] \leq \boldsymbol{b} \tag{5.13}$$

where

$\boldsymbol{x}^*$ a feasible solution which satisfies (5.9)

J_i is the set of all uncertain coefficients in constraint i

In this formulation, the second term $max\left[\sum_{j\in J_i} \hat{a}_{ij}y_j\right]$ stands for the maximum change due to the uncertainty of a_{ij} and clearly

$$max\left[\sum_{j\in J_i} \hat{a}_{ij}x_j^*\right] = \sum_{j\in J_i} \left|\hat{a}_{ij}x_j^*\right| \tag{5.14}$$

Thus, the ULO problem given in (5.9) becomes

$$\begin{gathered} max\, \boldsymbol{c}'\boldsymbol{x} \\ s.t. \sum_j a_{ij}x_j + \sum_{j\in J_i} \left|\hat{a}_{ij}x_j^*\right| \leq b_i \end{gathered} \tag{5.15}$$

However, the formulation is a non-linear problem due to the absolute value calculations. The control variable $\boldsymbol{x}$ is extended to $(\boldsymbol{x}, \boldsymbol{y})$ so that (5.15) can be solved as an LO problem

$$\begin{gathered} max\, \boldsymbol{c}'\boldsymbol{x} \\ s.t. \sum_j a_{ij}x_j + \sum_{j\in J_i} \hat{a}_{ij}y_j \leq \boldsymbol{b} \\ -y_j \leq x_j \leq y_j \\ \boldsymbol{y} \geq \boldsymbol{0} \end{gathered} \tag{5.16}$$

Thus, by solving the problem stated in (5.16) the ULO problem can be solved deterministically.

5.3.2 Ben-Tal and Nemirovski's formulation

The robust formulation (RF) proposed by Soyster is for the worst case scenario. Ben-Tal and Nemirovski proposed a less conservative approach compared to Soyster's formulation [189]. Instead of adopting the deterministic assumption, the worst case scenario as given by (5.16), by taking a probabilistic approach, Ben-Tal and Nemirovski proved that a ULO problem can be reformed as

$$max\ \boldsymbol{c}'\boldsymbol{x}$$
$$s.t. \sum_j a_{ij}x_j + \sum_{j\in J} \hat{a}_{ij}y_{ij} + \Omega\sqrt{\sum_{j\in J_i} \hat{a}_{ij}^2 z_{ij}^2} \leq b_i + \sigma \max[1, |b_i|] \quad \textbf{(5.17)}$$
$$-y_j \leq x_j - z_{ij} \leq y_j$$
$$\boldsymbol{y} \geq \boldsymbol{0}$$

where

σ	the infeasibility tolerance
Ω	a positive parameter which adjusts the level of conservatism

A detailed proof and explanation can be found in paper [189]. In this approach, if $\boldsymbol{x}^*$ is a feasible solution to the nominal ULO problem in (5.9), the probability of $\boldsymbol{x}^*$ satisfying the constraints κ is given by

$$\kappa \leq \exp(-\Omega^2/2) \quad \textbf{(5.18)}$$

5.3.3 Bertsimas and Sim's formulation

The formulation proposed by Ben-Tal and Nemirovski is a non-linear approach. Bertsimas and Sim examined the previous approaches and proposed the concept of budget of uncertainty (BoU) Γ. BoU is defined so that a feasible solution $\boldsymbol{x}^*$ at the BoU of Γ_i protects the ith constraint against the uncertainties within this constraint, when the uncertainties are given by

- Up to $\lfloor\Gamma_i\rfloor$ number of a_{ij} are uncertain and $-1 \leq \eta_{ij} \leq 1$, $\lfloor\Gamma_i\rfloor$ is the floor of Γ_i which means $\lfloor\Gamma_i\rfloor$ is the largest integer not greater than Γ_i. This set of uncertainties is denoted by S and $|S| = \lfloor\Gamma_i\rfloor$, $S_i \subseteq J_i$,
- One coefficient changes by $(\Gamma_i - \lfloor\Gamma_i\rfloor)\hat{a}_{it}$, this uncertainty is recorded as t_i and $t_i \in J_i \backslash S_i$

Based on this definition, the ULO problem becomes

$$max\ \boldsymbol{c}'\boldsymbol{x}$$
$$s.t. \sum_j a_{ij}x_j + \max_{\{S_i\cup\{t_i\}|S_i\subseteq J_i, |S_i|=\lfloor\Gamma_i\rfloor, t_i\in J_i\backslash S_i\}} \left\{\sum_{j\in S_i} \hat{a}_{ij}y_j + (\Gamma_i - \lfloor\Gamma_i\rfloor)\,\hat{a}_{it_i}y_t\right\} \leq b_i \quad \textbf{(5.19)}$$
$$-y_{ij} \leq x_j \leq y_{ij} \quad \forall i,j \in J_i$$
$$\boldsymbol{y} \geq \boldsymbol{0}$$

BoU can be understood as the number of uncertain coefficients that the constraints are being protected against. When BoU is 0, (5.19) becomes a normal LO problem. In this work normal

LO problems refers to LO problems without uncertainty. When BoU equals the number of uncertain coefficients n, (5.19) becomes the conservative formulation of Soyster as given in (5.13). However, BoU does not necessarily need to be an integral.

When Γ_i is smaller than n by a small margin, which means the number of uncertain coefficients is greater than the number of uncertain coefficients that constraints are protected against, the solution still guarantees a high probability of zero constraints violations or a high probability of success (PoS). This is due to the fact that, for a constraint with multiple uncertainties, it is not likely all uncertainty coefficients $\tilde{a}_{ij}$ take values near their maximum or minimum.

BoU enables the trade-off between the level of conservatism and the cost. For the rest of the thesis, a normalised BoU Γ/n is applied to measure the level of conservatism. Compared to Γ, this normalised value in percentage terms is more intuitive.

The formulation of (5.19) is non-linear. Bertsimas and Sim proved that (5.19) can be further transformed to

$$max\ \boldsymbol{c}'\boldsymbol{x} \tag{5.20}$$

$$s.t. \sum_j a_{ij}x_j + z_i\Gamma_i + \sum_{j\in J_i} p_{ij} \leq b_i \tag{5.21}$$

$$z_i + p_{ij} \geq \hat{a}_{ij}y_j \tag{5.22}$$

$$-y_j \leq x_j \leq y_j \tag{5.23}$$

$$l_j \leq x_j \leq u_j \tag{5.24}$$

$$p_{ij} \geq 0 \tag{5.25}$$

$$y_j \geq 0 \tag{5.26}$$

$$z_j \geq 0 \tag{5.27}$$

Unlike equation (5.19), equation (5.20) to (5.27) is a standard linear optimisation problem. The detailed proof is provided in [192]. By introducing extra control variables $\boldsymbol{z}, \boldsymbol{p}$ and $\boldsymbol{y}$, the ULO problem given in (5.9) can be solved deterministically. At the same time, by adjusting the BoU, the level of conservatism can be adjusted as well.

This research adopts the formulation of Bertsimas and Sim as it is a linearized and adjustable approach to solve ULO problems.

5.4 Probability bounds of constraint violation

BoU enables the trade-off between the probability of constraint violation and cost. This section shows how the probability of constraint violation changes with BoU. Based on the uncertainty model introduced in section 5.2.3 and the formulation in (5.20) to (5.27) three probability bounds have been proposed and compared in [192].

In section 4.3, methods to deal with uncertainty have been introduced. For the problem defined in (5.1), if a solution for this problem $\boldsymbol{x}^*$ is given, the methods introduced in section 4.3 can be used to calculate the probability of constraint violation for $\boldsymbol{x}^*$. The bounds introduced in this section provide an estimation of the probability of constraint violation without using these methods. The bounds are given as follows.

Bound 1

$$Pr\left(\sum_j \tilde{a}_{ij} x_j^* > b_i\right) \leq exp\left(-\frac{\Gamma_i^2}{2n}\right) \tag{5.28}$$

BoU controls the conservatism of the solution. At low BoU, $\Gamma_i \approx 0$ and thus $-\Gamma_i^2/2n \approx 0$. The probability of success (PoS), which is the opposite of probability of constraint violation given in (5.28) becomes

$$PoS = 1 - Pr\left(\sum_j \tilde{a}_{ij} x_j^* > b_i\right) = 1 - exp\left(-\frac{\Gamma_i^2}{2n}\right) \approx 1 - exp(0) \approx 0 \tag{5.29}$$

A low PoS means that the solution at this BoU still has a high probability of constraints violation. On the contrary, at high BoU, $\Gamma_i = n$ and thus $-\Gamma_i^2/2n = -n/2$. When n is a large number and $-n/2$ is large enough so that

$$PoS = 1 - Pr\left(\sum_j \tilde{a}_{ij} x_j^* > b_i\right) = 1 - exp\left(-\frac{\Gamma_i^2}{2n}\right) \approx 1 - exp(-\infty) \approx 1 \tag{5.30}$$

$PoS = 1$ indicates that the solution at high BoU is a robust solution and thus the solution is immune to uncertainty.

Bound 2

$$\Pr\left(\sum_{j \in J_i} \gamma_{ij} \eta_{ij} \geq \Gamma_i\right) \leq B(n, \Gamma_i) \tag{5.31}$$

$$B(n, \Gamma_i) = \frac{1}{2^n}\left\{(1-\mu)\binom{n}{\lfloor v \rfloor} + \sum_{l=\lfloor v \rfloor + 1}^{n} \binom{n}{l}\right\} \tag{5.32}$$

where $n = |J_i|, v = (\Gamma_i + n)/2$, $\mu = v - \lfloor v \rfloor$ and $l \in J_i \backslash S_i$ such that $\hat{a}_{il}|x_l| > \hat{a}_{ir}|x_r|$

In comparison with bound 1, bound 2 does not involve the feasible solution $\boldsymbol{x}^*$ however solving this presents computational difficulty. Bound 3 is proposed as an approximation of bound 2 to reduce computational difficulty.

Bound 3

$$\Pr\left(\sum_{j\in J_i}\gamma_{ij}\eta_{ij} \geq \Gamma_i\right) \leq B(n,\Gamma_i)$$
$$B(n,\Gamma_i) \approx 1-\Phi\left(\frac{\Gamma_i-1}{\sqrt{n}}\right) \quad \textbf{(5.33)}$$

Where Φ is the cumulative distribution function of a standard normal distribution and is given by

$$\Phi(\theta) = \frac{1}{\sqrt{2\pi}}\int_{-\infty}^{\infty} exp\left(-\frac{y^2}{2}\right)dy \quad \textbf{(5.34)}$$

where $\theta = \Gamma_i/\sqrt{n}$, y is the value or position on the standard normal distribution

Comparison

In [192], bound 1 and bound 2 have been compared with a ULO problem with 10 uncertain coefficients ($n = 10$). The comparison results are shown in this section. Results from this comparison are given in Figure 5.1. It can be observed that, the probability of constraints violation estimated by bound 1 is higher than that of bound 2. This means that for a ULO problem with a small number of uncertainties, bound 1 overestimates the probability of constraints being violated in comparison with bound 2.

Further tests with $n = 100$ and $n = 2{,}000$ show that, the probabilities estimated by bound 2 and bound 3 are very similar while that of bound 1 is always higher. This is consistent with the results obtained with $n = 10$.

In conclusion, bound 2 and 3 are normally more accurate than bound 1, especially for problems with large numbers of uncertainties, but are more difficult to calculate. Bound 1 has low computational difficulty and a more flexible structure. As a result, for the rest of this research, bound 1 will be used to calculate the probability of constraint violation.

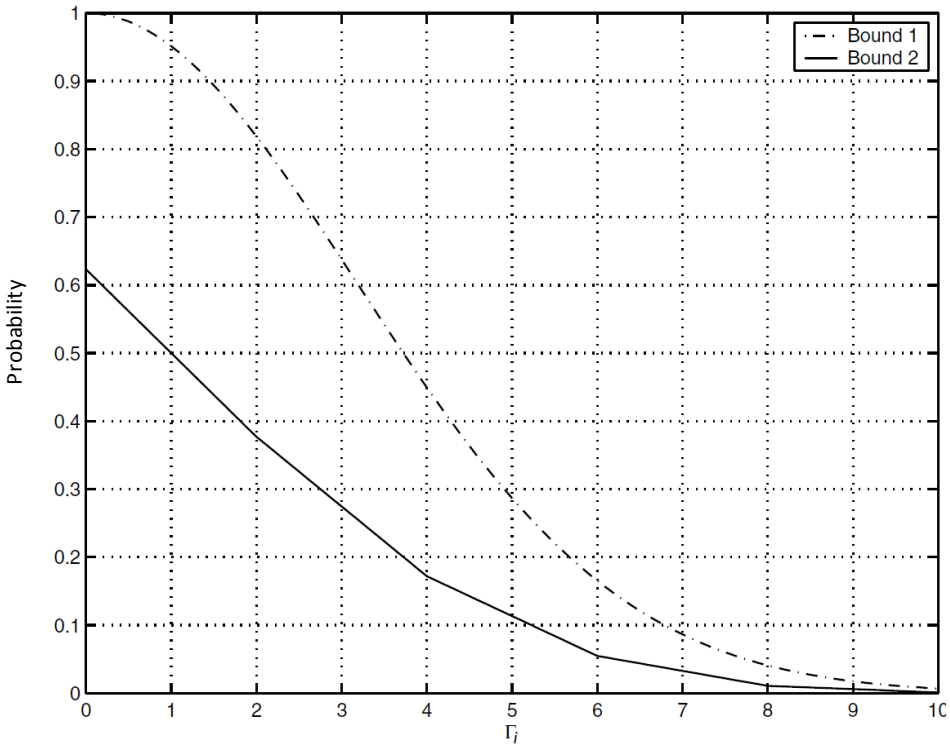

Figure 5.1 Probability of constraint violation with BoU of bound 1 and 2 for a ULO problem with $n = 10$ [192]

5.5 Probability of Success

In previous section, three methods for estimating probability of constraint violation are introduced. These methods ignore the distribution of uncertainty within the uncertainty interval therefore are only conservative estimation of the probability of constraint violation. In order to access more accurate probability of constraint violation, probabilistic methods such as Monte Carlo simulations (MCS) can be used.

Increasing the BoU will reduce the probability of constraints violation or increase the probability of success (PoS) of the solution. If MCS is applied, PoS can be defined as

$$PoS = \left(1 - \frac{N_{Vio}}{N_{Total}}\right) \times 100\% \tag{5.35}$$

where

N_{Total} the total number of Monte Carlo samples

N_{Vio} the number of violations recorded.

The selection of BoU is critical to the performance of the algorithm. A high BoU ensures high PoS however can be over-conservative. A low BoU reduces the cost but also lowers the PoS.

5.6 Algorithm Implementation

5.6.1 Python Implementation

There was no commercial software available to solve ULO problems with Bertsimas and Sim's formulation when this research was carried out. Therefore a solver based on Bertsimas and Sim's formulation was developed in Python by the author. This solver:

- Transforms ULO problems, as given in (5.1) to the formulation given from (5.20) to (5.27);
- Solves the problem in the form or (5.20) to (5.27) for a given BoU

The flow chart of the solver is given in Figure 5.2.

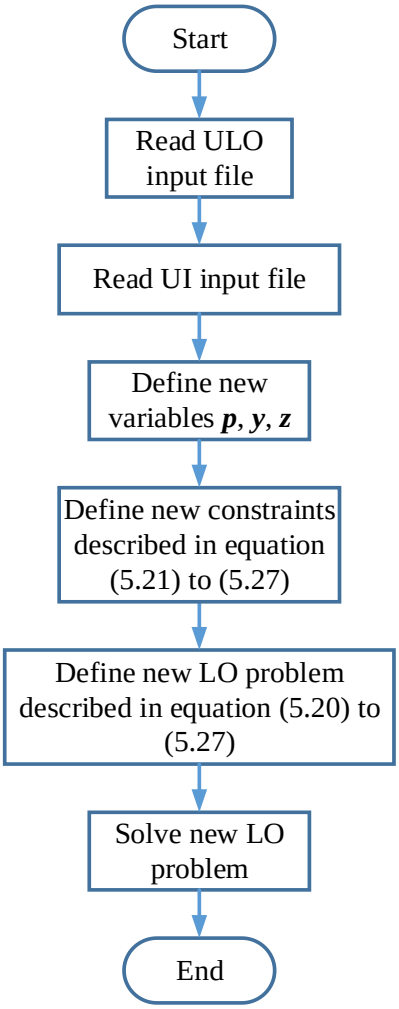

Figure 5.2 Flow Chart for the RO Solver in Python

Initially, the ULO problem definition and the uncertainty input files are read. The uncertainty input file contains the uncertainty intervals of uncertainty values and BoU for constraints if applicable. Next, extra parameters $\boldsymbol{p}$, $\boldsymbol{y}$, $\boldsymbol{z}$ and constraints are defined. The cost function remains the same. Once the new LO problem is defined, it can be solved with normal LO

solvers. In this script, Sequential Least SQuare Programming (SLSQP) method in SciPy has been used [195]. SLSQP method has been implemented previously in Python by Kraft [196].

5.6.2 Evaluation with a 30 Variable Problem

The Python script is tested with a 30 variable and 50 constraint problem. This problem is created and solved in Matlab. The parameters are detailed in Appendix D. It is assumed that, all coefficients of the 6th constraint a_{ij}, $i = 1,2,\dots,30, j = 6$ are uncertain. All the uncertain values have a UI of 10%. Thus, it becomes a ULO problem and $n = \Gamma_{max} = 30$. This problem is used to evaluate the solver. The evaluation process is illustrated below in Figure 5.3.

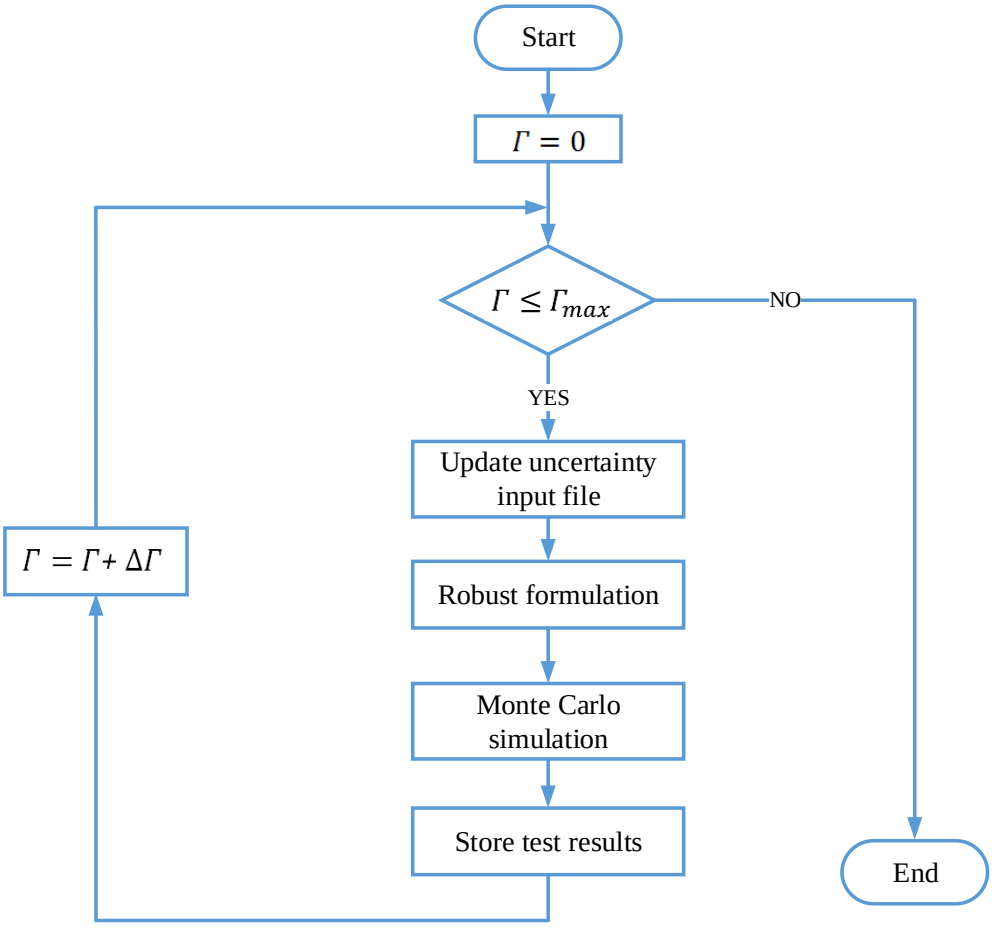

Figure 5.3 Testing for a 30 Variable Problem

The initial BoU is set to 0, as introduced in section 5.3.3, the RO formulation is equivalent to a normal LO problem. Thus, this solution only guarantees a low PoS. In each loop, the BoU Γ is increased by a step of $\Delta\Gamma = 0.5$, until $\Gamma = \Gamma_{max}$. For each updated Γ, an RO based ULO solver is executed to calculate a corresponding solution x. When the solution is available for the new BoU, Monte Carlo simulations (MCS) are carried out to test the probability of

constraint violation. In these MCS, each solution is evaluated with 10,000 samples. The uncertainty model has been introduced in (5.10) and (5.11). The error between the real value $\tilde{a}_{ij}$ and the nominal or the estimation of the value a_{ij} is given as

$$\tilde{a}_{ij} - a_{ij} \tag{5.36}$$

In this test, it is assumed that this error follows a uniform distribution. The choice of 10,000 samples for this problem guarantees a converged set of results. The results are depicted in Figure 5.4.

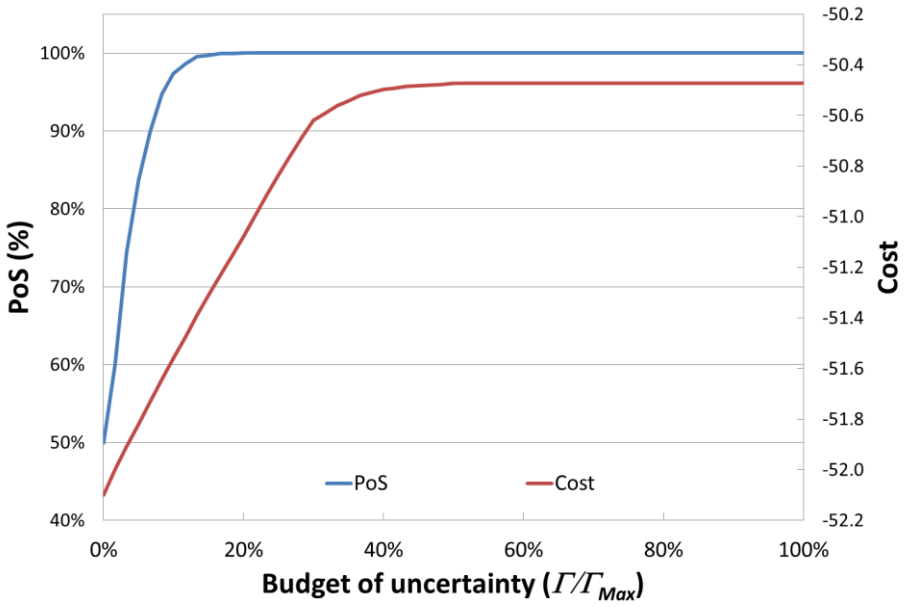

Figure 5.4 Test result of a 30 variable 50 constraints problem

Cost and PoS change with BoU

How the overall cost and PoS change with the increase of BoU can be observed from this figure. In this figure, the blue trace is the probability of success (PoS) and the red trace is the cost $\boldsymbol{c}'\boldsymbol{x}$. The PoS represents the reliability of the solution and is opposite to the probability of constraints violation. As can be observed, the PoS and the cost increase with BoU. When $\Gamma = 0$, the PoS is 50% approximately. The PoS increases to 100% when $\Gamma/\Gamma_{Max} = 20\%$.

Worst case scenario

The result when $\Gamma = \Gamma_{Max}$ is tested with the worst case scenario. The worst case is considered as all uncertain values $\tilde{a}_{ij}$ takes their values of either $\tilde{a}_{ij} = a_{ij} \mp \hat{a}_{ij}$ so that $\sum_j \tilde{a}_{ij} x_j$ has its maximum. In other words, the solution at $\Gamma = \Gamma_{Max}$, $\boldsymbol{x}_{\Gamma=\Gamma_{Max}}$ must satisfy

$$\max\left(\sum_j a_{ij}x_{j,\Gamma=\Gamma_{Max}} + \sum_j \hat{a}_{ij}x_{j,\Gamma=\Gamma_{Max}}\right) \leq b_j \quad \textbf{(5.37)}$$

It has been found that the solution for the worst case $\boldsymbol{x}_{\Gamma=\Gamma_{Max}}$ does not cause constraint violation.

Estimated PoS and Real PoS

The PoS from MCS is compared to the probability bound given in (5.28). In equation (5.28), the probability is given as the probability of constraint violation. This probability bound is based on Markov's inequality. Markov's inequality only provides an upper bound for the probability of violation $Pr\left(\sum_{j\in J_i}\gamma_{ij}\eta_{ij} \geq \Gamma_i\right)$, regardless of the distribution of the error $\tilde{a}_{ij} - a_{ij}$ or η_{ij}. Therefore, the probability bound can be seen as the most conservative estimation. On the other hand, due to the large number of samples, the results from MCS study can be seen as the "real" reliability. PoS derived from (5.28) and PoS from MCS study are compared in Figure 5.5. The red trace is the MCS result and the blue trace is the derived probability bound. Compared to the derived probability bound, the MCS result follow the trend of the derived bound but has a higher PoS at the same BoU.

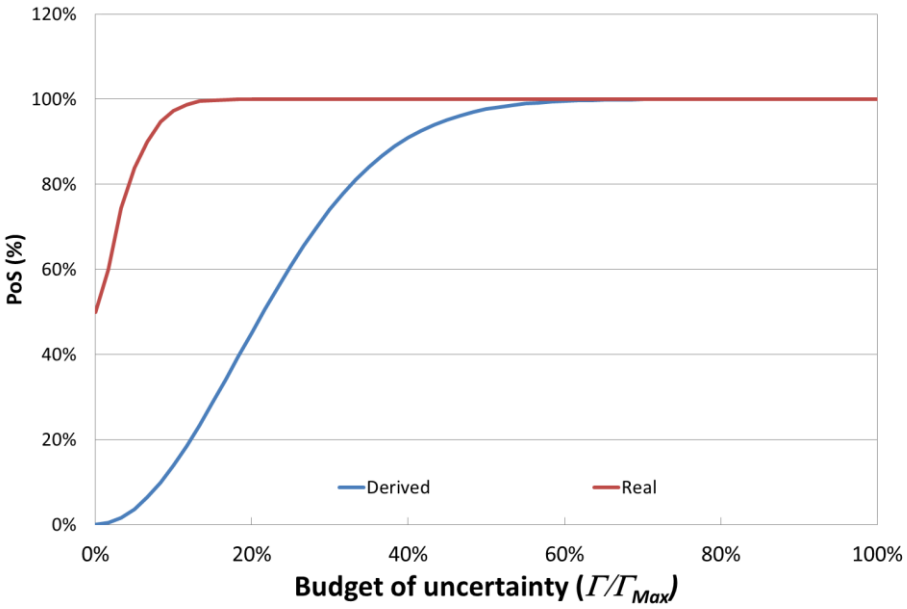

Figure 5.5 Comparison of derived PoS based on equation (5.28) and MCS results

The reasons why the real PoS is higher than the derived PoS are explained. Firstly, the derived PoS is based on the estimation given in equation (5.28) and is a very conservative bound for PoS. Secondly, this estimation has larger error when the number of uncertainties is small.

5.7 Discussion and conclusion

In this chapter, the importance of dealing with uncertainty and the concept of RO are introduced. This is followed by the presentation of the general form of the ULO problem. Three different formulations to solve the ULO problem are given. To enable the trade-off between probability of constraint violation and the cost, the bounds for the probability of constraint violation is discussed. The development of a Python based solver to RO problems was described. Finally, the operation of the Python solver is validated with a 30 variable, 50 constraint ULO problem.

Chapter 6. A Robust Optimisation Based Scheduling Scheme

6.1 Introduction

Solving uncertain linear optimization (ULO) problems with RO was introduced in the previous chapter. In this chapter, the RO technique is applied to solve a power system scheduling problem, which can be formulated as a ULO. The robust scheduling scheme is applied for energy storage systems (ESS) deployed in distribution networks to facilitate high penetrations of renewable energy sources (RES). This scheme schedules the charging and discharging of ESSs subject to State-of-Charge (SoC) limits, transmission line real-time thermal ratings (RTTRs) and voltage constraints.

Firstly, a scheduling scheme is proposed. This scheduling scheme consists of three stages, forecast stage, scheduling stage and post-event analysis stage. Next, the problem formulation in the scheduling stage is detailed. In section 6.3, the formulation without uncertainty is introduced first. This is followed by the formulation and solution with uncertainty in section 6.4. In this thesis, Budget of uncertainty (BoU) is used when solving an ULO problem. BoU controls the level of conservatism of the solution. The selection of UI, therefore, is critical to the performance of this RO based scheduling scheme. In section 6.5, two approaches of calculating BoU so that a required probability of success (PoS) can be achieved, are introduced. The first approach estimate the BoU with the probability bound introduced in section 5.4. The second approach, which uses a moderate number of MCS coupled with the Levenberg–Marquardt (LMA) curve fitting technique, has been proposed to estimate the optimal BoU, to ensure a desired level of PoS. Finally extensions of this scheme to take into consideration the uncertainty of DSR and reactive power are introduced.

6.2 Proposed Scheduling Scheme

In this section, the proposed scheduling scheme is introduced. The proposed scheduling scheme is illustrated in Figure 6.1. This scheme can be divided into three stages: Forecast, Scheduling and Post-event analysis stages.

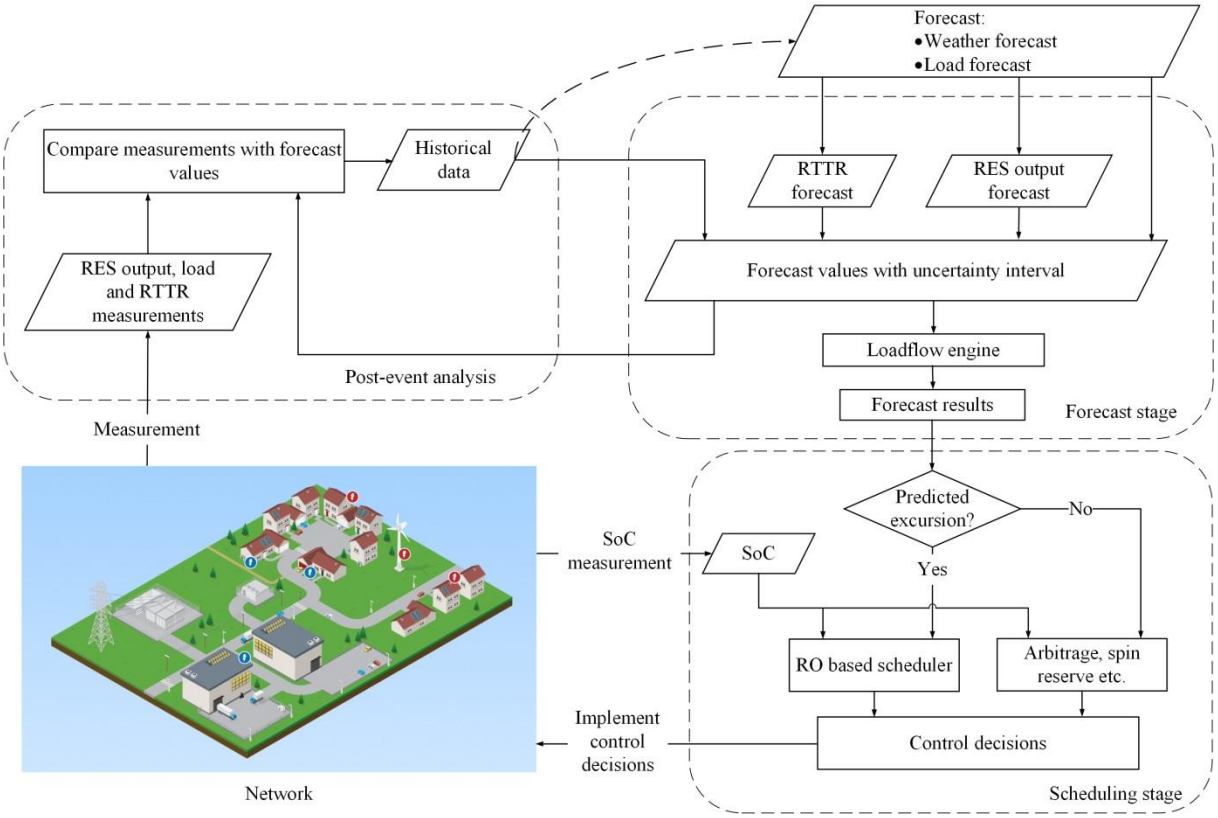

Figure 6.1 Proposed Scheduling Scheme

6.2.1 Forecast stage

Weather forecast data can be used to predict the RTTR of transformers and overhead lines, load and RES generation. The predicted RES generation output and load forecast (LF) data are used as input data to power flow calculations. Generating forecast values is beyond the scope of this research. It is assumed that forecast values, such as weather and load forecast, are already available. Both weather forecast and historical load profile from the post event analysis stage can be used as the input for load forecast.

The RO based approach adopted requires the UI of uncertainty associated with these input variables to be quantified. Therefore, the forecast values consist of forecast values and their UIs. However, depending on the forecast technique used and the variables of interest, UIs for each variable may not be always available. At the post-event analysis stage, historical data can be used to derive an estimation of this forecast error and can be used to derive the UI associated with this variable. This will be further explained in the description of the *Post-event analysis stage*.

6.2.2 Scheduling stage

At the scheduling stage, if a predicted line RTTR violation is found, based on the results from the forecast stage, RO based scheduling will be carried out. At this stage only nominal values

are used to check for excursions. Overhead line RTTR violation is based on the nominal forecast values. During the scheduling stage, state-of-charge (SoC) information from ESS will be used to inform the scheduler of the energy available. Based on this information, the RO based controller can decide the import or export from ESS. On the other hand, if there is no predicted line RTTR violation, the ESS unit(s) could be made available to provide other services such as arbitrage.

6.2.3 Post-event analysis

Finally, at the post-event stage, the real measurements of weather, generation, load and RTTR are compared to their forecast values. The selection of UIs is important for the performance of RO. If the UIs are too conservative, the decisions made by RO based approach will be conservative as well. On the contrary, if the uncertainty is underestimated, which means narrow UIs are adopted, the risk of constraints violations will increase. By comparing the predicted values to the real values, the quality of UIs can be improved. Therefore this feedback process can increase the robustness and reduce the conservatism of the scheme.

6.3 Problem Formulation without uncertainty

The scheduling scheme has been outlined in section 6.2 and uncertainties that involved in this scheme has been detailed in section 4.2. This section introduces the formulation of the RO based scheduling scheme. The formulation without uncertainty is introduced first. This is followed by an explanation of how the formulation is extended so that the aforementioned uncertainties can be managed.

The scheduling algorithm plans the import and export of ESS from time $t = 0$ to time $t = T$ so that line RTTR overloads and voltage violations can be avoided. This formulation uses power flow sensitivity factors (PFSFs) and voltage sensitivity factors (VSFs) to estimate the power flow and voltage change due to ESS and RES. In Chapter 3, two methods to calculate VSFs and PFSFs have been introduced. In this scheme, the incremental method is used. PFSFs and VSFs are calculated for each timestep. The network models for each timestep will be updated based on load and generation forecast.

6.3.1 Objective function

The objective function minimizes the cost of charging or discharging ESS during the scheduling period.

$$min \sum_{t=0}^{T} \sum_{m=1}^{N_{ESS}} C_{ESS_m} \cdot P_{ESS_m}^{t} \quad \textbf{(6.1)}$$

where

T	the total number of timesteps
t	number of timestep, integer between 0 to T
N_{ESS}	the total number of ESS
m	an integer indicating ESS
C_{ESS_m}	the cost of charging or discharging ESS m
$P_{ESS_m}^t$	the power import/export of ESS m at time t

C_{ESS_m} is determined by the capital cost per kW and the state-of-health (SoH) of ESS m and is not the actual cost of using ESS

$$C_{ESS_m} = k_1 \cdot C_{ESS_m,Capital} + k_2 \cdot SoH_{ESS_m} \quad \textbf{(6.2)}$$

where

k_1	positive coefficient for the capital cost
k_2	negative coefficient for the state of health
$C_{ESS_m,Capital}$	the capital cost of ESS m
SoH_{ESS_m}	the State-of-Health of ESS m

In this cost function, two weight factors k_1 and k_2 are introduced. k_1 is a positive coefficient so that ESSs with lower capital costs will result in a lower cost. On the other hand k_2 is a negative coefficient therefore ESSs with more useful lifetime are more likely to be chosen. By varying the weight factors k_1 and k_2, this cost function enables a trade-off between the capital cost and the SoH of ESS. SoH can be quantified by the number of cycles left before the remaining capacity of the system deteriorates to 80% [134].

6.3.2 Constraints

Constraints in this research include power flow constraints, voltage constraints and ESS SoC constraints.

Power flow constraint

The power flow constraint estimates the apparent power flow on each branch and ensures no RTTR of OHLs and transformers are violated. This constraint is detailed below.

$$-S^t_{ij,RTTR} \leq S^t_{ij,Estimate} \leq S^t_{ij,RTTR} \tag{6.3}$$

where

$S^t_{ij,RTTR}$ the RTTR of branch from bus i to bus j (branch ij) at time t

$S^t_{ij,Estimate}$ the estimated load flow through branch ij

$S^t_{ij,Estimate}$ is an estimation of the load flow through branch ij considering the impacts of ESS, RES output uncertainty and busbar load uncertainty using PFSFs, according to:

$$S^t_{ij,Estimate} = S^t_{ij,Forecast} + \sum_{m=1}^{N_{ESS}} PFSF^t_{ij,ESS_m} \cdot P^t_{ESS_m} + \sum_{n=1}^{N_{RES}} PFSF^t_{ij,RES_n} \cdot \Delta P^t_{RES_n} + \sum_{p=1}^{N_{Bus}} PFSF^t_{ij,Bus_p} \cdot \Delta P^t_{Bus_p} \tag{6.4}$$

where

$S^t_{ij,Forecast}$ the forecasted load flow through branch ij at time t, based on power flow calculations at the forecast stage

$PFSF^t_{ij,ESS_m}$ the PFSF of ESS m to branch ij at time t

$PFSF^t_{ij,RES_n}$ the PFSF of RES n to branch ij at time t

$PFSF^t_{ij,Bus_p}$ the PFSF of load at busbar p to branch ij at time t

N_{ESS} the total number of ESS

N_{RES} the total number of renewable energy sources

N_{Bus} the total number of buses

$\Delta P^t_{RES_n}$ the forecast error of RES power output at time t

$\Delta P^t_{Bus_p}$ the forecast error of load at time t

The forecast load flow through branch ij is based on predicted load and generation values and is calculated by running a full AC loadflow. Only nominal values of load and generation forecast are used. Based on this forecast, the load flow through this branch with the inclusion of ESS and the uncertainty of RES output and load can be calculated. In equation (6.4), PFSFs are used. PFSFs represent the apparent power change (in MVA) on branch ij due to per MW real power change from ESS m, RES n and load p.

In this formulation, only the power output and busbar load forecast error is used. The reason is explained below. If the actual power output of RES and the busbar load at time t is given by

$$P^t_{RES_n} = P^t_{RES_n,Forecast} + \Delta P^t_{RES_n} \quad \textbf{(6.5)}$$

$$P^t_{Bus_p} = P^t_{Bus_p,Forecast} + \Delta P^t_{Bus_p} \quad \textbf{(6.6)}$$

where

$P^t_{RES_n,Forecast}$ is the forecasted output of RES n at time t

$P^t_{Bus_p,Forecast}$ is the forecasted load of busbar p at time t

At the forecast stage, $P^t_{RES_n,Forecast}$ and $P^t_{Bus_p,Forecast}$ are used to calculate $S^t_{ij,Forecast}$ and as a result, to estimate the power flow on branch ij at time t, only the forecast error $\Delta P^t_{RES_n}$ and $\Delta P^t_{Bus_p}$ is needed.

The use of sensitivity factors is a linearization of the non-linear load flow equations. In this work, instead of constant values, PFSFs that vary depending on network conditions are used. It is found in [197] that, PFSFs are only insensitive to the operating point in networks with sufficient voltage support. With the increasing penetrations of RES and future load, voltage profiles of distribution networks will be more volatile. In this work, the PFSFs are calculated based on loadflow equations with updated load and generation values for each timestep to enhance the accuracy.

Constraint (6.3) is only applied to branches with high PFSF with respect to ESS unit(s) or renewables to reduce the size of the problem.

Voltage constraint

Similar to power flow constraints, voltage constraints estimate the voltage of busbar i and ensure that the estimated voltage $V_{i,Estimate}^{t}$ does not exceed its limits

$$V_{Min,i} \leq V_{i,Estimate}^{t} \leq V_{Max,i} \tag{6.7}$$

$V_{i,Estimate}^{t}$ is defined as follows

$$V_{i,Estimate}^{t} = V_{i,Forecast}^{t} + \sum_{m=1}^{N_{ESS}} VSF_{i,ESS_m}^{t} \cdot P_{ESS_m}^{t} + \sum_{n=1}^{N_{RES}} VSF_{i,RES_n}^{t} \cdot \Delta P_{RES_n}^{t} + \sum_{p=1}^{N_{Bus}} VSF_{i,Bus_p}^{t} \cdot \Delta P_{Bus_p}^{t} \tag{6.8}$$

where

$V_{Min,i}$ the lower voltage limits of busbar i

$V_{Max,i}$ the upper voltage limits of busbar i

$V_{i,Forecast}^{t}$ the forecasted voltage of busbar i at time t based on load flow calculations at the forecast stage

VSF_{i,EES_m}^{t} the voltage sensitivity factor from ESS m to busbar i at time t

VSF_{i,RES_n}^{t} the voltage sensitivity factor from RES n to busbar i at time t

VSF_{i,Bus_p}^{t} the voltage sensitivity factor from load at busbar p to busbar i at time t

This constraint guarantees all busbar voltage within limits. Similar to power flow constraints, only critical busbars with high VSFs with respect to ESSs will be added to this constraint.

ESS SoC constraint

The ESS SoC constraints include equality and inequality constraints. The equality constraints, given in equation (6.9), calculate the SoC of all ESSs for all timesteps. The inequality constraints are the SoC limits.

The SoC of ESS is calculated by

$$SoC_{ESS_m}^{t+1} = SoC_{ESS_m}^{t} + d_{ESS_m}^{t} \cdot \frac{\Delta t \cdot \frac{P_{ESS_m}^{t}}{\eta_{ESS_m,discharge}}}{E_{ESS_m}} \tag{6.9}$$

$$+(1-d_{ESS_m}^t)\cdot\frac{\Delta t\cdot P_{ESS_m}^t\cdot\eta_{ESS_m,charge}}{E_{ESS_m}}$$

where

$SoC_{ESS_m}^t$ the SoC of ESS at time t

Δt the duration of each timestep

$\eta_{ESS_m,discharge}$ the discharge efficiency of ESS m

$\eta_{ESS_m,charge}$ the charge efficiency of ESS m

$d_{ESS_m}^t$ a binary variable, $d=1$ if discharge and $d=0$ if charge

E_{ESS_m} the energy capacity of the ESS m

This equation calculates the SoC of ESS m for each timestep. The efficiencies for charging and discharging have been taken into consideration. The next constraint prevents the ESS from over charging or over discharging

$$SoC_{ESS_m,Min}^t \le SoC_{ESS_m}^t \le SoC_{ESS_m,Max}^t \quad \textbf{(6.10)}$$

where

$SoC_{ESS_m,Min}^t$ the lower limit of SoC for ESS m at time t

$SoC_{ESS_m,Max}^t$ the upper limit of SoC for ESS m at time t

It should be noted that the SoC limits in this constraint $SoC_{ESS_m,Min}^t$ and $SoC_{ESS_m,Max}^t$ can be defined by the DNO or the operator of the ESS. ESSs will be used for other purposes, such as frequency control and harmonics elimination, which are not included in this scheme, the ESSs may therefore be given lower SoC limits that are higher than the technical lower limits. For instance, although some Li-ion batteries are able to be discharged to 0% SoC [198], the lower limits $SoC_{ESS_m,Min}^t$ can be set to 40% so that the ESSs can still be used for frequency control during the peak periods.

6.3.3 Generalization of the Proposed Formulation

The objective function and constraints introduced in this section are summarised below

$$min \sum_{t=0}^{T} \sum_{m=1}^{N_{ESS}} C_{ESS_m} \cdot P_{ESS_m}^t$$

Subject to

$$-S_{ij,RTTR}^t \leq S_{ij,Forecast}^t + \sum_{m=1}^{N_{ESS}} PFSF_{ij,ESS_m}^t \cdot P_{ESS_m}^t + \sum_{n=1}^{N_{RES}} PFSF_{ij,RES_n}^t \cdot \Delta P_{RES_n}^t + \sum_{p=1}^{N_{Bus}} PFSF_{ij,Bus_p}^t \cdot \Delta P_{Bus_p}^t \leq S_{ij,RTTR}^t$$

$$V_{Min,i} \leq V_{i,Forecast}^t + \sum_{m=1}^{N_{ESS}} VSF_{i,ESS_m}^t \cdot P_{ESS_m}^t + \sum_{n=1}^{N_{RES}} VSF_{i,RES_n}^t \cdot \Delta P_{RES_n}^t + \sum_{p=1}^{N_{Bus}} VSF_{i,Busp}^t \cdot \Delta P_{Bus_p}^t \leq V_{Max,i} \quad \textbf{(6.11)}$$

$$SoC_{ESS_m,Min}^t \leq SoC_{ESS_m}^t \leq SoC_{ESS_m,Max}^t$$

$$SoC_{ESS_m}^{t+1} = SoC_{ESS_m}^t + d_{ESS_m}^t \cdot \frac{\Delta t \cdot \frac{P_{ESS_m}^t}{\eta_{ESS_m,discharge}}}{E_{ESS_m}} + (1 - d_{ESS_m}^t) \cdot \frac{\Delta t \cdot P_{ESS_m}^t \cdot \eta_{ESS_m,charge}}{E_{ESS_m}}$$

The meaning of this formulation is summarised. The cost function minimises the use of ESS. The first constraint estimates the power flow on the branches due to the import/export of ESS and the change of RES output and load. Similarly, the second constraint estimates the voltage of each busbar due to the import/export of ESS and the change of RES output and load. The last two constraints ensures ESS will not be over-charge or over-discharged.

The general form of a linear optimization problem has been introduced in section 4.3. This ESS scheduling problem given in (6.11) can be generalized as a LO problem as given in equation (4.10).

$$min\, f(\boldsymbol{P}_{ESS}^t) \quad \textbf{(6.12)}$$

Subject to

$$\boldsymbol{l} \leq \boldsymbol{h}\left(\boldsymbol{P}_{ESS}^t, \Delta \boldsymbol{P}_{RES}^t, \Delta \boldsymbol{P}_{Bus}^t, \boldsymbol{S}_{Branch,Forecast}^t, \boldsymbol{V}_{Bus}^t, \boldsymbol{SoC}_{ESS}^{t=0}\right) \leq \boldsymbol{u}$$
$$\boldsymbol{g}(\boldsymbol{P}_{ESS}^t, \boldsymbol{SoC}_{ESS}^{t=0}) = \boldsymbol{0} \quad \textbf{(6.13)}$$

where

$\boldsymbol{P}_{ESS}^{t}$	the real power import or export of ESS m at time t
$f()$	the cost function
$h()$	the function for inequality linear constraints
$\boldsymbol{l}$	the lower limit of inequality linear constraints
$\boldsymbol{u}$	the upper limit of inequality linear constraints
$g()$	the function for equality linear constraints
$\Delta\boldsymbol{P}_{RES}^{t}$	the error of RES power output at time t
$\Delta\boldsymbol{P}_{Bus}^{t}$	the error of busbar load at time t
$\boldsymbol{S}_{Branch,Forecast}^{t}$	the forecasted load flow of branch ij at time t
$\boldsymbol{SoC}_{ESS}^{t=0}$	the SoC of ESS at time $t = 0$
$\boldsymbol{V}_{\boldsymbol{Bus}}^{\boldsymbol{t}}$	the forecasted voltage of busbar i at time t based on power flow calculations

By finding a feasible solution $\boldsymbol{P}_{ESS}^{t}$, this formulation minimizes the cost of charging and discharging ESS and at the same time eliminates the risk of line RTTR overload, voltage limit violations and over use of ESSs. The equality constraints calculate the SoC of ESS from $t = 0$ to time $t = T$. The inequality constraints include power flow constraints, voltage constraints and SoC constraints.

6.4 Problem Formulation with Uncertainty

Considering the aforementioned uncertain inputs, the objective function remains the same. The constraints given in (6.13) become

$$\boldsymbol{l} \leq \boldsymbol{h}\left(\boldsymbol{P}_{ESS}^{t}, \Delta\widetilde{\boldsymbol{P}}_{RES}^{t}, \Delta\widetilde{\boldsymbol{P}}_{Bus}^{t}, \tilde{\boldsymbol{S}}_{Branch,Forecast}^{t}, \boldsymbol{V}_{Bus}^{t}, \widetilde{\boldsymbol{SoC}}_{ESS}^{t=0}\right) \leq \boldsymbol{u} \tag{6.14}$$

$$\boldsymbol{g}\left(\boldsymbol{P}_{ESS}^{t}, \widetilde{\boldsymbol{SoC}}_{ESS}^{t=0}\right) = \boldsymbol{0} \tag{6.15}$$

The objective function in (6.12) and constraints given in (6.14) and (6.15) form an uncertain linear optimization problem. It is assumed that all uncertain values are independent and each uncertain variable a is bounded by an interval given as

$$\tilde{a} \in [a - \hat{a}, a + \hat{a}] \tag{6.16}$$

The uncertainty model has been introduced in section 5.2.3. The new formulation is summarised as:

$$min\, f(\boldsymbol{P}_{ESS}^{t})$$

Subject to

$$\begin{gathered} \boldsymbol{l} \leq \boldsymbol{h}\left(\boldsymbol{P}_{ESS}^{t}, \Delta\widetilde{\boldsymbol{P}}_{RES}^{t}, \Delta\widetilde{\boldsymbol{P}}_{Bus}^{t}, \tilde{\boldsymbol{S}}_{Branch,Forecast}^{t}, \boldsymbol{V}_{Bus}^{t}, \widetilde{\boldsymbol{SoC}}_{ESS}^{t=0}\right) \leq \boldsymbol{u} \\ \boldsymbol{g}\left(\boldsymbol{P}_{ESS}^{t}, \widetilde{\boldsymbol{SoC}}_{ESS}^{t=0}\right) = \boldsymbol{0} \end{gathered} \tag{6.17}$$

And all uncertain values a follow

$$\tilde{a} \in [a - \hat{a}, a + \hat{a}]$$

The scheduling problem for ESS, formulated as (6.17), can be generalised as the problem given in equation (5.9). In Chapter 5, how to solve (5.9) with Bertsimas and Sim's formulation has been introduced. Bertsimas and Sim's formulation solves this problem by transforming (6.17) into another linear but certain formulation as given from (5.20) to (5.27).

In Bertsimas and Sim's formulation, budget of uncertainty (BoU) is used. The meaning of BoU in this application is explained with an example. The right-hand side of constraint (6.3) at time t is given as

$$\begin{gathered} S_{ij,Forecast}^{t} + \sum_{n=1}^{N_{ESS}} PFSF_{ij,ESS_m}^{t} \cdot P_{ESS_m}^{t} + \sum_{n=1}^{N_{RES}} PFSF_{ij,RES_n}^{t} \cdot \Delta P_{RES_n}^{t} + \\ \sum_{p=1}^{N_{Bus}} PFSF_{ij,Bus_p}^{t} \cdot \Delta P_{Bus_p}^{t} \leq S_{ij,RTTR}^{t} \end{gathered} \tag{6.18}$$

Considering the uncertainty of RES, load forecast and RTTR, (6.18) becomes

$$\begin{gathered} S_{ij,Forecast}^{t} + \sum_{n=1}^{N_{ESS}} PFSF_{ij,ESS_m}^{t} \cdot P_{ESS_m}^{t} + \sum_{n=1}^{N_{RES}} PFSF_{ij,RES_n}^{t} \cdot \Delta\tilde{P}_{RES_n}^{t} + \\ \sum_{p=1}^{N_{Bus}} PFSF_{ij,Bus_p}^{t} \cdot \Delta\tilde{P}_{Bus_p}^{t} \leq \tilde{S}_{ij,RTTR}^{t} \end{gathered} \tag{6.19}$$

where

$\tilde{S}_{ij,RTTR}^{t}$ the uncertainty value of predicted RTTR of branch ij at time t

$\Delta\tilde{P}_{RES_n}^{t}$ the uncertainty value of predicted power output of RES n at time t

$\Delta\tilde{P}_{Bus_p}^{t}$ the uncertainty value of load forecast of busbar p at time t

Therefore the total number of uncertainties N_u in constraint (6.19) is

$$N_u = N_{RES} + N_{Bus} + 1 \tag{6.20}$$

Denoting the BoU for this constraint as Γ_i^t, it follows that

$$0 \leq \Gamma_i^t \leq N_u \tag{6.21}$$

For this constraint, BoU means how many of these forecast values will greatly deviate from their nominal values, in other words, their real values $\tilde{a}_{ij}$ will be close or equal to their lower or upper bounds. For simplicity, the rest of this thesis uses the normalized value Γ/N_u to represent the BoU.

6.5 Optimal Budget of Uncertainty and Probability of Success Estimation

Increasing the BoU will reduce the probability of constraints violation or increase the probability of success (PoS) of the solution. PoS is defined as

$$PoS = \left(1 - \frac{N_{Vio}}{N_{Total}}\right) \times 100\% \tag{6.22}$$

where

N_{Total} the total number of Monte Carlo samples

N_{Vio} the number of violations recorded.

The selection of BoU is critical to the performance of the algorithm. A high BoU ensures high PoS however can be over-conservative. A low BoU reduces the cost but also lowers the PoS. In the following section, two approaches are introduced to estimate the PoS of a given BoU.

The minimum BoU which guarantees the required PoS is called the optimal BoU (OBoU). In the UK, for single and multi-circuit supply systems, the aggregate percentage of time when the design temperature of conductors can be exceeded is 0% and 3%, respectively [24, 199]. This standard is adopted by UK DNOs for operating systems with static ratings. Consistent with this approach, in this work PoSs of 100% and 97% have been used. In order to calculate charge or discharge profiles for ESSs which are able to provide the required level of PoS for the system, the corresponding OBoU needs to be calculated first.

In this section, two methods to estimate OBoU are proposed. The first approach estimates the relationship between the BoU and the PoS based on Bound 1 introduced in section 5.4. The

second approach combines this bound with moderate numbers of MCS and a curve fitting technique. These two approaches are introduced below.

6.5.1 Estimation of OBoU Based on Probability Bounds of Constraint Violation (Bound 1)

As has been shown in section 5.4, the PoS is a function of BoU Γ_i and can bounded by

$$PoS \geq 1 - \exp(-\frac{\Gamma_i^2}{2 \cdot N_u}) \tag{6.23}$$

where

i the index of constraints, i.e. this is the *i*th constraint in the formulation

Γ_i the budget of uncertainty for the ith constraint

Based on (6.23), the OBoU for a required PoS is given by

$$\Gamma_i = \sqrt{-2N_u \cdot \ln(1 - PoS)} \tag{6.24}$$

Once the required PoS is defined, the OBoU for this PoS can be calculated. However, as shown in Chapter 5, this estimation is easy to compute but can be conservative. This estimation is based on the assumption that the errors are symmetrically distributed regardless of the type of distributions. Furthermore, this estimation is less accurate when the maximum number of uncertainties N_u is small. To address the limitations of this estimation, extra parameters are introduced and detailed below.

6.5.2 Estimation of OBoU Based on MCS and Curve Fitting Technique

In this research, a new approach to estimate the corresponding PoS of a given BoU is proposed. Firstly, three new parameters are introduced into equation (6.23) to enable tuning of the shape of this curve. Secondly, a practical method is introduced to calculate the values of the introduced values. This method combines MCS and curve fitting technique. To depict the curve between BoU and PoS, a large number of Monte Carlo simulations are required. MCS is accurate but also time consuming. The method proposed in this section can reduce the required number of Monte Carlo simulations dramatically. This method is detailed below.

Extension of equation (6.23)

To describe the PoS curve accurately, three extra parameters are introduced and equation (6.23) can be expressed with the following

$$PoS = g(\Gamma_i, a, b, c) = a - b \cdot \exp(-c \cdot \Gamma_i^2) \tag{6.25}$$

where

$g(\Gamma_i, a, b, c)$ the function to estimate PoS

a, b, c parameters introduced to modify the curve

By calculating the values of a, b and c, $g(\Gamma_i, a, b, c)$ is capable of describing the PoS curve. The flexible structure of $g(\Gamma_i, a, b, c)$ enables the establishment of the relationship between the PoS and Γ_i. The values of a, b and c can be calculated by using curve fitting techniques.

Combining MCS with curve fitting method

To calculate the values of the parameters, only three inputs and outputs, Γ and corresponding PoS, are required. The PoS of a given BoU can be achieved by running a Monte Carlo simulation (MCS). This method is illustrated in Figure 6.2 below.

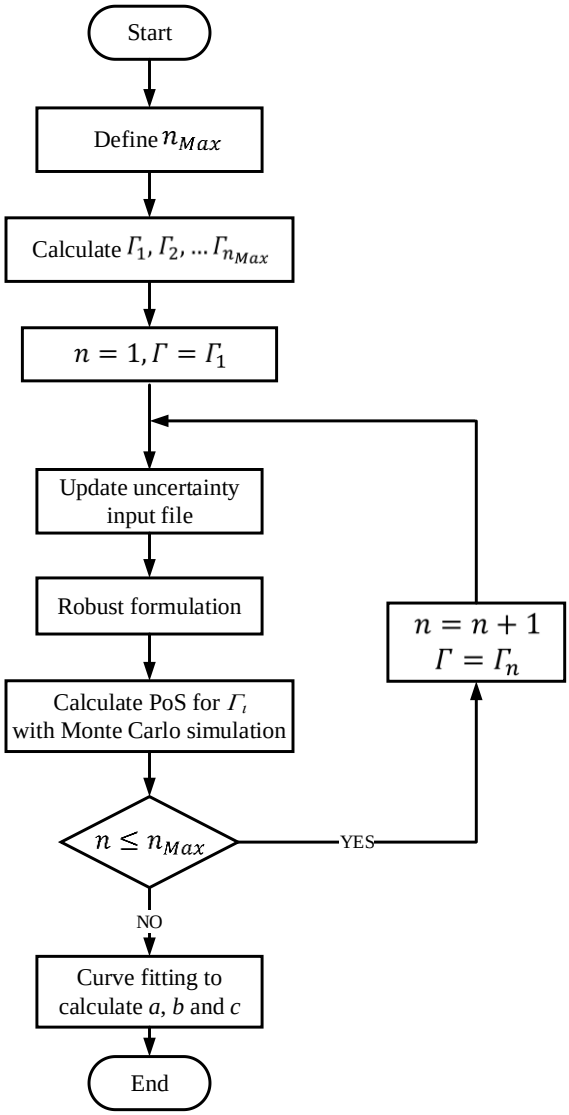

Figure 6.2 Estimation of OBoU Based on MCS and Curve Fitting Technique

First of all, the number of input values n_{Max} is decided. In this case, there are three parameters to be calculated and therefore the minimum number of input values is three and $n_{Max} \geq 3$. Based on the number of inputs, the range of BoUs can be decided. The BoUs should be chosen that the full range of the curve is covered. Next, the RO problem is solved for all the given BoU values with the RO solver introduced in section 5.5. The PoS of solutions at different BoU are tested with MCS. Once the set of data points, BoU $\Gamma_i, i = 1,2, \dots, n_{Max}$ and corresponding PoS, are available, the values of *a*, *b* and *c* can be calculated with curve fitting techniques. The aim is to find the suitable *a*, *b* and *c* values so that $g(\Gamma_i, a, b, c)$ is the best description for the input data points. In the next section, the curve fitting technique is detailed.

The Levenberg–Marquardt algorithm

The input to the curve fitting algorithm is the PoS at different Γ. In this thesis, Levenberg–Marquardt algorithm (LMA) has been adopted to solve the curve fitting problem. LMA is a technique for solving non-linear least square problems and is used widely to solve curve fitting problems. LMA minimizes the least square of the error between the inputs and the output, in this case, by finding the correct parameters *a*, *b* and *c*. The LMA technique minimises the least square between the real PoS, generated through MCS, and the estimated PoS by changing *a*, *b* and *c*. This can be expressed as

$$min\ S(a,b,c) = \sum_{n=1}^{n_{Max}} [PoS_n - g(\Gamma_n, a, b, c)]^2 \quad \textbf{(6.26)}$$

where

PoS_n is the PoS for the *n*th BoU Γ_n, this value is achieved from an MCS study detailed in section 6.5.2

LMA is available in the Matlab curve fitting toolbox.

The Effect of the Parameters

The parameters *a*, *b* and *c* have different effects on the fitting results. In the following section, the impact of changing the values of *a*, *b* and *c* on the maximum, minimum and derivatives of $g(\Gamma_i, a, b, c)$ is introduced. The aim of this section is to provide a guidance on how the change of the parameters *a*, *b* and *c* can affect the curve. The minimum value of the curve is decided by the difference between *a* and *b*. the maximum value of the curve is dependent on the value of *a*. The derivative, or the rate of the curve is a function of *b*, *c* and Γ_i.

- **Minimum PoS ($\Gamma = 0$)**

When $\Gamma/\Gamma_{Max} = 0$, $\exp(-c \cdot \Gamma_i^2) \rightarrow 1$ and PoS reaches its minimum,

$$\min[g(\Gamma_i, a, b, c)\ ] \approx a - b \tag{6.27}$$

- **Maximum PoS ($\Gamma = \Gamma_{Max}$)**

When $\Gamma/\Gamma_{Max} = 1$, if c is a large enough number then $\exp(-c \cdot \Gamma_i^2) \rightarrow 0$ and PoS reaches its maximum,

$$\max[g(\Gamma_i, a, b, c)\ ] \approx a \tag{6.28}$$

- **Derivative**

The derivative of $g(\Gamma_i, a, b, c)$ is given as

$$\frac{\partial g(\Gamma_i, a, b, c)}{\partial \Gamma_i} = 2b \cdot c \cdot \Gamma_i \cdot \exp(-c \cdot \Gamma_i^2) \tag{6.29}$$

6.6 Extension of this formulation

6.6.1 Demand Side Response

The formulation proposed in equation (6.11) can be extended to take the uncertainty of DSR into consideration.

$$min \sum_{t=0}^{T} \left(\sum_{m=1}^{N_{ESS}} C_{ESS_m} \cdot P_{ESS_m}^t + \sum_{q=1}^{N_{DSR}} C_{DSR_q} \cdot P_{DSR_q}^t \right)$$

Subject to

$$-S_{ij,RTTR}^t \leq S_{ij,Forecast}^t + \sum_{m=1}^{N_{ESS}} PFSF_{ij,ESS_m}^t \cdot P_{ESS_m}^t + \sum_{n=1}^{N_{RES}} PFSF_{ij,RES_n}^t \cdot \Delta\tilde{P}_{RES_n}^t + \sum_{p=1}^{N_{Bus}} PFSF_{ij,Bus_p}^t \cdot \Delta\tilde{P}_{Bus_p}^t + \sum_{q=1}^{N_{DSR}} PFSF_{ij,DSR_q}^t \cdot \tilde{P}_{DSR_q}^t \leq \tilde{S}_{ij,RTTR}^t \tag{6.30}$$

$$V_{Min,i} \leq V_{i,Forecast}^t + \sum_{m=1}^{N_{ESS}} VSF_{i,ESS_m}^t \cdot P_{ESS_m}^t + \sum_{n=1}^{N_{RES}} VSF_{i,RES_n}^t \cdot \Delta\tilde{P}_{RES_n}^t + \sum_{p=1}^{N_{Bus}} VSF_{i,Busp}^t \cdot \Delta\tilde{P}_{Bus_p}^t + \sum_{q=1}^{N_{DSR}} VSF_{i,DSR_q}^t \cdot \tilde{P}_{DSR_q}^t \leq V_{Max,i}$$

$$SoC_{ESS_m,Min}^t \leq \widetilde{SoC}_{ESS_m}^t \leq SoC_{ESS_m,Max}^t$$

$$SoC_{ESS_m}^{t+1} = \widetilde{SoC}_{ESS_m}^{t} + d_{ESS_m}^{t} \cdot \frac{\Delta t \cdot \frac{P_{ESS_m}^{t}}{\eta_{ESS_m,discharge}}}{E_{ESS_m}} + (1 - d_{ESS_m}^{t}) \cdot \frac{\Delta t \cdot P_{ESS_m}^{t} \cdot \eta_{ESS_m,charge}}{E_{ESS_m}}$$

where

N_{DSR} the total number of DSR q

$PFSF_{ij,DSR_q}^{t}$ the power flow sensitivity factor of DSR q to branch ij (MVA/MW)

VSF_{i,DSR_q}^{t} the voltage sensitivity factor of DSR q to bus i (p.u./MW)

$P_{DSR_q}^{t}$ the power decrease or increase due to DSR q

$\tilde{P}_{DSR_q}^{t}$ the uncertain power decrease of increase due to DSR q

In this formulation, DSR is formulated the same as ESS. As discussed in section 2.3. DSR can be seen as one type of energy storage. The cost function consists of the cost of using ESS and DSR. The power flow and voltage constraints use PFSF and VSF to estimate the impact of DSR.

6.6.2 Reactive Power

In the formulation proposed in (6.11) and (6.30), only real power from ESS and DSR has been considered. This formulation can be modified such that the scheduling problem can be solved with reactive power injection. The PFSFs used in this formulation represents the apparent power change through branch ij in MVA due to the real power injection or extraction from ESS or DSR. The VSFs used in this formulation represents the per unit voltage change at bus i due to real power injection or extraction from ESS or DSR. If the SFs are replaced by reactive power sensitivity factors, i.e. MVA/MVAr and pu/MVAr, this formulation can be used to solve scheduling problems with reactive power.

6.7 Discussion and Conclusion

In this chapter, the use of RO to solve a scheduling problem which is cognisant of the input data uncertainty is proposed. Firstly, the formulation without considering uncertainty is introduced. This is followed by a description of the robust formulation considering load, RTTR and RES generation uncertainty. This uncertain linear optimization problem is solved by the method proposed by Bertsimas and Sim. In this method, budget of uncertainty is introduced to control the level of conservatism. The solution at a higher BoU has a higher

probability of success (PoS). Based on BoU, the concept of OBoU is proposed in section 6.5 by the author. OBoU is the minimum BoU which guarantees a desired PoS. Two methods have been introduced to calculate the OBoU. The first method uses the probability bounds introduced in section 5.4. The second method uses a moderate number of MCSs coupled with the LMA curve fitting technique to estimate the relationship between BoU and PoS.

The proposed scheduling scheme presents several advantages compared to stochastic optimization and chance constraint techniques. In scenarios where, for uncertain values, only their UIs exist or their PDFs are only partially available or even inaccurate, techniques such as stochastic optimization or chance-constraint programming are unable to solve the problem. On the other hand, it has been shown that the proposed RO based scheduling scheme is still able to provide robust solutions to avoid branch line RTTR violation, cognizant of ESS SoC limits and network voltage constraints. In such scenarios, approach 1 based on equation (5.28) is able to provide robust solutions based on simple calculations in a very short time even for a large network. In scenarios where accurate PDFs are available for all the uncertain values, the advantages of RO based scheduling scheme still exist. Under such circumstances, both the estimation and the curve fitting based approaches can be used to calculate OBoU. The estimation approach can be applied to calculate a slightly conservative but robust solution in a very short time. Curve fitting based approach constructs the function between BoU and PoS through MCS. MCS runs a large number of load flow calculations to compute the PoS at different BoU. The MCS process is time consuming however it avoids any linearization of the network model. As a result, the curve fitting method is able to provide accurate solutions and ensure desired levels of PoS. The capability of adjusting the PoS is beneficial to the future deployment of ESS. As shown in the simulation results, by accepting a PoS requirement of 97%, the proposed method can further reduce the power and energy requirements of ESS.

The selection of UI is important to the performance of RO. Forecast techniques for UI prediction have been proposed [11, 27, 28]. Conservative UIs can compromise the benefits of the proposed approach. On the other hand, if the uncertainty is underestimated, the PoS of RO solutions will be reduced.

Chapter 7. Evaluation of the Robust Optimization Based Scheduling Scheme and Case Studies

7.1 Introduction

In Chapter 6, a robust scheduling scheme for energy storage systems (ESSs) deployed in distribution networks to facilitate high penetrations of renewable energy sources (RES) is presented. Two methods for calculating optimal budget of uncertainty (OBoU) have been introduced. In this chapter, the proposed scheduling scheme is tested with IEEE 14 busbar network and IEEE 118 busbar network with real load, generation and RTTR profiles. The curve fitting method has been used to estimate the OBoU for 97% and 100% probability of success (PoS) in the first case study with the IEEE 14 bus network. Both methods have been applied on the IEEE 118 busbar network. The scheduling scheme based on RO is compared to classical optimal power flow (OPF) approaches which do not consider uncertainty. OPF technique is introduced in section 7.2.

In this chapter, standard IEEE networks are used. Compared to the real distribution network used in Chapter 3, there are a few advantages using the standard IEEE networks. Frist of all, IEEE networks are well known and the case studies on these networks can be repeated easily. Secondly, two methods to estimate OBoU have been introduced in section 6.5. The first method uses bound 1, introduced in section 5.4 to estimate the OBoU. However, this method is more accurate for problems with large number of uncertainties. The use of standard IEEE networks can test the scalability of proposed methods and the accuracy of the first method for estimating OBoU.

7.2 Optimal power flow

Optimal power flow (OPF) is a well-established technique for solving power system problems. This technique has been introduced in [145, 151, 159]. In this section, the general form of OPF is introduced. Next, the general form of OPF is modified to model ESS and RTTR.

7.2.1 Standard alternate current optimal power flow

The aim of OPF is to minimise the cost of using generators and all constraints are satisfied.

A normal OPF is given as

$$\min \sum_{i \in S_G} f\left(P_{G_i}\right) \tag{7.1}$$

Subject to

$$P_{G_i} - P_{D_i} - V_i \sum_{j=1}^{N_{Bus}} V_j\left(G_{ij}\cos\theta_{ij} + B_{ij}\sin\theta_{ij}\right) = 0$$

$$Q_{G_i} - Q_{D_i} - V_i \sum_{j=1}^{N_{Bus}} V_j\left(G_{ij}\cos\theta_{ij} - B_{ij}\sin\theta_{ij}\right) = 0 \quad \textbf{(7.2)}$$

$$P_{G_i,Min} \le P_{G_i} \le P_{G_i,Max}$$

$$Q_{G_i,Min} \le Q_{G_i} \le Q_{G_i,Max} \quad \textbf{(7.3)}$$

$$V_{j,Min} \le V_j \le V_{j,Max} \quad \textbf{(7.4)}$$

$$\left|P_{ij}\right| = \left|V_i V_j\left(G_{ij}\cos\theta_{ij} + B_{ij}\sin\theta_{ij}\right) - V_i^2 G_{ij}\right| \le P_{ij,Rating} \quad \textbf{(7.5)}$$

where

P_{G_i} the real power export for generator at bus i

S_G the set of generators

P_{D_i} the real power demand at bus i

V_i voltage at bus i

N_{Bus} total number of buses

G_{ij} the per unit conductance of branch from busbar i to busbar j

B_{ij} the per unit susceptance of branch from busbar i to busbar j

θ_{ij} the angle difference between busbar i and busbar j

Q_{G_i} the reactive power export for generator at bus i

Q_{D_i} the reactive power demand for generator at bus i

$P_{G_i,Min}$ minimum real power export of generator at bus i

$P_{G_i,Max}$ maximum real power export of generator at bus i

$P_{Q_i,Min}$ minimum reactive power export of generator at bus i

$P_{Q_i,Max}$ maximum reactive power export of generator at bus i

$V_{j,Min}$ low voltage limit for bus j

$V_{j,Max}$ upper voltage limit for bus j

$P_{ij,Rating}$ real power rating of branch ij

In this formulation, the cost function equation (7.1) minimise the cost for all the generators. Constraints (7.2) are equality constraints for nodal real and reactive power balance. Constraints (7.3) are lower and upper limits for generators real and reactive power outputs. Constraints (7.4) ensure all bus voltage are within limits and constraints (7.5) are power flow constraints for branches which guarantee the real power flows on branches are below the ratings of branches.

7.2.2 Modified optimal power flow

The formulation introduced in the previous section does not include ESS and RTTR. The conventional OPF is modified so it includes ESS and RTTR. In the modified version of OPF, ESS is modelled as a generator with extra constraints to model the SoC constraints. RTTR is modelled with variable ratings in constraint (7.4). The modifications are detailed below.

The cost function is modified to minimise the cost of using ESS

$$\min \sum_{m=1}^{N_{ESS}} C_{ESS_m}^t \cdot P_{ESS_m}^t \tag{7.6}$$

The cost function is consistent with the cost function is RO.

The following constraints are added to model ESS.

$$-P_{ESS_m,Rating} \leq P_{ESS,m}^t \leq P_{ESS_m,Rating} \tag{7.7}$$

$$-Q_{ESS_m,Rating} \leq Q_{ESS,m}^t \leq Q_{ESS_m,Rating} \tag{7.8}$$

$$\begin{aligned} SoC_{ESS_m}^{t+1} &= SoC_{ESS_m}^t \\ &+ d_{ESS_m}^t \cdot \frac{\Delta t \cdot \frac{P_{ESS_m}^t}{\eta_{ESS_m,discharge}}}{E_{ESS_m}} + (1 - d_{ESS_m}^t) \cdot \frac{\Delta t \cdot P_{ESS_m}^t \cdot \eta_{ESS_m,charge}}{E_{ESS_m}} \\ SoC_{ESS_m,Min}^t &\leq SoC_{ESS_m}^t \leq SoC_{ESS_m,Max}^t \end{aligned} \tag{7.9}$$

where

$P_{ESS,m}^t$ the real power output of ESS m

$Q_{ESS,m}^t$ the reactive power output of ESS m

$P_{ESS_m,Rating}$ the real power rating of ESS m

$Q_{ESS_m,Rating}$ the reactive power rating of ESS m

Constraints (7.7) and (7.8) are real and reactive power constraints for ESS. Constraint (7.9) is the SoC constraint which guarantees that the ESSs are not over-charged or over-discharged.

RTTR is modelled as varying ratings of branches at different timesteps. Constraint (7.5) is modified as

$$\left|P_{ij}^{t}\right| \leq P_{ij,RTTR}^{t} \tag{7.10}$$

The modified cost function and constraints are included in the normal OPF formulation. The modified OPF formulation takes ESS and RTTR into consideration. The results of this form of OPF is called normal OPF (NOPF).

7.2.3 Conservative form of optimal power flow

The formulation of NOPF considers ESS and RTTR but not uncertainty. In this section, the NOPF formulation is modified to account for uncertainty. As stated in equation (6.16), the uncertainty can be described with uncertainty intervals. Conservative OPF (COPF) is introduced. COPF uses maximum or minimum possible values for uncertain values so that the solution is able to provide solution with high PoS.

For RTTR, the reduced values are used

$$P_{ij,RTTR}^{t} = P_{ij,RTTR}^{t} - \hat{P}_{ij,RTTR}^{t} \tag{7.11}$$

Depending on if thermal overloads and/or voltage excursions are due to generation or load, different values are used for DG and load. To be specific, if predicted excursions are due to load, the following values will be used:

$$\begin{aligned} P_{Bus_P}^{t} &= P_{Bus_p}^{t} + \hat{P}_{Bus_p}^{t} \\ P_{RES_n}^{t} &= P_{RES_n}^{t} - \hat{P}_{RES_n}^{t} \end{aligned} \tag{7.12}$$

If predicted excursions are due to generation, maximum generation values and minimum load values will be used.

$$\begin{aligned} P_{Bus_P}^{t} &= P_{Bus_p}^{t} - \hat{P}_{Bus_p}^{t} \\ P_{RES_n}^{t} &= P_{RES_n}^{t} + \hat{P}_{RES_n}^{t} \end{aligned} \tag{7.13}$$

7.3 Case Study on IEEE 14 Bus Network

7.3.1 Case Study Network

The RO based scheduling scheme is applied to a modified version of the IEEE 14 bus network as illustrated in Figure 7.1. Two windfarms have been connected to busbars 12 and 13 of this network with capacities of 25MVA and 35MVA respectively. A 20 MVA, 40MWh ESS unit is located at busbar 14. Wind generation at busbar 12 and 13 causes a continuous overload on the branch from busbar 13 to busbar 14. It is assumed that this branch is equipped with RTTR. In this case study, half-hourly real windfarm generation export, RTTR and load profile data from the north east of England have been used [200].

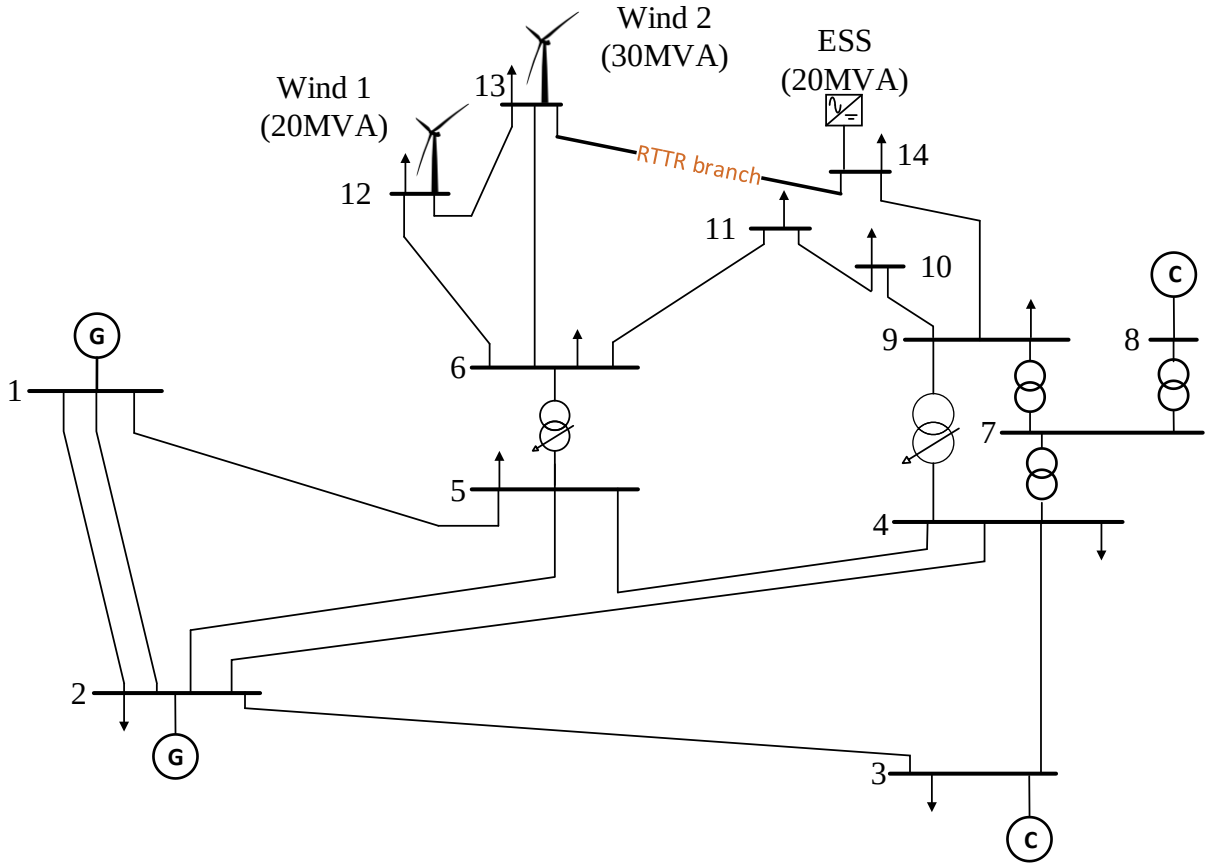

Figure 7.1 IEEE 14 Busbar network

Half-hourly windfarm outputs from the north east of England have been used for this case study. The output has been scaled for the purpose of this study. It is assumed that the generators are generating at unity power factor. By replacing the real power injections in the constraints by apparent power injections and apparent power PFSF (MVA powerflow change per MVA injection change), this method is able to solve the scheduling problems with reactive power. The windfarm export profiles are depicted in Figure 7.2.

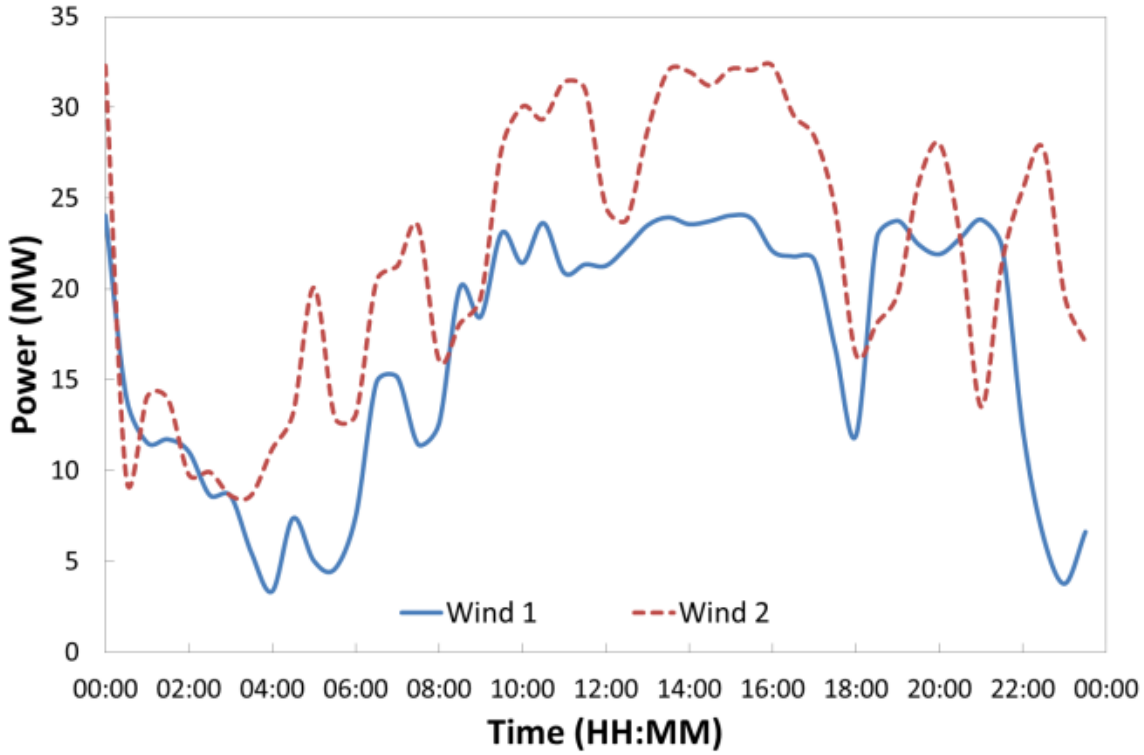

Figure 7.2 Windfarm Output

Powerflow through the branch and the RTTR of the branch are given in Figure 7.3.

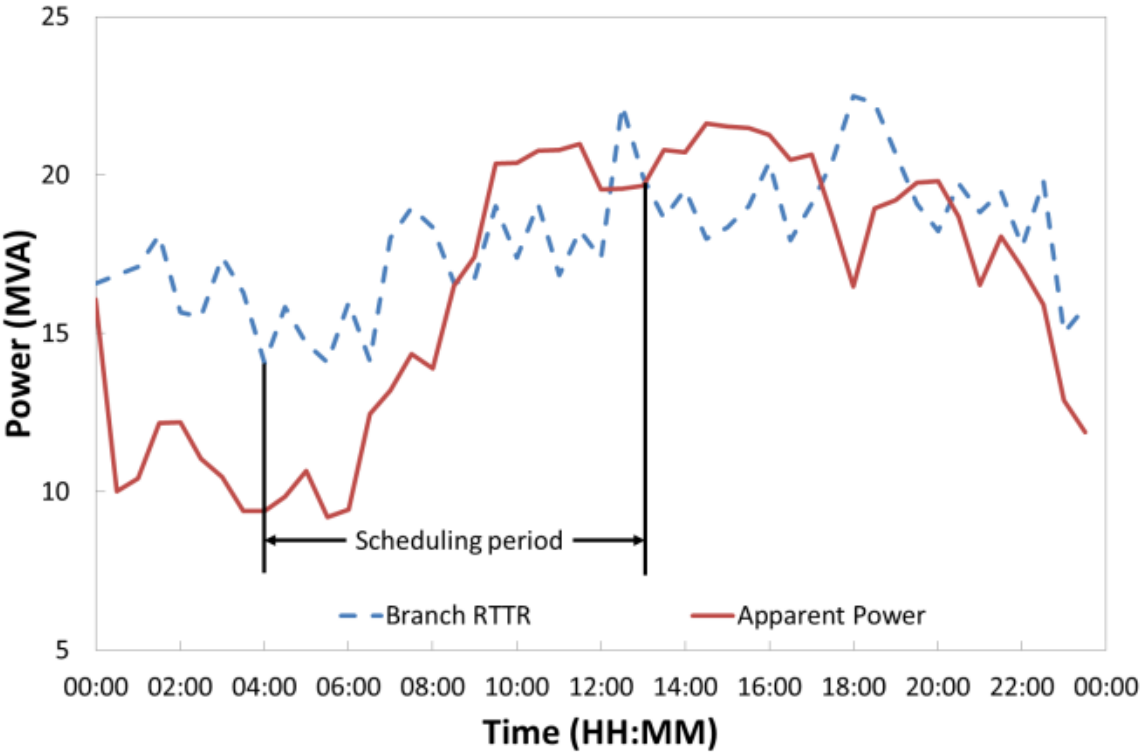

Figure 7.3 Apparent Power and RTTR of the Modelled Branch 13- 14

The scheduling scheme has been applied for the first excursion between 04:00 to 13:00 at a half-hourly interval. The total number of timesteps is 18.

7.3.2 Sources of Uncertainties

The sources of uncertainty considered in this case study include load, windfarm output and RTTR. The levels of uncertainties are informed by the literature review in section 4.2. The uncertainty intervals are given in Table 7.1. It is assumed that load for all busbars have 5% uncertainty. The RTTR forecast of the branch from bus 13 to bus 14 has an uncertainty of 5% as well. The power output uncertainty of both windfarms is 10%.

	Load	RTTR	Wind 1	Wind 2
Uncertainty interval	5%	5%	10%	10%

Table 7.1 Sources of Uncertainty and Uncertainty Intervals

Three test cases have been used to test the performance of the proposed scheduling scheme with different types of uncertainty distributions. In case 1 and 2, it is assumed that all errors are symmetrically distributed and follow normal and uniform distributions, respectively. In case 3, both left and right skewed Beta distributions have been used. The skewness of each error distribution is chosen so that the severity of violation is worse. For example, it is assumed that RTTR tends to be overestimated and wind speeds are likely to be underestimated. Therefore, the RTTR violation will be more severe than expected. Beta distributions are used for the asymmetrical test case due to its simplicity.

The specifications of the distributions in the test cases are detailed below in Table 7.2. For case 1, normal distribution, the ratio of standard deviation (SD) to mean is defined. For load uncertainty, the SD is chosen to be 1% of its mean value. Therefore, the UI selected, which is 5%, equals to five time the SD. This range represents a confidence interval of more than 99.99%. For case 2, uniform distribution, the maximum variation of uniform distribution is given as a percentage. The maximum variations are consistent with the UI.

	Load	RTTR	Wind 1	Wind 2
Uncertainty interval	5%	5%	10%	10%
Case 1 (SD/Mean)	1%	1%	2%	2%
Case 2 (Maximum variation)	5%	5%	10%	10%
Case 3 (α, β)	2, 1.5	2, 4	2, 1.5	2, 1.5

Table 7.2 Sources of Uncertainty and Uncertainty Intervals

For case 3, the parameters α and β for the Beta distributions are given. Changing the values of α and β changes the mean and skewness of the Beta distribution. Two sets of α and β values are used.

	α	β
Beta Distribution Series 1	2	1.5
Beta Distribution Series 2	2	4

Table 7.3 Two Sets of Beta Distributions

The PDF of two Beta distributions are plotted below in Figure 7.4.

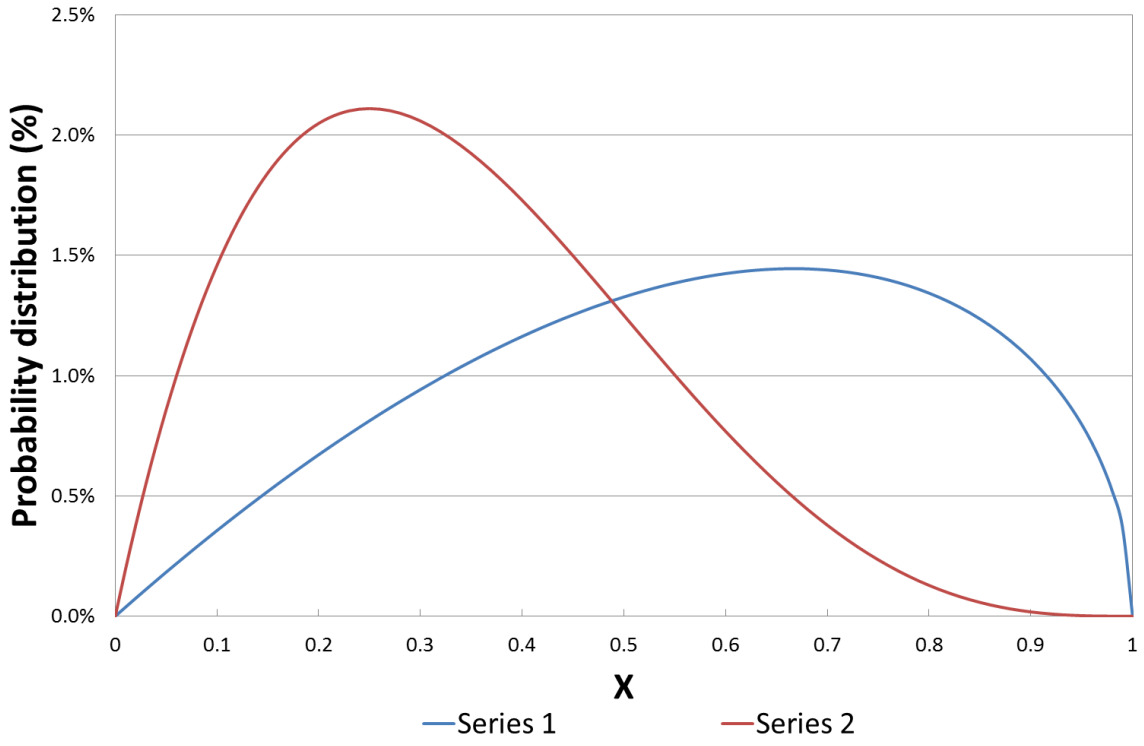

Figure 7.4 Two sets of Beta Distributions, for series 1, α = 2 and β = 1.5, for series 2 α = 2 and β = 4

The minimum and maximum value of Beta distribution function is 0 and 1, respectively. Series 1 has been scaled to model the uncertainties of load and DG output error. Series 2 has been scaled to describe the uncertainty of RTTR.

Considering the uncertainty defined in this section, the windfarm outputs are plotted below in Figure 7.5. This figure depicts the windfarm export profiles and uncertainty intervals. The

black traces are the nominal wind generation exports. These nominal values have been plotted in Figure 7.2. The blue shaded area surrounding the trace represents the forecast error bounds. Darker shades indicate higher probabilities. The centre of this graph is the predicted generation profile with nominal values. The distribution is assumed to be normal.

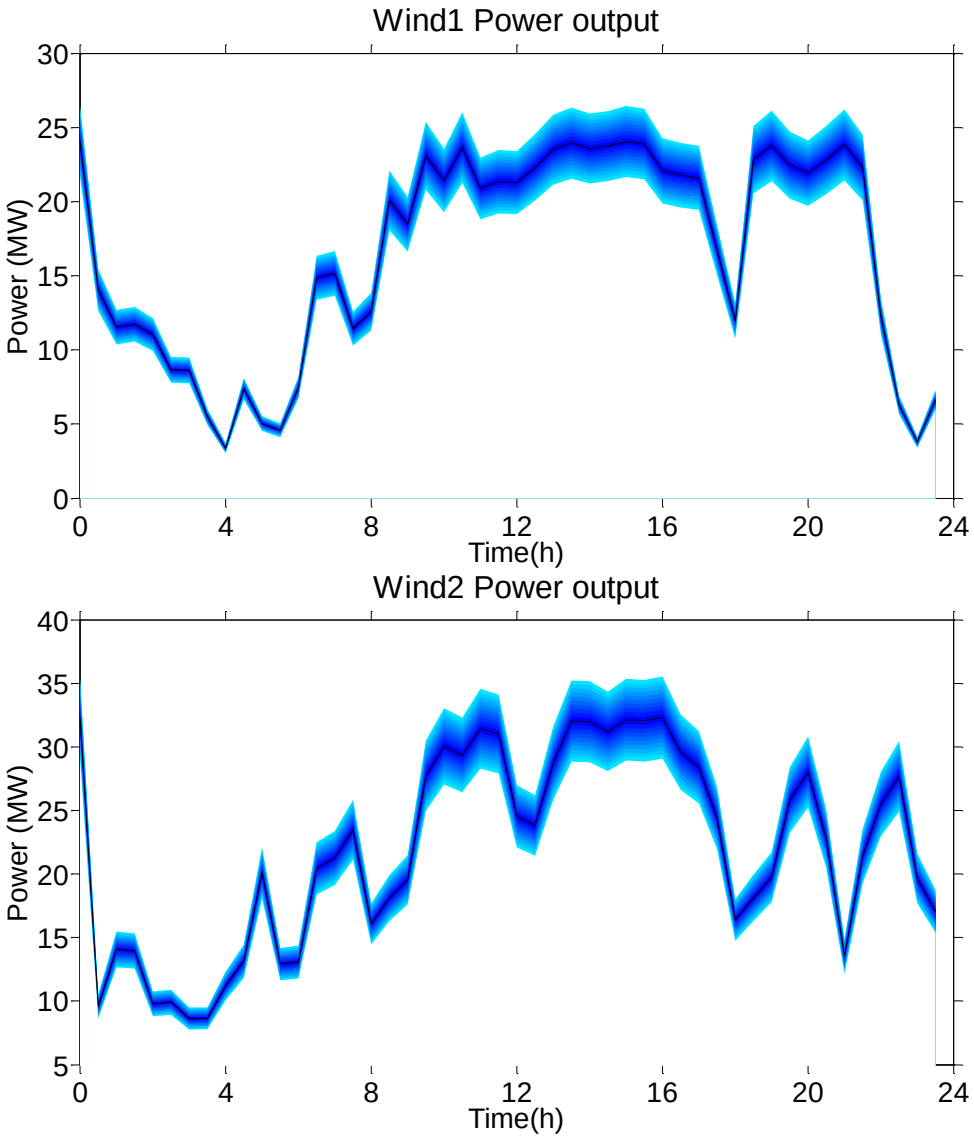

Figure 7.5 Windfarm Outputs with Uncertainty

Power flow through the branch and the RTTR of the branch 13-14 are given in Figure 7.6. The red curve with shaded area is the RTTR of the branch. The blue curve with the shaded area is the predicted power flow through the branch with the uncertainty of load and RES. Three distinct sustained branch overloads can be observed. The scheduling scheme has been applied for the first overload period between 04:00 to 13:00 at a half-hour interval. The total number of timesteps is 18.

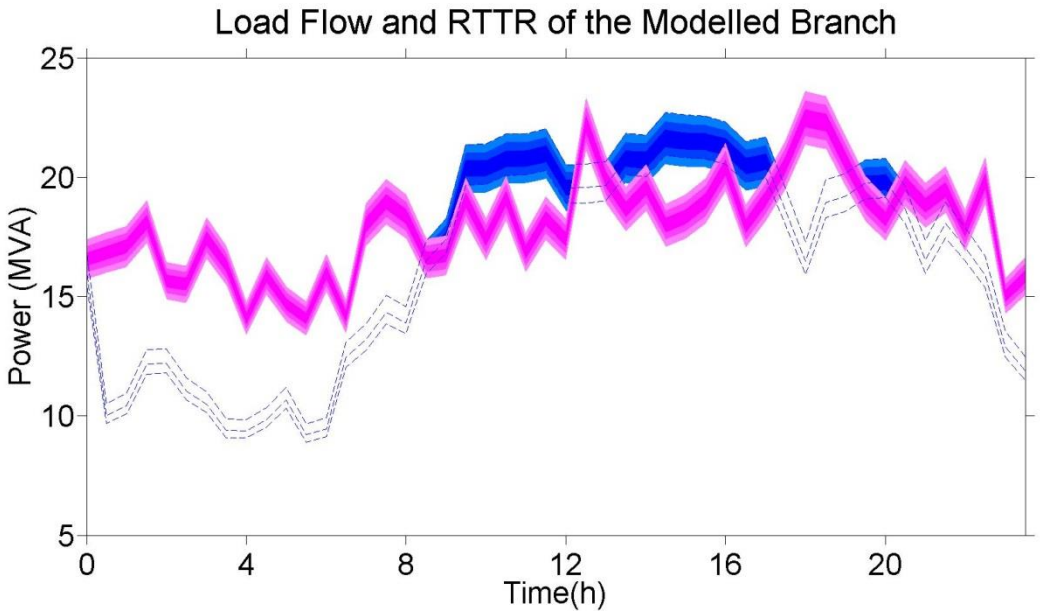

Figure 7.6 Apparent Power and RTTR of the Modelled Branch

7.3.3 Optimal Budget of Uncertainty and Probability of Success Test Results

Two approaches to calculate OBoU have been introduced in section 6.5. The first approach calculates based on bound 1 introduced in equation (6.24). The second approach uses a moderate number of MCS studies. Due to the relatively small number of forecast values used in this case study, only the curve fitting based technique is used to calculate OBoU. For each case, four groups ($n_{Max} = 4$) of BoU and its PoS have been used to calculate the parameters *a*, *b* and *c* in equation (6.24).

The input PoS is achieved by MCS. The parameters used for MCS are consistent with the specification given in Table 7.2. For case 1, the uncertain values used in MCS have not been truncated even though RO uses the intervals as input. MCS is carried out for all three cases for all 18 timesteps and each timestep is tested with 5,000 samples. Analysis shows that results converges at around 2,000 samples. Techniques for reducing the sample size of MCS are available however this is beyond the scope of this thesis. The sample size is selected to guarantee the convergence of the results. The OBoU for 97% and 100% PoS can be calculated based on these functions. The inputs used are given below in Table 7.4.

Input value	Case 1		Case 2		Case 3	
	BoU	PoS	BoU	PoS	BoU	PoS
1	0%	93.44%	0%	12.46%	0%	1.06%
2	10%	99.96%	15%	79.16%	15%	69.30%
3	15%	100.0%	30%	99.82%	30%	100.0%
4	20%	100.0%	45%	100.0%	45%	100.0%

Table 7.4 Input values for the curve fitting algorithm

With the input values in Table 7.4, the parameters *a*, *b* and *c* in equation (6.24) can be calculated. The calculated values of *a*, *b* and *c* are summarized below in Table 7.5.

	Case 1	Case 2	Case 3
PDF type	Normal	Uniform	Beta
a	1.00	1.00	1.01
b	0.07	0.88	0.99
c	856.40	63.71	51.25

Table 7.5 Calculated Parameters Based on LMA Curve Fitting Technique

Based on the parameters calculated above in Table 7.5, OBoUs for the three cases can be estimated by equation (6.24). The estimation results are summarized below in Table 7.6. OBoUs have been estimated for both 97% and 100% PoS.

	Estimated OBoU		
Case	Case 1	Case 2	Case 3
PDF type	Normal	Uniform	Beta
PoS 97%	4.0%	23.0%	26.0%
PoS 100%	9.8%	31.0%	32.0%

Table 7.6 Estimated OBoU for 97% and 100% PoS

7.3.4 Verification of Estimated OBoU

Next, tests are carried out to verify the accuracy of the OBoU estimation methods proposed in the previous section. PoSs for more BoUs in all three cases are tested with MCS. Initially the PoS of each case was tested with MCS for normalized BoU from 0% to 100% at a 5% interval. Next, more tests were conducted for BoU with PoS of more than 90% at 1% BoU interval. Test results are illustrated in Figure 7.7. As can be observed, in all cases, PoS increase with BoU. At the same BoU, the PoSs for the normal distribution case is higher in comparison with the uniform and Beta distribution cases.

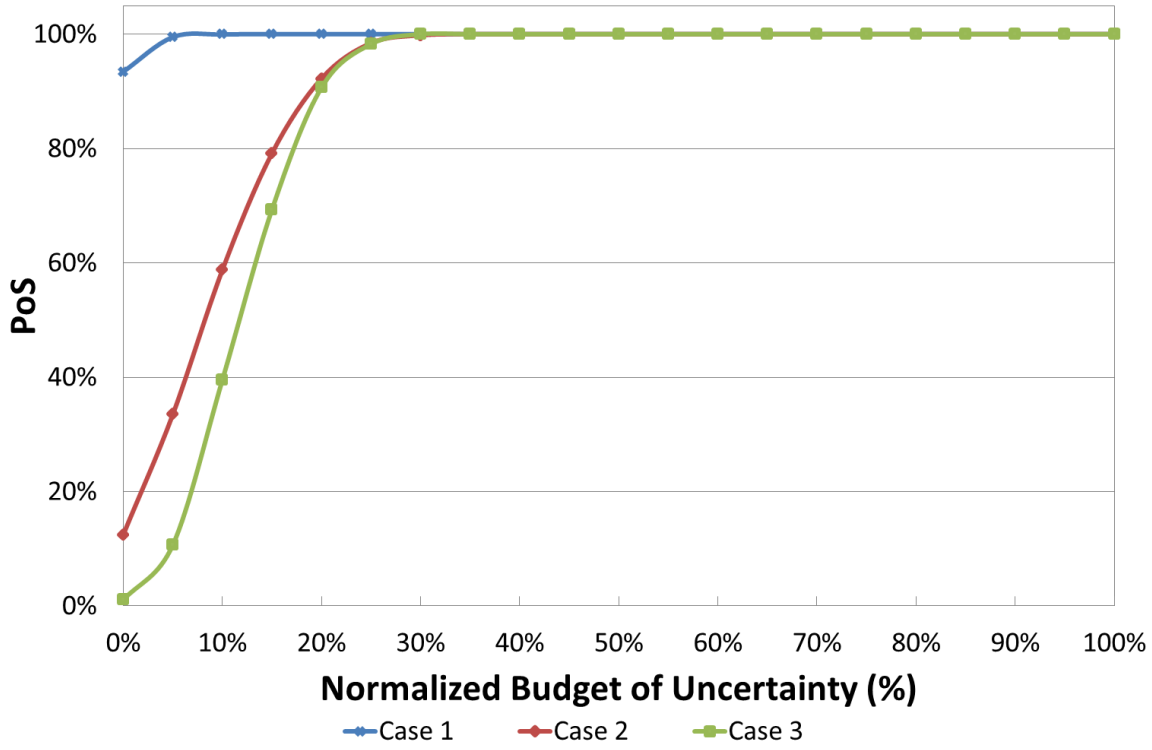

Figure 7.7 PoS Test Results for All Cases at different BoU

The reason why the PoS for normal distribution is higher than uniform and Beta distribution is explained below. At low BoU, the solutions provided by RO are able to deal with small errors. Constraint violations are mostly caused by large forecast errors. Therefore, the shapes of distributions of the forecast errors can influence the PoS. Example PDFs for three types of distributions of forecast errors are plotted. The blue curve is an example PDF of a normal distribution. The red dotted curve illustrates an example PDF for uniform distribution. The green and purple scattered curves are example PDF for Beta distribution with different skewness.

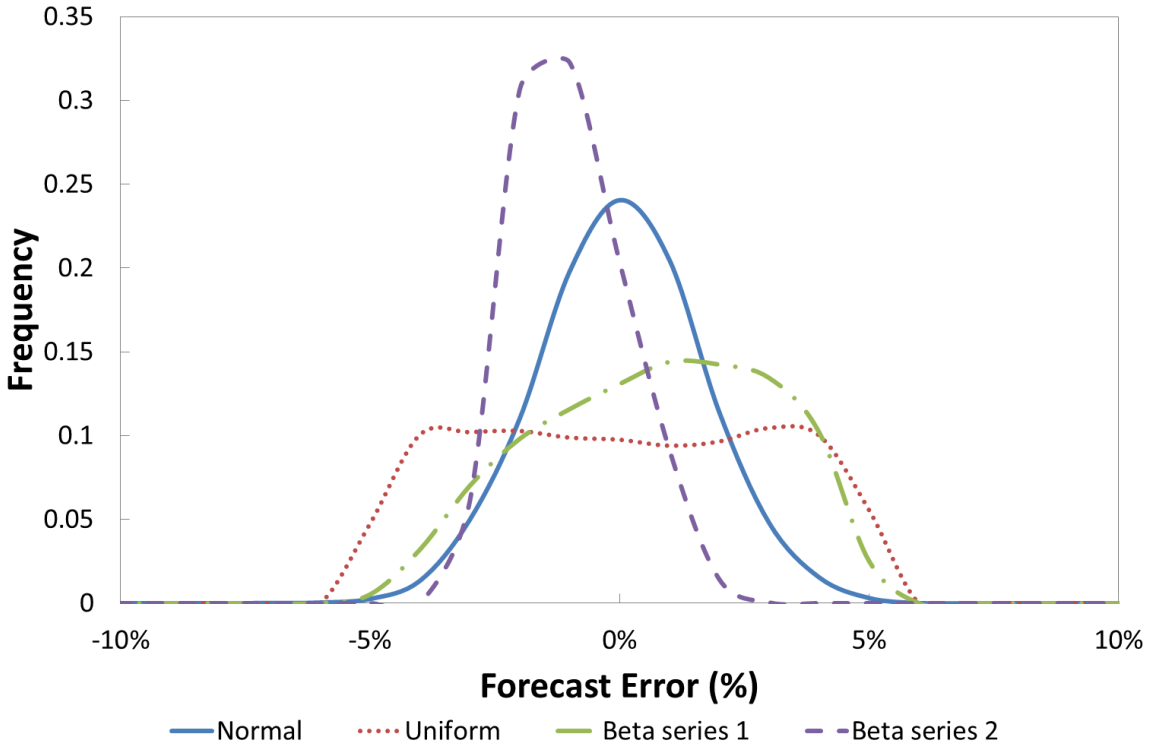

Figure 7.8 Illustration of Different Types of Distributions

If the errors between the real values and forecast values follow a normal distribution, as defined in Case 1, the probabilities of small errors (close to 0%) are relative higher. In other words, the probabilities that large errors occur are smaller. Therefore, the probability of constraint violation is smaller. On the contrary, for Beta and Uniform distributions, the probabilities that large errors occur are relatively higher. When probabilities of large errors occur are high and the BoU is low, the PoS is reduced.

Curve Fitting results for Case 1

The curve fitting results for Case 1 is plotted below in Figure 7.9. The red curve depicts the results from MCS. The green triangles indicate the input for curve fitting algorithm. The blue curve is the curve fitting result. The green triangles are selected points from the MCS results, depicted as the red curve. Based on these input, the values of *a*, *b* and *c* as shown in equation (6.25) can be calculated. The blue curve is depicted based on calculated *a*, *b* and *c*. As can be observed, the estimated curve follows the original curve well. The original curve and the fitting results have a high correlation coefficient of 0.9624.

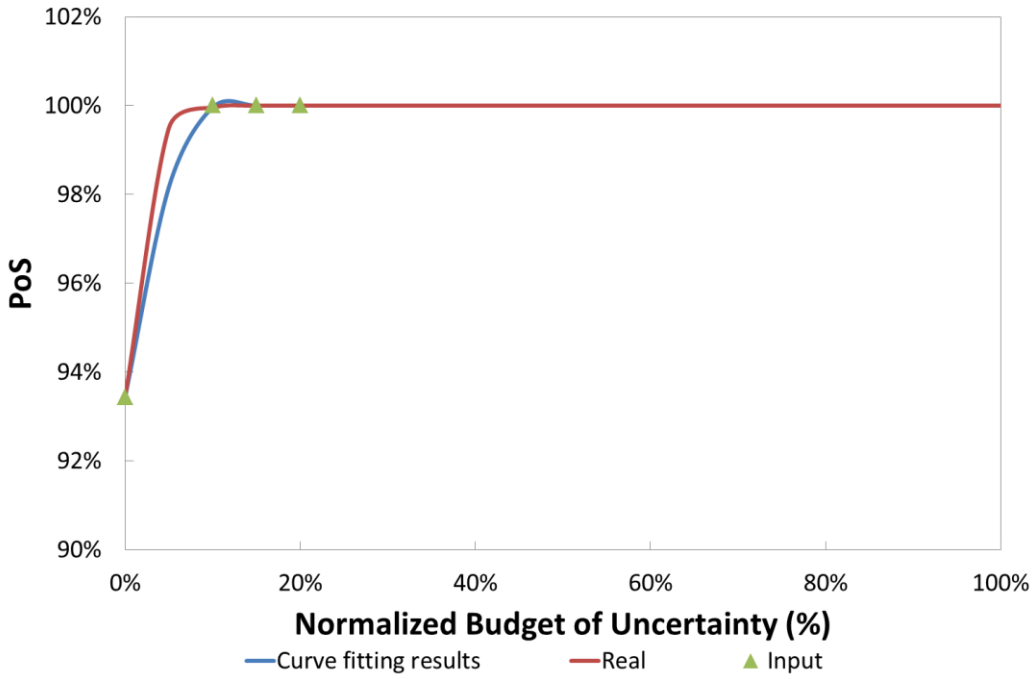

Figure 7.9 Curve Fitting Results of Case Study 1

Curve Fitting results for Case 2

The curve fitting results for Case 2 is plotted below in Figure 7.10. The red curve depicts the results from MCS. The green triangles indicate the input for curve fitting algorithm. The blue curve is the curve fitting result. The original curve and the fitting results have a high correlation coefficient of 0.9977.

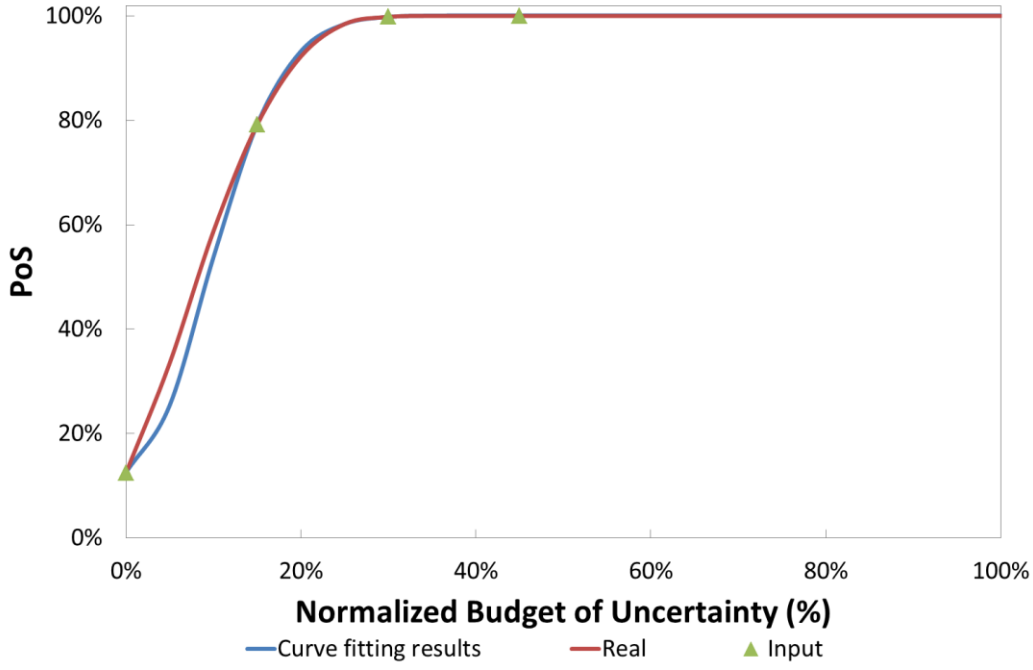

Figure 7.10 Curve Fitting Results of Case Study 2

Curve Fitting results for Case 3

The curve fitting results for Case 3 is plotted below in Figure 7.11. The red curve depicts the results from MCS. The green triangles indicate the input for curve fitting algorithm. The blue curve is the curve fitting result. The original curve and the fitting results have a high correlation coefficient of 0.9994.

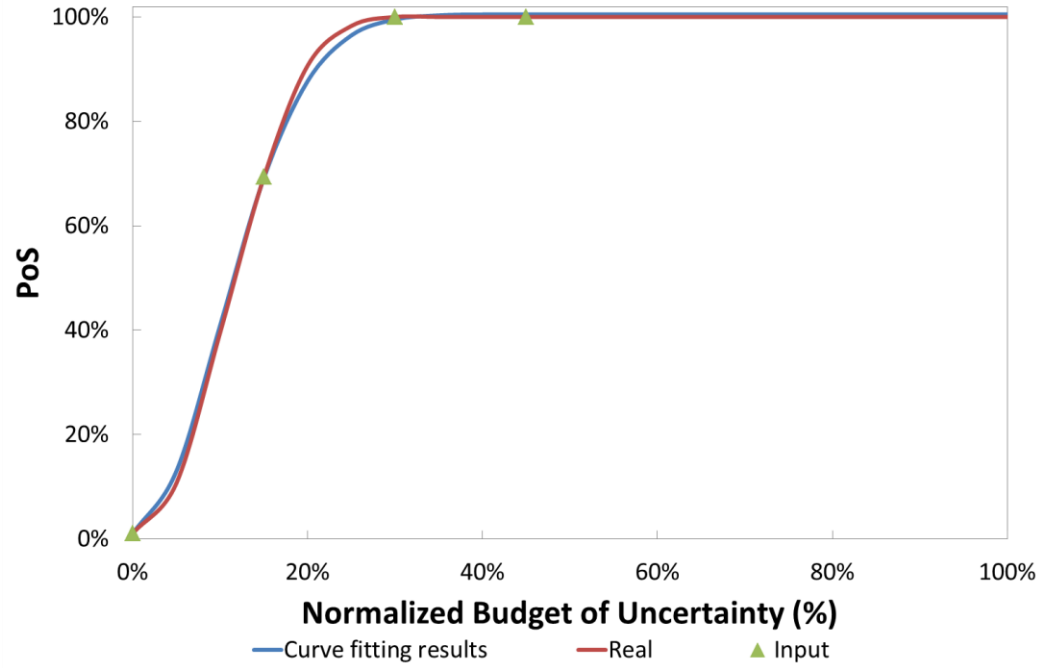

Figure 7.11 Curve Fitting Results of Case Study 3

Analysis of the Curve Fitting Results

The OBoU based on MCS study are summarised below in Table 7.7. Due to the large sample size of MCS, the OBoU obtained can be seen as the real OBoU. Comparing the estimated OBoU listed to the real OBoU in Table 7.6, it can be seen that the curve fitting based approach can provide a good estimation of OBoU. Moreover, this method can reduce the computational cost of running MCS. In case 1 and 2, 15 and 19 steps of MCS are required. By adopting this method, the computational cost is reduced to between 20% and 30%.

		OBoU	
Test case	Case 1	Case 2	Case 3
PDF type	Normal	Uniform	Beta
PoS 97%	2%	24%	21%
PoS 100%	15%	32%	29%

Table 7.7 OPTIMAL BOU FOR 97% AND 100% POS

As can be observed in Figure 7.10 and Figure 7.11, for case 2 and 3, at low BoU, the difference between the real PoS and the curve fitting results is relatively larger. However, at high BoU, the difference reduces. PoS represents the level of risk, in this case, the risk of RTTR violation of OHL and transformers happening. It is unlikely that the PoS is set to a small number. Therefore, this curve fitting technique, combined with MCS can provide accurate estimation of OBoU.

7.3.5 Comparison with Optimal Power flow

The proposed method is compared to two forms of optimal power flow (OPF) scheduling schemes, nominal OPF (NOPF) and conservative OPF (COPF). NOPF uses the nominal as input and therefore does not consider any uncertainty. On the other hand, COPF considers the worst case scenario. In this case, COPF uses the maximum possible wind speed and minimum RTTR. The PoSs of the calculated OBoU and OPF approaches are tested with MCS. Test results are summarized in Table 7.8.

		PoS	
Test	Case 1	Case 2	Case 3
PDF type	Normal	Uniform	Beta
NOPF	60.72%	41.52%	11.40%
97% Estimated OBoU	98.90%	95.97%	98.0%
100% Estimated OBoU	99.96%	99.90%	100.0%
COPF	100%	100%	100%
100% BoU	100%	100%	100%

Table 7.8 PoS Test Results

As can be observed, without considering the uncertainty, the solution of NOPF results in low PoS. Meanwhile, the result of the COPF method, results in 100% PoS. It can be also seen that, the estimated OBoU is able to provide reliable solutions. It can be observed that the proposed method is able to calculate the OBoU for a desired PoS. Therefore the level of conservatism can be adjusted.

Charge and discharge profiles in Case 1 for COPF, NOPF, and the RO scheme with 100% and 97% PoS are compared in Figure 7.12. As shown in this figure, compared to COPF, the proposed scheme can reduce the maximum discharge power from 11MW to 9MW and also ensuring that the constraints are fully protected against uncertainty.

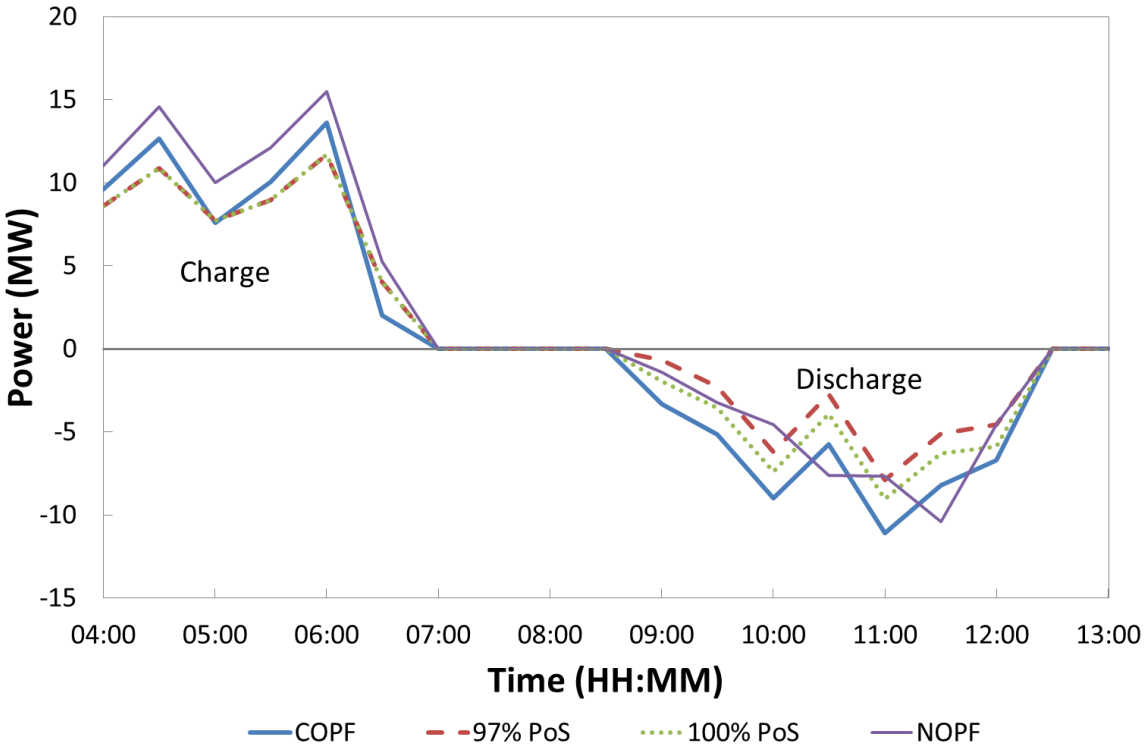

Figure 7.12 ESS Charge and Discharge Profiles in Case 1

The SoC change during this period is compared in Figure 7.13. During the discharge period between 09:00 to 13:00, compared to OPF, the ESS energy exchange requirement can be reduced by 9.9MWh and 5.6MWh at 97% and 100% PoS respectively.

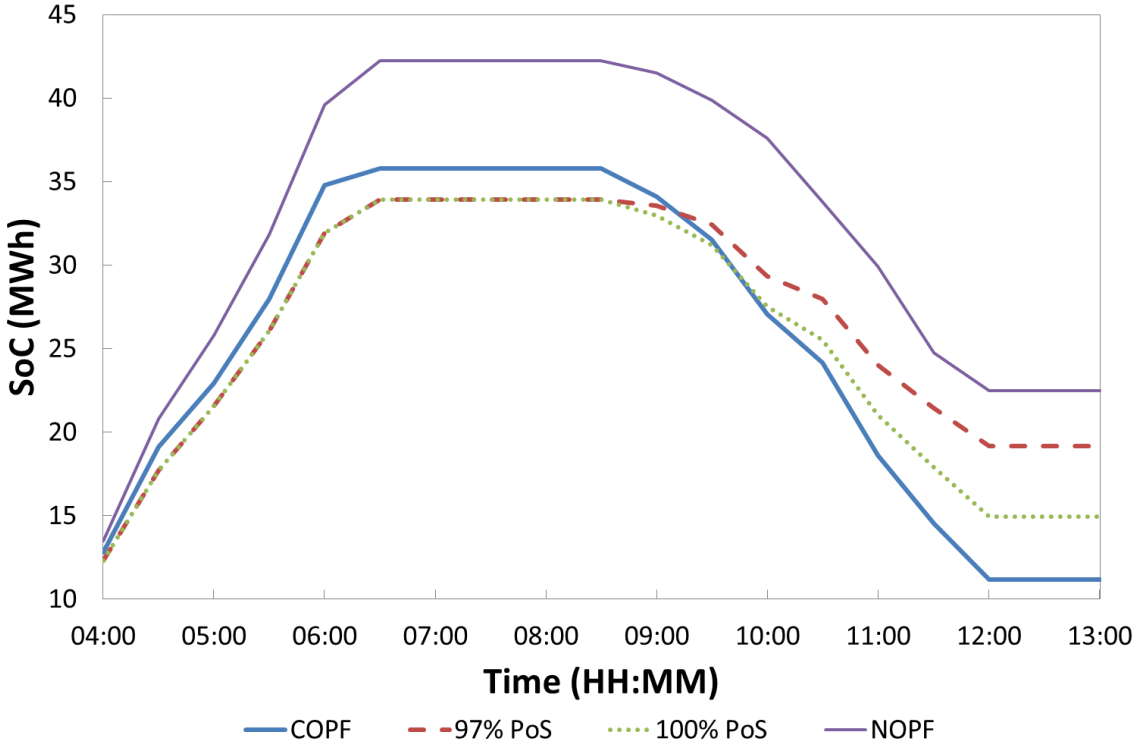

Figure 7.13 SoC Comparison in case 1

The maximum discharge power and the SoC change for 97% and 100% PoS in all test cases are listed in Table 7.9. As can be observed, instead of scheduling the system for 100% PoS, a reduced requirement of 97% can reduce the required rated power and energy capacity of the ESS unit. Furthermore, the reduced duty on the EES unit decelerates the degradation of the unit.

	Maximum Discharge (MW)			ΔSoC (MWh)		
	Case 1	Case 2	Case 3	Case 1	Case 2	Case 3
NOPF	10.4	10.4	10.4	19.76	19.76	19.76
97%	7.90	9.80	9.54	14.75	22.37	21.24
100%	9.00	10.41	10.18	19.00	25.26	24.19
COPF	11.10	11.10	11.10	24.62	24.62	24.62

Table 7.9 PoS of Estimated OBoU

7.4 IEEE 118 busbar network

The proposed scheduling scheme is applied to IEEE 118 busbar network. A diagram of the IEEE 118 network is given below.

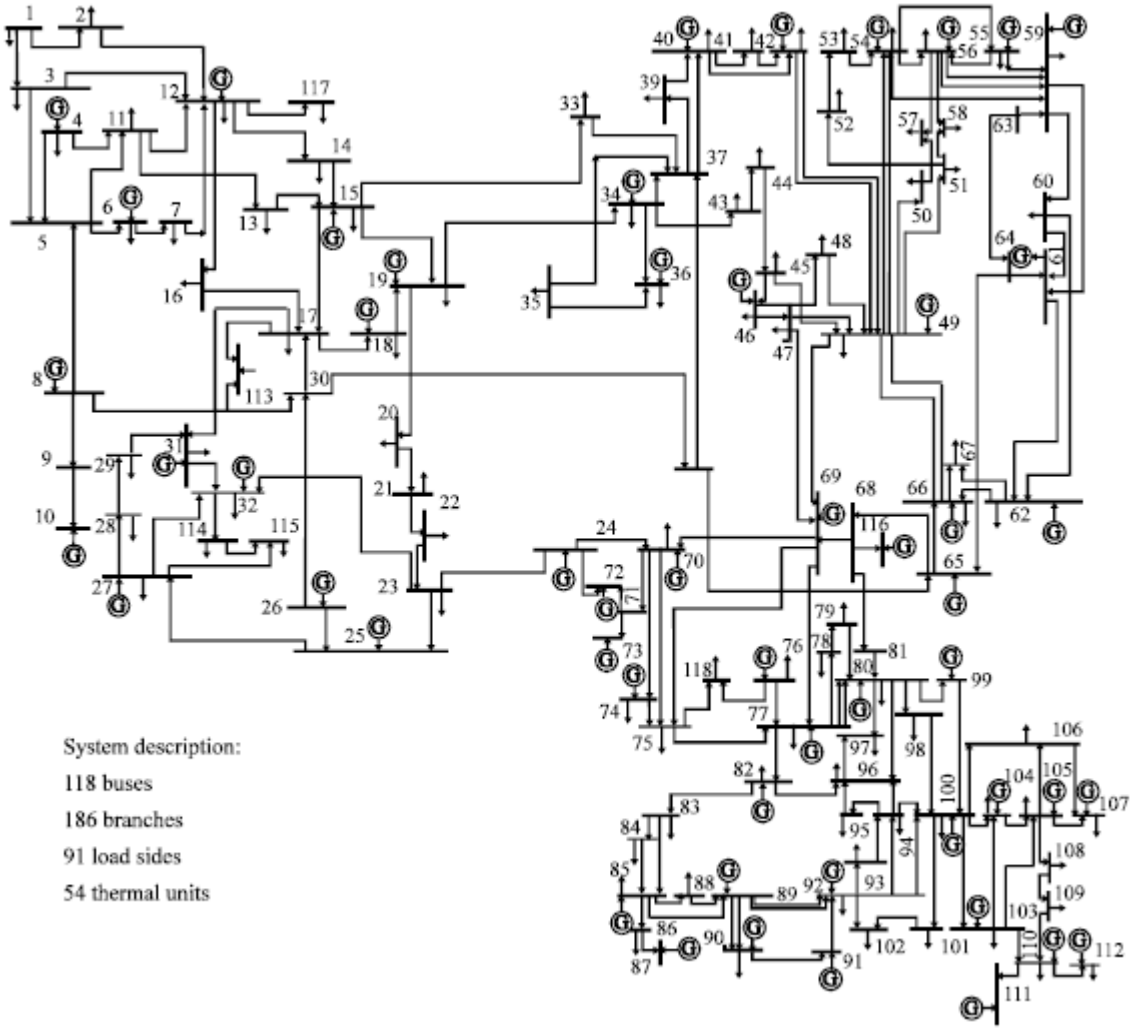

Figure 7.14 IEEE 118 busbar network

8 ESSs and 10 RESs have been connected to this network. The locations and ratings of ESSs are summarised below.

No.	Busbar	P Rating (MW)	Q Rating (MVAr)	S Rating(MVA)	Capacity (MWh)
1	11	100	100	100	500
2	20	100	100	100	500
3	24	80	80	80	240
4	37	50	50	50	200
5	38	75	75	150	300
6	71	100	100	100	500
7	116	100	100	100	500
8	117	80	100	100	500

Table 7.10 ESS in IEEE 118 Network

The locations and ratings of the RESs are summarised below.

No.	Busbar	P Rating (MW)	Type
1	3	75	Wind
2	4	75	Wind
3	11	75	Wind
4	12	80	Wind
5	28	80	Wind
6	31	80	Wind
7	35	40	Wind
8	36	40	Wind
9	72	50	Wind
10	73	60	Wind

Table 7.11 Locations and Ratings of RESs

The profiles for RES generation are plotted below

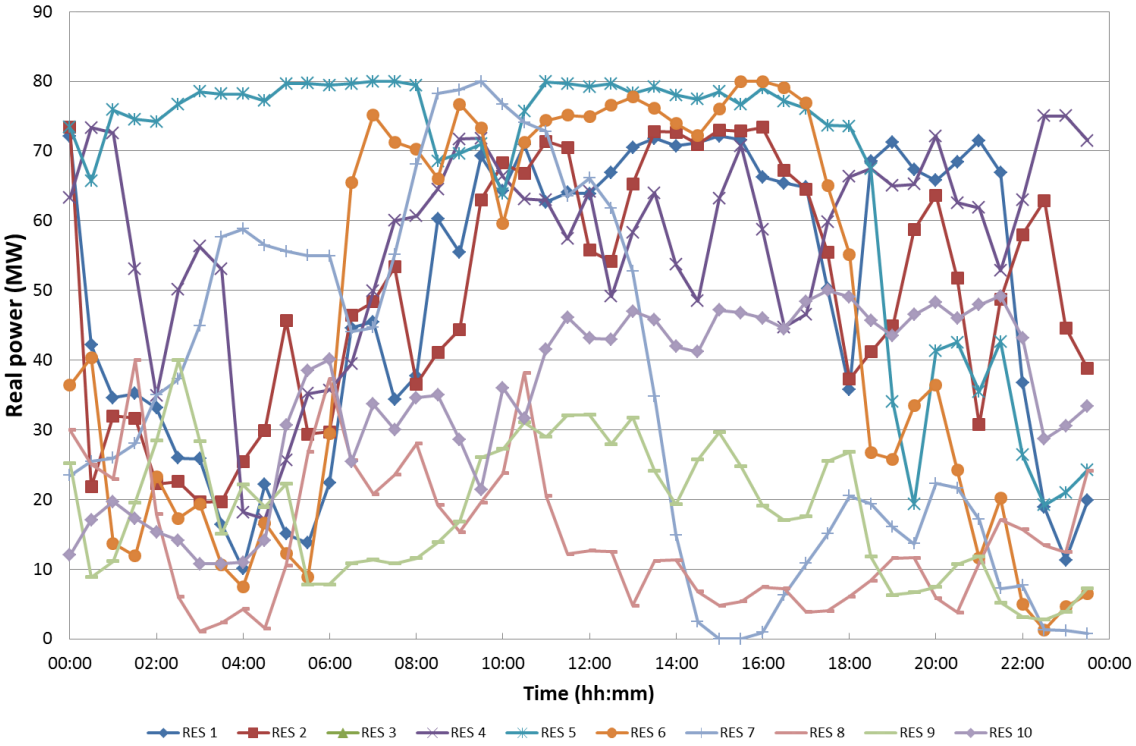

Figure 7.15 RES output plot

The same load profile used in the IEEE 14 busbar network has been used for this study. Half-hourly load data has been used. The load has been scaled for this case study. The ratings of 30 branches have been added. The scheduling algorithm was applied to a four-hour period thermal excursion.

It is assumed that all busbars have uncertain load. The uncertainty intervals are consistent with the previous study on the 14 busbar network. In this case study, both OBoU estimation approaches introduced in section 6.5 have been used. Based on the first approach, the estimated OBoU for 100% PoS is 45.6%. The curve fitting based approach, approach 2 is used to calculate OBoU for all three cases as well. Based on the estimated BoU, charging and discharging profiles for all six ESSs can be calculated. Next, the PoS for the solutions based on different methods are evaluated through MCS. The test results for 100% PoS are summarised below in Table 7.12.

PoS	Case 1	Case 2	Case 3
NOPF	48.96%	48.76%	13.90%
Approach 1 – 100%	100.0%	100.0%	99.98%
Approach 2 – 100%	100.0%	100.0%	100.0%
COPF	100.0%	100.0%	100.0%

Table 7.12 PoS Results for 100% PoS

As can be observed, both OBoU estimation approaches can guarantee high PoS. Meanwhile, the costs for all the approaches are compared below. COPF has the highest cost. The costs for NOPF and RO based methods are given as the percentage of COPF cost.

PoS	Case 1	Case 2	Case 3
NOPF	28.8%	28.8%	28.8%
Approach 1 – 100%	96.5%	96.5%	96.5%
Approach 2 – 100%	81.5%	88.3%	89.1%
COPF	1	1	1

Table 7.13 Cost Results

As can be observed, the RO based approach can provide solutions with high PoS and also reduces the cost. The reason RO can provide solutions with high PoS and reduced cost is that, COPF considers the worst case scenario, which means all uncertain values take values at their lower or upper bounds. However, it is unlikely that all uncertain values take values near their lower or upper bounds. On the other hand, the proposed scheme is able to realize the trade-off between the cost and the probability of constraint violations. Therefore the requirements for ESS power and energy rating can be reduced.

7.5 Discussion and Conclusion

In this case study, it is assumed that the uncertainty intervals remain the same for all the timesteps. For instance, it is assumed that the errors for load forecasts are 5% for all the timesteps for the next 24 hours. However, the errors of load forecast and generation forecast are different, 5% and 10% respectively in this case study. As shown in [121] and [123], the forecast errors increase with the length of time. The assumption of unified uncertainty intervals for the same type of input value for different timesteps does not affect the evaluation of the proposed scheduling scheme. As shown in equation (5.20) to (5.27), the uncertainty interval $\hat{a}_{i,j}$ is treated as constants in constraint equation (5.22). Therefore, the formulation proposed in this thesis is capable to deal with varying uncertainty intervals for the same value at different timesteps.

This work describes a new application of RO for solving an ESS scheduling problem considering new sources of uncertainty, namely the uncertainty of RTTR and ESS SoC. The scheduling of ESS, compared to aforementioned RO applications, involves bidirectional power flow and is constrained by the available energy resource from ESS. The formulation proposed in this work considers the SoC constraint so that ESSs, which are currently expensive and fragile, can be protected from over-charging and over-discharging. Furthermore, the proposed cost function takes into account the capital cost and the SoH of different ESSs. The uncertainty of RTTR is influenced by a number of factors including model limitations and measurement accuracy of environmental factors such as wind speed and direction. Therefore, developing appropriate PDFs for RTTR in large networks is almost an impossible task. This poses difficulties for techniques that demand PDFs.

The proposed RO scheduling scheme is compared to OPF techniques. Reliability test results through MCS with 5,000 samples for all scheduled timesteps on IEEE 14 and 118 busbar networks with real wind, load and RTTR data are presented. Test results show that classical OPF approaches which do not consider uncertainty, when coupled with RTTR and ESS, result in a low PoS In comparison with COPF, which also provides high PoS, the proposed RO scheduling scheme is able to reduce the power and energy requirement to solve a line RTTR violation under uncertainty. The reduced ESS requirements would reduce the power rating and energy capacities required for the ESS and slow the cyclic degradation of the system.

In addition, two methods have been introduced to estimate the trade-off between the cost and the probability of constraint violations. The first approach results in a slightly conservative solution for small networks. When applied to a large network, the approach can reduce the

requirements for ESS power rating and energy capacity. The second approach, which uses a moderate number of MCSs coupled with LMA curve fitting technique, has been proposed to estimate the optimal BoU, to ensure a desired level of PoS. Simulation results show that, the proposed methodology is able to provide an ESS charge and discharge profile that ensures a desired level of probability of success. It has also been found that, reducing the PoS requirement from 100% to 97%, the proposed method can further reduce the power and energy requirements of ESS. The case study results show that, reducing the PoS requirement by 3% reduces the capacity requirement of ESS by up to 4.25 MWh. The scheme proposed in this paper provides a practical solution to ESS scheduling problems under uncertainty to facilitate high penetrations of RES.

Chapter 8. Discussion

8.1 Introduction

In this thesis, an investigation of the use of ESS, DSR and RTTR as an alternative approach to network reinforcement to accommodate LCTs is presented. A discussion regarding using smartgrid technologies and techniques for deferring or avoiding network reinforcement is provided in section 8.2. Based on the review of the state of the art of control and scheduling systems presented in Chapter 2, it is found that most algorithms ignore the stochasticity of load, DG and as well as RTTR. In Chapter 3, control schemes based on sensitivity factors and cost sensitivity factors are presented and evaluated. The merits and drawbacks of SF and CSF based methods are given in section 8.3. In Chapter 4, sources of uncertainties are reviewed. The importance of considering and dealing with uncertainty appropriately is discussed in section 8.4. A study of the impact of EV charging on distribution networks is carried out. The implications of this study are summarised in section 8.5. In Chapter 6 and Chapter 7, a scheduling scheme for ESS and DSR based on RO is proposed and evaluated. RO uses uncertainty intervals (UIs) rather than probability distribution functions (PDFs). The relative strengths and weaknesses of this RO based ESS scheduling method are compared to other methods, such as MCS and PEM in 8.6.3.

8.2 Network Reinforcement vs Smartgrid Technologies and Techniques

In this section, the strengths and weaknesses of using smartgrid technologies and techniques compared to network reinforcement are discussed. The control and scheduling methodologies discussed in this thesis are shown to be alternative solutions to conventional network reinforcement in certain scenarios. It has been demonstrated that smartgrid enabled solutions with ESS, DSR and RTTR are more flexible than network reinforcement and are able to better utilise the current capacities of existing distribution network infrastructure.

- The cost of DSR and RTTR can be lower than network reinforcement
  Network infrastructure reinforcement is expensive and requires construction works. The implementation of ESS, DSR and RTTR, on the other hand, require minimum construction and the cost of DSR and RTTR can be much lower than that of network reinforcement. In Chapter 3 and Chapter 4, real world I&C DSR trial results have been reported. The cost of these DSR and network reinforcement has been compared in [201]. It is estimated that the cost of replacing a transformer at a substation to increase the capacity by 6MVA is approximately £1.5million. On the other hand, I&C DSR customers are paid for £200 per hour for 1MW of reduction. Therefore, if the overload

is not persistent and frequent, DSR and RTTR can be more cost effective than network reinforcement.

- Smartgrid technologies have higher flexibility
  The installation of ESS, DSR and RTTR is more flexible than network reinforcement. Besides, they can be installed in modules and are expandable. Smartgrid technologies and techniques can be installed at specific locations such as end of feeders or close to DGs and customers.
- Extra control capabilities
  ESS, DSR and RTTR have more control capabilities than conventional methods. Conventionally, it is difficult for the DNO to deal with unbalance between feeders and phases with conventional technologies, such as OLTCs. ESS and DSR can be used to deal with feeder and phase unbalance.
- ESS is a dependable and certain solution to deal with uncertainty
  The uncertainty in distribution networks due to the uptake of DGs and LCTs is likely to increase. Compared to DSR and RTTR, ESS is a dependable and certain solution to deal with network uncertainty.

On the other hand, there are also some drawbacks of smartgrid interventions.

- Requirements for the implementation of DSR
  First of all, the awareness of DSR customers needs to be improved. Secondly, the rollout of DSR requires the installation of smart meters and measurements. Finally, lack of market structure and supporting policies is also a hurdle for the widespread use of DSR.
- Requirements for Information Communication Technology (ICT)
  Compared to decentralised or conventional technologies and techniques, centralised smartgrid technologies and techniques rely on communication infrastructures. Centralised smartgrid technologies and techniques are likely to fail without a reliable communication system. Furthermore, network components will be used closer to their limits after the implementation of smartgrid. Therefore, the failure of the control system poses a higher risk than before.
- DSR and RTTR introduce extra uncertainty and risk
  The use of DSR and RTTR introduces new sources of uncertainty and increases the risk for the control and scheduling of distribution networks. Especially with RDSR enabled customers, it is difficult to predict the duration and magnitude of the response

that will be provided. The payback characteristics need to be well understood so that it does not cause any further network constraint violations.

The RTTRs of conductors depend on weather conditions. The implementation of RTTR can also bring uncertainty due to weather measurements and model accuracy. In most scenarios, RTTR is higher than static ratings, which means the conductors are operated closer to their physical limits. Therefore, errors in RTTR can lead to conductor damage.

- Limitation of ESS
  Currently, the cost of ESS is still high and the lifetime is relatively short. For instance, the cycling times (number of cycles) for Li-ion batteries are estimated to 1,000-10,000 at a cost of $600 to 2500 per kWh [202]. The deployment of ESS may not be cost effective if ESS is used for single application. On the other hand, considering its finite resource available, ESS may not have enough resource for later usage if its SoC is not managed well.
- Increased losses
  In some cases, the deployment of smartgrid technologies and techniques can increase network losses. For instance, RTTR allows higher current to go through the conductor. This will increase the losses.

8.3 Sensitivity Factors

8.3.1 Variation of Sensitivity Factors

In Chapter 3, two methods to calculate sensitivity factors are introduced. The first approach derives sensitivity factors from the Jacobian matrix or DC load flow equation. The second approach applies a small power injection/extraction change ΔP_k at bus k and calculates sensitivity factors based on the voltage and power flow change due to ΔP_k. Figure 8.1 illustrates the difference between these approaches. This plot is extrapolated from experimental results shown in Figure 3.31.

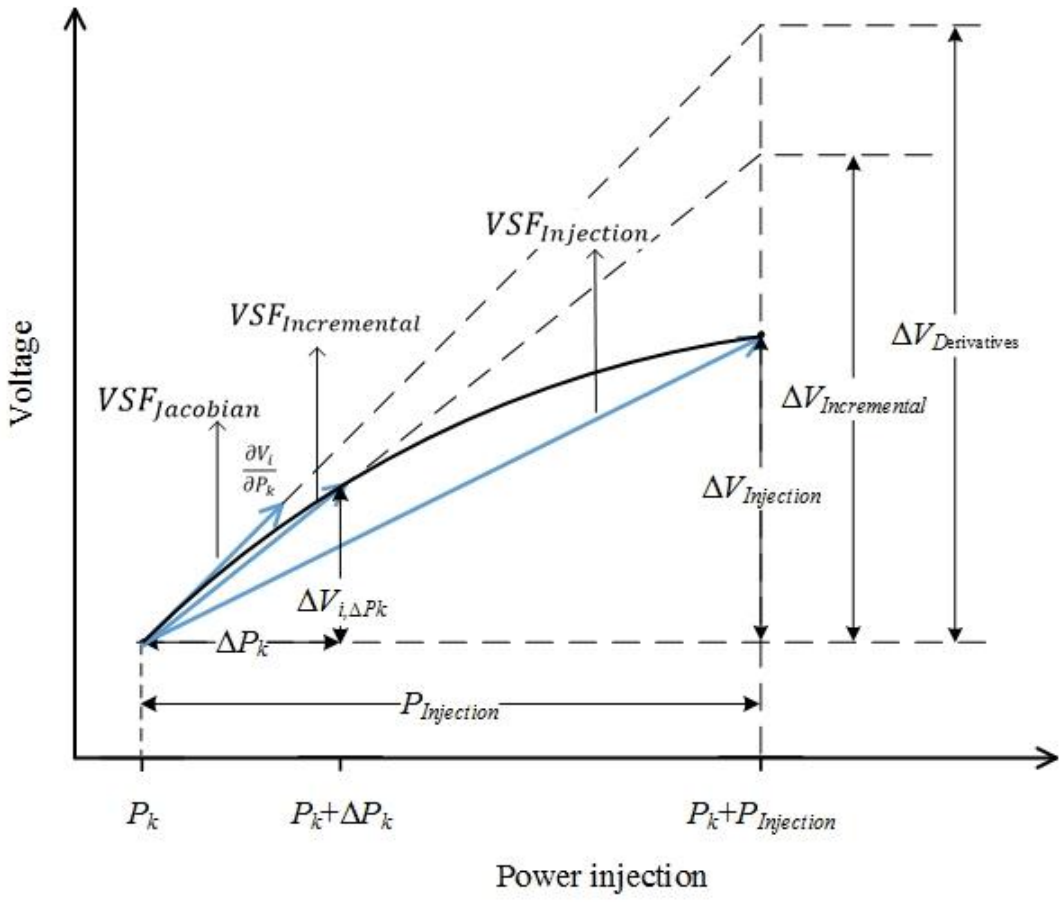

Figure 8.1 Comparison of Different Approaches to Calculate Sensitivity Factors

In this figure, the black curve is an example voltage trajectory of bus i due to power injection from bus k. The rates of the blue lines indicate the VSFs from bus k to bus i, calculated by different methods.

The first line from the top shows the VSF calculated based on Jacobian matrix. Denoting the original power injection from bus k as P_k, the VSF based on Jacobian matrix is given as

$$VSF_{Jacobian} = \frac{\partial V_i}{\partial P_k} = \frac{\Delta V_{Jacobian}}{P_{Injection}} \tag{8.1}$$

The line in the middle is the VSF calculated with the incremental method. Based on this method, the sensitivity factor is calculated as

$$VSF_{Incremental} = \frac{\Delta V_{i,\Delta P_k}}{\Delta P_k} = \frac{\Delta V_{Incremental}}{P_{Injection}} \tag{8.2}$$

The actual voltage change $\Delta V_{Injection}$ due to actual power injection $P_{Injection}$ is also illustrated on the graph. Based on $\Delta V_{Injection}$ and $P_{Injection}$, the real VSF is calculated. The real VSF is shown as the bottom line.

$$VSF_{Injection} = \frac{\Delta V_{Injection}}{\Delta P_k} = \frac{\Delta V_{Incremental}}{P_{Injection}} \quad \textbf{(8.3)}$$

In a voltage control scheme, $VSF_{Incremental}$ or $VSF_{Jacobian}$ can be used to calculate the required power injection $P_{Injection}$. As can be observed from this graph, sensitivity factors are related to the state or the operating point of the system. For the incremental method, the error of calculated sensitivity factors will reduce if ΔP_k is close to $P_{Injection}$. However, without knowing $P_{Injection}$, the state of the system is unknown and thus, it is not possible to calculate the exact sensitivity factor $VSF_{Injection}$.

8.3.2 Strength and Weakness of Sensitivity Factors

As shown in Chapter 4, most analytical methods for dealing with uncertain problems can only be applied to linear problems. The use of VSF and PFSF is a linearization of the full quadratic AC loadflow calculation. DC loadflow is another approach to linearize the full AC loadflow equation. Compared to DC loadflow, the advantages of SFs are:

- Reactive power
  Reactive power is neglected in DC loadflow based on the assumption that X>> R. At the same time, in DC loadflow it is assumed that all voltage magnitudes are 1.0. However, in distribution networks, the voltage profile will be more volatile and is not likely to be 1.0 pu constantly. Moreover, reactive power resource from ESS is not time limited. Using real power only will increase the power and energy requirement from ESS.
- Voltage control
  DC loadflow is not able to deal with voltage problems with either real or reactive power. Therefore, DC loadflow may not be suitable for the purpose of distribution network control.

However, the disadvantages of using sensitivity factors are

- Need to be updated
  The weakness of the use of sensitivity factor is that SFs are related to the state or the operating point of the network. This indicated that SFs need to be updated for each timestep based on the forecast. In this thesis, the SFs are calculated based on loadflow equations with updated load and generation values for each timestep to enhance accuracy.

- Assumption of small state change due to uncertainty

Most analytical methods for dealing with uncertainty require the linearization of the problem. If SFs are used for the linearization process, the underpinning assumption is that uncertainty does not cause dramatic changes in the state of the system. For instance, large variation between the real values and forecast of load and/or generation can change voltage magnitudes and even the direction of power flow. The sensitivity factors calculated based on the forecast values are therefore very different compared to the real sensitivity factors. As a result, decisions made with these methods are likely to be inaccurate or even fail.

- Superposition

  If multiple control interventions are included in the decision making process, the superposition of the effects due to the adopted interventions is not linear. The use of sensitivity factors cannot capture the interactions between the interventions.

8.4 The Importance of Considering Uncertainty

Without appropriate methods to deal with uncertainty, two extreme approaches can be taken to avoid network limit violations. These approaches can be separated into a scheduling stage and a control stage. Schedules can be made from hours to one day ahead. When the schedules are being implemented, real time control is required if an excursion occurs.

The first approach makes schedules without considering the presence of uncertainty. All scheduling decisions are made based on the nominal forecast values. During control stage when schedule is being implemented, if an excursion happens, real time control procedures will be taken to ensure the network operates within its limits. However, without considering uncertainty, ESSs may not have enough SoC to deal with the excursion. Therefore, more expensive solutions, such as DG curtailment or diesel generators, may be used. Besides, if ESS is used for multiple purposes, it may not be available when it is needed.

The second approach is fully conservative and makes schedules for the worst case scenario even though it is unlikely to happen. This approach considers the impacts of uncertainty but ignores the distributions of uncertainty within the uncertainty intervals. This approach increases the reliability and PoS but also increases unnecessary cost. Smartgrid interventions such as ESS and DSR are likely to be used more intensively in this approach.

The first approach is aggressive and ignores uncertainty. The second approach is conservative and prepares for the worst case. In scenarios where the level of risk is very low, which mean the possibilities of large errors happening are low, it is possible that the first aggressive approach incurs lower cost than the conservative approach.

8.5 The Impact of LCTs on Distribution Networks

The performance of conventional control and scheduling algorithms may not be adequate in the presence of a range of sources of uncertainty. In section 4.4, the impact of EV charging has been studied.

In this study two unique datasets of real world EV charging and load profile from smart meter measurement are combined using a probabilistic method. Previous work makes various assumptions regarding the spatial, temporal and behavioural diversity of EV charging. For instance, it is assumed EVs start to charge when they return home and/or charge from a low SoC until fully charged. In this work, the spatial, temporal and behavioural uncertainties have been taken into consideration using real world data and MCS. Using real charging profiles avoids the assumption of when EVs start to charge and the SoC change during charging. Compared to results which do not consider diversity, it is shown that, the spatial, temporal and behavioural diversity of EV charging alleviates the impacts on distribution networks. Therefore, compared with conservative consumptions such as all EVs start charging at the same time from low SoC to full, higher penetrations of EVs can be accommodated before triggering network reinforcement.

The results of this study demonstrate that:

- Uncertainty and diversity exist in LCT demands.
  As illustrated in Figure 4.15 and Figure 4.16, for a urban network with 60% penetration of EV, the mean peak apparent power demand is 400kVA and the 97.5 percentile of the samples has a peak demand of 500kVA.
- The diversity of LCT demand lessens its impact on distribution networks
- Without considering the uncertainty and diversity of LCT demands, the control, scheduling and planning decisions made by DNOs will be conservative

8.6 Robust Optimization

In Chapter 5, the principle of robust optimization (RO) is introduced. In Chapter 6, RO is applied to solve a scheduling problem for ESS and DSR. In this section, RO is compared with other techniques to deal with uncertainty such as chance constraint programming and MCS. How to select appropriate uncertainty intervals based on different types of distributions is discussed. Finally, the advantages and disadvantages of the MCS based curve fitting technique are introduced.

8.6.1 RO and Other Methods to Deal with Uncertainty

In Chapter 4, a series of methods to deal with uncertainty are introduced. It has been found that most of the methods require the PDF of uncertain values. In Chapter 6, RO has been applied for the scheduling of ESS and DSR. Two methods to calculate BoU have been proposed. The first approach estimates the relationship between BoU and PoS regardless of the distribution of uncertainty sets. The second approach combines MCS and curve fitting technique to provide a more accurate mathematical description of the relationship between BoU and PoS.

The proposed scheduling scheme presents several advantages compared to stochastic optimization and chance constraint programming techniques. Firstly, in scenarios where, for uncertain values, only their UIs exist or their PDFs are only partially available or even inaccurate, techniques such as stochastic optimization or chance-constraint programming are unable to solve the problem. On the other hand, it has been shown that the proposed RO based scheduling scheme is still able to provide robust solutions to avoid branch RTTR violation, with respect to ESS SoC limits and network voltage constraints. In such scenarios, the first PoS estimation approach is able to provide robust solutions based on simple calculations in a very short time even for a large network.

As shown in section 4.2, most techniques cannot provide accurate PDFs for uncertain values. Even in scenarios where accurate PDFs are available for all the uncertain values, the advantages of RO based scheduling scheme still exist. Under such circumstances, both the estimation and the curve fitting based approaches can be used to calculate OBoU. The estimation approach can be applied to calculate a slightly conservative but robust solution in a very short time. Once the optimization problem is solved, the OBoU can be calculated with the simple equation given in (6.23).

Curve fitting based approach constructs the function between BoU and PoS through MCS. MCS runs a large number of load flow calculations to compute the PoS at different BoU. The MCS process is relatively time consuming however it avoids any linearization of the network model. As a result, the curve fitting method is able to provide accurate solutions and ensure desired levels of PoS. The capability of adjusting the PoS is beneficial to the future deployment of ESS. As shown in Table 7.9, by accepting a PoS requirement of 97%, the proposed method can further reduce the power and energy requirements of ESS. In this case, the power requirement can be reduced by up to 12% and the energy requirement can be reduced by up to 22%.

8.6.2 Selection of Uncertainty Interval

The selection of UI is important to the performance of RO. Conservative UI selection compromises the benefits of the proposed RO based approach. On the other hand, if the UIs are too narrow, which means uncertainty is underestimated; the probability of success achieved by RO based solutions will be reduced.

Some forecast techniques, such as [126, 203, 204], are able to provide confidence intervals. The confidence intervals can be used as UIs. If the confidence intervals or the uncertainty intervals are 100%, RO based method can successfully solve the problem and tune the BoU to minimise the cost. However, if the confidence level of the confidence intervals is less 100%, 95% for instance, RO can still provide solutions with high PoS.

If PDFs for uncertainty values are available, depending on different types of uncertainty distribution, different strategies for selecting UI can be adopted. Data following uniform distributions and Beta distributions have relatively clear bounds so there is no need to define UIs. The upper and lower limits of uniform and Beta distributions can be used as UIs. Normal distributed data does not have clear bounds or minimum or maximum values. If uncertainty values follow normal distributions, UIs can be defined by three approaches. The three approaches are compared below.

1) Large UIs combined with MCS curve fitting technique
   In this approach, large UIs are used in combination with curve fitting technique to decide the OBoU. For instance, five times the standard deviation of the normal distribution can be used as UIs. The drawback of this approach is that it is time consuming due to the MCS process. However, once an accurate relationship between BoU and PoS is found, the BoU can be adjusted to achieve the required PoS. As has been found, the flexibility to adjust BoU reduces the power and energy requirement for ESS and the need for DG curtailment.
2) Large UIs without MCS curve fitting technique
   Similar to previous approach, large UIs are used. However, this approach only estimates the relationship between BoU and PoS based on the first bound introduced in section 5.4. This approach can be very conservative because this estimation ignores the distribution of the uncertainty values. However, this approach guarantees high PoS and is also time saving.
3) Small to medium intervals without MCS curve fitting technique
   This approach uses 3 to 4 times the standard deviation as UIs and does not run MCS based

curve fitting. If small to medium UIs, i.e. 3 to 4 times standard deviation, are used, the BoU can be set to 100%. This is a time-saving approach since there is no need to run MCS. However, depending on how the UIs are selected, this approach can be conservative or risky. If the UIs chosen are small, e.g. 3 times the standard deviation, the results of this approach will have a low PoS. If the UIs chosen are large, this approach can be conservative.

8.6.3 MCS Based Curve Fitting Technique

The second approach to estimate the relationship between BoU and PoS is based on MCS. MCS poses heavy computational burden and is therefore time consuming. To be specific, depending on the size of the network and the number of uncertainties, at least a few hundreds of loadflow calculations are needed for each solution at the given BoU. If there is enough time before the schedule needs to be implemented, the use of MCS to decide the accurate relationship between BoU and PoS present some advantages:

- As introduced earlier, SFs are a linearization of the system and may not always be accurate. If the state of the system varies greatly from the estimation, the SFs may not be adequate to make accurate and reliable decisions. In the MCS process, large numbers of loadflow calculations are carried out. The PoS are calculated based on full AC loadflow results. This process avoids any assumptions, including SFs, made in the linear optimization formulation.
- The establishment of the accurate relationship between BoU and PoS enables a fine tuning of BoU so that desired PoS can be achieved. It has been found that a reduced but high PoS can reduce the power and energy requirement for ESS and maintain a high reliability at the same time. By reducing the required PoS, the requirements for ESSs can be reduced. This is very important for maximizing the benefits of ESS, which is currently expensive and fragile.

Chapter 9. Conclusion

9.1 Overview

In this thesis, the impacts of high penetrations of DG and LCTs on future distribution networks in terms of voltage and power flow are studied first. The limitations of existing control strategies for ESS and DSR in future scenarios where high penetrations of DG and LCTs exist have been explored. Thirdly, the impacts of a range of sources of uncertainties on the performance of conventional control algorithms are discovered. Finally, control and scheduling strategies for ESS and DSR to facilitate DG and LCTs in the presence of a range of source of uncertainties based on robust optimization is developed and evaluated. In this chapter, conclusions are drawn and future work is suggested.

9.2 Conclusions

The research question of this research is posed at the beginning of this thesis: if and when ESS and DSR can be alternative to network reinforcement? It has been found that, the collaborative use of ESS and DSR can be alternative to network reinforcement in some cases. Furthermore, the use of smartgrid technologies and techniques can provide more benefits compared to conventional network reinforcement.

Key findings are summarized and explained below.

1) Most previous research ignores the uncertainty in DSR, DG, RTTR and load and little previous work has considered the coordinated operation of ESS and DSR.

In this thesis it has been found that, ESS and DSR have the capability to provide a number of services in assisting in the operation of distribution networks, especially in future networks with large penetrations of low carbon technologies such as wind generation, solar generation, EVs and heat pumps. Through literature review, it has been found that the majority of previous research ignores the uncertainty in DSR, DG, RTTR and load. Besides, most previous research has focused on DSM rather than DSR and ignores the uncertainty in the magnitude and duration of DSR. Besides, little previous work has considered the coordinated operation of ESS and DSR and has usually considered the control of these devices in isolation. ESS is a fully controllable and fast response device with relatively high cost and a limited energy resource. Compared to ESS, DSR is normally less controllable, slow to respond but with a relatively lower cost. At the same time, DSR resource or capacity is less constrained compared to ESS. Finally, for power flow management problems, much of the previous work

assumes a static asset rating rather than using RTTR. RTTR can enhance the utilization of cables and transformer and thus reduce the requirement for ESS and DSR.

2) Collaborative control algorithms for ESS and DSR based on sensitivity factors and cost sensitivity factors are proposed.

In chapter 3, VSFs and PFSFs are introduced. Two methods for calculate sensitivity factors have been introduced. The limitations and advantages of two methods are pointed out. Based on voltage and power flow sensitivity factors, the concept of voltage cost sensitivity factor and power flow cost sensitivity factors are proposed. Cost sensitivity factors evaluate an intervention using both technical and commercial considerations. Two control schemes based on sensitivity factors and cost sensitivity factors respectively, are presented. The proposed control algorithms use ESS and DSR collaboratively. This work has illustrated the complementary features of ESS and DSR which make the combination of ESS and DSR an attractive solution.

In this work, cost functions for ESS, I&C DSR and RDSR have been developed, based on the cost of real ESS systems, real I&C DSR trial contracts and the value of RDSR to DNOs respectively. Multiple forms of DSR with varying magnitudes, locations and characteristics have been considered in this work. The strategies have been evaluated using a validated real network model and a realistic future scenario extrapolated from a large smart meter data set. In this future scenario, the present voltage control system with on load tap changer and capacitor banks is no longer able to function successfully.

The proposed control schemes have been evaluated. Simulation results illustrate how the control strategy can be used as an attractive alternative to network reinforcement to solve the uncertain voltage problems due to the unpredictable rate and distribution of LCT installations. The proposed methods can deal with uncertainty to an extent and require no knowledge of the PDF of uncertainty. However, the proposed scheme is a passive control scheme which responds to measurements. Without forecast and planning, such schemes may be inadequate to deal with predictable future excursions. Moreover the proposed schemes are not able to provide a solution with minimum cost. Lastly, this control scheme does not take into consideration the timescale of ESS and DSR. ESS SoC management is critical to maximize its value. Due to the current high cost, under-utilised ESS is unlikely to be cost effective while unnecessary use of ESS can reduce its useful lifetime.

3) Most methods to deal with uncertain problems require the PDF of the uncertain values.

However, accurate PDF of uncertain values is difficult to access and unlikely to be normally distributed

In chapter 4, the sources of uncertainties are reviewed first. It has been found that, uncertainty exists in load, wind and wind power, RTTR, SoC and DSR. It can also be seen that the PDF of uncertainty is often difficult to access and unlikely to be normally distributed. Next, methods to deal with uncertainties have been reviewed and compared. The methods to deal with uncertainty include Monte Carlo simulation (MCS), chance constraint programming (CCP) and analytical probabilistic methods, such as point estimation method (PEM) and cumulant based method (CBM). The limitations of these methods are:

- These methods require the PDF of the uncertain values. If PDFs are not available or only partially available, these methods are not able to solve the problem;
- Some previous methods are not able to deal with asymmetrical distributions;
- Most of these methods are not able to adjust the probability of success (PoS) of their solutions;
- The results of MCS provide accurate description of the distribution of the output but is very time consuming.

4) Spatial and temporal diversities in EV charging alleviate the stress on the distribution networks therefore it is important to deal with uncertainty properly to avoid making overly conservative decisions.

In Chapter 4, the impact of EV charging on distribution networks is studied with MCS. Two real world datasets have been used to sample household load profiles and EV charging profiles. The use of real EV charging profiles avoids assumptions of EV charging patterns. This study shows the importance of dealing with uncertainty. If the diversity and the uncertainty of LCTs are not considered, decisions made for ESS and DSR will be conservative and the associated cost will increase. At the same time, it is also found that, the uncertainty of LCTs is difficult to describe mathematically.

5) A scheduling scheme for ESS and DSR based on robust optimisation is proposed and evaluated. The proposed method is shown to have advantages over conventional techniques.

In previous chapters, it has been found that there is a need for an algorithm to deal with uncertainty which:

- Requires minimum information about the uncertainty.
- Require small or moderate computation time
- Able to deal with asymmetrical distributions of uncertainties

Based on literature, robust optimization (RO) has proved to be able to fulfil these requirements. In chapter 5, the general form of an uncertainty linear optimization (ULO) problem is presented. Three different formulations of RO are introduced. Three types of bounds are discussed to enable the probability of constraint violation. An RO solver in python is developed and validated.

A new application of RO for solving an ESS scheduling problem considering new sources of uncertainty, namely the uncertainty of RTTR and ESS SoC is described. The proposed formulation considers the RTTR constraints, voltage constraints and ESS state-of-charge constraints. Furthermore, the proposed cost function takes into account the capital cost and the remaining cycles of ESSs.

The proposed RO scheduling scheme is compared to normal and conservative OPF techniques. Compared to OPF results without considering uncertainty, the proposed method can guarantee high probability of success. In comparison with conservative form of OPF, the proposed method is able to achieve high PoS with reduced cost.

6) The use of budget of uncertainty (BoU) can adjust the level of conservatism and therefore reduce the power and energy requirement from ESS.

In the proposed RO based approach, BoU is introduced to control the level of conservatism. A high BoU ensures high PoS and a low BoU reduces the cost and also the PoS. To enable the trade-off between the cost and the PoS, two methods have been introduced. The first approach estimates the OBoU ignoring the distribution of the uncertainty. This approach results in a slightly conservative solution for small networks. When applied to a large network, the approach can reduce the requirements for ESS power rating and energy capacity. The second approach, which uses a moderate number of MCSs coupled with LMA curve fitting technique, has been proposed to estimate the optimal BoU, to ensure a desired level of PoS. This approach is relatively time consuming but has been found to be able to estimate the relationship between BoU and PoS with high accuracy. Simulation results show that, the proposed methodology is able to provide an ESS charge and discharge profile that ensures a desired level of PoS.

The capability of adjusting the solution so that a PoS of less than 100% can be achieved has been found valuable. As shown in the case study in Table 7.9, by accepting a solution with 97% PoS, the energy requirement for ESS can be reduced by up to 22.4% and the power requirement can be reduced by up to 12.2%.

7) Simulation results also show that the proposed method based on RO is able to deal with asymmetrical uncertainty data.

As has been shown before in section 4.3, some analytical methods for dealing with uncertainty assume the distributions of uncertainty data are symmetrical. In reality, however, it is very unlikely that the uncertainty data is always symmetrically distributed. By testing the proposed approach with Beta distribution data, it is found that the proposed method is able to deal with both symmetrical and asymmetrical uncertainty data.

9.3 Future work

Future work to extend the research described in this thesis is suggested below.

First of all, ramp rates of ESSs are not considered in the RO formulation. If fast response storage systems are used, it is reasonable to assume that ESSs can change their output rapidly from the previous timestep to the required output in the next timestep. If shorter timesteps (e.g. 5 minutes) and slower response energy storage system such as hydro pump storage are considered, their ramp rates should be considered in the formulations.

In this thesis, a scheme problem for ESS has been formulated as an uncertain linear optimization (ULO) problem and solved by robust optimization. This formulation deals with uncertain values with uncertainty intervals. An uncertainty interval is a range that uncertain value varies. This formulation is not able to deal with mixed integer problems such as the uncertainty of if a I&C DSR customer is able to provide a response and an unpredicted N-1 condition. The formulation can be extended to deal with the uncertainty of if DSR can be delivered and contingency.

The correlation between different uncertainties is not considered although the formulation of RO is able to deal with correlated uncertainty datasets. For instance, if wind speed is underestimated, compared with forecast, both the output of windfarm and the RTTRs of adjacent OHLs will increase. Taking this correlation into consideration is likely to further increase the benefits of RO based approach.

Appendix A. Loadflow Calculation

Load flow calculations have been introduced in [100, 145, 151]. In section, load flow equation is introduced and solve with Newton-Raphson method. Next, P-Q decoupled methods and DC load flow, which are simplifications of the full AC load flow equations, are introduced.

Loadflow and Jacobian Matrix

In a network with N_{bus} busbars, the standard node voltage equations can be written as

$$\boldsymbol{I} = \boldsymbol{Y} \cdot \boldsymbol{V} \tag{A.1}$$

Where

$\boldsymbol{I}$	is the bus current injection vector
$\boldsymbol{Y}$	is the bus admittance matrix
$\boldsymbol{V}$	is the bus voltage vector

Non-diagonal elements of $\boldsymbol{Y}$ is calculated as

$$Y_{ij} = -\frac{1}{r_{ij} + jx_{ij}} = G_{ij} + jB_{ij}, i \neq j \tag{A.2}$$

Where

r_{ij}	the per unit resistance of branch from busbar i to busbar j
x_{ij}	the per unit reactance of branch from busbar i to busbar j
G_{ij}	the per unit conductance of branch from busbar i to busbar j
B_{ij}	the per unit susceptance of branch from busbar i to busbar j

Y_{ij} is a complex number and can be recorded in the polar form as

$$Y_{ij} = -y_{ij}\angle\phi_{ij}, i \neq j \tag{A.3}$$

Where

ϕ_{ij} is the angle of the vector

y_{ij} is the length of the vector

For the diagonal elements of $\boldsymbol{Y}$, as known as self-admittance of bus i can be calculated as

$$Y_{ii} = \sum_{j=1}^{n} y_{ij} \angle \phi_{ij} + \sum_{j=1}^{n} j \frac{B_{ij}}{2}, i \neq j \quad \textbf{(A.4)}$$

Where

B_{ij} is the charging capacitance of branch from busbar i to busbar j

The complex power injection of bus i is defined as

$$S_i^* = P_i - jQ_i = S_{Gi}^* - S_{Di}^* = (P_{Gi} - P_{Di}) - j(Q_{Gi} - Q_{Di}) \quad \textbf{(A.5)}$$

Where

S_i the complex power injection of busbar i

S_i^* the conjugation of S_i

P_i the net real power injection of busbar i

Q_i the net reactive power injection of busbar i

S_{Gi}^* the conjugation of S_{Gi} which is the apparent power generation of busbar i

S_{Di}^* the conjugation of S_{Di} which is the apparent power demand of busbar i

P_{Gi} the real power output of generators connected to busbar i

Q_{Gi} the reactive power output of generators connected to busbar i

P_{Di} the real power demand of busbar i

Q_{Di} the reactive power demand of busbar i

The complex power injection can be calculated by

$$S_i^* = V_i^* I_i \quad \textbf{(A.6)}$$

Substituting equation (A.5) into (A.6)

$$\boldsymbol{S}^{*} = \boldsymbol{P} - j\boldsymbol{Q} = \boldsymbol{V}^{*}\boldsymbol{Y}\boldsymbol{V} \tag{A.7}$$

Where

$\boldsymbol{P}$ is the vector of net real power injection of busbars

$\boldsymbol{Q}$ is the vector of net reactive power injection of busbars

Separating the real and imaginary parts of (A.7)

$$\begin{aligned} P_i &= V_i \sum_{j=1}^{n} V_j\left(G_{ij}\cos\theta_{ij} + B_{ij}\sin\theta_{ij}\right) \\ Q_i &= V_i \sum_{j=1}^{n} V_j\left(G_{ij}\sin\ \theta_{ij} - B_{ij}\cos\theta_{ij}\right) \end{aligned} \tag{A.8}$$

where

θ_{ij} the angle difference between busbar i and busbar j

Equation (A.8) can be written as

$$\begin{bmatrix}\boldsymbol{P}\\ \boldsymbol{Q}\end{bmatrix} = g\left(\begin{bmatrix}\boldsymbol{\theta}\\ \boldsymbol{V}\end{bmatrix}\right) \tag{A.9}$$

The equation in (A.9) can be solved with the Newton-Raphson method. Base on the Newton-Raphson method, for each PV and PQ busbar, the real and reactive power mismatch can be calculated as

$$\begin{bmatrix}\Delta\boldsymbol{P}\\ \Delta\boldsymbol{Q}\end{bmatrix} = \begin{bmatrix}\frac{\partial\Delta\boldsymbol{P}}{\partial\boldsymbol{\theta}} & \frac{\partial\Delta\boldsymbol{P}}{\partial\boldsymbol{V}}\\ \frac{\partial\Delta\boldsymbol{Q}}{\partial\boldsymbol{\theta}} & \frac{\partial\Delta\boldsymbol{Q}}{\partial\boldsymbol{V}}\end{bmatrix}\begin{bmatrix}\Delta\boldsymbol{\theta}\\ \Delta\boldsymbol{V}\end{bmatrix} = -\boldsymbol{J}\begin{bmatrix}\Delta\boldsymbol{\theta}\\ \Delta\boldsymbol{V}/\boldsymbol{V}\end{bmatrix} \tag{A.10}$$

Where

$\boldsymbol{J}$ the Jacobian matrix

$\partial\Delta\boldsymbol{P}/\partial\boldsymbol{\theta}$ the matrix for the partial derivatives of $\Delta\boldsymbol{P}$ to $\boldsymbol{\theta}$

$\partial\Delta\boldsymbol{P}/\partial\boldsymbol{V}$ the matrix for the partial derivatives of $\Delta\boldsymbol{P}$ to $\boldsymbol{V}$

$\partial\Delta\boldsymbol{Q}/\partial\boldsymbol{\theta}$ the matrix for the partial derivatives of $\Delta\boldsymbol{Q}$ to $\boldsymbol{\theta}$

$\partial \Delta \boldsymbol{Q} / \partial \boldsymbol{V}$ the matrix for the partial derivatives of $\Delta \boldsymbol{Q}$ to $\boldsymbol{V}$

Assuming bus 1 to bus N_{PQ} are PQ buses, bus $N_{PQ}+1$ to bus $N_{bus}-1$ are PV buses, bus N_{bus} is slack bus

$$\Delta \boldsymbol{P} = \begin{bmatrix} \Delta P_1 \\ \Delta P_2 \\ \vdots \\ \Delta P_{N_{bus}-1} \end{bmatrix}$$

$$\Delta \boldsymbol{Q} = \begin{bmatrix} \Delta Q_1 \\ \Delta Q_2 \\ \vdots \\ \Delta Q_{N_{PQ}} \end{bmatrix}$$

$$\Delta \boldsymbol{\theta} = \begin{bmatrix} \Delta \theta_1 \\ \Delta \theta_2 \\ \vdots \\ \Delta \theta_{N_{bus}-1} \end{bmatrix}$$

$$\Delta \boldsymbol{V} = \begin{bmatrix} \Delta V_1 \\ \Delta V_2 \\ \vdots \\ \Delta V_{N_{PQ}} \end{bmatrix}$$

N_{PQ} the number of PQ buses

N_{PV} the number of PV buses

The elements in (A.10) are calculated as

$$\frac{\partial \Delta P_i}{\partial \theta_i} = V_i^2 B_{ii} + Q_i \quad \textbf{(A.11)}$$

$$\frac{\partial P_i}{\partial \theta_j} = -V_i V_j \left(G_{ij} \sin \theta_{ij} - B_{ij} \cos \theta_{ij} \right), i \neq j \quad \textbf{(A.12)}$$

$$\frac{\partial \Delta P_i}{\partial V_i} V_i = -V_i^2 G_{ii} - P_i \quad \textbf{(A.13)}$$

$$\frac{\partial P_i}{\partial V_j} = -V_i \left(G_{ij} \cos \theta_{ij} + B_{ij} \sin \theta_{ij} \right), i \neq j \quad \textbf{(A.14)}$$

$$\frac{\partial Q_i}{\partial \theta_i} = V_i^2 G_{ii} - P_i \quad \textbf{(A.15)}$$

$$\frac{\partial Q_i}{\partial \theta_j} = V_i V_j \left(G_{ij} \cos \theta_{ij} + B_{ij} \sin \theta_{ij} \right), i \neq j \quad \textbf{(A.16)}$$

$$\frac{\partial Q_i}{\partial V_i} = V_i^2 B_{ii} - Q_i \tag{A.17}$$

$$\frac{\partial Q_i}{\partial V_j} = -V_i\left(G_{ij}\sin\theta_{ij} - B_{ij}\cos\theta_{ij}\right), i \neq j \tag{A.18}$$

P-Q Decoupling Method

The full AC loadflow calculation is of high accuracy but the Jacobian matrix needs to be calculated in each iteration. To simplify this process, P-Q decoupling method has been proposed [205]. P-Q decoupling method assumes that

i. the coupling between the real power and the magnitude of voltage is weak and thus

$$\frac{\partial \Delta P_i}{\partial V_j} \approx 0 \tag{A.19}$$

ii. the coupling between the reactive power and the angle of voltage is weak and thus

$$\frac{\partial Q_i}{\partial \theta_j} \approx 0 \tag{A.20}$$

Based on the assumptions (A.19) and (A.20), equation (A.10) becomes,

$$\begin{bmatrix}\Delta \boldsymbol{P}\\ \Delta \boldsymbol{Q}\end{bmatrix} = \begin{bmatrix}\frac{\partial \boldsymbol{P}}{\partial \boldsymbol{\theta}} & 0\\ 0 & \frac{\partial \boldsymbol{Q}}{\partial \boldsymbol{V}}\end{bmatrix}\begin{bmatrix}\Delta \boldsymbol{\theta}\\ \Delta \boldsymbol{V}\end{bmatrix} \tag{A.21}$$

$\partial \boldsymbol{P}/\partial \boldsymbol{\theta}$ and $\partial \boldsymbol{Q}/\partial \boldsymbol{V}$ as given in (A.11) - (A.18) can be further simplified. Assuming the angle between busbar i and j is small so that $\cos\theta_{ij} \approx 1$, (A.12) becomes

$$\frac{\partial P_i}{\partial \theta_j} \approx -V_i V_j\left(G_{ij}\sin\theta_{ij} - B_{ij}\right) \tag{A.22}$$

Assuming $\sin\theta_{ij}$ is a very small number and $G_{ij}\sin\theta_{ij} \ll B_{ij}$, (A.22) becomes

$$\frac{\partial P_i}{\partial \theta_j} \approx V_i V_j B_{ij} \tag{A.23}$$

Assuming $V_i^2 B_{ii} \gg Q_i$ and (A.11) becomes

$$\frac{\partial \Delta P_i}{\partial \theta_i} \approx V_i^2 B_{ii} \tag{A.24}$$

Similarly (A.17) and (A.18) become

$$\frac{\partial Q_i}{\partial V_i} \approx V_i^2 G_{ii} \tag{A.25}$$

$$\frac{\partial Q_i}{\partial V_j} = -V_i B_{ij} \tag{A.26}$$

Based on the above assumptions (A.21) becomes

$$\begin{bmatrix} \Delta \boldsymbol{P} \\ \Delta \boldsymbol{Q} \end{bmatrix} = \begin{bmatrix} \boldsymbol{V}\boldsymbol{B}'\boldsymbol{V} & 0 \\ 0 & \boldsymbol{V}\boldsymbol{B}''\boldsymbol{V} \end{bmatrix} \begin{bmatrix} \Delta \boldsymbol{\theta} \\ \Delta \boldsymbol{V} \end{bmatrix} \tag{A.27}$$

Where

$\boldsymbol{B}'$ is a $N_{Bus} - 1$ by $N_{Bus} - 1$ matrix

$\boldsymbol{B}''$ is a N_{PQ} by N_{PQ} matrix

$$\boldsymbol{B}' = -\begin{bmatrix} B_{11} & B_{12} & \cdots & B_{1,N_{Bus}-1} \\ B_{21} & B_{22} & \cdots & B_{2,N_{Bus}-1} \\ \vdots & \vdots & & \vdots \\ B_{N_{Bus}-1,1} & B_{N_{Bus}-1,2} & \cdots & B_{N_{Bus}-1,N_{Bus}-1} \end{bmatrix}$$

$$\mathbf{B}'' = -\begin{bmatrix} B_{11} & B_{12} & \cdots & B_{1,N_{PQ}} \\ B_{21} & B_{22} & \cdots & B_{2,N_{PQ}} \\ \vdots & \vdots & & \vdots \\ B_{N_{PQ},1} & B_{N_{PQ},2} & \cdots & B_{N_{PQ},N_{PQ}} \end{bmatrix}$$

(A.27) can be divided into two separate parts, given as

$$\begin{aligned} \Delta \boldsymbol{P} &= \boldsymbol{V}\boldsymbol{B}'\boldsymbol{V}\Delta\boldsymbol{\theta} \\ \Delta \boldsymbol{Q} &= \boldsymbol{V}\boldsymbol{B}''\boldsymbol{V}\Delta\boldsymbol{V} \end{aligned} \tag{A.28}$$

Thus, real power *P* and reactive power *Q* are decoupled and the iteration can be carried out separately. The relationship between real power and voltage magnitude and the relationship between reactive power and reactive power and voltage angle are ignored.

There are two methods to calculate the elements of $\boldsymbol{B}'$ and $\boldsymbol{B}''$, BX and XB versions. For the XB version, it is assumed that $r_{ij} \ll x_{ij}$ and the shunt reactance to the ground is ignored $B_{i0} = 0$, $\boldsymbol{B}'$ and $\boldsymbol{B}''$ are calculated as

$$B'_{ij} = -\frac{1}{x_{ij}} \tag{A.29}$$

$$B'_{ii} = \sum_{j \neq i} \frac{1}{x_{ij}} \tag{A.30}$$

$$B''_{ij} = -\frac{x_{ij}}{r_{ij}^2 + x_{ij}^2} \tag{A.31}$$

$$B''_{ij} = -\sum_{j \neq i} B''_{ij} \tag{A.32}$$

DC Loadflow

DC loadflow is a further simplification of XB version P-Q decoupling method. The relationship between reactive power and voltage is ignored. (A.27) can be rewritten as

$$\Delta \boldsymbol{P} = \boldsymbol{V}\boldsymbol{B}'\boldsymbol{V}\Delta\boldsymbol{\theta} \tag{A.33}$$

In DC loadflow, it is assumed that $V_i = 1.0$. Therefore (A.33) will be

$$\Delta \boldsymbol{P} = \boldsymbol{B}'\Delta\boldsymbol{\theta} \tag{A.34}$$

Thus, the nonlinear relationship between real and reactive power and voltage angle and magnitude, as defined in (A.10) can be simplified to a linear function between real power and voltage angle. The power flow on each branch can be calculated as

$$P_{ij} = -B_{ij}(\theta_i - \theta_j) = \frac{\theta_i - \theta_j}{x_{ij}} \tag{A.35}$$

Appendix B. Code for Running Loadflows with EV and Smart Meter Profiles

```
def backup():
    #get the network P and Q demand without scaling
    P_noscale = 0.0
    Q_noscale = 0.0
    #Set_Load(otherloadname, 0 ,0)
    net.DoLoadFlow()

    P_noscale, Q_noscale = Total_Load_Noloss()

    #back up P and Q load at each busbar
    count = 0 ###'count' is used to count the number of load
in the original model
    for load in loads.itervalues():

Load_P.append(float(load.GetDValue(ipsa.IscLoad.RealMW)))

Load_Q.append(float(load.GetDValue(ipsa.IscLoad.ReactiveMVAr)))
        count = count + 1
    return count, P_noscale, Q_noscale#'count' is the number
of busbars,P and Q without scale

def setupnetwork(gridinfeed_voltage_pu, networkP, pqratio):
    networkQ = networkP * pqratio
    loadP = networkP
    loadQ = networkQ
    #otherloadQ = otherloadP * pqratio # estimate Q on all
other feedes based on the estimated power factor of 0.97
    #loadP = networkP - otherloadP # active power demand on
feeder Hecley high house and Hecley North SW
    #loadQ = loadP * pqratio

    #scale factor based on original model
```

```
    Pscale = float(loadP/float(P_noscale))
    Qscale = float(loadQ/float(Q_noscale))

    #66kV side voltage
    for infeed in infeeds.itervalues():
        infeedname = infeed.GetRealName()
        if (infeedname == Grid_Infeed_Name):
            infeed.SetDValue(ipsa.IscGridInfeed.VoltPU,
gridinfeed_voltage_pu)

    #work out new P Q value
    i = 1
    for load in loads.itervalues():
        load.SetDValue(ipsa.IscLoad.RealMW, Load_P[i]*Pscale)
        load.SetDValue(ipsa.IscLoad.ReactiveMVAr,
Load_Q[i]*Qscale)
        i += 1

def loadflow():

    wrt = Write_Results()
    wrt.write_new_titles('')

    with open(SCADA_Data_File,'rb') as filereader:
        reader = csv.reader(filereader, dialect='excel')

        #skip first four row of the file (Loadline list row,
measurement error row, RTTR row, title row)
        skip_line_number = 1
        skip_i = 1
        while skip_i <= skip_line_number:
            reader.next()
            skip_i += 1
```

```
        # read data for each time step
        for row in reader:
            # break when the row being read gets to a Null
statement in the CSV file
            if (row[0]== 'null'):
                break

            elif (row[0] != 'null'):
                readtime = row[0]
                if float(readtime) == 24:
                    readtime = 0

                readtime = str(readtime) + ':00'
                print readtime
                format = "%H:%M"
                t = time.strptime(readtime,format)
                tnumber = int(t.tm_hour *60) +
int(t.tm_min)#tnumber is the float format of time, for
example,00:30 is 0.5 and 01:00 is 1
                shorttime = str(t.tm_hour) + ':' +
str(t.tm_min)

                #print shorttime
                Gridinfeed_Voltage_pu = 1

                feed5120 = float(row[1]) * 3
                Set_Load_kW('Busbar2', feed5120, power_factor)

                feed128 = float(row[2]) * 3
                Set_Load_kW('Busbar15', feed128, power_factor)
                Set_Load_kW('Busbar16', feed128, power_factor)
                Set_Load_kW('Busbar17', feed128, power_factor)
                Set_Load_kW('Busbar18', feed128, power_factor)
                Set_Load_kW('Busbar19', feed128, power_factor)
                Set_Load_kW('Busbar20', feed128, power_factor)
```

```
                Set_Load_kW('Busbar21', feed128, power_factor)

                feed384 = float(row[3])
                Set_Load_kW('Busbar22', feed384, power_factor)


                net.DoLoadFlow()
                if Add_LCT_Flag == True:
                    PDOMtotal, PEVtotal, PHPtotal, PPVtotal =
Add_LCT(tnumber, extra_percentage, Add_Shop_Flag, Add_DOM_Flag,
Add_EV_Flag, Add_ASHP_Flag, Add_PV_Flag)#add LCT ,return the
total consumption/generation of customers, EV, HP and PV
                elif Add_LCT_Flag == False:
                    PDOMtotal, PEVtotal, PHPtotal, PPVtotal  =
0, 0, 0, 0

                totalP, totalQ =
Get_Grid_Infeed_Output(Grid_Infeed_Name)
                Network_Total_Load = (totalP ** 2 + totalQ **
2)**0.5
                extrastr = ''
                wrt.write_results(shorttime,
Network_Total_Load, totalP, totalQ, Gridinfeed_Voltage_pu,
PDOMtotal, PEVtotal, PHPtotal, PPVtotal, extrastr)

execfile('Config.py')
execfile('lib0.10.5.py')
#read LCT busbars and the numbers of customers
LCTbusbars, Customer_Numbers, SHOPpercentage, DOMpercentage,
EVpercentage, HPpercentage, PVpercentage =
Read_LCT_Busbars(LCTBusbar_Input_File)
#load LCT profile, this the average value for a single
household in kW
SHOPprofile, DOMprofile, EVprofile, HPprofile, PVprofile =
Read_LCT_Profile(Profile_Input_File)
```

```
Load_P = ['Back-up for P loads']
Load_Q = ['Back-up for Q loads']
number, P_noscale, Q_noscale = backup()

cmp = Components()
cmp.filename = Components_Input_File
"""
Define busbars
"""
Output_Busbar_List, Busbar_List = cmp.Read_Output_Busbar()
Busbar_Number = len(Busbar_List)

#define transformers
Transformer_List = cmp.Read_Transformer()
Transformer_Number = len(Transformer_List)
for i in range (0, Transformer_Number):
    Transformer_List[i].Index = i

"""
define branches
"""
Branch_List = cmp.Read_Branch()
Branch_Number = len(Branch_List)
for i in range (0, Branch_Number):
    Branch_List[i].Index = i

Add_LCT_Flag = False
Add_DOM_Flag = False
Add_Shop_Flag = False
Add_EV_Flag = False
Add_ASHP_Flag = True
Add_PV_Flag = False

Debug_Flag = True
```

```
t0 = time.clock()

study_name = 'generic-mean-384-0.4-IPSA'
SCADA_Data_File = study_name + '.csv'
All_Output_File = study_name + ' results.csv'

loadflow()

print 'Done!'
t1 = time.clock()
print 'Computing time taken: ', "%.2f" % float(t1 - t0), '
seconds'
#execfile('all_loadflow_results.py')
```

Appendix C. Moment, Central Moment and Cumulant

Mathematical Explanation of Moment, Central Moment and Cumulant is detailed in this section.

Moment

If the density function of variable x is given as $g(x)$, the $v-th$ moment of x is defined as

$$\propto_v = \int_{-\infty}^{\infty} x^v g(x)dx \quad \textbf{(C.1)}$$

When $v = 0$,

$$\propto_0 = \int_{-\infty}^{\infty} g(x)dx \quad \textbf{(C.2)}$$

$\propto_0$ is the total probability of x

When $v = 1$,

$$\mu = \propto_1 = \int_{-\infty}^{\infty} x \cdot g(x)dx = E(x) \quad \textbf{(C.3)}$$

$\propto_1$ is the expectation or mean of x

Central moment

Central moment of x is defined as

$$M_v = \int_{-\infty}^{\infty} (x-\mu)^v g(x)dx \quad \textbf{(C.4)}$$

When $v = 2$

$$M_2 = \int_{-\infty}^{\infty} (x-\mu)^2 g(x)dx = \sigma^2 \quad \textbf{(C.5)}$$

M_2 is the variance of x

Cumulant

Cumulant of x is defined as

$$\begin{aligned} K_1 &= \propto_1 \\ K_2 &= \propto_2 - \propto_1^2 = M_2 \end{aligned} \quad \textbf{(C.6)}$$

Unlike the moment and central moment of x, the cumulants can be summed up directly

$$K_v^{(t)} = K_v^{(1)} + K_v^{(2)} (v = 1,2, \dots, k) \quad \textbf{(C.7)}$$

Appendix D. Test case for Python Based Robust optimization solver

The test case used in chapter 5 for testing the Python based Robust optimization solver is detailed in this appendix. The standard form of linear optimization is

$$\begin{aligned} &\min c'\boldsymbol{x} \\ &\boldsymbol{Ax} \leq \boldsymbol{b} \end{aligned} \tag{D.1}$$

The values in equation (D.1) is given below

Cost function:

Symbol	Value	Symbol	Value	Symbol	Value
c_1	0.303466	c_{11}	-0.58595	c_{21}	-0.52384
c_2	-0.37585	c_{12}	0.232108	c_{22}	-0.05013
c_3	-0.85944	c_{13}	0.783697	c_{23}	-0.88983
c_4	0.299917	c_{14}	0.432824	c_{24}	0.680962
c_5	0.697796	c_{15}	0.730441	c_{25}	0.19975
c_6	-0.79734	c_{16}	0.676498	c_{26}	-0.44109
c_7	-0.31528	c_{17}	-0.96087	c_{27}	0.930087
c_8	-0.57674	c_{18}	-0.33751	c_{28}	-0.82453
c_9	-0.81759	c_{19}	-0.88749	c_{29}	-0.9062
c_{10}	-0.49477	c_{20}	0.345291	c_{30}	0.23525

Constraints

Symbol	Value	Symbol	Value
b_1	577.2281	b_{26}	383.0781
b_2	502.3159	b_{27}	569.3523
b_3	530.2045	b_{28}	489.9169
b_4	552.9091	b_{29}	381.1728
b_5	504.456	b_{30}	457.5401
b_6	434.6779	b_{31}	413.4519
b_7	503.4637	b_{32}	512.7421
b_8	448.0199	b_{33}	449.3519
b_9	359.998	b_{34}	561.4997
b_{10}	472.1379	b_{35}	512.9653
b_{11}	605.5079	b_{36}	449.7469
b_{12}	486.3126	b_{37}	419.2331

b_{13}	402.6164	b_{38}	464.0361
b_{14}	423.4678	b_{39}	416.7912
b_{15}	420.4441	b_{40}	539.9676
b_{16}	447.191	b_{41}	431.3303
b_{17}	385.3514	b_{42}	480.9181
b_{18}	567.582	b_{43}	452.2597
b_{19}	451.514	b_{44}	466.4683
b_{20}	552.2505	b_{45}	401.3201
b_{21}	407.4321	b_{46}	496.0582
b_{22}	461.8815	b_{47}	471.4336
b_{23}	455.2449	b_{48}	501.6898
b_{24}	465.3611	b_{49}	490.8632
b_{25}	448.3807	b_{50}	464.6249

Constraints coefficients

	1	2	3	4	5	6	7	8	9	10
1	-4.15937	-1.6223	-9.17984	-3.8424	-6.08298	-6.53527	-4.21985	-2.92418	-2.81498	-2.52576
2	-7.94779	-9.20078	-0.5594	-8.56078	-5.75595	-6.65701	-6.30274	-4.05151	-7.77496	-5.99596
3	-8.76723	-1.06895	-7.04677	-3.55627	-9.85993	-5.03434	-0.39344	-5.02758	-4.18112	-2.41295
4	-3.53212	-1.43541	-4.97978	-8.58591	-9.86563	-0.31432	-4.45958	-7.89678	-1.08362	-3.39136
5	-8.15069	-6.39571	-3.6581	-4.20061	-4.59389	-7.63345	-3.28194	-0.93268	-4.14292	-6.6437
6	-1.23163	-2.6501	-9.98213	-2.304	-3.76222	-7.86841	-7.975	-2.01485	-9.12228	-0.56811
7	-3.48026	-0.09964	-9.54996	-7.23318	-0.31795	-8.23928	-8.55603	-0.24774	-5.63897	-9.89177
8	-4.6059	-8.5261	-5.13322	-0.93562	-7.19117	-3.82846	-9.23347	-6.81364	-7.94531	-9.03988
9	-4.55368	-3.08223	-6.70281	-1.5323	-2.5188	-3.53607	-2.95944	-7.35351	-3.0825	-7.94057
10	-3.86113	-9.08528	-0.0189	-9.05066	-4.06763	-3.30518	-9.02589	-1.4947	-0.95809	-0.84792
11	-0.62243	-4.5835	-4.92954	-5.73733	-8.25746	-7.0245	-0.95264	-3.09903	-0.7924	-9.28222
12	-4.20736	-3.28645	-5.31262	-6.82354	-5.6693	-3.83894	-3.94988	-3.31821	-5.59236	-5.56182
13	-9.91166	-9.91286	-3.05873	-0.78246	-5.76152	-0.31135	-6.78003	-1.86597	-3.59132	-2.92185
14	-8.0854	-8.13539	-8.59838	-3.52072	-3.04169	-4.56642	-1.5342	-6.87619	-8.05319	-0.12561
15	-5.4967	-2.95061	-0.66211	-3.53324	-2.89527	-2.79415	-0.65262	-5.64631	-0.46511	-4.18293
16	-8.06739	-8.75884	-5.34419	-1.15064	-2.71407	-3.36279	-1.06374	-5.44207	-6.27885	-9.99462
17	-4.55625	-3.16912	-0.06309	-4.92438	-7.09458	-0.52184	-0.96461	-9.3355	-3.38972	-6.73541
18	-5.87205	-9.59782	-6.62005	-4.33285	-2.40387	-5.39986	-3.95889	-0.31417	-0.0629	-5.49846
19	-9.98786	-9.28595	-5.38829	-2.32297	-5.59984	-3.80937	-9.8517	-6.62305	-9.20627	-7.71955
20	-7.33665	-4.9614	-4.45592	-1.99393	-3.26029	-9.9844	-5.68954	-7.75173	-1.91105	-3.19691

	11	12	13	14	15	16	17	18	19	20
1	-1.23207	-6.69396	-8.84165	-6.9648	-6.39132	-6.36516	-9.31689	-3.14834	-9.17995	-3.064
2	-1.64285	-5.56997	-9.26836	-5.26419	-7.55559	-7.47234	-3.93036	-4.09903	-9.47034	-2.02702
3	-5.71671	-9.59815	-9.4526	-6.28979	-6.46204	-9.03188	-4.44071	-5.15374	-3.32316	-8.46972
4	-5.67418	-8.94698	-5.17882	-6.20644	-6.68417	-9.99971	-2.1739	-2.82738	-2.5261	-6.98103
5	-7.57666	-1.25927	-1.78178	-7.20116	-5.92287	-9.7721	-7.96887	-4.7488	-4.48691	-3.47188
6	-1.10493	-4.53215	-8.21974	-0.45182	-7.40318	-4.75983	-8.70033	-0.28603	-7.40191	-6.60611
7	-7.35379	-3.03367	-0.48909	-8.05834	-4.6408	-4.77735	-7.26231	-1.38782	-0.97148	-3.84381
8	-5.33138	-1.26961	-1.29157	-3.94447	-1.43579	-0.68609	-1.2906	-1.18843	-7.81908	-5.44648
9	-4.64071	-3.20432	-9.31925	-1.65014	-3.18717	-3.04733	-0.94574	-5.11004	-2.70679	-1.40265
10	-5.94426	-3.69398	-2.80907	-8.97292	-8.47849	-9.23096	-0.93669	-9.38911	-1.28615	-6.63147
11	-9.83212	-8.57049	-9.44096	-8.9234	-6.57818	-6.86173	-1.95152	-3.56678	-9.49147	-4.70088
12	-3.65178	-1.80934	-6.84338	-8.4507	-3.88958	-2.86382	-4.42469	-9.42203	-8.18688	-4.38483
13	-2.75456	-0.99291	-6.74147	-5.97013	-9.17013	-4.33905	-3.18537	-3.04624	-1.26506	-7.79341
14	-3.27956	-0.17634	-3.76699	-4.17742	-5.27603	-3.67408	-6.44221	-2.24912	-7.31121	-1.09263
15	-8.87818	-7.9786	-8.681	-5.57039	-1.58905	-5.00261	-7.41278	-1.08812	-2.39111	-6.94751
16	-7.75767	-2.56535	-5.58541	-5.4389	-6.93014	-1.57612	-3.32797	-6.04342	-1.11631	-0.60601
17	-2.31675	-3.59831	-3.03373	-7.18481	-7.83406	-4.47576	-8.17164	-5.55532	-2.30791	-5.8173
18	-6.50618	-8.0853	-8.49239	-3.7279	-8.4645	-9.14742	-2.52956	-6.04739	-8.17439	-3.74173
19	-0.3186	-5.66247	-7.84557	-2.40192	-4.57292	-0.8877	-6.13676	-7.92676	-1.96988	-3.59104
20	-9.75115	-7.82076	-9.70628	-6.68806	-0.8896	-3.72123	-8.56544	-0.20924	-8.78282	-7.17434

	21	22	23	24	25	26	27	28	29	30
1	-9.27458	-5.72857	-5.62481	-5.68297	-6.47127	-4.19896	-8.64555	-7.31976	-9.22519	-7.60016
2	-2.00732	-5.27214	-6.17681	-3.10964	-7.25606	-6.59262	-0.78845	-9.87856	-4.36466	-0.88641
3	-6.71622	-2.5529	-1.52082	-1.03373	-6.1478	-4.19539	-4.32604	-4.02041	-2.37317	-6.82712
4	-4.70321	-8.09671	-9.52579	-0.53193	-9.76314	-9.35489	-8.04789	-8.84561	-2.28835	-9.09111
5	-8.42512	-7.54944	-2.09944	-9.7007	-2.50711	-7.12397	-5.09566	-1.90363	-2.71372	-1.54181
6	-0.25456	-7.08336	-8.76372	-0.94182	-2.81078	-9.52563	-4.04993	-6.66796	-8.10064	-9.39228
7	-4.51386	-8.21029	-2.32427	-6.55904	-5.502	-9.15369	-4.65695	-4.89389	-4.43933	-9.41512
8	-4.18901	-3.33056	-4.58679	-3.70817	-9.55751	-1.82677	-3.68572	-4.69883	-9.10145	-4.36477
9	-0.46928	-4.88565	-9.04723	-5.58479	-2.51833	-6.68525	-5.62034	-3.84859	-4.45266	-2.45903
10	-9.25967	-9.81008	-5.86465	-8.49392	-5.38198	-0.96526	-5.52353	-1.47443	-4.14109	-0.71456
11	-9.6323	-9.44987	-0.39817	-7.96043	-5.8284	-9.84181	-1.82624	-8.17223	-5.90384	-8.53744
12	-2.36607	-1.52519	-2.77391	-7.23252	-4.83676	-7.4369	-6.72909	-1.10309	-4.43905	-5.94739
13	-3.7233	-9.94647	-2.51373	-5.71249	-4.81453	-2.13358	-6.42394	-8.15535	-0.73021	-5.75805
14	-6.59505	-6.27006	-2.14859	-3.85127	-2.91564	-6.1739	-8.163	-8.20402	-4.48342	-3.51989
15	-3.05838	-0.82083	-6.76132	-8.7719	-1.81599	-3.35598	-2.64969	-2.68209	-9.07709	-8.64627
16	-9.31434	-4.45801	-5.53316	-7.46549	-2.32751	-6.32607	-7.99167	-0.96805	-5.0118	-0.67735
17	-1.87917	-3.0606	-2.02787	-0.67616	-4.88348	-5.15757	-3.11439	-5.56982	-1.66128	-2.01058
18	-7.12404	-4.48694	-9.8611	-0.41245	-6.64511	-7.86918	-7.15284	-8.31541	-1.92406	-9.08284
19	-1.03807	-2.72363	-0.28451	-8.51654	-0.42035	-5.0261	-9.13258	-6.76971	-5.28491	-1.92611
20	-3.12319	-2.38821	-6.50584	-5.86979	-9.50519	-1.64536	-7.03561	-2.5518	-9.14204	-1.3114

	1	2	3	4	5	6	7	8	9	10
21	-4.66716	-4.9176	-7.84126	-2.57131	-2.7817	-5.2962	-2.82274	-6.47946	-5.95906	-6.89302
22	-6.16419	-9.92205	-1.60567	-0.9397	-2.65387	-8.86439	-6.68623	-9.84728	-8.03434	-3.64838
23	-1.29083	-3.94865	-1.54572	-2.69591	-5.02469	-8.15573	-6.19357	-9.55027	-2.27016	-0.73261
24	-8.9675	-9.47273	-8.12342	-1.96449	-5.67901	-3.2469	-9.15463	-7.50747	-8.62346	-9.17887
25	-1.66532	-0.91402	-9.77881	-4.17498	-1.2611	-2.66163	-2.07402	-0.96796	-8.94409	-1.02759
26	-2.22409	-3.82747	-2.85138	-0.17978	-0.48868	-2.77812	-0.50989	-4.69069	-2.59314	-7.48447
27	-6.2833	-7.3052	-6.57305	-1.91955	-8.13172	-7.54442	-7.03059	-1.04149	-8.0291	-7.84292
28	-4.94231	-7.46189	-8.06738	-2.65424	-2.01446	-9.78925	-1.59723	-3.72154	-3.44282	-3.53137
29	-4.61079	-1.73407	-8.20034	-5.96612	-7.18906	-6.4246	-6.71057	-0.69776	-1.42989	-0.21157
30	-1.0364	-3.61959	-3.05139	-1.1649	-6.84992	-8.52242	-0.68315	-9.11742	-7.8233	-0.16422
31	-0.88081	-6.61359	-0.74208	-1.53745	-1.63903	-8.55239	-0.29748	-5.9991	-8.81019	-3.38993
32	-9.07459	-6.27767	-6.17595	-4.20944	-8.46761	-5.58858	-8.41617	-9.81303	-8.30308	-7.20457
33	-3.9857	-7.24736	-1.36161	-0.44102	-4.75994	-2.53089	-7.53925	-9.1276	-3.83631	-9.01398
34	-0.24451	-6.72603	-8.09157	-4.77712	-7.09035	-3.76631	-0.97785	-5.00368	-1.97119	-4.73656
35	-4.66885	-0.42894	-9.77885	-9.5113	-2.97092	-5.45043	-2.08485	-0.47345	-5.122	-0.55742
36	-8.58291	-2.99763	-9.00426	-8.91556	-2.26897	-0.44818	-0.86949	-6.94075	-2.77808	-4.07768
37	-8.63568	-4.87373	-1.82757	-9.11167	-9.02526	-3.34692	-8.65738	-0.74033	-1.0312	-3.35756
38	-5.05456	-3.43927	-9.22028	-2.15062	-6.20063	-8.0258	-0.24588	-5.3236	-1.8975	-3.04103
39	-4.87883	-0.75561	-1.36559	-6.25266	-2.32256	-4.93565	-2.51565	-6.31307	-1.29547	-2.96485
40	-2.36818	-3.36204	-0.43354	-0.14954	-6	-2.588	-6.15623	-8.46676	-2.4061	-9.71418

	11	12	13	14	15	16	17	18	19	20
21	-1.14792	-4.87805	-9.78249	-0.36679	-1.35624	-0.52508	-1.79064	-9.88731	-7.60349	-6.97901
22	-1.42389	-4.41566	-6.03268	-3.85584	-5.71318	-8.22365	-5.04528	-0.86877	-8.75324	-7.9496
23	-7.19137	-3.37946	-0.14928	-7.8306	-6.23538	-8.05051	-7.11514	-9.00475	-0.26959	-5.84939
24	-3.27901	-0.54782	-2.56933	-3.4348	-6.97154	-8.4305	-2.3082	-2.38097	-2.37345	-4.55038
25	-6.77925	-6.92343	-3.10051	-5.66018	-4.15731	-6.62031	-8.07886	-8.09264	-4.1012	-1.88877
26	-1.01735	-0.17722	-2.27289	-3.18262	-1.38734	-9.61039	-5.78898	-6.15093	-4.11547	-1.65631
27	-5.59869	-4.21418	-7.22565	-9.93082	-3.10096	-5.97839	-9.7846	-2.79211	-2.37576	-8.77429
28	-1.22771	-8.81376	-6.49138	-0.27324	-7.12355	-8.78388	-8.8833	-6.50908	-8.75958	-4.27953
29	-2.50905	-0.0148	-9.29584	-2.72539	-2.12451	-0.52432	-7.63848	-8.86883	-0.89086	-4.12068
30	-5.70175	-5.00703	-5.43996	-5.02337	-7.33805	-0.23191	-8.83261	-3.80867	-6.65838	-5.00384
31	-0.08883	-7.54797	-4.41847	-3.69673	-3.89342	-2.05225	-3.26172	-8.68585	-2.47574	-5.54813
32	-4.68463	-6.75507	-6.4023	-2.21938	-0.21103	-5.77727	-7.23128	-9.12902	-1.12286	-4.26188
33	-2.94044	-1.81102	-2.20179	-3.86383	-6.5083	-7.7126	-4.6319	-9.11107	-6.02881	-7.93675
34	-2.59341	-9.96023	-0.49502	-8.04266	-6.34358	-8.72091	-7.39967	-8.80493	-9.69136	-4.18207
35	-5.19479	-8.91461	-2.10454	-7.84626	-7.18429	-0.80858	-5.6125	-2.15967	-7.45809	-2.19293
36	-5.01066	-6.95988	-8.6419	-6.55413	-8.01617	-8.50041	-4.11575	-0.14207	-1.12134	-6.51012
37	-0.64558	-1.02007	-1.10842	-3.57426	-6.80867	-9.30426	-0.60425	-0.92013	-1.75653	-9.30816
38	-4.84831	-8.71677	-9.64972	-3.39016	-2.76987	-5.37625	-5.00383	-7.19365	-3.23499	-2.00151
39	-8.19297	-9.08354	-4.03663	-0.527	-6.54458	-0.52655	-5.15677	-3.08382	-0.86871	-7.93945
40	-6.59665	-9.06082	-1.82369	-8.62862	-7.6478	-8.86802	-5.17554	-2.13074	-7.65125	-3.90883

	21	22	23	24	25	26	27	28	29	30
21	-7.89863	-9.56796	-0.97227	-6.61009	-4.45707	-5.07462	-0.8689	-2.73456	-0.35803	-7.75047
22	-1.44471	-8.40242	-3.82759	-5.87978	-4.30396	-8.22814	-5.07838	-2.76803	-1.63792	-7.13657
23	-3.14614	-8.82117	-3.24331	-2.57621	-7.47576	-4.28819	-7.76182	-7.26294	-1.55852	-4.69052
24	-7.66362	-9.26713	-0.89585	-6.80488	-2.45066	-1.57685	-5.0325	-7.49991	-4.88406	-3.57224
25	-2.99607	-9.53286	-2.70708	-8.95247	-7.42839	-6.74891	-0.58534	-3.51855	-3.8102	-1.3509
26	-6.37472	-0.62521	-8.97833	-3.81129	-2.84623	-2.76631	-6.67996	-9.5373	-7.71004	-1.1212
27	-7.26788	-9.0778	-6.77032	-3.14339	-0.61385	-3.74786	-4.09678	-9.51615	-1.40931	-4.82631
28	-7.10525	-8.6857	-4.98199	-1.57746	-6.12765	-3.96795	-0.01048	-5.99929	-6.70325	-9.25901
29	-6.64987	-0.11051	-4.60753	-6.70918	-3.78552	-1.32116	-6.7428	-7.16602	-5.75109	-2.26152
30	-3.44483	-2.40953	-5.50776	-5.31718	-8.18756	-9.66226	-4.61382	-8.96796	-8.19015	-0.89469
31	-7.47392	-9.29979	-3.30677	-8.10936	-0.50719	-9.61159	-9.57661	-1.14232	-6.07294	-5.07072
32	-7.78581	-4.60176	-1.86522	-5.14935	-8.8273	-0.1401	-3.86581	-4.34841	-7.30765	-3.00966
33	-6.77135	-4.47748	-1.15152	-1.88584	-0.81084	-5.09365	-2.60176	-8.44348	-7.43769	-7.74959
34	-1.85073	-0.71533	-5.85895	-7.78516	-8.36279	-1.95088	-2.08079	-6.29701	-6.19258	-0.07375
35	-3.0505	-5.02911	-3.64339	-9.04952	-6.96701	-8.5302	-6.34651	-8.20248	-2.48066	-2.51136
36	-3.13981	-3.80775	-0.75328	-5.63703	-6.03339	-8.52883	-3.5434	-0.73181	-1.44826	-6.65212
37	-9.98258	-3.49153	-3.30602	-5.99766	-5.13717	-5.74297	-1.3537	-9.79764	-4.85612	-1.96058
38	-7.85791	-0.06572	-5.94124	-6.19911	-2.47802	-3.16956	-2.16727	-7.19745	-3.84776	-9.93618
39	-7.00463	-7.69738	-5.01841	-6.50537	-7.04223	-3.86754	-6.06093	-9.66511	-0.47642	-7.56182
40	-8.34182	-9.70747	-7.813	-1.31966	-5.46724	-7.64808	-4.43802	-3.47965	-0.33204	-3.28468

	1	2	3	4	5	6	7	8	9	10
41	-9.70516	-1.22452	-6.72789	-7.83935	-1.34316	-2.84679	-4.68386	-6.23685	-5.63202	-5.75293
42	-1.46043	-1.42741	-1.27698	-0.0847	-0.5369	-8.16923	-7.38356	-0.75724	-7.28274	-2.37375
43	-1.21724	-3.7643	-2.19268	-7.61137	-2.05987	-5.91343	-1.95218	-2.9975	-7.56581	-9.11665
44	-3.09361	-7.58628	-6.58854	-3.31213	-2.29544	-3.93866	-5.48258	-8.83229	-1.46859	-0.37761
45	-8.79646	-8.64535	-3.22587	-1.04548	-6.40687	-1.1091	-4.59119	-7.33457	-1.21084	-5.57034
46	-2.79961	-8.5662	-5.02479	-9.08801	-2.19685	-9.96487	-9.71373	-5.90627	-1.6636	-6.74468
47	-6.01304	-1.33034	-5.34424	-7.72216	-6.69061	-0.053	-3.24202	-6.27892	-4.38433	-9.32526
48	-2.69368	-8.63232	-4.59094	-1.24303	-6.61126	-2.51523	-2.02608	-7.59784	-2.96908	-9.88483
49	-9.13623	-5.94296	-5.1868	-9.59683	-3.03377	-6.70354	-5.67275	-2.4736	-5.42572	-1.72388
50	-6.05382	-5.90262	-5.72167	-3.39898	-5.66837	-6.2119	-4.83129	-2.20996	-9.24436	-0.02981
	11	12	13	14	15	16	17	18	19	20
41	-1.94152	-5.67137	-5.62838	-0.73851	-2.91975	-1.59849	-5.06286	-1.17141	-5.15275	-5.01841
42	-9.5887	-4.08238	-4.12363	-6.84605	-8.18491	-7.95752	-4.22329	-3.63304	-1.67267	-9.13344
43	-9.53934	-1.00638	-7.88408	-5.73587	-0.77722	-3.07297	-6.54975	-3.32813	-5.80673	-4.05492
44	-9.06896	-5.43877	-0.77033	-4.30952	-9.0888	-6.52484	-7.20879	-6.08786	-2.13657	-6.39676
45	-3.81069	-4.40186	-0.27241	-4.86191	-9.97674	-8.74288	-6.66025	-0.10912	-1.55619	-4.00631
46	-6.41791	-6.30545	-8.41852	-6.78527	-4.18799	-1.45382	-4.93629	-0.88534	-5.99246	-1.79643
47	-8.20315	-2.14494	-1.20679	-2.03212	-2.6591	-8.69352	-0.96119	-5.54977	-2.91514	-8.66369
48	-4.16961	-6.3981	-9.52648	-3.68278	-2.59965	-8.62284	-8.09998	-9.68146	-4.84783	-8.89202
49	-7.1782	-9.6842	-6.1217	-7.59893	-3.40114	-7.47525	-3.95437	-7.64444	-2.00759	-5.09091
50	-8.32303	-6.97213	-2.63514	-1.05001	-7.88581	-6.67506	-3.72102	-3.48554	-0.99033	-2.2834

	21	22	23	24	25	26	27	28	29	30
41	-3.65648	-3.65561	-8.23396	-2.51546	-8.81587	-6.80434	-4.80427	-5.97929	-6.31183	-5.41216
42	-8.29688	-4.34835	-8.97216	-6.9087	-1.34556	-1.25304	-8.86996	-4.83224	-3.09439	-4.78347
43	-7.66676	-8.70895	-5.69581	-3.81261	-8.68822	-6.19837	-0.12599	-8.30738	-1.87699	-2.1677
44	-6.47249	-0.90617	-0.39997	-5.59234	-9.80886	-6.87666	-5.78491	-0.71397	-7.65854	-7.93502
45	-0.30901	-9.5874	-9.57487	-1.9737	-3.69981	-7.60281	-0.66439	-4.64272	-6.10777	-6.38214
46	-9.99539	-5.23866	-8.99389	-7.84785	-1.94443	-2.27134	-2.92447	-2.0843	-7.19972	-7.6457
47	-7.76822	-3.27724	-1.52342	-6.20492	-4.83866	-2.24294	-4.8701	-6.9878	-5.94066	-7.39809
48	-3.27458	-4.91007	-6.66174	-2.29646	-4.38065	-0.15016	-1.76221	-7.31939	-7.22799	-1.27164
49	-0.42785	-7.09152	-0.57671	-0.89151	-1.59591	-5.8533	-4.96054	-0.80464	-9.0879	-6.84025
50	-4.61977	-1.90939	-8.68069	-9.81866	-9.23499	-7.32774	-6.21845	-3.98793	-1.27078	-7.47283

Appendix E. Robust Optimization Detailed Formulation

The constraints given in (6.13) can be written as

$$\begin{bmatrix} -S_{RTTR} \\ V_{Min} \\ SoC_{Min} \end{bmatrix} \leq \begin{bmatrix} PFSF \\ VSF \\ D \end{bmatrix} \cdot P + \begin{bmatrix} S_{Forecast} \\ V_{Forecast} \\ SoC^{t=0} \end{bmatrix} \leq \begin{bmatrix} S_{RTTR} \\ V_{Max} \\ SoC_{Max} \end{bmatrix} \tag{E.1}$$

Where

$\boldsymbol{P}$ is the power injection from busbars and

$$P = \begin{bmatrix} P_{ESS} \\ \Delta P_{RES} \\ \Delta P_{Bus} \end{bmatrix} \tag{E.2}$$

$\boldsymbol{PFSF}$ is the matrix of PFSF

$\boldsymbol{VSF}$ is the matrix of VSF

Considering the uncertainty of RTTR, load forecast, RES output forecast and SoC estimation, (E.1) becomes

$$\begin{bmatrix} -\tilde{S}_{RTTR} \\ V_{Min} \\ SoC_{Min} \end{bmatrix} \leq \begin{bmatrix} PFSF \\ VSF \\ D \end{bmatrix} \cdot \begin{bmatrix} P_{ESS} \\ \Delta\tilde{P}_{RES} \\ \Delta\tilde{P}_{Bus} \end{bmatrix} + \begin{bmatrix} \tilde{S}_{Forecast} \\ \tilde{V}_{Forecast} \\ \widetilde{SoC^{t=0}} \end{bmatrix} \leq \begin{bmatrix} \tilde{S}_{RTTR} \\ V_{Max} \\ SoC_{Max} \end{bmatrix} \tag{E.3}$$

Constraint (E.3) can be rewritten as the form below

$$\begin{bmatrix} PFSF \\ VSF \\ D \\ -PFSF \\ -VSF \\ -D \end{bmatrix} \cdot \begin{bmatrix} P_{ESS} \\ \Delta\tilde{P}_{RES} \\ \Delta\tilde{P}_{Bus} \end{bmatrix} + \begin{bmatrix} \tilde{S}_{Forecast} \\ \tilde{V}_{Forecast} \\ \widetilde{SoC^{t=0}} \\ -\tilde{S}_{Forecast} \\ -\tilde{V}_{Forecast} \\ -\widetilde{SoC^{t=0}} \end{bmatrix} + \begin{bmatrix} -\tilde{S}_{RTTR} \\ -V_{Max} \\ -SoC_{Max} \\ -\tilde{S}_{RTTR} \\ V_{Min} \\ SoC_{Min} \end{bmatrix} \leq 0 \tag{E.4}$$

In (E.4), only $\boldsymbol{P_{ESS}}$ is the control variable. Uncertain values include $\Delta\widetilde{\boldsymbol{P}}_{\boldsymbol{RES}}$, $\Delta\widetilde{\boldsymbol{P}}_{\boldsymbol{Bus}}$, $\tilde{\boldsymbol{S}}_{\boldsymbol{Forecast}}$, $\tilde{\boldsymbol{V}}_{\boldsymbol{Forecast}}$, $\tilde{\boldsymbol{S}}_{\boldsymbol{RTTR}}$ and $\widetilde{\boldsymbol{SoC}^{\boldsymbol{t=0}}}$. Extra control variables are introduced to reform the problem.

$$\begin{aligned} &\min C \cdot P_{ESS} \\ &s.t. \\ &A \cdot X \leq 0 \end{aligned} \tag{E.5}$$

Where

$\boldsymbol{C}$ is the cost vector

$\boldsymbol{A}$ is the coefficient matrix

$\boldsymbol{X}$ is the control variables

$$\boldsymbol{A} = \begin{bmatrix} \boldsymbol{PFSF} & \boldsymbol{PFSF} \cdot \Delta\widetilde{\boldsymbol{P}}_{\boldsymbol{RES}} & \boldsymbol{PFSF} \cdot \Delta\widetilde{\boldsymbol{P}}_{\boldsymbol{Bus}} & \tilde{\boldsymbol{S}}_{\boldsymbol{Forecast}} & -\tilde{\boldsymbol{S}}_{\boldsymbol{RTTR}} \\ \boldsymbol{VSF} & \boldsymbol{VSF} \cdot \Delta\widetilde{\boldsymbol{P}}_{\boldsymbol{RES}} & \boldsymbol{VSF} \cdot \Delta\widetilde{\boldsymbol{P}}_{\boldsymbol{Bus}} & \widetilde{\boldsymbol{V}}_{\boldsymbol{Forecast}} & -\boldsymbol{V}_{\boldsymbol{Max}} \\ \boldsymbol{D} & & & \widetilde{\boldsymbol{SoC}^{\boldsymbol{t=0}}} & -\boldsymbol{SoC}_{\boldsymbol{Max}} \\ -\boldsymbol{PFSF} & -\boldsymbol{PFSF} \cdot \Delta\widetilde{\boldsymbol{P}}_{\boldsymbol{RES}} & -\boldsymbol{PFSF} \cdot \Delta\widetilde{\boldsymbol{P}}_{\boldsymbol{Bus}} & -\tilde{\boldsymbol{S}}_{\boldsymbol{Forecast}} & -\tilde{\boldsymbol{S}}_{\boldsymbol{RTTR}} \\ -\boldsymbol{VSF} & -\boldsymbol{VSF} \cdot \Delta\widetilde{\boldsymbol{P}}_{\boldsymbol{RES}} & -\boldsymbol{VSF} \cdot \Delta\widetilde{\boldsymbol{P}}_{\boldsymbol{Bus}} & -\widetilde{\boldsymbol{V}}_{\boldsymbol{Forecast}} & \boldsymbol{V}_{\boldsymbol{Min}} \\ -\boldsymbol{D} & & & -\widetilde{\boldsymbol{SoC}^{\boldsymbol{t=0}}} & \boldsymbol{SoC}_{\boldsymbol{Min}} \end{bmatrix} \quad \textbf{(E.6)}$$

And

$$\boldsymbol{X} = \begin{bmatrix} \boldsymbol{P}_{\boldsymbol{ESS}} \\ 1 \\ \vdots \\ 1 \end{bmatrix} \Bigg\} N_{RES} + N_{Bus} + 2 \quad \textbf{(E.7)}$$

Appendix F. Curve fitting results

Normal distribution

BoU	PoS	Curve fitting results
0%	0.9344	0.9344
5%	0.9950	0.9817
10%	0.9996	0.9996
15%	1.0000	1.0000
20%	1.0000	1.0000
25%	1.0000	1.0000
30%	1.0000	1.0000
35%	1.0000	1.0000
40%	1.0000	1.0000
45%	1.0000	1.0000
50%	1.0000	1.0000
55%	1.0000	1.0000
60%	1.0000	1.0000
65%	1.0000	1.0000
70%	1.0000	1.0000
75%	1.0000	1.0000
80%	1.0000	1.0000
85%	1.0000	1.0000
90%	1.0000	1.0000
95%	1.0000	1.0000
100%	1.0000	1.0000

Uniform distribution

BoU	PoS	Curve fitting results
0%	0.125	0.13
5%	0.335	0.25
10%	0.588	0.54
15%	0.792	0.79
20%	0.922	0.93
25%	0.985	0.98
30%	0.998	1.00
35%	1.000	1.00
40%	1.000	1.00

45%	1.000	1.00
50%	1.000	1.00
55%	1.000	1.00
60%	1.000	1.00
65%	1.000	1.00
70%	1.000	1.00
75%	1.000	1.00
80%	1.000	1.00
85%	1.000	1.00
90%	1.000	1.00
95%	1.000	1.00
100%	1.000	1.00

Beta distribution

BoU	PoS	Curve fitting results
0%	1.06%	1.02%
5%	10.66%	12.98%
10%	39.52%	40.91%
15%	69.30%	69.10%
20%	90.66%	87.69%
25%	98.28%	96.46%
30%	100.00%	99.51%
35%	100.00%	100.31%
40%	100.00%	100.47%
45%	100.00%	100.50%
50%	100.00%	100.50%
55%	100.00%	100.50%
60%	100.00%	100.50%
65%	100.00%	100.50%
70%	100.00%	100.50%
75%	100.00%	100.50%
80%	100.00%	100.50%
85%	100.00%	100.50%
90%	100.00%	100.50%
95%	100.00%	100.50%
100%	100.00%	100.50%

Reference

[1] "Climate change act 2009 impact assessment," Department of Energy and Climate Change2009.

[2] "2013 UK Greenhouse Gas Emissions, Final Figures," Department of Energy & Climate Change, London2015.

[3] "Renewable sources of energy: Chapter 6, Digest of United Kingdom Energy Statistics (DUKES)," Department of Energy & Climate Change, London2015.

[4] F. Madonna and F. Bazzocchi, "Annual performances of reversible air-to-water heat pumps in small residential buildings," *Energy and Buildings,* vol. 65, pp. 299-309, 10// 2013.

[5] A. Navarro-Espinosa and P. Mancarella, "Probabilistic modeling and assessment of the impact of electric heat pumps on low voltage distribution networks," *Applied Energy,* vol. 127, pp. 249-266, Aug 2014.

[6] R. G.-V. J. A. P. Lopes, *Electric Vehicle Integration into Modern Power Networks*. New York: Springer, 2013.

[7] A. G. Boulanger, A. C. Chu, S. Maxx, and D. L. Waltz, "Vehicle Electrification: Status and Issues," *Proceedings of the IEEE,* vol. 99, pp. 1116-1138, 2011.

[8] B. Sungwoo and A. Kwasinski, "Spatial and Temporal Model of Electric Vehicle Charging Demand," *Smart Grid, IEEE Transactions on,* vol. 3, pp. 394-403, 2012.

[9] J. de Hoog, T. Alpcan, M. Brazil, D. A. Thomas, and I. Mareels, "Optimal Charging of Electric Vehicles Taking Distribution Network Constraints Into Account," *Power Systems, IEEE Transactions on,* vol. 30, pp. 365-375, 2015.

[10] Y. Mu, J. Wu, N. Jenkins, H. Jia, and C. Wang, "A Spatial–Temporal model for grid impact analysis of plug-in electric vehicles," *Applied Energy,* vol. 114, pp. 456-465, 2// 2014.

[11] L. M. Cipcigan and P. C. Taylor, "Investigation of the reverse power flow requirements of high penetrations of small-scale embedded generation," *Renewable Power Generation, IET,* vol. 1, pp. 160-166, 2007.

[12] I. Ziari, G. Ledwich, A. Ghosh, and G. Platt, "Optimal distribution network reinforcement considering load growth, line loss, and reliability," *IEEE Transactions on Power Systems,* vol. 28, pp. 587-597, 2013.

[13] Y. Zhang, F. Li, Z. Hu, and G. Shaddick, "Quantification of low voltage network reinforcement costs: A statistical approach," *IEEE Transactions on Power Systems,* vol. 28, pp. 810-818, 2013.

[14] A. Keane, L. F. Ochoa, C. L. T. Borges, G. W. Ault, A. D. Alarcon-Rodriguez, R. A. F. Currie, *et al.*, "State-of-the-Art Techniques and Challenges Ahead for Distributed Generation Planning and Optimization," *Power Systems, IEEE Transactions on,* vol. 28, pp. 1493-1502, 2013.

[15] J. Valenzuela, M. Mazumdar, and A. Kapoor, "Influence of temperature and load forecast uncertainty on estimates of power generation production costs," *Power Systems, IEEE Transactions on,* vol. 15, pp. 668-674, 2000.

[16] C. Lowery and M. O'Malley, "Impact of Wind Forecast Error Statistics Upon Unit Commitment," *Sustainable Energy, IEEE Transactions on,* vol. 3, pp. 760-768, 2012.

[17] A. Dunbar, F. Tagliaferri, I. M. Viola, and G. P. Harrison, "The impact of electricity price forecast accuracy on the optimality of storage revenue," in *Renewable Power Generation Conference (RPG 2014), 3rd*, 2014, pp. 1-6.

[18] I. Hadjipaschalis, A. Poullikkas, and V. Efthimiou, "Overview of current and future energy storage technologies for electric power applications," *Renewable and Sustainable Energy Reviews,* vol. 13, pp. 1513-1522, 8// 2009.

[19] G. C. Jim Eyer, "Energy Storage for the Electricity Grid: Benefits and Market Potential Assessment Guide," Sandia National Laboratories, Albuquerque, New Mexico 87185 and Livermore, California 945502010.

[20] E. E. Paul Denholm, Brendan Kirby and Michael Milligan, "The Role of Energy Storage with Renewable Electricity Generation," National Renewable Energy Laboratory2010.

[21] S. M. Rezvanizaniani, Z. C. Liu, Y. Chen, and J. Lee, "Review and recent advances in battery health monitoring and prognostics technologies for electric vehicle (EV) safety and mobility," *Journal of Power Sources,* vol. 256, pp. 110-124, Jun 2014.

[22] Ofgem, "Demand Side Response Discussion Paper," 2010.

[23] G. Strbac, "Demand side management: Benefits and challenges," *Energy Policy,* vol. 36, pp. 4419-4426, 2008.

[24] "ER P27: Current Rating Guide for High Voltage Overhead Lines Operating in the UK Distribution System," ed: Energy Networks Association, 1986.

[25] A. Michiorri, P. C. Taylor, S. C. E. Jupe, and C. J. Berry, "Investigation into the influence of environmental conditions on power system ratings," *Proceedings of the Institution of Mechanical Engineers Part A-Journal of Power and Energy,* vol. 223, pp. 743-757, Nov 2009.

[26] L. C. Cradden and G. P. Harrison, "Adapting overhead lines to climate change: Are dynamic ratings the answer?," *Energy Policy,* vol. 63, pp. 197-206, 12// 2013.

[27] A. Michiorri, "Power system real-time thermal rating estimation," Durham university, 2010.

[28] A. Michiorri, P. C. Taylor, and S. C. E. Jupe, "Overhead line real-time rating estimation algorithm: description and validation," *Proceedings of the Institution of Mechanical Engineers Part a-Journal of Power and Energy*, vol. 224, pp. 293-304, 2010.

[29] M. Z. Degefa, M. Humayun, A. Safdarian, M. Koivisto, R. J. Millar, and M. Lehtonen, "Unlocking distribution network capacity through real-time thermal rating for high penetration of DGs," *Electric Power Systems Research*, vol. 117, pp. 36-46, 12// 2014.

[30] D. M. Greenwood and P. C. Taylor, "Investigating the Impact of Real-Time Thermal Ratings on Power Network Reliability," *Power Systems, IEEE Transactions on*, vol. PP, pp. 1-9, 2014.

[31] N. S. Wade, P. C. Taylor, P. D. Lang, and P. R. Jones, "Evaluating the benefits of an electrical energy storage system in a future smart grid," *Energy Policy*, vol. 38, pp. 7180-7188, 11// 2010.

[32] N. Powergrid. (2015, January). *Customer Led Network Revolution*. Available: http://www.networkrevolution.co.uk/

[33] A. A. Thatte, X. Le, D. E. Viassolo, and S. Singh, "Risk Measure Based Robust Bidding Strategy for Arbitrage Using a Wind Farm and Energy Storage," *Smart Grid, IEEE Transactions on*, vol. 4, pp. 2191-2199, 2013.

[34] H. Khani and M. R. Dadash Zadeh, "Real-Time Optimal Dispatch and Economic Viability of Cryogenic Energy Storage Exploiting Arbitrage Opportunities in an Electricity Market," *Smart Grid, IEEE Transactions on*, vol. 6, pp. 391-401, 2015.

[35] UKPN. (2016, January). *Smarter Network Storage*. Available: http://innovation.ukpowernetworks.co.uk/innovation/en/Projects/tier-2-projects/Smarter-Network-Storage-(SNS)/

[36] C. L. Moreira, F. O. Resende, and J. A. Peas Lopes, "Using Low Voltage MicroGrids for Service Restoration," *Power Systems, IEEE Transactions on*, vol. 22, pp. 395-403, 2007.

[37] F. Qiang, A. Nasiri, V. Bhavaraju, A. Solanki, T. Abdallah, and D. C. Yu, "Transition Management of Microgrids With High Penetration of Renewable Energy," *Smart Grid, IEEE Transactions on*, vol. 5, pp. 539-549, 2014.

[38] A. Arulampalam, M. Barnes, N. Jenkins, and J. B. Ekanayake, "Power quality and stability improvement of a wind farm using STATCOM supported with hybrid battery

energy storage," *Generation, Transmission and Distribution, IEE Proceedings-,* vol. 153, pp. 701-710, 2006.

[39] I. Wasiak, R. Pawelek, and R. Mienski, "Energy storage application in low-voltage microgrids for energy management and power quality improvement," *Generation, Transmission & Distribution, IET,* vol. 8, pp. 463-472, 2014.

[40] F. Qiang, L. F. Montoya, A. Solanki, A. Nasiri, V. Bhavaraju, T. Abdallah, *et al.*, "Microgrid Generation Capacity Design With Renewables and Energy Storage Addressing Power Quality and Surety," *Smart Grid, IEEE Transactions on,* vol. 3, pp. 2019-2027, 2012.

[41] R. K. Edmunds, T. T. Cockerill, T. J. Foxon, D. B. Ingham, and M. Pourkashanian, "Technical benefits of energy storage and electricity interconnections in future British power systems," *Energy,* vol. 70, pp. 577-587, 6/1/ 2014.

[42] "Engineering Recommendation P2/6 Security of Supply," ed: Energy Networks Association 2006.

[43] S. Blake, Y. Jialiang, P. Taylor, D. Miller, and I. Lloyd, "Using electrical energy storage to support customers under faulted network conditions," in *Electricity Distribution (CIRED 2013), 22nd International Conference and Exhibition on,* 2013, pp. 1-4.

[44] S. Vazquez, S. M. Lukic, E. Galvan, L. G. Franquelo, and J. M. Carrasco, "Energy Storage Systems for Transport and Grid Applications," *Industrial Electronics, IEEE Transactions on,* vol. 57, pp. 3881-3895, 2010.

[45] H. Zhao, Q. Wu, S. Hu, H. Xu, and C. N. Rasmussen, "Review of energy storage system for wind power integration support," *Applied Energy,* vol. 137, pp. 545-553, 1/1/ 2015.

[46] D. O. Akinyele and R. K. Rayudu, "Review of energy storage technologies for sustainable power networks," *Sustainable Energy Technologies and Assessments,* vol. 8, pp. 74-91, 12// 2014.

[47] X. Luo, J. Wang, M. Dooner, and J. Clarke, "Overview of current development in electrical energy storage technologies and the application potential in power system operation," *Applied Energy,* vol. 137, pp. 511-536, 1/1/ 2015.

[48] K. C. Divya and J. Ostergaard, "Battery energy storage technology for power systems-An overview," *Electric Power Systems Research,* vol. 79, pp. 511-520, Apr 2009.

[49] C. A. Hill, M. C. Such, C. Dongmei, J. Gonzalez, and W. M. Grady, "Battery Energy Storage for Enabling Integration of Distributed Solar Power Generation," *Smart Grid, IEEE Transactions on,* vol. 3, pp. 850-857, 2012.

[50] J. Tant, F. Geth, D. Six, P. Tant, and J. Driesen, "Multiobjective Battery Storage to Improve PV Integration in Residential Distribution Grids," *Sustainable Energy, IEEE Transactions on,* vol. 4, pp. 182-191, 2013.

[51] S. Grillo, M. Marinelli, S. Massucco, and F. Silvestro, "Optimal Management Strategy of a Battery-Based Storage System to Improve Renewable Energy Integration in Distribution Networks," *Smart Grid, IEEE Transactions on,* vol. 3, pp. 950-958, 2012.

[52] N. Wade, P. Taylor, P. Lang, and J. Svensson, "Energy storage for power flow management and voltage control on an 11kV UK distribution network," in *Electricity Distribution - Part 1, 2009. CIRED 2009. 20th International Conference and Exhibition on,* 2009, pp. 1-4.

[53] M. A. Kashem and G. Ledwich, "Energy requirement for distributed energy resources with battery energy storage for voltage support in three-phase distribution lines," *Electric Power Systems Research,* vol. 77, pp. 10-23, 1// 2007.

[54] M. A. Kashem and G. Ledwich, "Multiple Distributed Generators for Distribution Feeder Voltage Support," *Energy Conversion, IEEE Transactions on,* vol. 20, pp. 676-684, 2005.

[55] M. Zillmann, Y. Ruifeng, and T. K. Saha, "Regulation of distribution network voltage using dispersed battery storage systems: A case study of a rural network," in *Power and Energy Society General Meeting, 2011 IEEE,* 2011, pp. 1-8.

[56] A. Gabash and P. Li, "Active-Reactive Optimal Power Flow in Distribution Networks With Embedded Generation and Battery Storage," *Ieee Transactions on Power Systems,* vol. 27, pp. 2026-2035, Nov 2012.

[57] A. Gabash and L. Pu, "Flexible Optimal Operation of Battery Storage Systems for Energy Supply Networks," *Power Systems, IEEE Transactions on,* vol. 28, pp. 2788-2797, 2013.

[58] Y. Levron, J. M. Guerrero, and Y. Beck, "Optimal Power Flow in Microgrids With Energy Storage," *Power Systems, IEEE Transactions on,* vol. 28, pp. 3226-3234, 2013.

[59] D. Gayme and U. Topcu, "Optimal Power Flow With Large-Scale Storage Integration," *Power Systems, IEEE Transactions on,* vol. 28, pp. 709-717, 2013.

[60] S. Teleke, M. E. Baran, S. Bhattacharya, and A. Q. Huang, "Rule-Based Control of Battery Energy Storage for Dispatching Intermittent Renewable Sources," *Sustainable Energy, IEEE Transactions on,* vol. 1, pp. 117-124, 2010.

[61] P. Wang, D. H. Liang, J. Yi, P. F. Lyons, P. J. Davison, and P. C. Taylor, "Integrating Electrical Energy Storage Into Coordinated Voltage Control Schemes for Distribution Networks," *Smart Grid, IEEE Transactions on,* vol. 5, pp. 1018-1032, 2014.

[62] L. Xiaohu, A. Aichhorn, L. Liming, and L. Hui, "Coordinated Control of Distributed Energy Storage System With Tap Changer Transformers for Voltage Rise Mitigation Under High Photovoltaic Penetration," *Smart Grid, IEEE Transactions on,* vol. 3, pp. 897-906, 2012.

[63] P. Palensky and D. Dietrich, "Demand Side Management: Demand Response, Intelligent Energy Systems, and Smart Loads," *Industrial Informatics, IEEE Transactions on,* vol. 7, pp. 381-388, 2011.

[64] D. S. Popovic, V. A. Levi, and Z. A. Gorecan, "Co-ordination of emergency secondary-voltage control and load shedding to prevent voltage instability," *Generation, Transmission and Distribution, IEE Proceedings-,* vol. 144, pp. 293-300, 1997.

[65] N. Ruiz, I. Cobelo, and J. Oyarzabal, "A Direct Load Control Model for Virtual Power Plant Management," *Power Systems, IEEE Transactions on,* vol. 24, pp. 959-966, 2009.

[66] A. Gomes, C. H. Antunes, and A. G. Martins, "A Multiple Objective Approach to Direct Load Control Using an Interactive Evolutionary Algorithm," *Power Systems, IEEE Transactions on,* vol. 22, pp. 1004-1011, 2007.

[67] M. Ali, J. Jokisalo, K. Siren, and M. Lehtonen, "Combining the Demand Response of direct electric space heating and partial thermal storage using LP optimization," *Electric Power Systems Research,* vol. 106, pp. 160-167, Jan 2014.

[68] O. Malik and P. Havel, "Active Demand-Side Management System to Facilitate Integration of RES in Low-Voltage Distribution Networks," *Sustainable Energy, IEEE Transactions on,* vol. 5, pp. 673-681, 2014.

[69] B. Ramanathan and V. Vittal, "A Framework for Evaluation of Advanced Direct Load Control With Minimum Disruption," *IEEE Transactions on Power Systems,* vol. 23, pp. 1681-1688, Nov 2008.

[70] B. M. Davis and T. H. Bradley, "The Efficacy of Electric Vehicle Time-of-Use Rates in Guiding Plug-in Hybrid Electric Vehicle Charging Behavior," *Smart Grid, IEEE Transactions on,* vol. 3, pp. 1679-1686, 2012.

[71] Y. Peng, T. Gongguo, and A. Nehorai, "A game-theoretic approach for optimal time-of-use electricity pricing," *Power Systems, IEEE Transactions on,* vol. 28, pp. 884-892, 2013.

[72] L. Xiaohui, L. Xu, L. Rongxing, L. Xiaodong, and S. Xuemin, "UDP: Usage-Based Dynamic Pricing With Privacy Preservation for Smart Grid," *Smart Grid, IEEE Transactions on,* vol. 4, pp. 141-150, 2013.

[73] S. Misra, S. Bera, and T. Ojha, "D2P: Distributed Dynamic Pricing Policyin Smart Grid for PHEVs Management," *Parallel and Distributed Systems, IEEE Transactions on,* vol. 26, pp. 702-712, 2015.

[74] M. A. Zehir and M. Bagriyanik, "Demand Side Management by controlling refrigerators and its effects on consumers," *Energy Conversion and Management,* vol. 64, pp. 238-244, 12// 2012.

[75] M. Tokudome, K. Tanaka, T. Senjyu, A. Yona, T. Funabashi, and K. Chul-Hwan, "Frequency and voltage control of small power systems by decentralized controllable loads," in *Power Electronics and Drive Systems, 2009. PEDS 2009. International Conference on*, 2009, pp. 666-671.

[76] Y. Kinjyo, T. Senjyu, A. Yona, and T. Funabashi, "Autonomous distribution system control by decentralized controllable loads," in *Industrial Electronics and Applications (ICIEA), 2012 7th IEEE Conference on*, 2012, pp. 1212-1217.

[77] A. Arteconi, N. J. Hewitt, and F. Polonara, "State of the art of thermal storage for demand-side management," *Applied Energy,* vol. 93, pp. 371-389, May 2012.

[78] T. Ericson, "Direct load control of residential water heaters," *Energy Policy,* vol. 37, pp. 3502-3512, September 2009.

[79] T. Jiang, G. Putrus, Z. Gao, M. Conti, S. McDonald, and G. Lacey, "Development of a decentralized smart charge controller for electric vehicles," *International Journal of Electrical Power & Energy Systems,* vol. 61, pp. 355-370, 10// 2014.

[80] O. Erdinc, N. G. Paterakis, T. D. P. Mendes, A. G. Bakirtzis, and J. P. S. Catalao, "Smart Household Operation Considering Bi-Directional EV and ESS Utilization by Real-Time Pricing-Based DR," *Smart Grid, IEEE Transactions on,* vol. 6, pp. 1281-1291, 2015.

[81] M. H. Albadi and E. F. El-Saadany, "A summary of demand response in electricity markets," *Electric Power Systems Research,* vol. 78, pp. 1989-1996, 2008.

[82] P. Finn, C. Fitzpatrick, and D. Connolly, "Demand side management of electric car charging: Benefits for consumer and grid," *Energy,* vol. 42, pp. 358-363, Jun 2012.

[83] N. Venkatesan, J. Solanki, and S. K. Solanki, "Residential Demand Response model and impact on voltage profile and losses of an electric distribution network," *Applied Energy,* vol. 96, pp. 84-91, Aug 2012.

[84] V. Stanojevic, V. Silva, D. Pudjianto, G. Strbac, P. Lang, and D. MacLeman, "Application of storage and Demand Side Management to optimise existing network capacity," in *Electricity Distribution - Part 1, 2009. CIRED 2009. 20th International Conference and Exhibition on*, 2009, pp. 1-4.

[85] M. J. Lawson, P. C. Taylor, S. Bell, D. Miller, and N. S. Wade, "An interdisciplinary method to demand side participation for deferring distribution network reinforcement," in *Innovative Smart Grid Technologies (ISGT Europe), 2011 2nd IEEE PES International Conference and Exhibition on*, 2011, pp. 1-8.

[86] Y. S. Lim, S. White, G. Nicholson, and P. Taylor, "Additional applications of demand side management techniques in power systems integrated with distributed generation," in *Electricity Distribution, 2005. CIRED 2005. 18th International Conference and Exhibition on*, 2005, pp. 1-5.

[87] R. Garcia-Valle, L. C. P. da Silva, Z. Xu, and J. Ostergaard, "Smart demand for improving short-term voltage control on distribution networks," *Generation, Transmission & Distribution, IET*, vol. 3, pp. 724-732, 2009.

[88] P. Samadi, H. Mohsenian-Rad, R. Schober, and V. W. S. Wong, "Advanced Demand Side Management for the Future Smart Grid Using Mechanism Design," *Smart Grid, IEEE Transactions on*, vol. 3, pp. 1170-1180, 2012.

[89] T. Logenthiran, D. Srinivasan, and S. Tan Zong, "Demand Side Management in Smart Grid Using Heuristic Optimization," *Smart Grid, IEEE Transactions on*, vol. 3, pp. 1244-1252, 2012.

[90] W. Wei, L. Feng, and M. Shengwei, "Energy Pricing and Dispatch for Smart Grid Retailers Under Demand Response and Market Price Uncertainty," *Smart Grid, IEEE Transactions on*, vol. 6, pp. 1364-1374, 2015.

[91] A. Agnetis, G. de Pascale, P. Detti, and A. Vicino, "Load Scheduling for Household Energy Consumption Optimization," *Smart Grid, IEEE Transactions on*, vol. 4, pp. 2364-2373, 2013.

[92] A. H. Mohsenian-Rad, V. W. S. Wong, J. Jatskevich, R. Schober, and A. Leon-Garcia, "Autonomous Demand-Side Management Based on Game-Theoretic Energy Consumption Scheduling for the Future Smart Grid," *Smart Grid, IEEE Transactions on*, vol. 1, pp. 320-331, 2010.

[93] N. Yaagoubi and H. T. Mouftah, "User-Aware Game Theoretic Approach for Demand Management," *Smart Grid, IEEE Transactions on*, vol. 6, pp. 716-725, 2015.

[94] M. T. Wishart, F. Shahnia, A. Ghosh, and G. Ledwich, "Multi objective decision making method for demand side management of LV residential distribution networks with plug-in electric vehicles," in *Power and Energy Society General Meeting, 2011 IEEE*, 2011, pp. 1-8.

[95] G. Yuanxiong, P. Miao, F. Yuguang, and P. P. Khargonekar, "Decentralized Coordination of Energy Utilization for Residential Households in the Smart Grid," *Smart Grid, IEEE Transactions on*, vol. 4, pp. 1341-1350, 2013.

[96] C. Gouveia, C. L. Moreira, and J. A. P. Lopes, "Microgrids emergency management exploiting EV, demand response and energy storage units," in *PowerTech (POWERTECH), 2013 IEEE Grenoble*, 2013, pp. 1-6.

[97] C. Gouveia, J. Moreira, C. L. Moreira, and J. A. Pecas Lopes, "Coordinating Storage and Demand Response for Microgrid Emergency Operation," *Smart Grid, IEEE Transactions on*, vol. 4, pp. 1898-1908, 2013.

[98] C. Xu and T. J. Overbye, "PTDF-based power system equivalents," *Power Systems, IEEE Transactions on*, vol. 20, pp. 1868-1876, 2005.

[99] C. E. M.-S. a. R. J. T. R. D. Zimmerman, "MATPOWER: Steady-State Operations, Planning, and Analysis Tools for Power Systems Research and Education," *Power Systems, IEEE Transactions on*, vol. 26, pp. 12-19, 2011.

[100] B. F. W. Allen J. Wood, *Power generation, operation, and control*. New York: John Wiley & Sons, Inc, 1996.

[101] J. Yi, P. Wang, P. C. Taylor, P. J. Davison, P. F. Lyons, D. Liang, *et al.*, "Distribution network voltage control using energy storage and demand side response," in *Innovative Smart Grid Technologies (ISGT Europe), 2012 3rd IEEE PES International Conference and Exhibition on*, 2012, pp. 1-8.

[102] T. Sansawatt, L. F. Ochoa, and G. P. Harrison, "Smart Decentralized Control of DG for Voltage and Thermal Constraint Management," *IEEE Transactions on Power Systems*, vol. 27, pp. 1637-1645, 2012.

[103] Q. Zhou and J. W. Bialek, "Generation curtailment to manage voltage constraints in distribution networks," *Generation, Transmission & Distribution, IET*, vol. 1, pp. 492-498, 2007.

[104] E. E. Limited, "Strategies for the uptake of electric vehicles and associated infrastructure implications," 2009.

[105] S. Abu-Sharkh, R. J. Arnold, J. Kohler, R. Li, T. Markvart, J. N. Ross, *et al.*, "Can microgrids make a major contribution to UK energy supply?," *Renewable and Sustainable Energy Reviews*, vol. 10, pp. 78-127, 2006.

[106] P. Mancarella, G. Chin Kim, and G. Strbac, "Evaluation of the impact of electric heat pumps and distributed CHP on LV networks," in *PowerTech, 2011 IEEE Trondheim*, 2011, pp. 1-7.

[107] C. B.-H. Robin Wardle, David Miller,Elisabeth Sidebotham, "Initial Load Profiles from CLNR Intervention Trials," Available: http://www.networkrevolution.co.uk/industryzone/projectlibrary2013 2013.

[108] DECC/OFGEM, "Smart Grid Forum," 2012, 3rd August 2012.

[109] I. Richardson, M. Thomson, and D. Infield, "A high-resolution domestic building occupancy model for energy demand simulations," *Energy and Buildings*, vol. 40, pp. 1560-1566, // 2008.

[110] I. Richardson, M. Thomson, D. Infield, and C. Clifford, "Domestic electricity use: A high-resolution energy demand model," *Energy and Buildings*, vol. 42, pp. 1878-1887, 10// 2010.

[111] I. Richardson, M. Thomson, D. Infield, and A. Delahunty, "Domestic lighting: A high-resolution energy demand model," *Energy and Buildings*, vol. 41, pp. 781-789, 7// 2009.

[112] Ofgem, "Demand Side Response Discussion Paper," ed, 2010.

[113] Office of National Statistics, "Sub-national energy consumption statistics," D. o. E. a. C. Change, Ed., ed, 2011.

[114] M. Alamaniotis, A. Ikonomopoulos, and L. H. Tsoukalas, "Evolutionary Multiobjective Optimization of Kernel-Based Very-Short-Term Load Forecasting," *Power Systems, IEEE Transactions on*, vol. 27, pp. 1477-1484, 2012.

[115] Z. Rui, D. Zhao Yang, X. Yan, M. Ke, and W. Kit Po, "Short-term load forecasting of Australian National Electricity Market by an ensemble model of extreme learning machine," *Generation, Transmission & Distribution, IET*, vol. 7, pp. 391-397, 2013.

[116] K. Nose-Filho, A. D. P. Lotufo, and C. R. Minussi, "Short-Term Multinodal Load Forecasting Using a Modified General Regression Neural Network," *Power Delivery, IEEE Transactions on*, vol. 26, pp. 2862-2869, 2011.

[117] F. Shu and R. J. Hyndman, "Short-Term Load Forecasting Based on a Semi-Parametric Additive Model," *Power Systems, IEEE Transactions on*, vol. 27, pp. 134-141, 2012.

[118] F. Shu and C. Luonan, "Short-term load forecasting based on an adaptive hybrid method," *Power Systems, IEEE Transactions on*, vol. 21, pp. 392-401, 2006.

[119] Y. Goude, R. Nedellec, and N. Kong, "Local Short and Middle Term Electricity Load Forecasting With Semi-Parametric Additive Models," *Smart Grid, IEEE Transactions on*, vol. 5, pp. 440-446, 2014.

[120] A. P. Douglas, A. M. Breipohl, F. N. Lee, and R. Adapa, "Risk due to load forecast uncertainty in short term power system planning," *Power Systems, IEEE Transactions on,* vol. 13, pp. 1493-1499, 1998.

[121] M. Lange, "On the Uncertainty of Wind Power Predictions—Analysis of the Forecast Accuracy and Statistical Distribution of Errors," *Journal of Solar Energy Engineering,* vol. 127, pp. 177-184, 2005.

[122] A. L. S. Bofinger, and H. G. Beyer, "Qualification of wind power forecasts," presented at the Global Wind Power Conf. GWPC'02, Paris, France, 2002.

[123] H. Bludszuweit, J. A. Dominguez-Navarro, and A. Llombart, "Statistical Analysis of Wind Power Forecast Error," *Power Systems, IEEE Transactions on,* vol. 23, pp. 983-991, 2008.

[124] B. Hodge and M. Milligan, "Wind power forecasting error distributions over multiple timescales," in *Power and Energy Society General Meeting, 2011 IEEE,* 2011, pp. 1-8.

[125] R. B. C. Monteiro, V. Miranda, A. Botterud, J. Wang, and G. Conzelmann, "Wind Power Forecasting: State-of-the-Art 2009," Argonne National Laboratory Rep. ANL/DIS-10-1, November 6, 2009 2009.

[126] A. Khosravi, S. Nahavandi, and D. Creighton, "Prediction Intervals for Short-Term Wind Farm Power Generation Forecasts," *Sustainable Energy, IEEE Transactions on,* vol. 4, pp. 602-610, 2013.

[127] W. Can, X. Zhao, P. Pinson, D. Zhao Yang, and W. Kit Po, "Probabilistic Forecasting of Wind Power Generation Using Extreme Learning Machine," *Power Systems, IEEE Transactions on,* vol. 29, pp. 1033-1044, 2014.

[128] W. Can, X. Zhao, P. Pinson, D. Zhao Yang, and W. Kit Po, "Optimal Prediction Intervals of Wind Power Generation," *Power Systems, IEEE Transactions on,* vol. 29, pp. 1166-1174, 2014.

[129] D. Villacci and A. Vaccaro, "Transient tolerance analysis of power cables thermal dynamic by interval mathematic," *Electric Power Systems Research,* vol. 77, pp. 308-314, Mar 2007.

[130] A. Piccolo, A. Vaccaro, and D. Villacci, "Thermal rating assessment of overhead lines by Affine Arithmetic," *Electric Power Systems Research,* vol. 71, pp. 275-283, Nov 2004.

[131] A. Michiorri, H.-M. Nguyen, S. Alessandrini, J. B. Bremnes, S. Dierer, E. Ferrero, *et al.*, "Forecasting for dynamic line rating," *Renewable and Sustainable Energy Reviews,* vol. 52, pp. 1713-1730, 12// 2015.

[132] R. J. Millar and M. Lehtonen, "A robust framework for cable rating and temperature monitoring," *IEEE Transactions on Power Delivery,* vol. 21, pp. 313-321, Jan 2006.

[133] A. H. Ranjbar, A. Banaei, A. Khoobroo, and B. Fahimi, "Online Estimation of State of Charge in Li-Ion Batteries Using Impulse Response Concept," *Smart Grid, IEEE Transactions on,* vol. 3, pp. 360-367, 2012.

[134] K. Jonghoon and B. H. Cho, "State-of-Charge Estimation and State-of-Health Prediction of a Li-Ion Degraded Battery Based on an EKF Combined With a Per-Unit System," *Vehicular Technology, IEEE Transactions on,* vol. 60, pp. 4249-4260, 2011.

[135] K. Il-Song, "Nonlinear State of Charge Estimator for Hybrid Electric Vehicle Battery," *Power Electronics, IEEE Transactions on,* vol. 23, pp. 2027-2034, 2008.

[136] Z. Fei, L. Guangjun, F. Lijin, and W. Hongguang, "Estimation of Battery State of Charge With H Observer Applied to a Robot for Inspecting Power Transmission Lines," *Industrial Electronics, IEEE Transactions on,* vol. 59, pp. 1086-1095, 2012.

[137] L. Der-Tsai, S. Shaw-Ji, L. Chien-Ming, and W. Ying-Chung, "State-of-Charge Estimation for Electric Scooters by Using Learning Mechanisms," *Vehicular Technology, IEEE Transactions on,* vol. 56, pp. 544-556, 2007.

[138] J. C. Alvarez Anton, P. J. Garcia Nieto, C. Blanco Viejo, and J. A. Vilan Vilan, "Support Vector Machines Used to Estimate the Battery State of Charge," *Power Electronics, IEEE Transactions on,* vol. 28, pp. 5919-5926, 2013.

[139] G. L. Plett, "Extended Kalman filtering for battery management systems of LiPB-based HEV battery packs Part 2. Modeling and identification," *Journal of Power Sources,* vol. 134, pp. 262-276, 8/12/ 2004.

[140] P. F. Lyons, N. S. Wade, T. Jiang, P. C. Taylor, F. Hashiesh, M. Michel, *et al.*, "Design and analysis of electrical energy storage demonstration projects on UK distribution networks," *Applied Energy,* vol. 137, pp. 677-691, 1/1/ 2015.

[141] J. Yi and P. Lyons, "CLNR Trial Analysis: I&C Demand Side Response+ GUS Voltage Control," 2014.

[142] J. Yi and S. Blake, "Analysis of I&C DSR for Powerflow Management," 2014.

[143] S. Chun-Lien, "Probabilistic load-flow computation using point estimate method," *Power Systems, IEEE Transactions on,* vol. 20, pp. 1843-1851, 2005.

[144] G. L. Torres and V. H. Quintana, "An interior-point method for nonlinear optimal power flow using voltage rectangular coordinates," *Power Systems, IEEE Transactions on,* vol. 13, pp. 1211-1218, 1998.

[145] Y. S. Xifan Wang, Malcolm Irving, *Modern Power Systems Analysis*. New York: Springer US, 2008.

[146] G. Verbic and C. A. Canizares, "Probabilistic Optimal Power Flow in Electricity Markets Based on a Two-Point Estimate Method," *Power Systems, IEEE Transactions on,* vol. 21, pp. 1883-1893, 2006.

[147] J. M. Morales, L. Baringo, A. J. Conejo, and R. Minguez, "Probabilistic power flow with correlated wind sources," *Generation, Transmission & Distribution, IET,* vol. 4, pp. 641-651, 2010.

[148] C. S. Saunders, "Point Estimate Method Addressing Correlated Wind Power for Probabilistic Optimal Power Flow," *Power Systems, IEEE Transactions on,* vol. 29, pp. 1045-1054, 2014.

[149] M. Aien, M. Fotuhi-Firuzabad, and M. Rashidinejad, "Probabilistic Optimal Power Flow in Correlated Hybrid Wind-Photovoltaic Power Systems," *Smart Grid, IEEE Transactions on,* vol. 5, pp. 130-138, 2014.

[150] L. Yiming, L. Wenyuan, Y. Wei, Y. Juan, and Z. Xia, "Probabilistic Optimal Power Flow Considering Correlations of Wind Speeds Following Different Distributions," *Power Systems, IEEE Transactions on,* vol. 29, pp. 1847-1854, 2014.

[151] J. Zhu, *Optimization of power system operation.* New Jersey: John Wiley & Sons, 2009.

[152] H. Ying-Yi and L. Yi-Feng, "Optimal VAR Control Considering Wind Farms Using Probabilistic Load-Flow and Gray-Based Genetic Algorithms," *Power Delivery, IEEE Transactions on,* vol. 24, pp. 1441-1449, 2009.

[153] F. Miao, V. Vittal, G. T. Heydt, and R. Ayyanar, "Probabilistic Power Flow Studies for Transmission Systems With Photovoltaic Generation Using Cumulants," *Power Systems, IEEE Transactions on,* vol. 27, pp. 2251-2261, 2012.

[154] A. Schellenberg, W. Rosehart, and J. Aguado, "Cumulant-based probabilistic optimal power flow (P-OPF) with Gaussian and gamma distributions," *Power Systems, IEEE Transactions on,* vol. 20, pp. 773-781, 2005.

[155] A. Tamtum, A. Schellenberg, and W. D. Rosehart, "Enhancements to the Cumulant Method for Probabilistic Optimal Power Flow Studies," *Power Systems, IEEE Transactions on,* vol. 24, pp. 1739-1746, 2009.

[156] F. Miao, V. Vittal, G. T. Heydt, and R. Ayyanar, "Probabilistic Power Flow Analysis With Generation Dispatch Including Photovoltaic Resources," *Power Systems, IEEE Transactions on,* vol. 28, pp. 1797-1805, 2013.

[157] T. Williams and C. Crawford, "Probabilistic Load Flow Modeling Comparing Maximum Entropy and Gram-Charlier Probability Density Function Reconstructions," *Power Systems, IEEE Transactions on,* vol. 28, pp. 272-280, 2013.

[158] N. T. Thomopoulos, *Essentials of Monte Carlo Simulation*. New York: Springer, 2013.

[159] L. L. Grigsby, *Electric Power Engineering Handbook Second Edition*. Boca Raton, Florida: Taylor & Francis Group, LLC, 2007.

[160] H. Zhang and P. Li, "Probabilistic analysis for optimal power flow under uncertainty," *Generation, Transmission & Distribution, IET,* vol. 4, pp. 553-561, 2010.

[161] Z. Hui and L. Pu, "Application of sparse-grid technique to chance constrained optimal power flow," *Generation, Transmission & Distribution, IET,* vol. 7, pp. 491-499, 2013.

[162] Z. Hui and L. Pu, "Chance Constrained Programming for Optimal Power Flow Under Uncertainty," *Power Systems, IEEE Transactions on,* vol. 26, pp. 2417-2424, 2011.

[163] C. Yijia, T. Yi, L. Canbing, and C. Rehtanz, "Chance-Constrained Optimization-Based Unbalanced Optimal Power Flow for Radial Distribution Networks," *Power Delivery, IEEE Transactions on,* vol. 28, pp. 1855-1864, 2013.

[164] M. Neaimeh, G. Hill, P. Blythe, R. Wardle, Y. Jialiang, and P. Taylor, "Integrating smart meter and electric vehicle charging data to predict distribution network impacts," in *Innovative Smart Grid Technologies Europe (ISGT EUROPE), 2013 4th IEEE/PES*, 2013, pp. 1-5.

[165] M. Neaimeh, R. Wardle, A. M. Jenkins, J. L. Yi, G. Hill, P. F. Lyons, *et al.*, "A probabilistic approach to combining smart meter and electric vehicle charging data to investigate distribution network impacts," *Applied Energy*, vol. 157, pp. 688-698, Nov 1 2015.

[166] G. A. Hill, P. T. Blythe, and V. Suresh, "How does the use of a continuously updating database allow for the analysis of a user's changing behaviour in electric vehicles?," in *Road Transport Information and Control Conference and the ITS United Kingdom Members' Conference (RTIC 2010) - Better transport through technology*, 2010, pp. 1-7.

[167] H. G. Blythe PT, Huebner Y, Suresh V, Austin J, Grey L, Wardle J, "The North East of England Electric Vehicle and Infrastructure Trials," in *Electric Vehicle Symposium (EVS26)*, Los Angeles, USA;, 6-9 May 2012.

[168] D. P. Wardle R, "Initial load and generation profiles from CLNR monitoring trials," 2012.

[169] P. S. Ingram S, Jackson K., "The impact of small scale embedded generation on operating parameters of distribution networks," PB Power 2003.

[170] "The electricity safety, quality and continuity regulations," Department of Trade and Industry, London, UK2002.

[171] Z. Shu, S. Yonghua, H. Zechun, and Y. Liangzhong, "Robust optimization method based on scenario analysis for unit commitment considering wind uncertainties," in *Power and Energy Society General Meeting, 2011 IEEE*, 2011, pp. 1-7.

[172] A. Street, F. Oliveira, and J. M. Arroyo, "Contingency-Constrained Unit Commitment With n-K Security Criterion: A Robust Optimization Approach," *Power Systems, IEEE Transactions on,* vol. 26, pp. 1581-1590, 2011.

[173] J. Hao, Z. Shu, H. Zechun, S. Yonghua, and C. Yi, "Robust optimization method for unit commitment with network losses considering wind uncertainties," in *Power and Energy Society General Meeting, 2012 IEEE*, 2012, pp. 1-5.

[174] Z. Long and Z. Bo, "Robust unit commitment problem with demand response and wind energy," in *Power and Energy Society General Meeting, 2012 IEEE,* 2012, pp. 1-8.

[175] J. Ruiwei, W. Jianhui, and G. Yongpei, "Robust Unit Commitment With Wind Power and Pumped Storage Hydro," *Power Systems, IEEE Transactions on,* vol. 27, pp. 800-810, 2012.

[176] Z. Chaoyue, W. Jianhui, J. P. Watson, and G. Yongpei, "Multi-Stage Robust Unit Commitment Considering Wind and Demand Response Uncertainties," *Power Systems, IEEE Transactions on,* vol. 28, pp. 2708-2717, 2013.

[177] Z. Chaoyue and G. Yongpei, "Unified Stochastic and Robust Unit Commitment," *Power Systems, IEEE Transactions on,* vol. 28, pp. 3353-3361, 2013.

[178] W. Qianfan, J. P. Watson, and G. Yongpei, "Two-stage robust optimization for N-k contingency-constrained unit commitment," *Power Systems, IEEE Transactions on,* vol. 28, pp. 2366-2375, 2013.

[179] J. Ruiwei, W. Jianhui, Z. Muhong, and G. Yongpei, "Two-Stage Minimax Regret Robust Unit Commitment," *Power Systems, IEEE Transactions on,* vol. 28, pp. 2271-2282, 2013.

[180] L. Changhyeok, L. Cong, S. Mehrotra, and M. Shahidehpour, "Modeling Transmission Line Constraints in Two-Stage Robust Unit Commitment Problem," *Power Systems, IEEE Transactions on,* vol. 29, pp. 1221-1231, 2014.

[181] X. Peng and P. Jirutitijaroen, "Two-stage adjustable robust optimisation for unit commitment under uncertainty," *Generation, Transmission & Distribution, IET,* vol. 8, pp. 573-582, 2014.

[182] D. Bertsimas, E. Litvinov, X. A. Sun, Z. Jinye, and Z. Tongxin, "Adaptive Robust Optimization for the Security Constrained Unit Commitment Problem," *Power Systems, IEEE Transactions on,* vol. 28, pp. 52-63, 2013.

[183] A. J. Conejo, J. M. Morales, and L. Baringo, "Real-Time Demand Response Model," *Smart Grid, IEEE Transactions on,* vol. 1, pp. 236-242, 2010.

[184] C. Zhi, W. Lei, and F. Yong, "Real-Time Price-Based Demand Response Management for Residential Appliances via Stochastic Optimization and Robust Optimization," *Smart Grid, IEEE Transactions on,* vol. 3, pp. 1822-1831, 2012.

[185] K. Seung-Jun and G. B. Giannakis, "Scalable and Robust Demand Response With Mixed-Integer Constraints," *Smart Grid, IEEE Transactions on,* vol. 4, pp. 2089-2099, 2013.

[186] L. Ping and F. Yong, "Optimal operation of energy-efficiency building: A robust optimization approach," in *Power and Energy Society General Meeting (PES), 2013 IEEE*, 2013, pp. 1-5.

[187] Y. W. Yang, R. J. Zhou, X. H. Ran, and Ieee, "Robust Optimization with Box Set for Reactive Power Optimization in Wind Power Integrated System," presented at the 2012 Ieee Power and Energy Society General Meeting, New York, 2012.

[188] A. H. Hajimiragha, C. A. Canizares, M. W. Fowler, S. Moazeni, and A. Elkamel, "A Robust Optimization Approach for Planning the Transition to Plug-in Hybrid Electric Vehicles," *Power Systems, IEEE Transactions on,* vol. 26, pp. 2264-2274, 2011.

[189] A. Ben-Tal and A. Nemirovski, "Robust solutions of Linear Programming problems contaminated with uncertain data," *Mathematical Programming,* vol. 88, pp. 411-424, Sep 2000.

[190] L. E. G. Aharon Ben-Tal, and Arkadi Nemirovski, *Robust Optimization*. Princeton and Oxford: Princeton University Press, 2009.

[191] S. A. Malcolm and S. A. Zenios, "Robust optimization for power-systems capacity expansion under uncertainty," *Journal of the Operational Research Society,* vol. 45, pp. 1040-1049, Sep 1994.

[192] D. Bertsimas and M. Sim, "The price of robustness," *Operations Research,* vol. 52, pp. 35-53, Jan-Feb 2004.

[193] A. L. Soyster, "Technical Note—Convex Programming with Set-Inclusive Constraints and Applications to Inexact Linear Programming," *Operations Research,* vol. 21, pp. 1154-1157, 1973.

[194] D. Bertsimas and M. Sim, "Robust discrete optimization and network flows," *Mathematical Programming,* vol. 98, pp. 49-71, Sep 2003.

[195] T. E. Oliphant, "Python for Scientific Computing," *Computing in Science & Engineering,* vol. 9, pp. 10-20, 2007.

[196] D. Kraft, "A software package for sequential quadratic programming," DLR German Aerospace Center –Institute for Flight Mechanics, Koln, Germany1988.

[197] R. Baldick, "Variation of distribution factors with loading," *Power Systems, IEEE Transactions on,* vol. 18, pp. 1316-1323, 2003.

[198] C. K. V. C. M. Campbell, "A123's Advanced Grid Storage, Extending Our Experience to Distributed Resource Applications and Microgrids " in *MicronGen,* Glasgow, 2011.

[199] D. M. Greenwood, J. P. Gentle, K. S. Myers, P. J. Davison, I. J. West, J. W. Bush, *et al.*, "A Comparison of Real-Time Thermal Rating Systems in the U.S. and the U.K," *Power Delivery, IEEE Transactions on,* vol. 29, pp. 1849-1858, 2014.

[200] Northern Powergrid. (2014, April 2015). *Customer Led Network Revolution*. Available: http://www.networkrevolution.co.uk/

[201] A. Spencer, "Developing the smarter grid: the role of industrial and commercial and distributed generation customers," Northern Powergrid2014.

[202] H. Chen, T. N. Cong, W. Yang, C. Tan, Y. Li, and Y. Ding, "Progress in electrical energy storage system: A critical review," *Progress in Natural Science,* vol. 19, pp. 291-312, 3/10/ 2009.

[203] P. Mathiesen, J. M. Brown, and J. Kleissl, "Geostrophic Wind Dependent Probabilistic Irradiance Forecasts for Coastal California," *Sustainable Energy, IEEE Transactions on,* vol. 4, pp. 510-518, 2013.

[204] D. Saez, F. Avila, D. Olivares, C. Canizares, and L. Marin, "Fuzzy Prediction Interval Models for Forecasting Renewable Resources and Loads in Microgrids," *Smart Grid, IEEE Transactions on,* vol. 6, pp. 548-556, 2015.

[205] B. Stott and O. Alsac, "Fast Decoupled Load Flow," *Power Apparatus and Systems, IEEE Transactions on,* vol. PAS-93, pp. 859-869, 1974.